MODELLING AND CONTROL OF TRANSATMOSPHERIC VEHICLE DYNAMICS

CHRIS F. O'NEILL

Thesis Submitted to the Faculty of Engineering, University of Glasgow, for the Degree of Doctor of Philosophy. All aspects of the work presented herein are original in content except where indicated.
The research was conducted between October 1992 and October 1995 at the Department of Aerospace Engineering, University of Glasgow.

Chris O'Neill, January 1996

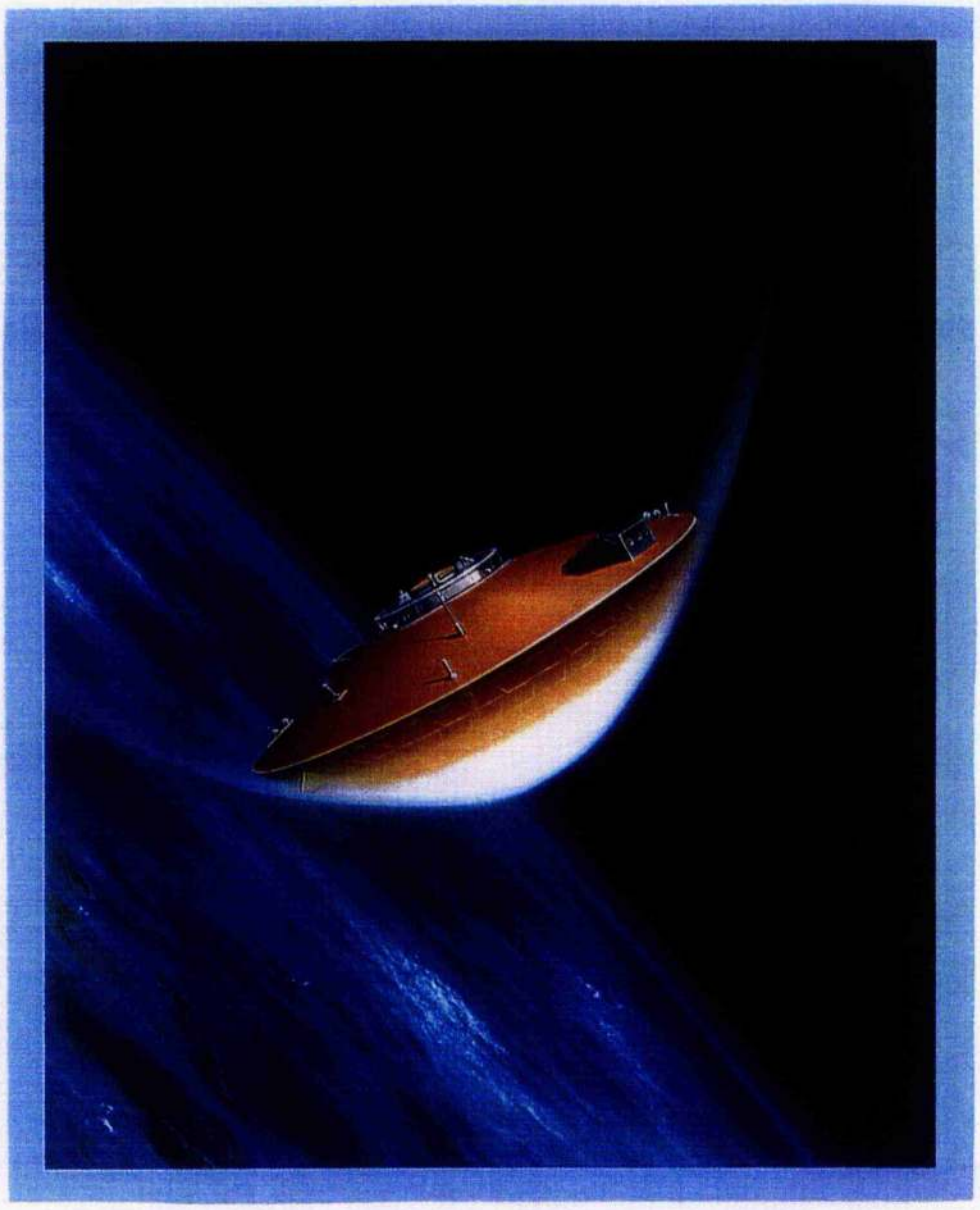

Artists impression of the Orbital Re-entry Experiment (OREX) designed to acquire re-entry data as part of the Japanese H-II Orbiting Plane (HOPE) program. Other vehicles in the program include the Hypersonic Flight Experiment (HYFLEX), a lifting vehicle intended to demonstrate hypersonic flight technologies, and the Automatic Landing Flight Experiment (ALFLEX) .
OREX was successfully flown in February 1994.

(Picture Taken from OREX publicity pamphlet)

"We shall not cease from exploration, and the end of all our exploring will be to arrive where we started and know the place for the first time."

T.S. Eliot

"As far as the laws of mathematics refer to reality they are not certain: and as far as they are certain, they do not refer to reality"

Albert Einstein

Abstract

The development of a flexible, high-fidelity, generic simulation of transatmospheric and interplanetary motion is described. The simulation incorporates aerodynamic and gravitational force modelling implemented in a Cartesian reference co-ordinate set. Propagation of the motion of a vehicle is carried out in a "working" reference frame whose origin is determined by the current gravitational sphere of influence. A semi-analytic model of planetary motion propagates the motion of the nine planets and six major moons, allowing simulation at any point within the solar system. Expansion and improvement of the model is facilitated through the vector formulation of the problem.

The use and applicability of the method of matched asymptotic expansions is examined as a means of producing high quality trajectory predictions quickly and easily. Ballistic launch and entry trajectories are considered incorporating a velocity dependent model for the aerodynamic drag coefficient. Using the derived relations direct launch is considered as a low-cost means of transporting acceleration insensitive payloads to a space station in low Earth orbit. In addition, it is shown that the high quality trajectory predictions may be obtained using a simple spreadsheet package.

Analytic modelling is also used as the basis of a highly robust, computationally efficient, controller design for autonomous aerocapture in the context of the lunar return problem. The validity of this approach to lunar return is examined and found to be of considerable potential in both its robustness and the potential improvements in payload mass-fraction available through the substantial fuel savings over direct return to Earth or propulsive return to a space station. The study shows that, using the derived control, the aerocapture manoeuvre can be successfully performed with existing material and technological capabilities.

Acknowledgements

I was once told that if, by the time you had finished a Ph.D., you did not hate your work, then you hadn't done it properly. This one should be good then.

The long and frequently tortuous days and nights often took their toll on my humour and I fear at times I inflicted my frustrations on those around me. I would like to apologise to those whom I consider to be some of the most genuine friends any man could ask for and to thank them for their unique contributions to my (in)sanity.

To "Uncle Col'", who put up with any number of bouts of apathy and resisted the temptation to push me off the top of a Munro. I hope supervising a paranoid neurotic held a few laughs for you. To Karen, for keeping Colin off the streets. To Stephen, who shared many a trouble over cups of coffee and chocolate. Your candour and blunt humour have been much appreciated and by way of showing that appreciation I'm going to resist the temptation to immortalise your nickname in print. To Reineke, inspiration and friend for always, and cause of many an oversized phone bill. You talk too much sense but you do always know what to say. To Zoi, friend, companion, fellow shopper, cook and daughter (?!...Answers on a postcard.....). Lots of late nights and lots of fun. To Frank. What can I say? It's been a long time. I think that we still talk to each other after all this time says it all. To Stewart "SS" Houston, the only man in the world who can say he watches Baywatch for the helicopters and be believed. To Scott, friend and partner, rowing has never quite been the same. "You've lost that balanced feeling,.....". To Mike and Linda, firm friends, I wish you many happy years together. To my many friends and co-sufferers in halls, Rose, Donna, Moira, Lindsey, Pauline, Jenny, Dougy, Stuart, Gaby, Claire, Viki, William, Koon-Huat, Eleanor, and especially to those who provided support and a much needed ear from time to time, Adele, Shihan, Michael, Brian, and Ingrid (bet you're wishing you never moved in now), and a supporting cast of thousands. To Katrine, Julie, Kate, Mitch, Fiona, and all the senior girls from the rowing club, who are definitely worse than the guys. To my parents, who have always supported me, whatever, and who must by now be senile enough to think I know what I'm doing. To the guys, Mark, Sean, and Adam, comrades in arms, Disney Club members, and nutcases one and all, what will happen to us all? Oops, I forgot, Mark's life's over already. Not to forget the MacLellans, Kay & "Wee" Chris, and the McQuades. To Laurent, Angus (wooOOOooose), Franck and Marivi.

You're all mad too. Do I spy a pattern developing here? And all those now gone, Gianmarco, Sergio, Fernando and Ismael. Goon but not forgotten. To my "wee" brother Kevin, for legal advice. To "Auntie Em's" Stationary, Postal, Cake & Cookie Service. To the staff at the Exchequer, the Aragon, the Research Club, and of course Shobha and Tracey at Chimmyz. To Thump'm, my calculator, which I'm convinced is the father of most, if not all, modern computers. Unfortunately. To Gavin Hastings, or God, as we call him. To God, just in case.... To Winona, and why not? Regrettably, I should also thank my older brother Greg, the real inspiration behind this work. If I get this that makes me a real 'Doctor' while you're busy working your way back to 'Mister'. Ever feel like you've been doing things the wrong way 'round?

And finally, to any and all I may have missed. I've met too many people during my time in Glasgow to keep track of and I haven't always shown my appreciation when I should have. Take it from me, I did appreciate it. To quote the Big Yin, "Appreciate, appreciate, appreciate....".

This work is dedicated to John and Linda O'Neill, *parents extraordinaires*.

Formal Acknowledgements

The author wishes to acknowledge the contributions made by his supervisors, Dr. Colin R. McInnes and Dr. Stewart S. Houston, towards the direction and completion of this work. Their guidance and assistance have been much appreciated.

I should also like to acknowledge the support and assistance of the entire Department of Aerospace Engineering, secretaries, staff, and fellow researchers. Because of their help no problem went unsolved.

This work was funded by a University of Glasgow Postgraduate Scholarship.

Contents

Figures and Tables

FIGURES

Notes : **a)** "average" refers to time averaged values for the variables shown.

b) "absolute" refers to the magnitude of the values shown.

c) where the term "peak heating rate" has been used this refers to the maximum value on the vehicle surface (i.e. the nosetip) at that time **not** the peak value achieved over the entire trajectory.

d) all errors are absolute unless otherwise stated.

Ballistic Entry

Ballistic Launch

TABLES

Nomenclature

Notes: 1) Where a symbol has more than one meaning in the list below the appropriate meaning can be understood from the text.
2) Where a symbol is for explanatory means the context of the symbol is given in the text.
3) All quantities are given in standard S.I. units except where noted.
4) A bar above a symbol usually denotes a non-dimensionalised quantity. Where this is not the case this is clear from the text.

A, A' - periapsis and apoapsis
a - semi-major axis, acceleration
C_D - aerodynamic drag coefficient
C_L - aerodynamic lift coefficient
C_Y - aerodynamic side force coefficient
$\overline{C}_{lm}, \overline{S}_{lm}$ - tesseral harmonics
D - aerodynamic drag
E - eccentric anomaly
e - eccentricity
F - force
G - Universal gravitational constant
g - local gravitational acceleration
H - atmospheric scale height
h - altitude (dimensioned or non-dimensional)
I - moment/product of inertia
J_n - zonal harmonics
L - aerodynamic lift
L/D - aerodynamic lift to drag ratio
m, M - mass
M - mean anomaly, mass, Mach number
N, N' - ascending and descending orbital nodes
P - pseudocontrol, North celestial pole
P_o - orbital period
$P_n(z), P_l^m(z)$ - Legendre polynomials of the function z
p, q, r - vehicle roll rates about x, y, z co-ordinate axes
$\dot{p}, \dot{q}, \dot{r}$ - vehicle angular accelerations about x, y, z co-ordinate axes
$\dot{Q}$ - convective heating rate
q - dynamic pressure, y-axis roll rate
R - planetary/lunar/solar radius
R_{soi} - radius of sphere of influence
r - orbital radius, vehicle roll rate about z-axis
S - reference area, focus (of ellipse)
T - torque, temperature
t - time
U - gravitational potential
u - square of non-dimensionalised velocity
v, V - velocity
V_a - airspeed
x, y, z - Cartesian reference axes
X, Y, Z - Cartesian reference axes
Y - aerodynamic side force
$y, \dot{y}, \ddot{y}$ - altitude error, climb rate error, radial acceleration error

Greek Symbols

α - control gain, angle of attack
β - ecliptic latitude, angle of sideslip
γ - flight path angle
Δi - change in inclination
ΔV - change in velocity
$\Delta\psi$ - change in heading angle
δ - bias
ε - small parameter, flattening parameter
ϕ - longitude, inclination (spherical polar co-ordinates), control gain, roll (bank) angle
ϕ, θ, ψ - roll (bank), pitch, yaw (azimuth) angles
$\dot{\phi}, \dot{\theta}, \dot{\psi}$ - roll (bank), pitch, yaw (azimuth) rates
λ - aerodynamic lift-to-drag ratio, ecliptic latitude
λ, ϕ - latitude and longitude
μ - planetary gravitational constant
ϖ - longitude of periapsis
θ - latitude, polar angle, range angle, pitch angle
$\dot{\theta}_i$ - angular rate about the ith axis
ρ - (local) atmospheric density
σ - roll (bank) angle, sub-satellite planetary radius
τ - time of periapsis passage
ω - Cosine of flight path angle, argument of periapsis, angular velocity
Ω - longitude of the ascending node
ψ - heading (track) angle, yaw (azimuth) angle
ζ - filter gain

Subscripts

a - airspeed, apogee
aero - aerodynamic
b - body
bp - body with respect to parent
c - command
d - demand
E - equatorial
e - entry
exo - exoatmospheric
exp - exponential atmosphere
grav, gravity - gravitational
i - initial, *i*th axis
l, m, n - indices
m, M - mass
max - maximum
o - sea-level, initial, zeroth order
p - parent, planet, perigee
po - initial perigee
ref - reference
s - heliocentric
soi - sphere of influence
x, y, z - Cartesian reference axes
* - constant of integration
∞ - planetocentric, exospheric

Acronyms & Abbreviations

AFE - Aeroassisted Flight Experiment
AGA - Aerogravity Assist
AOT - Aeroassisted Orbital Transfer
AOTV - Aeroassisted Orbital Transfer Vehicle
ARD - Atmospheric Re-entry Demonstrator

CM - Command Module
CPU - Central Processing Unit
ESA - European Space Agency
GEO - Geostationary Earth Orbit
IMU - Inertial Measurement Unit
ISSA - International Space Station Alpha
LCA - Lightweight Ceramic Ablator
LEDA - Lunar European Demonstration Approach
LEO - Low Earth Orbit
LSSG - Lunar Study Steering Group
LTV - Lunar Transfer Vehicle
MAE - Matched Asymptotic Expansions
NASA - National Aeronautics and Space Administration
PAO - Planet Acting as Origin
SRP - Solar Radiation Pressure
SSTO - Single Stage To Orbit
US – 62 - 1962 United States Standard Atmosphere

Chapter I.

INTRODUCTION

I.A. Comment

If mankind is ever to expand beyond the confines of the Earth, we must first look at and learn about the worlds around us. Examination and exploration of these bodies will enable us to learn more about the mechanisms of the Universe: how things develop, grow and decay, and how the human mind and physiology react to the varied environments to be encountered. Careful utilisation of the resources we may find should assist us to expand further into the Solar system.

All this has to begin somewhere and perhaps the "small step"[1] that was Apollo could be regarded as the first significant step towards man's expansion into space. Alas, since Apollo, man has not returned to the moon and, although missions such as Voyager and Viking have taught us more about our solar system, the advances that were envisaged at that time have not been achieved. Twenty-six years later, man has still not journeyed to Mars.

To be fair, the cost of a Mars mission, extrapolated from Apollo, would have been exorbitant (the cost of the Apollo program translates to over $120*billion* in 1990 Dollars[2], equivalent to over 600

shuttle missions) and the advances that have been made in technology and design in the interim may show that it was wise to wait (if that were the intention). But perhaps now the time for man to return to space has come.

What motivations can we find for the effort that will be required?

- **Human Expansion**

Man has long been driven by the desire to examine and to advance his understanding of his environment. The urges to explore, to discover, and to achieve took Columbus to the Americas, led the Egyptians to build the Pyramids, and cause our finest minds to look deeper into the atom or further into the skies. These aspirations alone should be justification enough for the manned exploration and colonisation of space.

More recently, our understanding of our environment and its past proposes another reason for manned space exploration; the continuation of the species. History suggests that sudden (geologically), periodic extinction of species such as the dinosaurs may be the result of cataclysmic events such as comet or meteorite impacts. Within the last year the effects of the impact of fragments of the comet Shoemaker-Levy on Jupiter have clearly demonstrated the destructive potential of such collisions. Even with the advanced technologies of today we must concede that we may not be able to avoid such an impact.

In addition possible climate changes, whether natural or man-made, would suggest that it is in the interests of the entire race then to expand into the Solar system, lest this planet become uninhabitable.

- **Scientific Knowledge**

As the Hubble Space Telescope has shown, much can be learned through such space-based astronomy about the evolution of our solar system and indeed the universe. From space we may observe the universe without the attenuating effect of the Earth's atmosphere and the clutter of radio waves which fill it.

- **Energy**

  Some appraisals of our fossil fuel consumption have us running out of economically viable sources in around 50years[3,4]. The most promising replacement source is currently nuclear power with fusion likely to be more productive in the long run. However, both fission and deuterium-tritium fusion (currently proposed for future reactors) produce large amounts of waste heat and radioactivity.

  Alternative energy sources such as geothermal, solar power, hydroelectricity, wind and wave power although renewable are unlikely to be able to replace fossil fuels even at today's energy consumption levels[4].

A first step in addressing these concerns is a return to the moon.

- **Human Expansion**

  A lunar colony is essential in developing our understanding of how human physiology reacts to prolonged exposure to reduced gravity and artificial environments (any lunar base will by necessity be an artificial environment) and in developing radiation protection and the aforementioned artificial ecosystems[5].

  Knowledge gained from lunar experience could be used in developing artificial ecosystems for other planets, in particular Mars, which would be an essential first step even if highly futuristic concepts such as terraforming (the transformation of an alien environment into a human-habitable one) were to prove feasible.

- **Scientific Knowledge**

  The science of the moon, in spite of the success of the Apollo and Lunokhod missions, is still incomplete and there is still much to be learned about its composition and history[5]. In addition access to the moon allows experimentation in unique gravitational and radiation environments[6].

The building of a radio-telescope and other observatories on the moon should be seriously considered. As has been remarked "the Moon is a God-given, spin-stabilised platform waiting for a payload"[7]. The Moon would appear an ideal site for a radio-telescope in particular, with the far side being permanently hidden from the Earth and its radio outputs.

- Energy

Deuterium-helium-3 fusion produces significantly less radioactive waste (almost none) than current fission and proposed fusion reactions and would provide energy with almost double the efficiency of current fission reactors[4].

Natural terrestrial helium-3 is scarce but deposits on the moon are abundant[3,4]. In addition, as helium-3 is deposited by the solar wind, it will be found in the surface soils aiding excavation.

One account suggests that Lunar mining could prove a highly lucrative business, with a single shuttle load of 25 metric tons valued at $75billion[3].

The concern over energy may seem the more immediate and is more likely to receive commercial backing. The use of other resources, such as oxygen, iron and aluminium may also prove commercially viable for in-orbit or lunar construction and it is likely that this will prove very important in terms of future funding for space efforts[2]. In addition there is the possibility of rare earth metal extraction which would certainly help the aforementioned commercial viability.

Of course, expansion onto the Moon and into space should be carried out under careful management. Leaving aside terrestrial concerns, we have already polluted the skies above us with orbital debris and through achieving our goals in an unthinking or naïve fashion we have created a problem which hinders us in continuing to achieve those goals. It is all part of the learning process but we should now know to think before we act.

I.B. Problem Statement: Lunar and Planetary Exploration

It is likely that the majority of early missions in the next phase of lunar exploration will be unmanned. Proposals by groups such as the ESA Lunar Study Steering Group (LSSG)[5] have lead to the conception of the Lunar European Demonstration Approach (LEDA)[6] which calls for a lunar lander carrying a small rover vehicle. It is proposed that the mission carry out soil analysis and assess the suitability of the Moon as a base for optical and radio-astronomy in addition to evaluating the operational environment on the Moon.

Whilst missions such as LEDA investigate the soil and rock structure and composition, a polar orbiter could be used to map the surface and survey the global chemical and physical make-up of the Moon. Other missions proposed include surface penetrators for examination of Lunar geology, the development of a network of small surface stations and sample-return missions[5]. In the future, technologies developed for and understanding gained from sample-return vehicles would be crucial in establishing a supply infrastructure to and from a lunar base. Given the likely limitations on energy consumption it will be important that we use what we can in the most efficient way possible. The economics to be gained over rocket propulsion from the effective use of aerobraking and aerocapture may make their use essential in the lunar return problem.

Further afield, we come first to Mars and then the other planets. For those planets with atmospheres, aerobraking and aerocapture could be used to perform the vital function of slowing the vehicle on arrival at its destination. Mars is likely to be the first planet, other than our own, to be explored by man and the approach to Martian exploration will probably be similar to that for Lunar exploration.

The work presented here describes:

- The development of a generic simulation (*genL*) for the analysis of space vehicle motion, investigation of control techniques and methodologies, and validation of analytic models.
- The development, implementation, and investigation of analytic models of transatmospheric vehicle motion.
- The development, implementation, and investigation of controls based on these models, in particular investigating the control of terrestrial aerocapture in the Lunar return context.

I.C. Aero-assisted Trajectories

The use of aerodynamic forces for the control of (transatmospheric) space vehicles is by no means a new concept. London's[8] 1961 paper on orbital plane changing is generally regarded as the first on the subject and although Walberg[9] gives one example of a paper published prior to London's he adds that London's "appears to be the first to convincingly demonstrate a significant performance gain.".

Most vehicles subject to aerodynamic forces will experience only the retarding effect of drag, and this may be either a help or a hindrance depending on the mission scenario. Lack of an atmosphere on the moon required the Apollo orbiter and Eagle lander to achieve all of their deceleration propulsively, requiring the transport of large amounts of fuel to the moon. A recent example of the benefits of aerodynamic braking was provided by the Magellan Venus mission[10], where atmospheric drag was successfully used to shrink the spacecraft's orbit apoapsis from $8467km$ to $541km$. This manoeuvre was carried out using only a fraction of the fuel that would be required to propulsively reduce the orbit and avoiding the extra cost of transporting the additional fuel to Venus.

Walberg[9] describes three classes of aeroassisted mission:

- synergetic plane change
- planetary mission applications
- orbital transfer vehicle applications.

This classification of aeroassisted missions is somewhat arbitrary as there is a degree of overlap among the classes. For example, the transfer between Geostationary Earth Orbit (GEO) and Low Earth Orbit (LEO) is an orbital transfer manoeuvre and may also require a change of plane.

In keeping with this arbitrary style of classification then we shall discuss aeroassisted manoeuvring in four sections:

- aerobraking
- aerocapture
- plane changing
- aerogravity assist.

These are presented in the order most appropriate to the work described here. As shall be seen the distinction between aerocapture and aerobraking can be considered more quantitative than qualitative. A review of the dynamics of the motion is included where appropriate.

I.C.1. Aerobraking

Aerobraking is a simple manoeuvre conceptually. Any body passing through an atmosphere experiences drag and is thus subject to aerodynamic braking. The aerobrake manoeuvre is designed to take advantage of this effect in order to achieve a desired reshaping of the orbit.

A propulsive burn would be used to transfer the vehicle from its initial trajectory into an elliptical orbit about the planet that skims the upper atmosphere at periapsis. The drag experienced during this atmospheric pass will lower the apoapsis and in this manner the orbit is gradually lowered and circularised[10,11]. Once the required apoapsis has been achieved a further burn is required to raise the periapsis out of the atmosphere if a surface impact is not desired. Fig I.C.1-1 below illustrates the multi-pass aerobraking scheme.

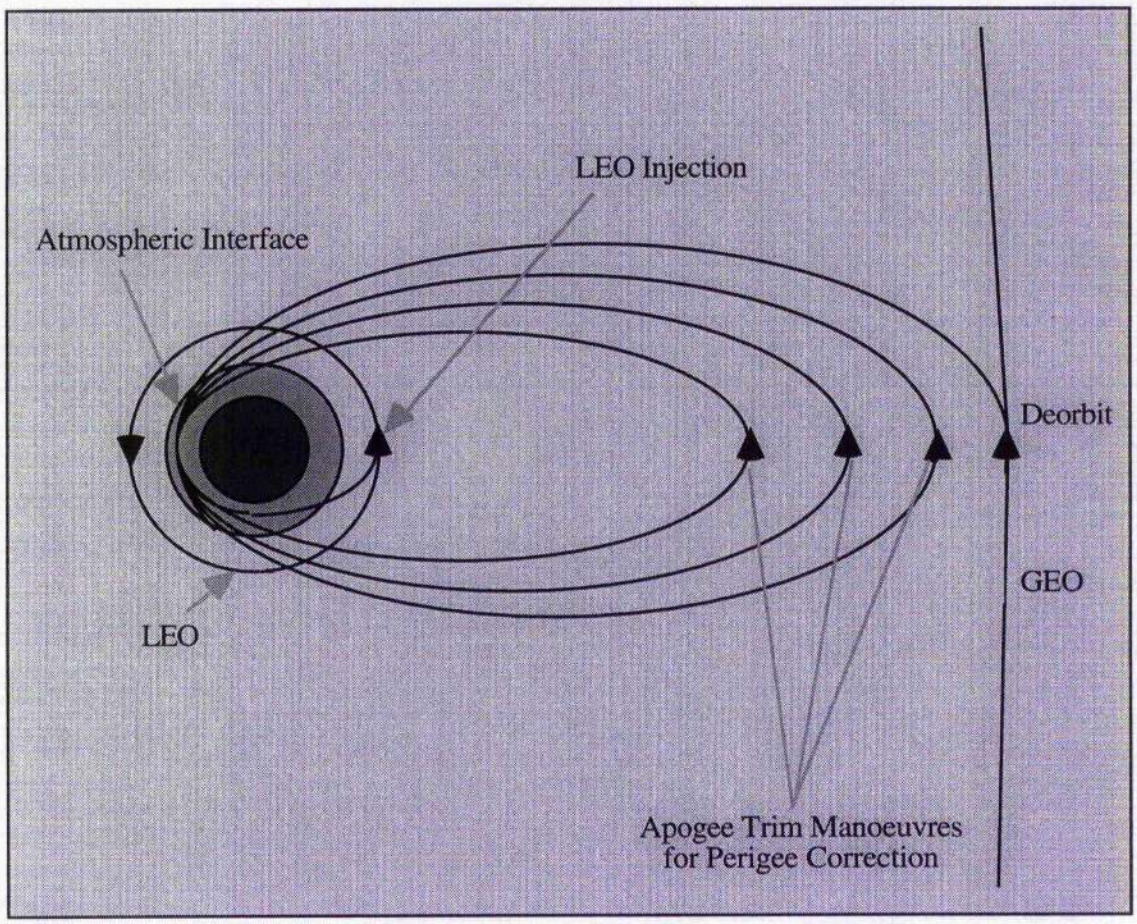

Fig. I.C.1-1 : Schematic of a Multi-pass Aerobrake mission: GEO to LEO

As mentioned above aerobraking was used to great effect on the Magellan mission[10]. What was particularly remarkable about this demonstration was that Magellan was not designed with aerobraking in mind. The possibility of extending the mapping mission using aerobraking only arose as a result of the

success of the original mission. The extension was intended to provide an accurate gravity map of Venus and this would require lowering the orbit from its $8467km$ apoapsis to $541km$. To achieve this propulsively would have required an order of magnitude more propellant than Magellan possessed, leaving aerobraking as the only means of lowering the orbit.

The aerobraking phase lasted 70 days during which time the vehicle performed several hundred passes. The length of an aerobraking operation allows time to "walk" the vehicle into an atmosphere and collect data to allow calibration of the manoeuvres and any necessary propulsive corrections. This allows the design of fail-safe missions even into previously unknown atmospheres. In addition, because of the high altitude of the atmospheric passes involved, an aerobraking vehicle will experience relatively low heat and deceleration loadings.

An aerobraking precursor to Magellan, the Atmospheric Explorer vehicle[11] was also not designed to take advantage of aerobraking. For this mission, the perigee was kept sufficiently high that the aerodynamic heating experienced by the vehicle was negligible.

As Magellan has shown, multi-pass aerobraking may be accomplished at low deceleration loads and with less stringent heat shielding requirements allowing greater flexibility in vehicle design[9,10].

I.C.2. Aerocapture

An aerocapture manoeuvre can be regarded as a single aerobraking manoeuvre (atmospheric skip) on a bigger scale. While aerobraking begins from propulsive insertion into an elliptical orbit about the planet, the aerocapture approach trajectory is directly into the atmosphere. The required velocity decrement is achieved through a single deep atmospheric pass such that upon atmospheric exit the vehicle can no longer escape from the planet's gravity field and is captured into an elliptical orbit about the planet. On achieving apogee a single

rocket motor burn would circularise the vehicle's orbit outside the atmosphere.

Aerocapture has been successfully used in the Apollo Lunar-return[12] and was proposed for use in manned Mars missions in the sixties[9]. An analysis of lifting entry was also carried out in advance of the Viking Mars[13] missions. In these cases a surface landing was required as will be the case in the Cassini-Huygens[14,15] mission to Saturn and one of its moons, Titan. Because of the double-dip (see below) manoeuvre performed at Earth re-entry, Apollo remains the closest match to the capture-to-orbit manoeuvres proposed for future planetary and lunar return missions[16,17,18,19].

During atmospheric entry of the Apollo capsules aerodynamic lift was used to augment vehicle control. Graves and Harpold[12] describe in detail the "double-dip" scheme employed to alleviate high pressure, deceleration, and heating loads by using the less dense upper atmosphere to slow the vehicle twice (see fig. I.C.2-1).

The necessity for load-alleviation through a double-dip manoeuvre has been lessened by the advances made in materials technology and the increasing likelihood that the vehicle will be unmanned. In addition, the complexity of performing an autonomous double-dip manoeuvre at a remote planet in uncertain atmospheric conditions makes it likely that a simple single pass will be adopted for off-world capture-to-ground applications.

Although Mars may be sufficiently close to contemplate relaying commands from Earth to a vehicle in orbit it is doubtful that such a signal could be sent through the plasma sheath that would engulf an entry vehicle.

Even if this were possible, the dynamics of the motion are so fast that the light time delay would make any received commands obsolete. This leads to the requirement for autonomous vehicle control[9].

The use of aerodynamic lift greatly increases the controllability of aeromanoeuvring[9,12,20,21]. Drag modulation is a possible means for trajectory control (e.g. inflatable ballute or

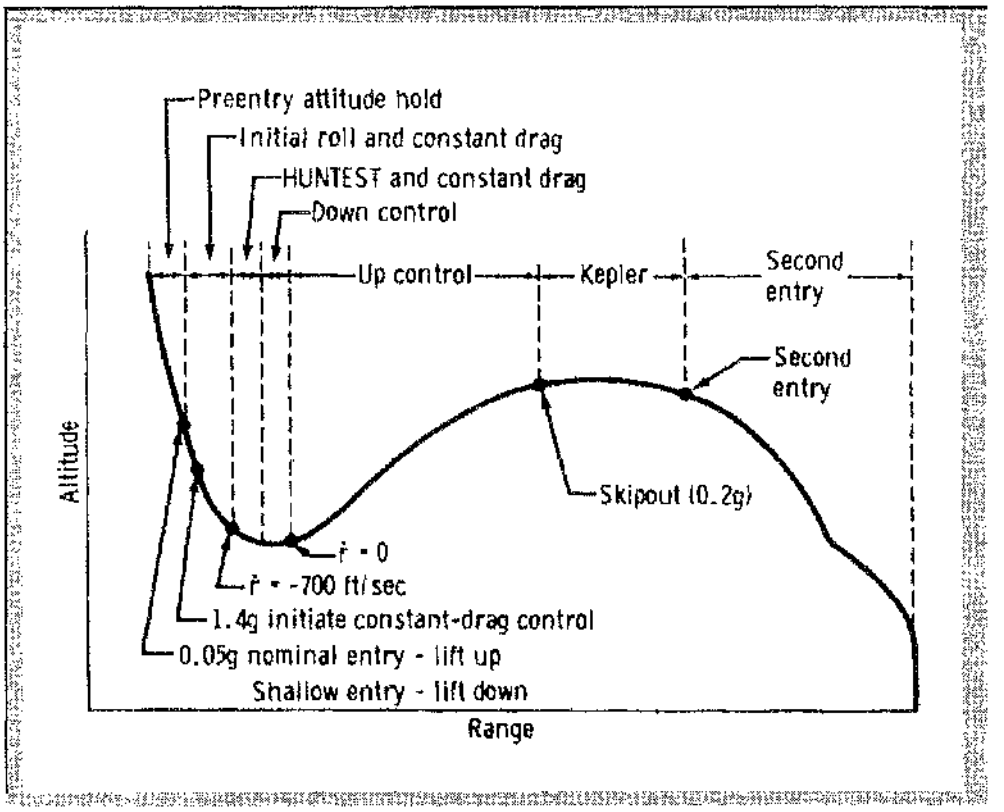

Fig. I.C.2-1 Double-dip manoeuvre schematic showing the guidance phases. Taken from Graves, C. A. and Harpold, J. C., *Apollo Experience Report*[12]

angle of attack modulation) but will only allow control of the deceleration acting along the line of motion, whereas lift allows control over accelerations perpendicular to the plane of motion. A more detailed consideration of the methods of controlling transatmospheric vehicles follows later in the chapter.

Walberg[9] describes two periods of high interest in aerocapture missions. The first, between 1964 and 1968, was primarily concerned with the manned Mars mission NASA proposed as a follow-up to the Apollo program. Funding never materialised for this program and it was not until 1979 that interest rose again, this time in the context of unmanned planetary missions. Walberg describes as a flight control requirement a hypersonic L/D of 1.0-1.5, although Graves and Harpold[12] give values for the Apollo capsule averaging around 0.35. The discrepancy between these two values is mostly due to

the former being for unmanned vehicles, which will operate with higher g-load limits.

The deep hypervelocity pass into the atmosphere brings with it significant heat and pressure loadings, the heat loadings being such that ablative heat shielding may be required, if not all over, then on the nose and leading edges of the vehicle. The vehicle may need to be completely enclosed in a protective aeroshell, further restricting vehicle design[9].

One scenario for a mission to Saturn and Titan proposed prior to Cassini-Huygens was designated SO2P-Titan[9]. This Saturn Orbiter would achieve capture into an orbit around Saturn by passing through the atmosphere of Titan. The vehicle would have used a full aeroshell to protect the probes during the atmospheric pass.

The complication with aeroshell design is that it will tend to trap the heat generated by the on-board power supply and instrumentation. As a result of this, thermal radiation shielding would be required for the sensitive instrumentation and systems and active cooling would be necessary to maintain the temperature of the spacecraft within an acceptable band. In addition expendable surface-mounted telemetry equipment may be required for tracking and navigation en route. This would avoid opening doors within the aeroshell during transit for deployment of subsystems which would introduce questions about the integrity of the aeroshell during atmospheric passage.

It appears that the use of aeroassist will significantly complicate the spacecraft design but it may also significantly improve payload margins, perhaps by as much as 100%[9].

Using the atmosphere to slow a vehicle at, for example, Mars would greatly reduce the amount of propellant required for the mission and thus the mass of vehicle which must be placed into Mars orbit. Any mass reduction here would be valuable in that an increase of $1kg$ mass in Mars orbit would require about $10kg$ extra mass in LEO[9]. In 1990 Ariane 4 was one of the cheapest

launch vehicles available at a cost of over £3000 / *kg* to LEO[2], so the savings would be considerable.

Early proposals for a manned Mars mission[22] envisaged blunt nosed biconic configurations. The vehicle would be controlled in much the same way as the Apollo re-entry capsules. An off-set centre of gravity would cause the vehicle to fly at a non-zero angle of attack, producing lift. Roll modulation would be used for control.

The optimism of the times is perhaps reflected in the vehicle concepts analysed. One design would have carried a crew of eight and a 9100*kg* payload to Mars[9]. This contrasts with the ill-fated 1018*kg* (total mass) unmanned Mars Observer mission.

I.C.3. Plane Changing

The term orbital plane change is generally used to refer to an alteration in the inclination of the plane, although it could equally well be used to refer to an orientation change with or without a concomitant change in inclination.

The ability to vary the orbital plane would be useful in allowing a vehicle such as the Shuttle[23] to rendezvous with satellites in varying orbital planes or as London[8] suggests it could be used to establish a vehicle in an orbital plane which does not pass through the launch site.

However, changing the orbit plane requires a large characteristic velocity (ΔV). It is well known that the ΔV required to achieve a 60° change in the orbital inclination is as large as that required to place the vehicle into LEO[24].

London showed that these changes in inclination could be achieved aerodynamically by passage of the vehicle through the atmosphere. A retro-propulsive burn would slow the vehicle causing it to dip into the atmosphere. During the atmospheric pass the vehicle's lift vector would be directed so as to produce the required out of plane force and thus the required change of

inclination. Once outside the atmosphere again a further rocket burn would circularise the orbit.

The effectiveness of the atmospheric turn depends on the point within the orbit at which it is effected. Walberg[9] shows that a turn at one of the orbital nodes will translate directly into an inclination change, whereas a turn at the apex (highest latitude) of the orbit merely rotates the orbit about the poles, effecting no inclination change at all.

An important parameter in orbital plane changing is the lift-to-drag ratio for the vehicle as this determines the speed loss due to drag for any given change in inclination, Δi. This loss forms the greatest part of the ΔV required to return the vehicle to orbit[8] after the pass and as such is a measure of the usefulness of the aerodynamic manoeuvre in comparison to a purely propulsive exoatmospheric manoeuvre. Fig. I.C.3-1 shows the ideal characteristic velocity required for a given inclination change for both the aerodynamic manoeuvre (for a range of L/D values) and the exoatmospheric propulsive manoeuvre (for the single impulse case and the three impulse cases requiring two and three orbital periods, P_n).

As stated, the ability to change the inclination of the orbital plane allows the insertion into orbit of equatorial satellites from non-equatorial launch sites and rendezvous with a target when the vehicle cannot be launched directly into the plane of the target. It also allows some control of the inclination of the orbital plane during an aeroassisted manoeuvre. This ability may prove particularly useful for supply missions to the International Space Station Alpha (ISSA) when construction is completed as it will have an orbital inclination of 51.6° [25] in order to allow access to the Russian launch sites.

Cuadra and Arthur[24] describe the plane change manoeuvre as either an aeroglide or an aerocruise manoeuvre. In aeroglide the vehicle is unpowered (during atmospheric passage), whereas in aerocruise rocket thrust is used to balance aerodynamic drag and maintain a constant altitude and velocity.

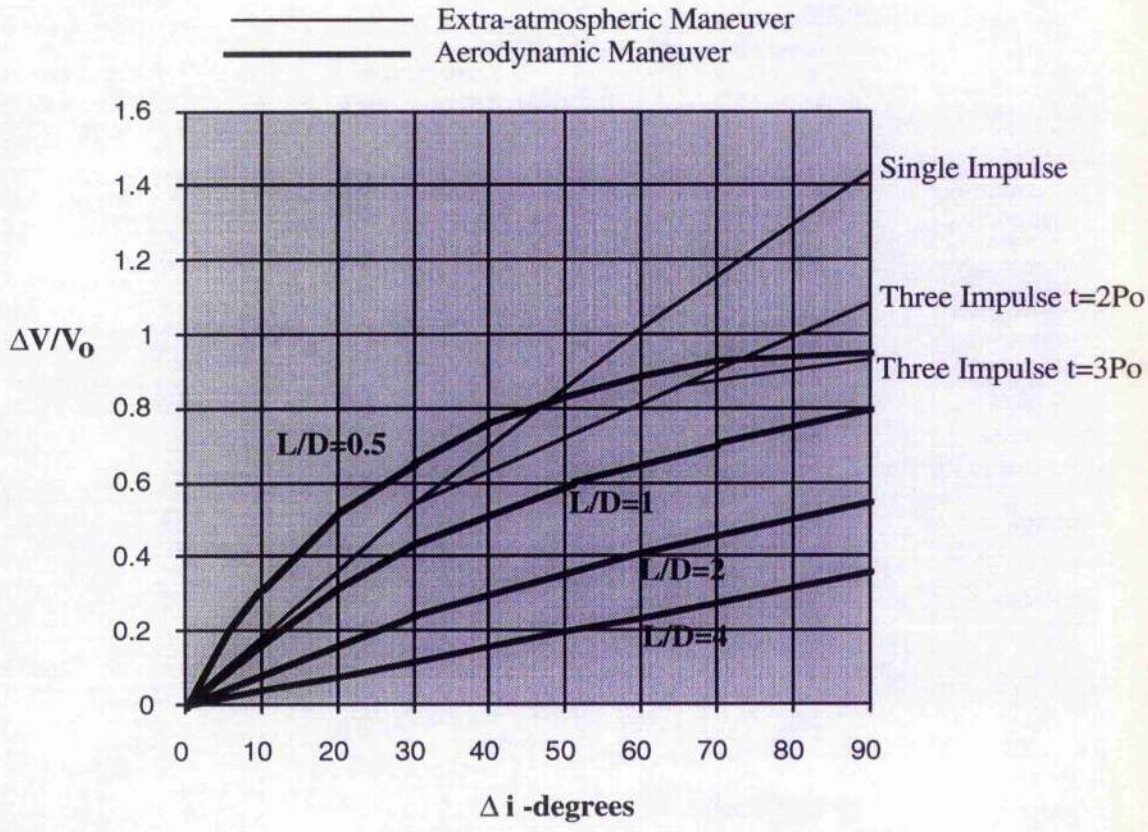

Fig. I.C.3-1 Ideal Characteristic Velocity for Changing Inclination
Replicated from London[8]

The ability to maintain a constant velocity is useful in controlling the heating and pressure environments for the vehicle and as Cervisi[26] asserts this would facilitate the design and control of both the manoeuvre and the vehicle.

I.C.4. Aerogravity-Assist

The aerogravity-assist (AGA) manoeuvre is an extension of the gravity assist or "slingshot" manoeuvres used by the Voyager spacecraft in their "Grand Tours" of the solar system.

In gravity-assist trajectories the vehicle is launched not directly to the distant target planet, with its correspondingly large

launch energy, but to a nearer planet which will require a much lower launch energy.

The vehicle will use that planet's gravity field to bend its trajectory thus changing the direction and magnitude of its sun-relative (heliocentric) velocity.

To do so propulsively would require a large fuel mass and some means of transporting that fuel to its point of use, greatly increasing the launch mass and launch energy requirement. Instead the vehicle gains energy from the planet as its trajectory is altered by the planet's gravitational field. Fig. I.C.4-1 illustrates the effect on the vehicle's heliocentric velocity, V_S, of rotating the planet relative (planetocentric) velocity vector, V_∞, through an angle $\Delta\psi$, called the bending angle. V_P is the heliocentric planetary velocity vector and primed quantities (e.g. V_S') are values after rotation through $\Delta\psi$.

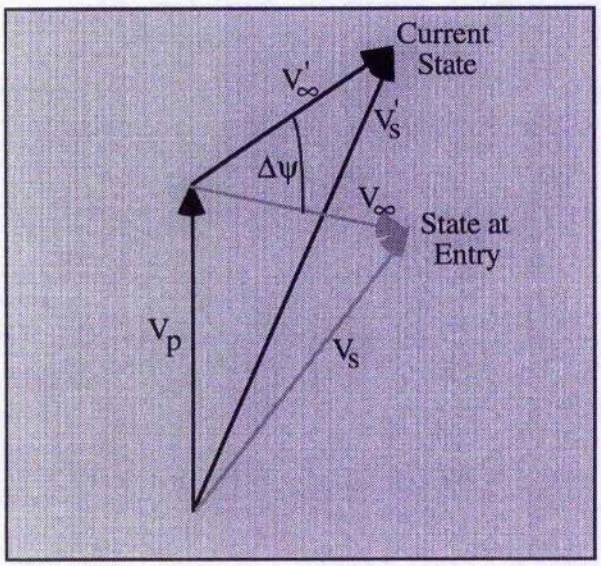

Fig. I.C.4-1 Rotation of the planetocentric velocity vector during an AGA manoeuvre

McRonald and Randolph[27] state that the heliocentric velocity change is directly proportional to the bending angle.

In aerogravity-assist the vehicle uses the planet's atmosphere to hold it within the gravity field for longer, enabling a larger bending angle and hence a larger ΔV. Obviously some speed is lost to the atmosphere of the planet but by using high lift-to-drag

vehicles such as Nonweiler's waverider concept[28] this loss can be minimised.

AGA manoeuvres are likely to be employed where travel times are long or launch windows are limited, for example the Solar Probe or Pluto missions described by McRonald and Randolph[27,29], or planetary missions to, for example, Saturn and Jupiter. There remain many technical and technology issues which have so far prevented the use of AGA, as well as the understandable reluctance of the world's space agencies to risk using an untried and dynamically unstable[30] manoeuvre on expensive deep space missions.

I.D. Dynamics and Control of Transatmospheric Vehicle Motion

The dynamics of transatmospheric vehicle motion are usually represented in polar co-ordinates for a vehicle travelling over a spherical planet with a non-rotating atmosphere, and for ease of illustration they are so represented here. Fig I.D.-1 represents ballistic vehicle motion for a single pass through an atmosphere and consequently the motion lies entirely within the orbital plane.

The symbols are described in the nomenclature. It should be noted that the flight path angle, γ, is measured as positive away from the planet. The forces acting on the vehicle are simply the gravitational attraction of the planet and aerodynamic drag. The full equations of motion for this system are given in Chapter II (eqn.s II.A.1-1:6) with the addition of aerodynamic lift.

The system is simple to analyse but difficult to control. The high velocities associated with atmospheric entry and the accordingly high pressure and heat loads make the use of aerodynamic control surfaces limited if not impossible. Stabilising the motion in such a system could be achieved through spin-vanes on the surface of the

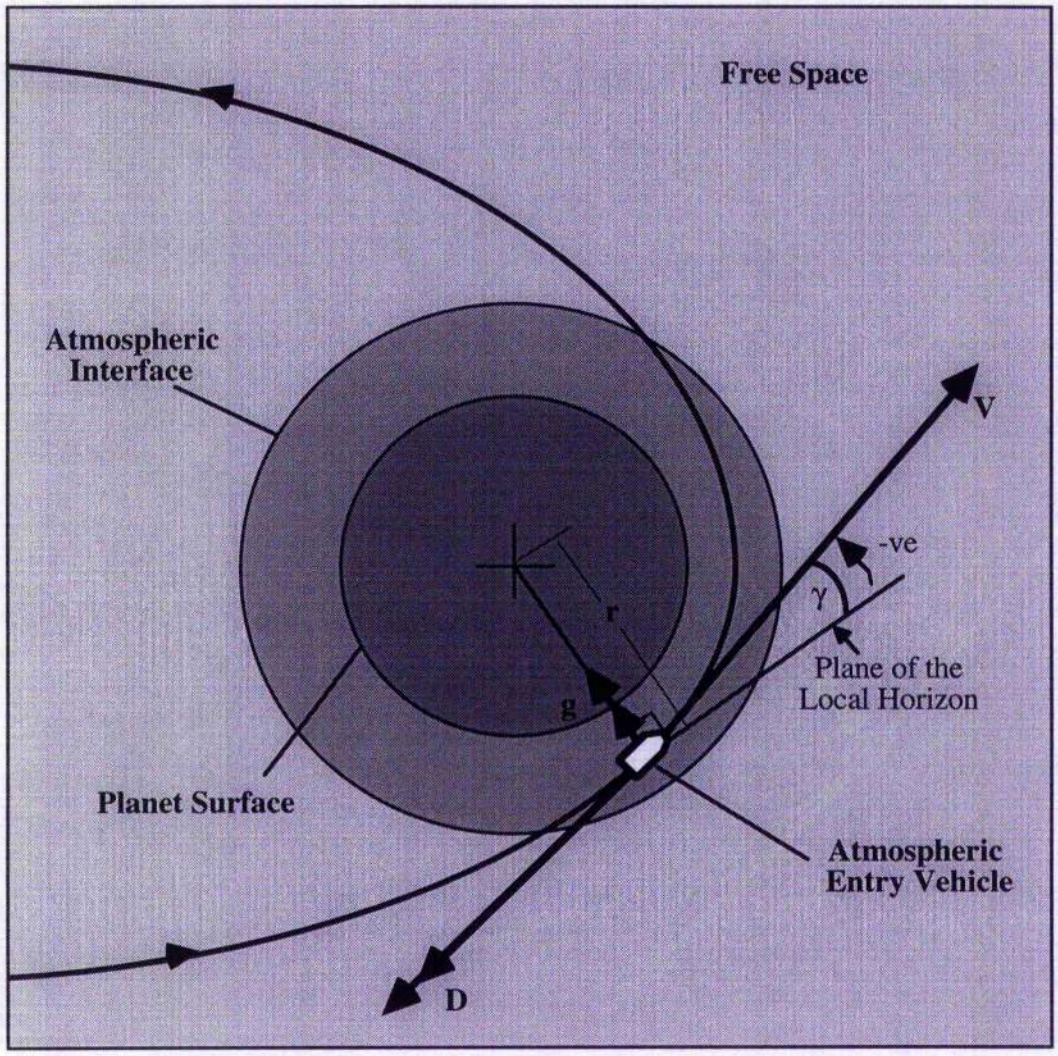

Fig. I.D-1 System schematic for an atmospheric pass

vehicle[14] (for slower entry speeds) or through reaction control thrusters.

One method of drag-only control is described by Walberg[9] for use as an orbital transfer or aerobraking vehicle. The inflatable ballute concept is essentially a balloon at the front of the entry vehicle which determines the drag characteristics of the vehicle.

By varying the internal pressure of the ballute a range of ballistic coefficients is possible and this allows limited control over the vehicle's trajectory. Unfortunately control authority is somewhat limited, but the concept is light for an aeroassisted orbital transfer vehicle (AOTV), and the payload gains possible from the use of aeroassist in the orbital transfer problem may yet lead to its use.

Vinh et al.[31] present a drag-only control scheme for an optimal orbital transfer manoeuvre. No practical method of implementation is given rather it is assumed that the vehicle is capable of modulating its drag coefficient between limits. The results obtained for an aeroassisted orbital transfer are described as excellent but an order of magnitude variation in the drag parameter is required.

For the higher speeds associated with aerocapture, ballistic vehicle control has been all but ignored and lifting vehicles seem to be the only viable option for controlled aerocapture.

The benefit of adding aerodynamic lift to the control problem can be seen when we consider that a lifting vehicle may mimic a ballistic entry by rolling the lift vector perpendicular to the orbital plane thus removing it from consideration for motion within that plane. If we then roll the vehicle away from the perpendicular we produce a component of lift which acts within the orbital plane and in this way we achieve a degree of control over the radial acceleration acting on the vehicle and consequently the altitude (fig.s I.D-2a&2b).

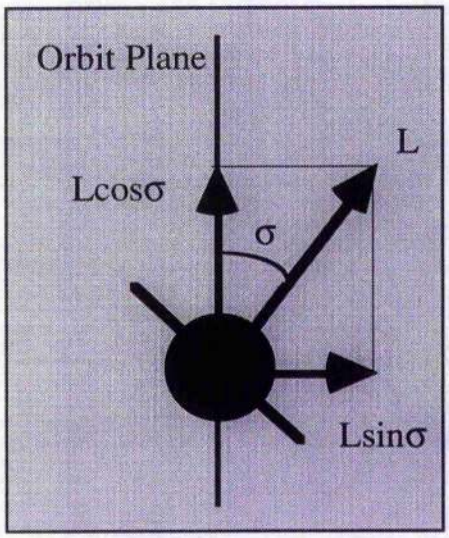

Fig. I.D-2a

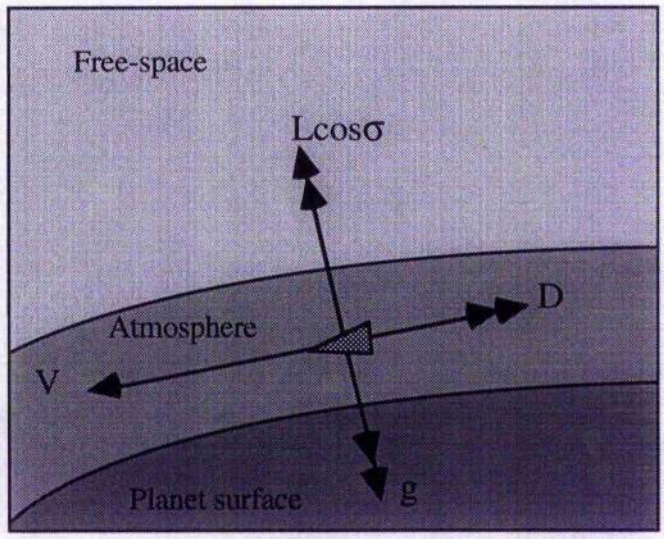

Fig. I.D-2b

Aerodynamic lift acting on a transatmospheric vehicle

2a) Orbital Plane: End Elevation

2b) Orbital Plane: Plan view

Such a control allows us to widen the range of entry states from which we can achieve an acceptable end state. This range or error margin is known as the entry corridor (fig. I.D-3).

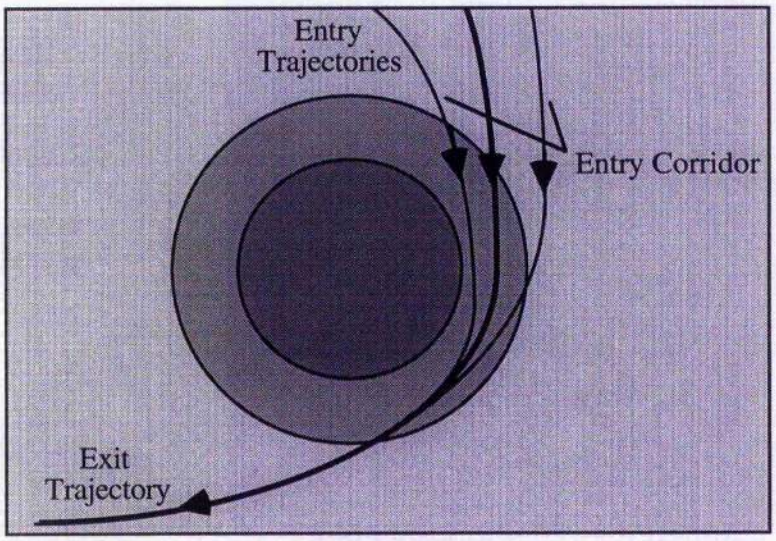

Fig. I.D-3 Schematic representation of the entry corridor concept

Graves and Harpold[12] define the concept of an entry corridor,

> *"The entry corridor is defined as the set of space trajectories for which aerodynamic capture within the atmosphere of the earth* [sic] *can be achieved and for which entry-trajectory control can be accomplished without exceeding either flight-crew or CM* [command module] *stress limits. Therefore, definition of the corridor limits includes four basic considerations: aerodynamic capture within the atmosphere, the aerodynamic load factor, aerodynamic heating, and landing-point control."*

This defines the entry corridor as a set of trajectories which lie between two extremes, the overshoot and the undershoot.

- **overshoot** - the entry is too shallow and consequently the vehicle does not lose enough energy to achieve capture and continues out of the target sphere of influence.

- **undershoot** - the entry angle is too steep and the vehicle impacts on the surface.

It should be noted that these definitions assume there are no structural or material limitations.

The difference between these two extremes is referred to as the corridor width, and this is usually given in terms of a range of atmospheric entry angles. A fuller discussion of entry corridor concepts and definitions is given in Chapter V.

The introduction of an out of plane force ($L\sin\sigma$, fig.I.D-2a) will also cause changes in the orbital plane. Where this is undesirable frequent roll-reversals (redirecting of the lift from one side of the orbital plane to the other side) can be used to minimise any lateral movement.

Tauber[32] describes the benefit of roll-modulated lift control for aerocapture over alternative methods such as pitch-modulation, as having a full range of control values from maximum positive to maximum negative lift (along the radius vector), increasing the entry corridor. In addition the physiological constraint of deceleration loads favours bank-angle modulation over pitch-modulation in that the crews tolerance to g-loads is at its highest when the load is applied perpendicular to the upper torso. It should also be noted that, as stated above, aerodynamic surfaces cannot be used during aerocapture so control is effected through reaction controls, and consequently requires fuel. As Tauber goes on to state, the amount of fuel used to implement roll control is significantly less than that which would be required to maintain off-trim pitch angles.

Control proposals for many aeroassisted manoeuvres are based on non-linear feedback control (Chapter III). A feedback controller uses a set of reference data in conjunction with current state evaluations to assess the vehicle's departure from the nominal or ideal trajectory and implements an appropriate control to cause convergence of the actual state to the reference state.

Mease and Kremer[33] present a non-linear feedback derivative of the current Shuttle entry guidance scheme which shows improvement over the current control, albeit limited within the present operating domain. Current shuttle entry guidance follows a drag reference trajectory and Mease and Kremer show that it is, in fact, similar in its derivation to non-linear feedback control.

Roenneke and Markl[34] present a similar controller following a drag-vs-energy reference.

Non-linear control has also been shown to be useful for aeroassisted orbital transfer (AOT)[35], and Lee[36] presents an optimal solution for AOT. A deterministic feedback law has been developed by Mease and McCreary[21] for control of atmospheric skip trajectories, which uses the desired apoapsis state as its reference and analytically recalculates the trajectory which will result in that state at each time point.

Given the uncertainties associated with high speed atmospheric passage it is perhaps not surprising that the use of optimal control is somewhat limited. Meyer et al.[37] study fuel-optimal bank angle control concluding that impulsive bank-angle control is possible with predictor corrector techniques adjusting the magnitude of the impulses to compensate for atmospheric uncertainties, navigation errors etc. Even here the optimisation process can only try to optimise the trajectory from the current vehicle state necessitating a fuel safety-margin. Given that any practical implementation will have a fuel safety-margin to accommodate the aforementioned uncertainties it is questionable whether there is anything to be gained by attempting to optimise the control in any sense other than robustness.

I.E. Simulation and Current Work

Commercially available packages such as *Orbital Workbench*[38] and *DAB Ascent*[39] have been written to provide ready-made analysis tools for space vehicle analysis. Whilst these packages perform their tasks well they are limited in the tasks they can perform. The author of *DAB Ascent* readily admits that his work is a three degree of freedom simulation and does not model rotational dynamics, nor does *Orbital Workbench* possess such a capability. In addition, control in *Orbital Workbench* is effected through magnitude and directional control of thrust alone, with no capability of modelling lifting bodies, although it will model a

change in the drag parameters such as that caused by the opening of a parachute.

Propagation in *Orbital Workbench* can be carried out in a number of ways from Keplerian models to numerical integration of vector models. This latter approach is also used in *DAB Ascent* and *POST* (Program to Optimize Simulated Trajectories)[40]. Like *DAB Ascent*, *POST* is a three of freedom program, which simulates and optimises point-mass trajectories. There is also a six degree of freedom version of *POST*.

The author's impression throughout has been that the vast majority of computer simulations were either purpose written for the work presented, or had been written prior to the work either by the respective authors or at least at that place of work. This suggests that simulations specifically tailored to the research at hand are easier to work with.

Part of the work presented here details the development of a generic six degree of freedom aerospace vehicle simulation, *genL*, which is capable of simulating any type of trajectory or manoeuvre and can easily incorporate unique control strategies. In order to remain as generic as possible the simulation incorporates a solar system model to allow analysis of interplanetary trajectories and aeroassisted manoeuvres at other planets.

As mentioned previously, the Apollo re-entry strategy employed a double-dip manoeuvre to alleviate the high pressure, deceleration, and heat loads experienced during re-entry. Graves and Harpold[12] describe the phases in detail, and it is interesting to note that any predictions required during the motion are made analytically. The use of analytic predictions is undoubtedly indicative of the limited computing power of the times, but its successful use shows that effective control does not require high-performance computers.

The use of analytic predictions as a basis for both modelling the motion of transatmospheric vehicles and controlling said motion is investigated here, firstly in the context of the launch and re-entry problems and then for aerocapture in the Lunar return problem.

Chapter II.

SIMULATION

II.A. Introduction : *genL*

"There is a car that has more computing power than it took to take man to the moon."[41]

So we are told. This is more a reflection on the scale of the achievements of the Apollo program than on the car but it makes a valid point. Year by year, computing power advances in leaps and bounds, the current journey from product birth to obsolescence being around three years. These advances have, in many cases, outstripped requirements, and consequently there is a great deal more flexibility in programming style available to researchers. The rapid increase in processor speeds and the corresponding reduction of program run times allows the researcher to move away from pure efficiency of code towards modularity and ease of use.

The modular approach allows the programs to be written in a more clearly structured manner and makes upgrading of programs simpler. Rather than rewriting large portions of code to incorporate an improved system model the model is broken down into sections and the appropriate sections upgraded. For example, in the *genL*

spacecraft simulation developed here, there is a module which evaluates the force of gravitational attraction acting on the vehicle towards the Earth. To change from a spherical gravity model to a sixth-order oblate Earth gravity model requires nothing more than a change in the call statement as it is the value of the gravitational potential which differs rather than its interaction with the rest of the system. This approach fits neatly with the Cartesian co-ordinate system used in *genL* which is essentially a modular way of thinking. By breaking down the system into suitable modules it becomes conceptually simpler and easier to adapt for differing scenarios.

The *genL* simulation makes use of this approach to programming whilst introducing a novel concept for the propagation of vehicle motion; propagation within an arbitrary reference frame.

Using this approach the equations of motion (Newton II) are applied to the vehicle within some undefined Cartesian reference axes set which will represent the current "working" frame. For example, in the trans-earth trajectory the vehicle moves from the Lunar sphere of influence into the Terrestrial sphere of influence. In *genL* the motion of the vehicle will be propagated firstly in selenocentric co-ordinates and then geocentric co-ordinates, switching between the two at the interface of their spheres of influence.

The frame of reference within which we are working then becomes a "working" frame rather than a fixed one. This approach allows force and moment calculations to be made in the frame most appropriate to them, thus minimising computational errors. These interactions are then transformed into the working frame and their combined effects analysed through Newton II. The use of an arbitrary reference frame is discussed in greater depth later in this chapter.

GenL is a generic spacecraft simulation program written in vector formulation for implementation in Cartesian reference frames.

The simulation incorporates a simple but accurate model of the Solar System called *Holst*. *Holst* models the motion of all nine

planets, the Sun and the six major moons (Titan, the Galilean Moons of Jupiter and our Moon). The gravitational effects of the other moons are considered too small to warrant consideration as are the major asteroids, although inclusion of further bodies into the simulation is quite straightforward. These bodies are included to allow analysis of outer planet aerocapture and interplanetary trajectories. From *Holst* are obtained the position and velocity vectors of the planets in the working reference frame.

Propagation of the motion of the vehicle requires knowledge of the forces acting on it, principally gravitational, aerodynamic and control forces:

For the analysis of transatmospheric motion *genL* has four different atmosphere models:

- Exponential
- US-62 standard atmosphere
- Oblate Earth exponential atmosphere
- Biased sine waves

The biased sine wave models are not actually models in themselves but provide perturbations to the nominal values derived from one of the other models. Each of these atmosphere models is described later in the text (section II.C.2).

Evaluation of the aerodynamic forces acting on the vehicle is made using the standard expressions and reference frames for aerodynamic forces and moments and transforming these into the working frame.

The modelling of the Terrestrial gravitational field is done in one of two ways:

- Standard Newtonian inverse square model
- 6^{th}-order geoid model with tesseral and zonal harmonics.

The inverse square model is adequate for the majority of scenarios particularly hypervelocity transatmospheric motion. The higher

order model is more useful for long-term orbit analysis or transatmospheric motion over a particular area of the Earth, e.g., shuttle re-entry to a landing at Kennedy Space Center.

The majority of the motion analysed in the chapters following is unpowered and consequently no propulsive control forces are applied for these analyses. Where control forces are applied they take the form of a force vector in body-fixed axes.

In this chapter we examine some of the characteristics and capabilities required of a transatmospheric motion simulation and detail the way in which they are incorporated into the development of the generic spacecraft simulation *genL*.

II.A.1. Modelling Requirements

The standard equations of motion as used in transatmospheric vehicle dynamics are, for a gliding vehicle[42],

$$\frac{dV}{dt} = -\frac{\rho V^2 S C_D}{2m} - \frac{\mu}{r^2}\sin\gamma \qquad \text{II.A.1-1}$$

$$V\frac{d\gamma}{dt} = -\left\{\frac{-V^2}{r} + \frac{\mu}{r^2}\right\}\cos\gamma + \frac{\rho V^2 S C_L}{2m}\cos\sigma \qquad \text{II.A.1-2}$$

$$\frac{dr}{dt} = V\sin\gamma \qquad \text{II.A.1-3}$$

$$\frac{d\theta}{dt} = \frac{V}{r}\cos\gamma \qquad \text{II.A.1-4}$$

$$\frac{d\phi}{dt} = \frac{V\cos\gamma\sin\psi}{r} \qquad \text{II.A.1-5}$$

$$V\frac{d\psi}{dt} = \frac{\rho V^2 S C_L}{2m\cos\gamma}\sin\sigma - \frac{V^2}{r}\cos\gamma\cos\psi\tan\phi \qquad \text{II.A.1-6}$$

where the symbols are described in the nomenclature.

Using these expressions the motion of a vehicle orbiting a planet may be modelled in terms of its radial displacement from

the centre of the planet, orbital velocity, spherical polar angles (ϕ, θ, effectively latitude and longitude measured with respect to the initial orbit plane) and flight path angle.

This system of equations makes use of certain assumptions, viz.,

- a non-rotating atmosphere
- spherical non-rotating planet
- constant vehicle lift and drag coefficients
- unpowered flight
- fixed alignment of the vehicle with the flight path.

These are all standard assumptions and indeed they are all used at some point in the guidance work presented later. However, the development of a robust controller is somewhat different from the development of a high-fidelity numerical simulation. The capabilities of the simulation are limited if this formulation is used. Certainly corrections can and are made to remove these assumptions[43,44] but these often involve different formulations of the equations in terms of the orbital elements and perturbations to these equations. The implementation of these equations in a computer simulation would be straightforward enough but would often require completely replacing the equations of motion to include a new effect.

In looking for alternatives to this approach we must first consider the potential requirements of a high-fidelity numerical simulation suitable for Earth-orbiting, interplanetary, and trans-atmospheric vehicle motion.

- Propagation of the motion of the vehicle in a suitable reference frame.
  (Section II.B.2)
- Derivation of the orbital elements.

  The position and velocity may be expressed directly in Cartesian co-ordinates and propagation of the motion may be

carried out in such a reference. However, the orbital elements provide a standard, easily understood data set and knowledge of these would still be preferred.
(Section II.B.2.1 and Appendix III)

- Gravitational field model.
  The Earth and most of the other planets are not perfect spheres and while it is often convenient to consider them as such this assumption may not always prove valid.
  (Section II.C.1 and Appendix IIb)

- Solar and Lunar gravity model.
  (Section II.C.1, II.C.3, and Appendix I)

- Terrestrial atmosphere model.
  The true atmosphere is neither non-rotating nor exponential and the consequences of this need to be considered.
  (Section II.C.2)

- Modelling of vehicle dynamics and aerodynamics
  Including rotational motion.
  (Sections II.B.2.2 and II.D)

- Ease of upgrade.
  The ability to incorporate additional physical effects with minimal additional programming complexity is desirable.
  (Section II.B.2 and below)

Ease of upgrade is perhaps the most important in terms of the design and development of *genL*, or indeed any simulation. In defining the approach taken in writing *genL*, this concern also ensures ease of use.

As will be discussed later, the clearest presentation of a problem is often provided by data in a form other than that which it is easiest to work with. For example, the position of a satellite may be most clearly visualised in spherical polar co-ordinates as it is visually referenced to the spherical planet it orbits. However, as will be shown, the most convenient reference in which to propagate the motion is Cartesian. Hence a transformation of co-ordinates is required to obtain the data in

the desired format. The Cartesian vector formulation employed to facilitate the upgrading of the simulation is also the most convenient for conversion between reference sets.

The other concerns and their incorporation into the generic spacecraft simulation *genL* are discussed in the sections shown.

II.B. The Orbit in Space

II.B.1. Introduction : Working Frame and Origin Switching

When we consider the motion of a body around a planet a convenient reference point for the motion would appear to be the centre of the planet, as this is the focus of the orbit.

If we then consider the motion of a vehicle in, for example, a trans-lunar trajectory it becomes less clear where we should locate the origin of the system. The barycentre of the system would seem to be a suitable choice but there are also arguments for the use of the Earth, Moon or switching between the two.

The description of motion about the barycentre becomes a solution to the three body problem[44], and the inclusion of aerodynamic effects (and hence the need to evaluate relative velocities) to this model would complicate things further still.

The possibilities for errors are huge and the ease with which they might be tracked down greatly reduced by the complexity of the system and the expressions.

Other effects we might wish to include range from the gravitational effect of the Sun and other planets, to an oblate Earth model, or Solar Radiation Pressure (SRP).

The increasing complexity of the system suggests the use of vectors is essential in maintaining a clearly constructed problem. This then defines the type of reference frame, but leaves the issue of which frame is most suitable unanswered.

In *genL* the factors influencing the vehicle's motion are evaluated in the Cartesian reference frames most appropriate to them. The forces of lift and drag are most conveniently evaluated in body axes, the gravitational force due to the Sun in heliocentric axes and so on. In this way the forces (and moments) acting on the vehicle are calculated with minimal error. What remains now is to transform these forces into a single frame in which the motion of the vehicle may be propagated using Newton II.

As stated above certain reference origins appear to lend themselves to certain problems. In *genL* the choice of frame is decided by a simple algorithm that determines which of the celestial bodies is currently exerting the greatest gravitational effect on the vehicle. This defines the current working frame or the 'planet acting as origin' (PAO).

Switching between frames ('origin switching') then occurs when the vehicle passes from one sphere of influence to another. The gravitational effects of the other bodies are evaluated in their own reference frames, e.g. the effect of the Earth is evaluated in a geocentric frame, the moon in a selenocentric frame, and so on. This follows the most appropriate frame concept described above and transformation to the PAO (working) frame ensures that numerical errors are minimised for the most significant gravitational contribution. Position and velocity vector integration errors are also minimised as in the majority of cases the PAO will be the geometrically closest body.

The working frame is then the frame of reference in which propagation of the motion of the vehicle is actually carried out. It can be seen, however, that the PAO may change during a simulation and so propagation is actually carried out in an undefined reference set into which is fed the current working data. In effect the integration routine blindly integrates the state vectors it is given with the appropriate conversions being made at the point of origin switching.

Fig. II.B.1-1 is a flowchart representation of the working frame/origin switching scheme.

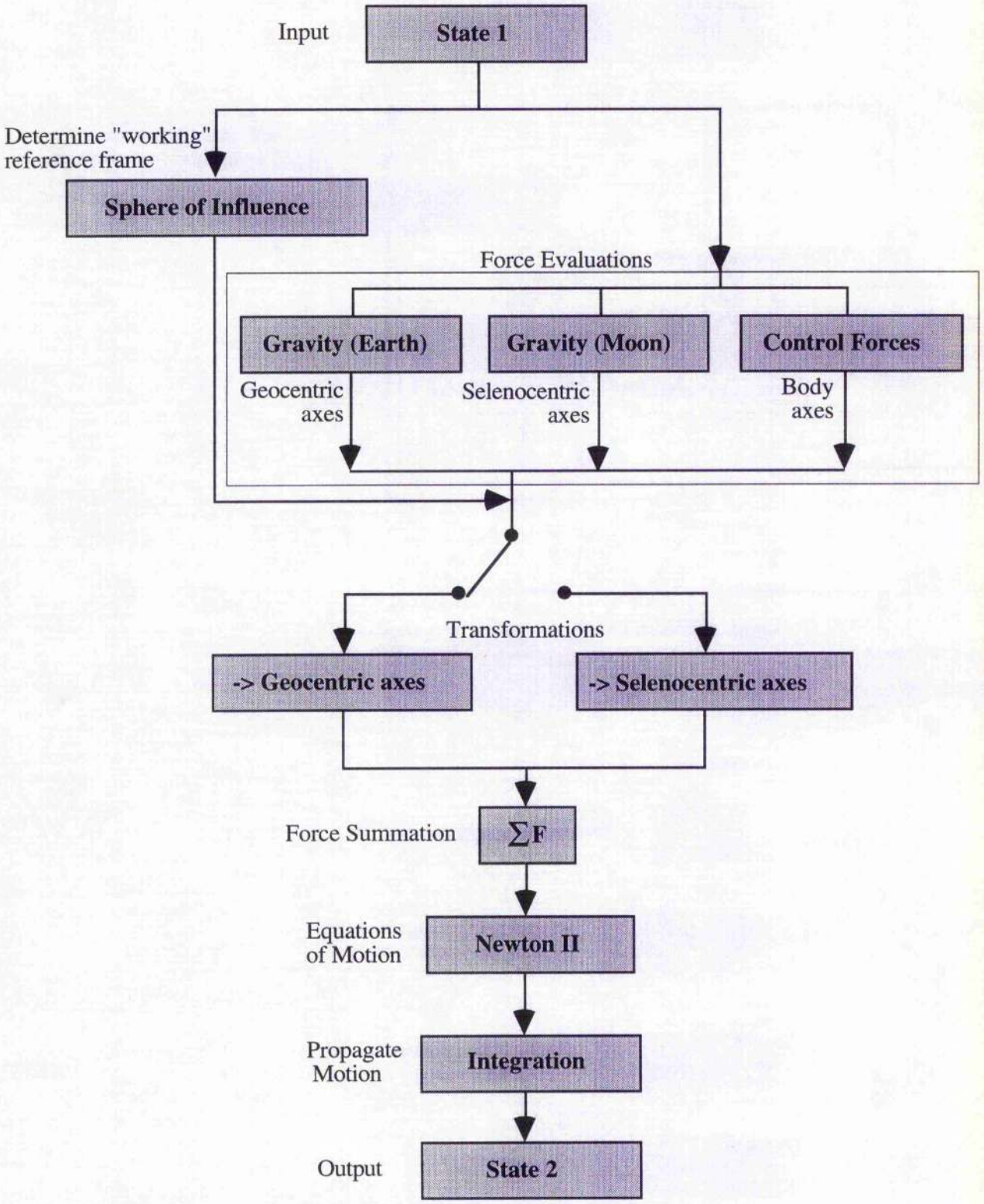

Fig. II.B.1-1 Simplified flowchart showing the operation of the "working" frame co-ordinate approach. **State 2** will be given in the current working frame as determined by the sphere of influence calculations. Changes of working frame require transformation of input variables from the original working frame to the new.

As is shown, once the influencing forces have been evaluated they are transformed into the working frame where vector summation produces the global force vector used in the equations of motion.

In this way a previously unmodelled effect, such as SRP, can be introduced into the simulation with no change in the existing code other than the introduction of a new term to the force summation. This approach also allows effects to be "turned on" or "turned off" as required without affecting the remainder of the simulation by simply removing them from the appropriate summation.

II.B.2. Co-ordinate Systems

There are a number of approaches to defining the position of a body, natural or artificial, in space. Those currently in use are there because of their suitability to astrodynamics. The choice of system depends on the position of the observer, or desired reference location. This might be a point on the surface of a planet, the centre of the planet or of the sun, or of the barycentre (centre of mass) of a planet-moon system.

A suitable system could be devised for each of the cases mentioned but whilst the majority of the information required may be best presented in the reference system used it may be more conveniently updated in another reference and it is often more useful to express some quantities in another system.

For example, for a vehicle travelling between the Earth and Moon it might seem appropriate to express its position in terms of a barycentric co-ordinate system for the majority of the journey, but it is clearly more useful to know the position relative to a given body when the vehicle is close to it. Even if a geocentric reference system were used we would want to know the position of the vehicle relative to the moon once it was in the lunar sphere of influence.

The conversion of data from one reference system to another can be a complicated and laborious process and this concern assists in choosing a co-ordinate system in which to work.

The other major consideration in choosing an appropriate co-ordinate system is how best to propagate the motion of the vehicle. This will depend largely on the type of motion to be studied.

As stated above, the *genL* simulation was intended to be suitable for use in all types of mission analyses. It was necessary, therefore, to use a co-ordinate system which would facilitate simple changes of reference, both for computational and conceptual simplicity.

We will now consider some of the references which could be used and explain their place within the simulation where appropriate.

II.B.2.1 The Ecliptic System and the Orbital Elements

Observation of the Sun from Earth reveals that it appears to progress eastwards against the celestial background at the rate of around 1°/day. It takes a year for the Sun to trace out this path, *the ecliptic,* and return to its starting point. The path of the ecliptic lies in the plane of the Earth's motion around the Sun which is hence named the ecliptic plane.

The ecliptic plane is the basis of the reference system of orbital elements used to describe the orbits of all the Sun-orbiting bodies in the solar system as the majority of these bodies follow orbits which lie at small inclinations to the ecliptic, with the notable exception of Pluto. A similar system of elements is used for planetary satellites, with the equatorial plane standing in for the ecliptic.

The ecliptic system of co-ordinates itself comprises the two quantities ecliptic latitude, β, and ecliptic longitude, λ (fig. II.B.2.1-1).

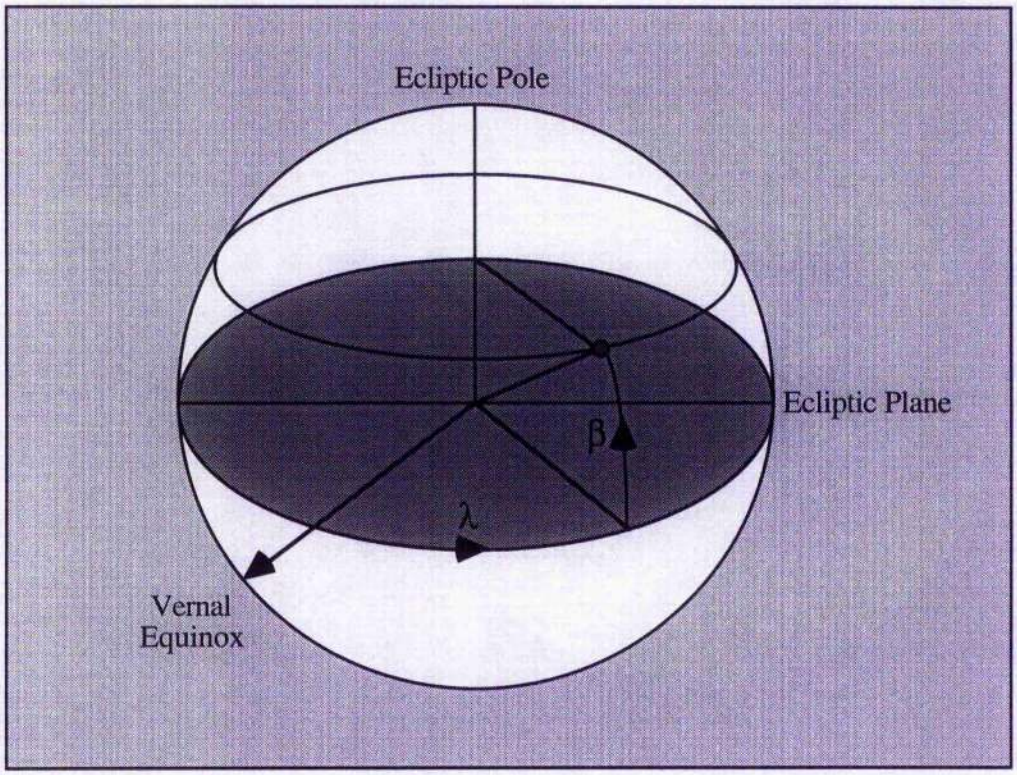

Figure II.B.2.1-1 Schematic of ecliptic system of co-ordinates

Ecliptic longitude is measured eastwards of the First Point of Aries, or vernal equinox, a fixed point in the celestial sky. Ecliptic latitude is measured north or south of the plane of the ecliptic.

This system of co-ordinates is simple to use and visualise but defines only the position of a body in space. To define the orbit and the position of a body it is customary to use the *elements* of the orbit.

Figure II.B.2.1-2 shows a schematic orbit showing the orientation of an orbit and the angular elements used to define a position within that orbit relative to the vernal equinox in the ecliptic plane.

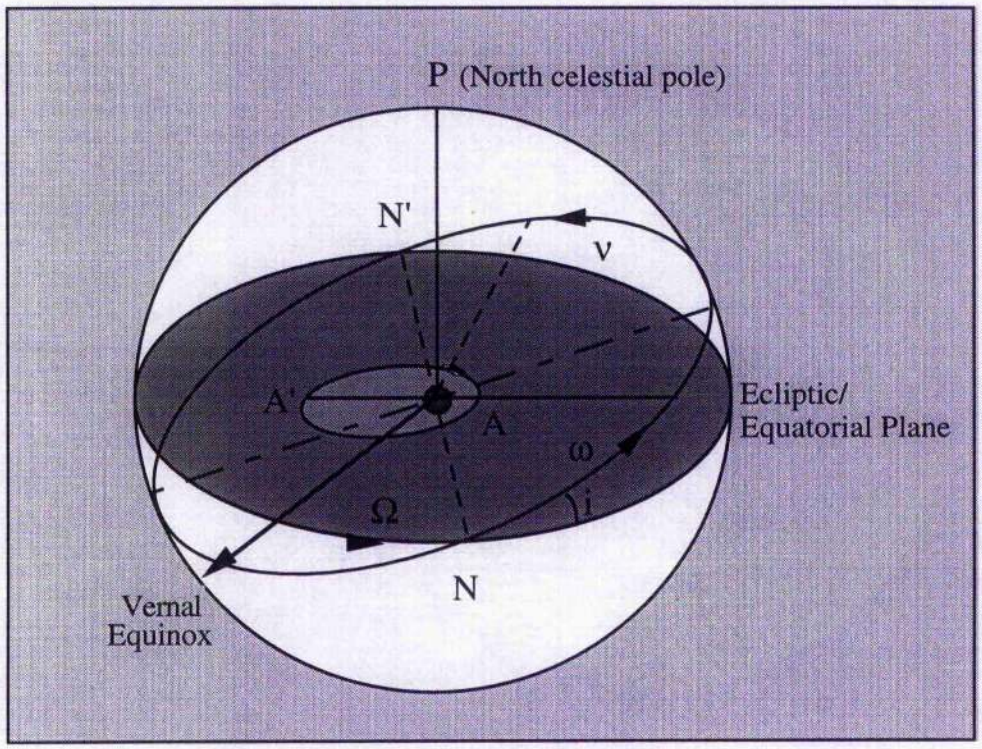

Fig. II.B.2.1-2 Angular orbital elements

Referring to fig. II.B.2.1-2 the first three elements are:

- Ω, the longitude of the ascending node.
  The nodes (ascending, N, and descending, N') are the points at which the orbital path crosses the ecliptic plane. Ω is measured eastwards along the ecliptic plane from the First Point of Aries.

- i, the inclination.
  The inclination of the orbit is the angle between the orbit plane and the plane of the ecliptic.
  Together Ω and i orientate the orbital plane in space.

- ϖ, the longitude of periapsis
  This defines the orientation of the orbit within the orbital plane. ϖ is measured along the ecliptic from the First Point of Aries to the ascending node and then along the orbit plane to perihelion, such that $\varpi = \Omega + \omega$.

These elements define the orientation of the orbit in space it remains now to define the nature of the orbit.

The motion of one body about another, under only the force of their mutual gravitational attraction will be a conic section. The standard orbital elements assume an elliptical orbit and the next two elements describe that ellipse: with reference to fig. II.B.2.1-3 they are,

- a, the semi-major axis.
- e, the eccentricity.

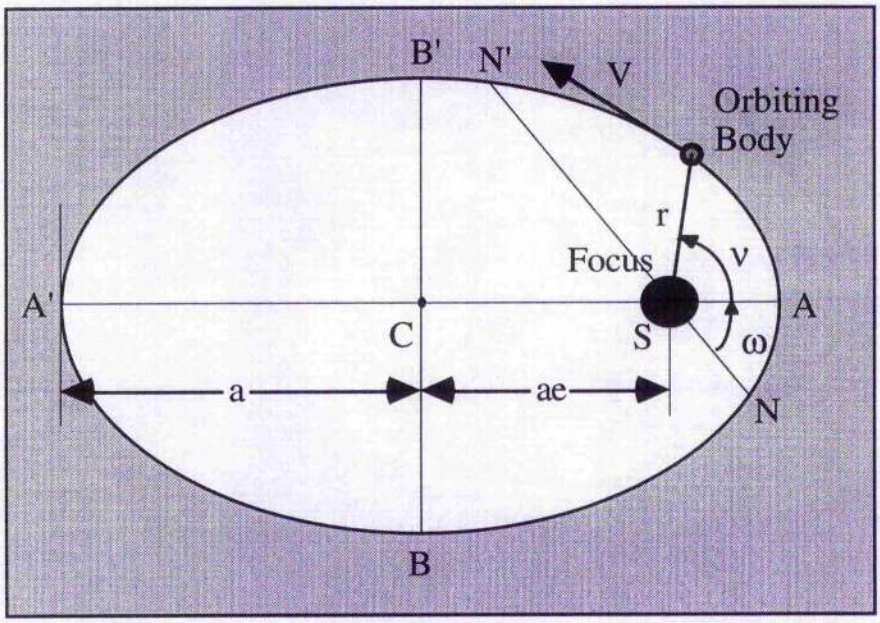

Fig. II.B.2.1-3 The elliptic orbit plane

The final element defines the time when the body was last at periapsis (A).

- τ, the time of periapsis passage

Together with the current time this defines the present position of the body within its orbit.

These are the standard orbital elements which in addition to defining the position of the body in space, are also used to define the body's orbital plane, its orientation, and the position of the body within that plane.

The orbital information presented in this format is highly descriptive and easily interpreted. As such it is desirable to have at least some of this information available even when the orbit is not elliptical. Propagation of vehicle motion could be carried out through propagation of these elements then. However, this would require a separate expression for each element and perturbations due to atmospheric passage require additions to these expressions.

In addition, the orbital elements are best used for perturbation problems, long-term orbit decay for example, where variations are slow. This makes them unsuitable for transatmospheric motion although again the inclination of the orbit in particular is still a useful quantity to know.

King-Hele[43] derives a number of relations for changes in the orbital elements for small orbital eccentricities, atmospheric drag, atmospheric drag in an oblate atmosphere, meridional winds, oblate Earth gravity models, and so on. These demonstrate the increasing complexity of the mathematics, conflicting with the design goal of a low-complexity easily upgraded model.

As a basis for a numerical simulation therefore, it is much more complicated to implement than would be desired.

It would seem to be more convenient to model the vehicle motion in one simple set of co-ordinates and derive the orbital elements quantities from them.

Cornelisse[45] provides relations for obtaining the orbital elements from both rectangular (Cartesian) co-ordinates and spherical co-ordinates, though the vector formulation used by Weisel[46] is by far the clearest and simplest to implement.

The argument for using Cartesian co-ordinates is presented in section II.B.2.2 following.

II.B.2.2 Vector Formulation in Cartesian co-ordinates.

Vector analysis fits neatly to the modular philosophy used in developing *genL* by allowing us to consider the motion of the vehicle as the sum of the three component directions. This partially solves the problem of increasing complexity as the inclusion of a new piece of physics, such as solar radiation pressure, therefore requires simply the evaluation of its effect and inclusion of each component (transformed into the working frame of reference) in the appropriate vector sum. Effects such as different atmospheric models are incorporated directly into the simulation without the need to replace the propagating equations.

The motion of the body then comprises six parts; three rotational and three translational. Each degree of freedom (fig II.B.2.2-1) is treated separately so that the motion of a body along, for example, the x-axis is determined solely by the forces, or force components, along that line of action, and similarly the rotational motion about the x-axis is determined solely by the torques, or moments, acting about it. This last consideration is important in that the rotational rates, p,q,r, are not considered in the orbital elements or in the standard astrodynamic equations of motion given above.

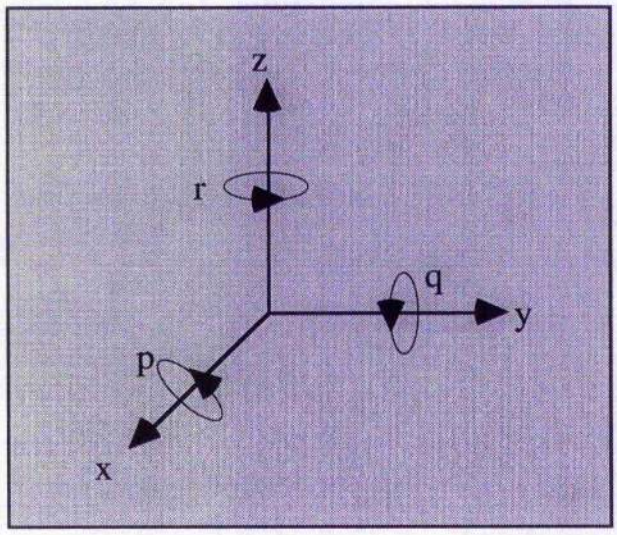

fig. II.B.2.2-1 : Cartesian reference frame showing p,q,r rotational directions.

Using this formulation we reduce the translational motion of the vehicle to relations of the form

$$\sum F_i = m\frac{d^2 r_i}{dt^2} \qquad \textbf{II.B.2.2-1}$$

where $i = x, y, z$ refer to the co-ordinate displacements along the reference axes.

As stated before each force is evaluated in the reference frame most appropriate to it. The summation however, is always carried out in the current working frame.

The beauty of this formulation now becomes clear. In order to introduce a new effect to the simulation, for example, onboard propulsive systems, we have only to obtain the components of the applied force in each of the axial directions (in this case body axes), transform these to the working frame and add to the summation term $\sum F_i$. The basic formulation remains unchanged.

For example,

$$\sum F_i = F_{i_{gravity}} + F_{i_{thrust}} \qquad i = x, y, z \qquad \textbf{II.B.2.2-2}$$

would cover the basic forces acting on the vehicle.

Fig. II.B.2.2-2 illustrates the incorporation of a new effect (in this case solar radiation pressure).

A new routine to evaluate the magnitude and direction of its effect is incorporated. The resulting vector transformed to the working frame and the components added to the force summation.

This approach facilitates the aforementioned modularity in the simulation, with the introduction and removal of various influences simply a case of introducing or removing the appropriate term from the summation.

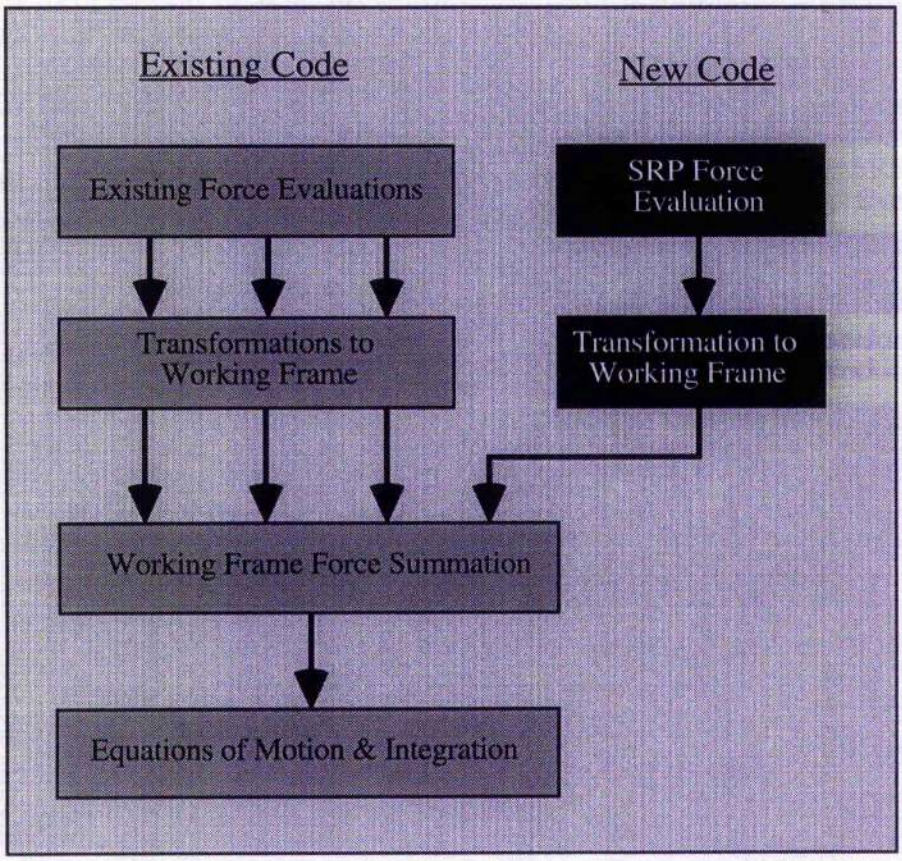

Fig. II.B.2.2-2 Schematic describing incorporation of a new force effect into *genL*. (See also Fig. II.B.1-1)

The rotational motion of the vehicle is described by the standard moment equations

$$\dot{p} = \frac{(I_{yy} - I_{zz})qr + I_{xz}(\dot{r} + pq) + M_x}{I_{xx}} \qquad \textbf{II.B.2.2-3a}$$

$$\dot{q} = \frac{(I_{zz} - I_{xx})rp + I_{xz}(r^2 + p^2) + M_y}{I_{yy}} \qquad \textbf{II.B.2.2-3b}$$

$$\dot{r} = \frac{(I_{xx} - I_{yy})pq + I_{xz}(\dot{p} + qr) + M_z}{I_{zz}} \qquad \textbf{II.B.2.2-3c}$$

which determine the body axes angular accelerations, $\dot{p},\dot{q},\dot{r}$ from the angular rates, p,q,r, the moments, M_x,M_y,M_z, and the vehicle inertia matrix.

The variables $\dot{p},\dot{q},\dot{r}$, and p,q,r refer to the x,y,z axes respectively.

Angular rates about the working frame axis set could be used, but it is more convenient to use the body axis set. This set provides a consistent reference set throughout the motion which will suffer minimal numerical errors in propagation.

The description of the vehicle's position and orientation with respect to some Cartesian reference frame is given by six variables; x,y,z, describing the displacement from the origin, and ϕ,θ,ψ, describing the angular transformation from the reference orientation (working frame) to that of the vehicle (body axes).

The angles ϕ,θ,ψ are termed roll (bank), pitch and yaw (azimuth), respectively, and the symbol σ may be used in place of ϕ to denote the bank angle. It remains to relate the orientation (Euler) angles, ϕ,θ,ψ, to the rotational rates p,q,r about the vehicle axes. This is done through the kinematic relations, viz.,

$$p = -\dot{\psi}\sin\theta + \dot{\phi} \qquad \textbf{II.B.2.2-4a}$$

$$q = \dot{\psi}\cos\theta\sin\phi + \dot{\theta}\cos\phi \qquad \textbf{II.B.2.2-4b}$$

$$r = \dot{\psi}\cos\theta\cos\phi - \dot{\theta}\sin\phi \qquad \textbf{II.B.2.2-4c}$$

often used in the inverse form

$$\dot{\psi} = (q\sin\phi + r\cos\phi)\sec\theta \qquad \textbf{II.B.2.2-5a}$$

$$\dot{\theta} = q\cos\phi - r\sin\phi \qquad \textbf{II.B.2.2-5b}$$

$$\dot{\phi} = p + \tan\theta(q\sin\phi + r\cos\phi) \qquad \textbf{II.B.2.2-5c}$$

We now have a complete set of relations which describe the propagation of angular and translational motion for the vehicle.

II.B.2.3 Reference Origins and Co-ordinate Transformations

Having established how we are to represent the spatial displacement and orientation of the vehicle it remains to establish with respect to what we are evaluating these variables.

It would be simple enough to define the Sun as the centre of the system and orientate a right-handed axis set, the xy plane lying within the plane of the ecliptic such that the x-axis, for example, is directed towards the First Point of Aries, and the z-axis "North" from the ecliptic. This system would be simple to implement and could be used for the analysis of any mission within the solar system without need for modification.

Now consider a lunar return mission and the type of data that would be required. We would certainly want to know the altitude of the vehicle above the surface of the Earth during re-entry and probably for the entire mission. Similarly, there would be a requirement for data with respect to the Moon.

If our working reference frame is heliocentric, in order to obtain Earth or Moon-relative positional (or other) data we would have to transform the information from heliocentric to geocentric or selenocentric co-ordinates.

It can be appreciated that the difference in the position vectors of a near-Earth vehicle and the Earth itself will be small if both are measured relative to the Sun. Numerically it might even be considered insignificant, and numerical accuracy would certainly be lost if evaluation of the vehicle's orbit about the Earth were to be calculated in a heliocentric frame. Conversely, the displacement from the vehicle to the geocentre will certainly not be insignificant if measured with respect to the geocentre.

In terms of numerical accuracy then, it would make sense to work with a reference originating at the centre of the nearest celestial body. However, there is another

consideration. The celestial body which is geometrically closest to the vehicle may not have the greatest gravitational effect on the vehicle. In order to minimise the loss of accuracy in the largest gravitational attraction during co-ordinate transformation it might seem more appropriate to use that body as the current reference origin.

Given that in the majority of cases the body exerting the largest gravitational effect on the vehicle will be the geometrically closest the gravitational concern is allowed to override the geometrical and a reference set with origin located at the centre of the celestial body exerting the largest gravitational attraction on the vehicle is used.

In this way the body which has the greatest effect on the motion of the vehicle in reality also exerts the greatest effect in the simulation.

In order to achieve this a gravitational sphere of influence calculation is used to determine the planet (or moon) to act as the origin of the reference frame. The sphere of influence of a celestial body is an abstract region of space within which the gravitational influence of the body can be said to predominate over the influences of any other bodies. After Cornelisse[45], the sphere of influence of a planet or moon is found as

$$R_{soi} = r_{bp}\left(\frac{m_b}{m_p}\right)^{2/5} \qquad \text{II.B.2.3-1}$$

where R_{soi} is the radius of the sphere of influence, r_{bp} denotes the radial displacement from the body to its parent (for a planet this would be the Sun, for a moon its parent planet), and m_b and m_p the masses of the body and its parent respectively.

This then forms the basis of the switching routine, employed within the simulation which checks for the current sphere of influence and, if a change has occurred from the previous time step, carries out the appropriate co-ordinate transformations. The actual integration variables are

declared with respect to an undefined reference and a "translation" routine supplies the values appropriate to the current reference frame.

II.C. Planet models

II.C.1. Gravitational

II.C.1.1 Introduction

The corner stone of astrodynamics is undoubtedly Newton's Law of Universal Gravitation. Put simply, it states that "every particle of matter in the universe attracts every other particle of matter with a force directly proportional to the product of the masses and inversely proportional to the square of the distances between them"[44].

Mathematically this becomes,

$$F = \frac{GMm}{r^2} \qquad \text{II.C.1.1-1}$$

where F is the force of gravitational attraction, M and m are the two masses, r is the separation distance of the two mass centres, and G is an empirical constant of proportionality.

Whilst this law is universally applicable, it is often used in conjunction with the assumption that any distributed mass system may be considered equivalent to a point mass.

If the Earth were spherical and homogenous in composition, this would be a valid assumption since the resulting gravitational field would indeed be uniform.

Unfortunately this is not the case, and the shape of the Earth is closer to an oblate spheroid with the equatorial diameter of our world some $43km$ greater than that between the poles.

Since the Earth is not an exact sphere it follows that the normal to the surface will not, in general, follow the radius vector to the geocentre. This "deflection of the vertical" is small, of the order of $10^{-1} mrad$, but may be significant in evaluating the motion of an orbiting vehicle as it is along the normal to the surface that the gravity gradient is a maximum. Consequently the assumption that the gravitational attraction of the Earth acts towards the geocentre will not prove valid for all analyses.

A close approximation to the geopotential surface of the Earth, the geoid, is an ellipsoid of revolution. The shape of the geoid is that of the mean sea-level surface of the Earth. As an equipotential surface, the geoid will possess an irregular shape, reflecting the irregularities in the composition of the Earth's various layers.

A gravitational model which takes account of these irregularities would be useful in the analysis of long-term orbital motion or in considering accurate transatmospheric motion above particular areas of the Earth.

II.C.1.2 Application to the Simulated Environment

The force of gravitational attraction is, by Newton's third law, independent of which body we look at. The accelerating effect of that force is, however, dependent on the body.

From application of Newton's second law the accelerations on each mass are found to be directly proportional to the mass of the other, i.e., from eqn. II.C.1.1-1

$$a_M = \frac{Gm}{r^2} \qquad \text{II.C.1.2-1a}$$

and

$$a_m = \frac{GM}{r^2} \qquad \text{II.C.1.2-1b}$$

For a typical Earth orbiting satellite the ratio $\frac{Gm}{r^2}$, the accelerating effect of the satellite on the Earth, is of order $10^{-21} kg/m^2$, which is generally considered insignificant, particularly in comparison to the effect of the Moon which is of order $10^{-5} kg/m^2$. In contrast the acceleration on the satellite due to the Earth is of order unity.

The effects of the other bodies in the solar system deserve similar consideration. A deep-space vehicle performing a swing-by at Jupiter or Saturn, for example, may be affected by the gravitational attraction of their moons, or for long duration Earth orbits the effect of the solar and lunar gravitational fields may warrant consideration, depending on the orbital altitude.

GenL includes the option of incorporating the effects of all nine major planets, the Sun, the terrestrial Moon, the Galilean Moons of Jupiter and Titan, Saturn's largest moon, allowing simulation at any point within the solar system.

II.C.1.3 Gravitational model

As the area of prime interest in the work presented here is the motion of a vehicle close to and within the terrestrial atmosphere, the Earth's gravitational field is modelled as a sixth order oblate spheroid. The gravitational fields for the Sun and Moon are modelled using the simple inverse square law because their fields are not as well known and the effects of any asymmetry they possess will be muted by their distance from the area of primary concern. Even further away, in a gravitational sense, the remaining planets in the solar system are available in the full simulation as are the Galilean moons and Titan.

The increased computational load resulting from the inclusion of a further thirteen bodies into the simulation is significant, with their exclusion halving the run time of the simulation. Consequently the transatmospheric work presented later concerns at most the four body Vehicle-Earth-Sun-Moon system.

The sixth-order gravity model is the Goddard Earth Model L2 (GEM-L2) which is based on satellite observational data[43]. The form of this data ranges from photographic to Doppler and radar, and some models derived from these analyses are reliable up to order 36. This 36*th* order model, however, requires 1296 coefficients and would obviously require a larger amount of computing power, especially given the requirement for updating the gravitational attractions every (sometimes very small) time step. It was decided therefore, that where a higher order gravity model were required a sixth order model would be sufficiently accurate whilst also retaining a reasonable program run-time.

As we know the Earth is not spherical, but if we assume for the moment that it is symmetrical about the polar axis then we may look at the zonal harmonics of the Earth's gravitational potential. These are terms in the expression for the Earth's geopotential which represent a modification to the shape of the Earth from the ideal sphere. The second harmonic, for example, represents the effect of the Earth's flattening at the poles, making its cross-section look more elliptical than circular, the third tends towards a triangular shape, the fourth a square, etc. Some of these harmonics are more evident in the shape of the Earth than others and consequently each is modified by a constant J_n, where n is the order of the harmonic. It is these constants that are evaluated from the satellite data.

The Earth is, however, not perfectly symmetrical about the polar axis either and so we require a second set of harmonics, the tesseral harmonics. Tesseral harmonics are dependent not only on latitude but also on longitude. With these included in the expression for the Earth's geopotential, the resultant form is given below (eqn. II.C.1.3-1).

$$U=\frac{\mu}{r}\left[\begin{array}{l}1-\sum_{n=2}^{\infty}J_n\left(\frac{R}{r}\right)^n P_n(\sin\phi)+\\ \sum_{l=2}^{\infty}\sum_{m=1}^{l}\left(\frac{R}{r}\right)^l P_l^m(\sin\phi)\left\{\overline{C}_{lm}\cos m\lambda+\overline{S}_{lm}\sin m\lambda\right\}N_{lm}\end{array}\right] \quad \text{II.C.1.3-1}$$

where the J_n terms represent the zonal harmonics, and the $\overline{C}_{lm}$ and $\overline{S}_{lm}$ terms represent the tesseral harmonics.
$P_n(z)$ is a Legendre polynomial of form

$$P_n(z)=\left(\frac{1}{2^n n!}\right)\frac{d^n\left(z^2-1\right)^n}{dz^n} \quad \text{II.C.1.3-2}$$

and $P_l^m(z)$ a Legendre polynomial of form

$$P_l^m(z)=\frac{\left(1-z^2\right)^{m/2}}{2^l l!}\frac{d^{l+m}\left(z^2-1\right)^l}{dz^{l+m}} \quad \text{II.C.1.3-3}$$

It can be seen that $P_n(z)$ is simply $P_l^m(z)$ with $m=0$ and $n=l$.
Values for the constants are given in Appendix VI.

II.C.2. Atmosphere

II.C.2.1 Introduction

The passage of a body through an atmosphere produces thermal and pressure loadings on the body which can affect not only the path the body will follow but also its survival. Within the subsonic/supersonic realm of aeronautics the major effect is that of the distributed pressure loading, although thermal effects cannot be neglected for higher velocity vehicles (eg. Concorde). Control of the vehicle is achieved through the use of aerodynamic control surfaces which effect alterations in the local flow field, modifying the forces and moments acting on the vehicle.

The velocities associated with re-entry extend beyond supersonic into the hypersonic region and the vehicle now experiences both distributed thermal and pressure loads. Regan[47] cites the example of an interplanetary vehicle re-entering from a near-parabolic orbit which would have a specific kinetic energy of around $6\times10^{7} J/kg$, approximately the specific energy of vaporisation of carbon. When we consider that carbon possesses one of the highest heats of vaporisation the magnitude of the problem becomes clear, the vehicle may not survive re-entry. This rather dramatic statement assumes that all the kinetic energy of the vehicle is converted into thermal energy absorbed solely by the vehicle. As Regan goes on to point out the survival of natural atmospheric entry bodies such as meteorites shows us that this is not the case and some of the thermal energy is transferred to the surrounding air through atmospheric friction.

How much of this energy is absorbed by the vehicle is dependent on the shape of the body and its trajectory. These factors in turn may be influenced by the thermal and pressure loads experienced by the vehicle through, for example, asymmetric ablation altering the shape of the vehicle and hence producing a non-zero trim angle. A variation in trim angle carries a concomitant variation in the aerodynamic forces acting on the vehicle.

The way in which the thermal and pressure loadings, and the vehicle shape and trajectory interact is highly complex but their interplay becomes less significant when compared to the variation in atmospheric density encountered during re-entry.

The atmospheric density-altitude profile is perhaps the most significant external factor to be considered in transatmospheric vehicle motion. However, the uncertainty that surrounds the prediction of atmospheric conditions is actually of help in simplifying the atmospheric model. There would seem to be little point in modelling the effect of a

variation in atmospheric scale height for a vehicle which will only spend a short time traversing an uncertain atmosphere.

Similarly, the effect of day-to-night variation may be neglected when considering atmospheric entry vehicles. The "daytime bulge" exhibited by the atmosphere is only really significant at altitudes over $400km$ where the atmosphere is vulnerable to solar activity, and consequently somewhat unpredictable. Below about $250km$, still outwith the sensible atmosphere, the effect of the day-to-night variation is small, and can be considered negligible for high velocity motion.

In the design of a control system one of the most important considerations is the robustness of the control to atmospheric perturbations. Assessing this will require off-nominal atmospheric profiles and this also lessens the need for a more precise model. The design of an atmospheric model then becomes that of a simpler 'mean atmosphere' model onto which perturbations can be applied as required.

GenL contains four types of atmosphere models:

- Standard exponential (Section II.C.2.3.1)
- Oblate Earth exponential atmosphere (Section II.C.2.3.2)
- US-62 standard atmosphere (Section II.C.2.3.4)
- Biased sine waves (Section II.C.2.3.5)

with the last of these a perturbation model to be applied to a nominal density profile derived from one of the other three.

The oblate exponential atmosphere is intended more for satellite orbital analysis than hypervelocity transatmospheric vehicle motion and is a concession to the generic nature of *genL*.

In the sections that follow we describe the terrestrial atmosphere, some of the atmospheric models available and explain the simplifications that can be made to the atmospheric model when considering hypervelocity motion.

II.C.2.2 Structure of the Terrestrial Atmosphere

The shaping and structuring of the Earth's atmosphere is for the most part due to radiation, both from the Sun and the surface of the Earth. The seasons, time of day, phases of the moon and solar activity also go some way to shaping the air above us.

All these factors might lead to the assumption that a highly complex model of the atmosphere would be needed for accurate analysis of the motion of a vehicle through the atmosphere.

However, though a deviation from the anticipated atmospheric conditions can cause significant changes in the vehicle's trajectory, this uncertainty can be used as an argument for simplification of the atmospheric model. Is there any point in using a highly complex model when the disparity between it and a more simplistic model may well be less than the accuracy of the prediction?

Some model types and the arguments for and against their use are presented in the section II.C.2.3 below.

An examination of the basic structure of the terrestrial atmosphere is of some help in appreciating the problem of accurate prediction of atmospheric conditions.

Figure II.C.2.2-1 shows the classification of the atmosphere by temperature (described below).

- **Troposphere.**

Altitude range = ground to $8-18km$ dependent on latitude.

This is the thinnest region of the atmosphere although it is by far the most dense, containing around 80% of the total mass. The density decreases with altitude until it is around 30% of the sea-level value at the upper edge of the troposphere. The troposphere can be highly turbulent, much more so than any other region, and consequently difficult to predict. Atmospheric heating in this region is carried out primarily by infra-red radiation from the Sun and the surface of the Earth.

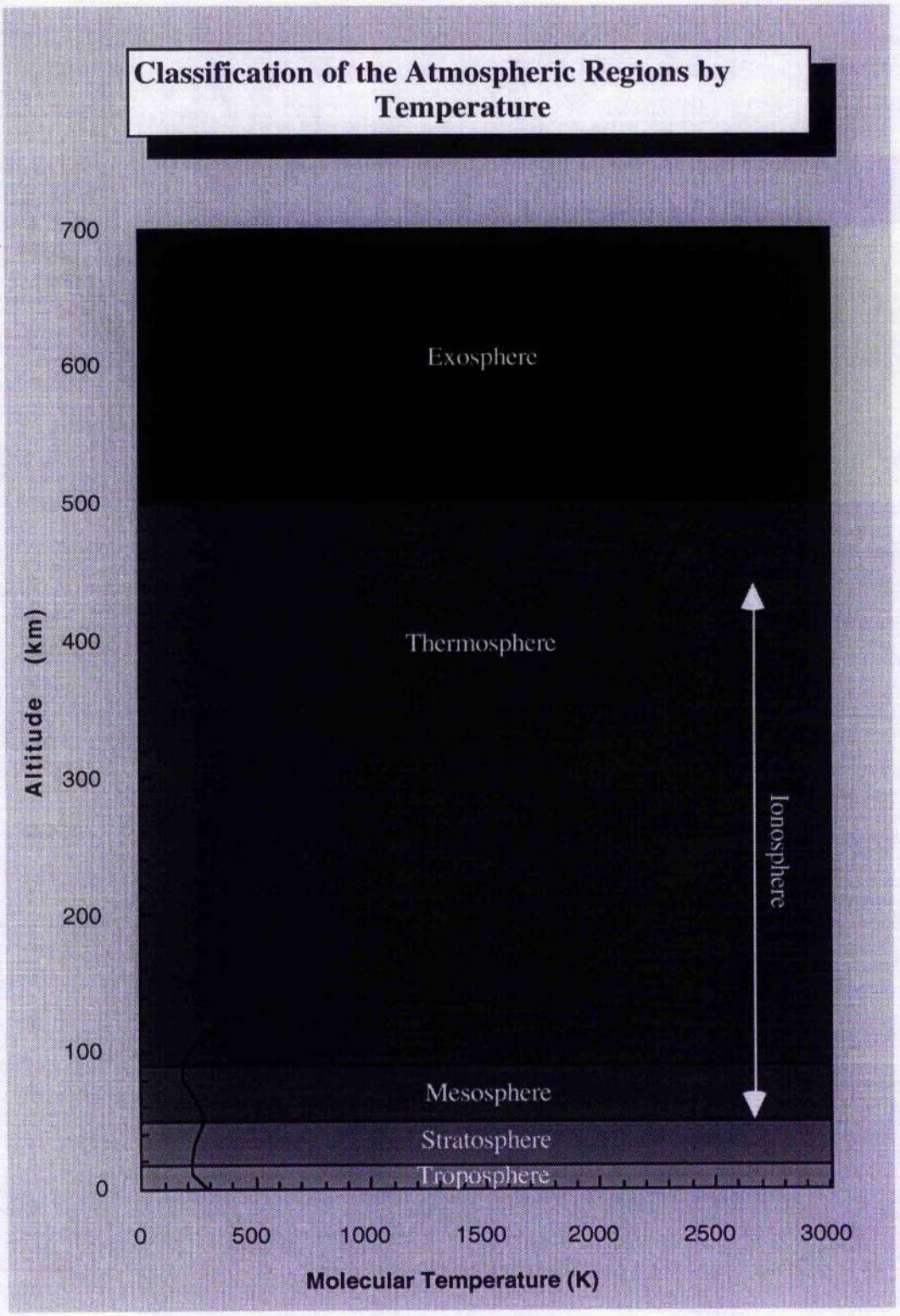

Fig. II.C.2.2-1 Classification of Atmospheric Regions by Temperature

- **Stratosphere.**

  Altitude range = $8-18km$ to $50km$

  The stratosphere extends from the top of the troposphere to around $50km$ altitude and contains the ozone layer. Decomposition of the ozone produced by absorption of ultraviolet radiation not absorbed by the upper atmosphere is largely responsible for heating of the stratosphere, and research suggests that this effect is seasonal.

  At the top of the stratosphere density is already approaching 0.08% of its sea-level value. For this reason some studies consider the stratosphere to be the limit of the sensible atmosphere[48].

- **Mesosphere.**

  Altitude Range = $50km$ to $90km$.

  The composition of the mesosphere is similar to that of the stratosphere but it lacks the heating produced by the presence of ozone.

- **Ionosphere.**

  Altitude Range = $50km$ to (several hundred) km

  The ionosphere overlaps both the mesosphere and the thermosphere (described below). Its name derives from the relatively large concentration of free radicals and electrons within the region. The majority of these ions are produced by atmospheric absorption of solar radiation. Because of the low density within the ionosphere the ions do not tend to recombine quickly and consequently the ionosphere exists even the regions of the atmosphere where it is currently night-time.

- **Thermosphere.**

  Altitude Range = $90km$ to $500km$

  The temperature within this region reaches the exospheric temperature T_∞ and the kinetic temperature remains constant from this altitude. Heating is due mainly to solar radiation, and solar activity has a large influence with periods of high solar activity causing additional heating in the upper part of the atmosphere increasing the density within this region.

The sensible atmosphere is generally considered to end in this region at around $200-300km$ altitude where the density has dropped to around $10^{-10} kg/m^3$. For high speed vehicles the atmosphere ceases to have a significant effect above this altitude.

- **Exosphere.**
  Altitude Range = $>500km$

  The exosphere extends from the top of the thermosphere out to the edges of what could be called the atmosphere. Some atoms escape from here to free space. At an altitude of around $1000km$ the density is less than $10^{-13} kg/m^3$ and aerodynamic forces can be safely neglected for most vehicles above this altitude. For rocket vehicles the atmosphere ceases to have a measurable effect at much lower altitudes.

For transatmospheric vehicle motion then the atmospheric density becomes numerically insignificant beyond about $300km$, and the temperature within this region (the thermosphere) stabilises to the value of the surrounding free-space. With these concerns in mind we now turn our attention to the construction of an atmospheric model suitable for transatmospheric vehicle analysis.

Various models of the terrestrial atmosphere exist and some of these are considered below. The arguments presented for and against are so done from the view point of an atmospheric entry vehicle but are equally applicable to other high-velocity transatmospheric motion.

II.C.2.3 Atmospheric Models

Prediction of atmospheric conditions is a complicated and uncertain matter, atmospheric dynamics being highly chaotic. One result of this is that a truly accurate computer testing of a vehicle or vehicle control system could only really be carried out during that period of time within which the mission planners could have confidence in their estimates of the

atmospheric conditions the vehicle would experience. By then it is of course too late, and the control must already be in place. So any control system must be developed with the required degree of robustness to accommodate expected perturbations. It is the mean atmosphere model to which these perturbations are applied which then becomes the analyst's concern.

The aim of a good atmospheric model must be to match this mean as closely as possible. Wind models can be put on top of this to allow for anticipated regional and seasonal variations, though the accuracy of these will again be uncertain. Thankfully, for a high-velocity atmospheric entry vehicle these winds are not of great concern. Tropospheric winds rarely exceed $0.05km/s$ so for entry speeds approaching $10km/s$ these winds will make a difference but not a greatly significant one. Because of the much reduced density at high altitudes, the effects of upper atmospheric winds may be safely ignored.

Above about $100km$ altitude the atmospheric density is so low that there is an argument for neglecting aerodynamic effects on the motion of an entry vehicle[47]. This is not done in *genL* but is worth bearing in mind when considering how precise an atmospheric model is required. For example, density values above $150km$ are subject to large variations due to fluctuations in solar radiation, but given the low value of the atmospheric density at these altitudes it would again seem more appropriate to model these fluctuations as perturbations to the mean.

The most commonly used mean atmosphere is the exponential density model which is a low order approximation but perfectly adequate for many purposes. Other models, such as the so-called standard atmospheres, are obtained from re-entry data and physical modelling. Even these can only be said to be truly accurate if the model density profile happens to coincide with that actually experienced during entry. They do, however, provide us with a look at

the general trends in the atmosphere and if large sets of such data were to be averaged then a more accurate mean model could be produced. The atmosphere is not stagnant though and never will be, leading to the possibility that an averaging process might produce a model which differs noticeably from the conditions experienced in the future and again the question of necessity arises.

Let us now look at the candidates for our atmospheric model.

II.C.2.3.1 Spherically symmetric exponential atmosphere.

The simplest of the commonly used atmospheric density models is the spherically symmetric exponential model wherein the density is given by

$$\rho = \rho_o \exp\left(-\frac{r - r_o}{H_o}\right) \qquad \text{II.C.2.3.1-1}$$

The subscript o usually denotes sea-level values although it may be used to denote perigee values depending on the type of motion being analysed. However, perigee values can only really be used for orbit decay analysis where the perigee change is relatively slow.

It is also assumed that H_o is constant over the range of interest.

II.C.2.3.2 Oblate exponential atmosphere.

One extension of this model is the inclusion of the effect of the oblateness of the Earth. According to King-Hele[42] the atmosphere comprises of surfaces of constant density with approximately the same shape as the Earth. Obviously a LEO satellite in a circular orbit will experience a variation in atmospheric drag as it travels along its orbit and this will affect the shape of the orbit.

Such motion will not remain truly circular for long. Once again though the effect is most noticeable for satellite orbits.

King-Hele[43] illustrates the development of an oblate exponential atmosphere, with the density at a height $(r-\sigma)$ given by

$$\rho = \rho_{po} \exp\left\{\frac{-(r-\sigma)}{H}\right\} \qquad \textbf{II.C.2.3.2-1}$$

with

$$\sigma = r_{po}\frac{1-\varepsilon\sin^2\phi}{1-\varepsilon\sin^2\phi_{po}} \qquad \textbf{II.C.2.3.2-2}$$

or

$$\sigma = \sigma_E\left\{1-\varepsilon\sin^2\phi+O(\varepsilon^2)\right\} \qquad \textbf{II.C.2.3.2-3}$$

where r is the orbit radius, σ the radius of the oblate spheroid at the current latitude, ϕ, and ρ the atmospheric density at the initial perigee. The subscript po usually refers to values at initial perigee, though it may be used to refer to sea-level values, while the subscript E refers to the value at the equator.

Using this model it is essential to remember to modify the altitude evaluation of the vehicle accordingly though the orbital radius evaluation will remain unaffected. The shape of the Earth model resulting from eqn. II.C.2.3.2-3 with a flattening $\varepsilon = 0.003352$ [44] has dimensions:

- Equatorial radius = 6378.14*km*
- Polar radius = 6356.74*km*

these match the "true Earth" values.

The radius of the oblate Earth at the sub-satellite point is automatically evaluated in *genL* whenever this atmosphere model is used.

II.C.2.3.3 Altitude varying scale height

One other extension to the model could be the inclusion of an altitude varying scale height. Once again such an approach is more appropriate for long-term orbit decay than atmospheric entry, particularly as the variation in scale height is most noticeable at altitudes above $150km$ where the atmospheric density is already less than $10^{-8} kg/m^3$. The model assumes a linear variation,

$$\lambda = \frac{dH}{dr} \qquad \text{II.C.2.3.3-1}$$

of scale height, H, with altitude such that

$$H = H_p + \lambda\left(r - r_p\right) \qquad \text{II.C.2.3.3-2}$$

and

$$\rho = \rho_p \exp\left(\frac{-\left(r - r_p\right)}{H}\right) \qquad \text{II.C.2.3.3-3}$$

Again the subscript p refers to perigee values.

The assumption that scale height varies linearly with altitude holds true over the probable range of interest for a satellite in a slowly decaying orbit. As this was not an area of prime concern this atmospheric model was not included in the simulation.

II.C.2.3.4 The U.S.-62 Standard Atmosphere

The atmosphere model ultimately chosen as the "real" mean atmosphere for *genL* is based on the 1962 U.S. standard atmosphere[49]. The US-62 standard atmosphere is a reference atmosphere derived from physical modelling and re-entry data.

The model used here takes the form of a fourteenth order Chebyshev polynomial approximation to the US-62

atmosphere. The series coefficients have been optimised for the region from ground zero to $200km$ altitude.

The series has the form

$$f(z)=\frac{a_o}{2}+\sum_{k=1}^{\infty}a_k C_k(z) \qquad \textbf{II.C.2.3.4-1}$$

where

$$z=\cos\phi \text{ and } -1\le z\le 1, \qquad \textbf{II.C.2.3.4-2}$$

$$a_k=\frac{2}{\pi}\int_0^{\pi} f(\cos\phi)\cos k\phi d\phi \qquad \textbf{II.C.2.3.4-3}$$

and

$$C_k=\cos\left(k\cos^{-1}z\right)=\cos k\phi \qquad \textbf{II.C.2.3.4-4}$$

Where $C_k(z)$ is a polynomial in z of order k, called a Chebyshev polynomial. Chebyshev polynomials are the solutions to the differential equation

$$\left(1-z^2\right)\ddot{x}-z\dot{x}+k^2x=0 \qquad \textbf{II.C.2.3.4-5}$$

The solutions have the form

$$C_k(z)=2zC_{k-1}(z)-C_{k-2}(z) \qquad \textbf{II.C.2.3.4-6}$$

with

$$C_o(z)=1 \qquad \textbf{II.C.2.3.4-7a}$$

and

$$C_1(z)=z \qquad \textbf{II.C.2.3.4-7b}$$

The approximation to the U.S. standard atmosphere is then given by setting

$$z=\frac{2h}{h_{\max}}-1 \qquad \textbf{II.C.2.3.4-8}$$

where h is the altitude above sea-level and $h_{\max}$ the upper limit of the model's validity, in this case $200km$, or

roughly the upper edge of the "sensible" atmosphere. This guarantees $-1 \le z \le 1$.
We also set

$$f(z) = \ln \frac{\rho(h)}{\rho_o} \qquad \textbf{II.C.2.3.4-9}$$

where ρ_o is sea-level air density.

Equation II.C.2.3.4-1 is now

$$\ln \frac{\rho(h)}{\rho_o} \approx \frac{a_o}{2} + \sum_{k=1}^{n} a_k C_k(z) \qquad \textbf{II.C.2.3.4-10}$$

and hence

$$\rho(h) \approx \rho_o \exp\left(\frac{a_o}{2} + \sum_{k=1}^{n} a_k C_k(z)\right) \qquad \textbf{II.C.2.3.4-11}$$

The coefficients a_k for a fourteenth order series with $h_{max} = 200km$ are given in table II.C.2.3.4-1 below.

k	a_k
0	-0.25415229E+02
1	-0.11684380E+02
2	+0.18721406E+01
3	+0.81660876E+00
4	-0.93811118E-01
5	-0.30155735E-00
6	-0.77593291E-01
7	+0.21640168E-00
8	-0.34918422E-01
9	-0.70126799E-01
10	+0.36014616E-01
11	+0.14951351E-01
12	-0.21450283E-01
13	-0.12497995E-02
14	+0.18421866E-01

Table II.C.2.3.4-1 Coefficients for US-62 Atmosphere Model

Figure II.C.2.3.4-1 shows how this model compares to the standard exponential atmospheric density model.

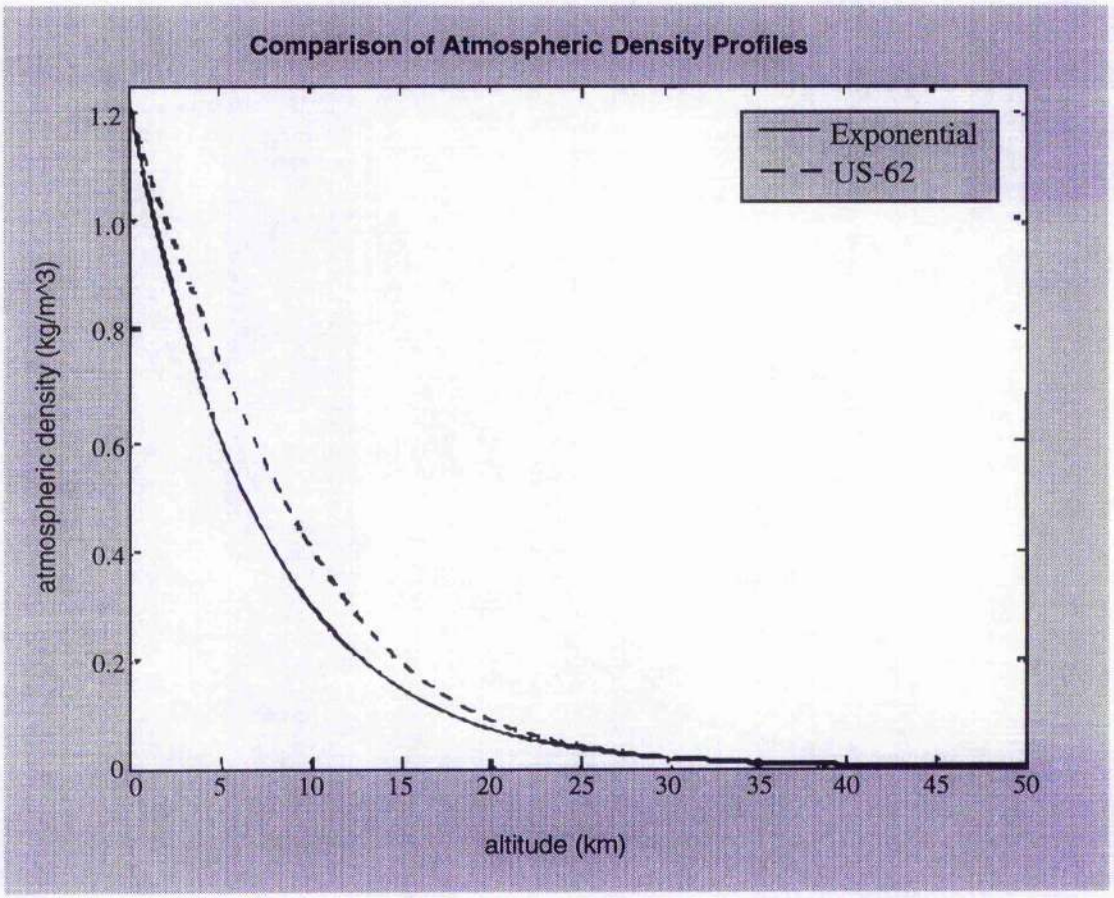

Fig. II.C.2.3.4-1 Comparison of Exponential and US-62 Standard Atmosphere Models

II.C.2.3.5 Modelling Off-Nominal Atmospheric Conditions

As has been stated, of primary concern for transatmospheric flight is the robustness of the control to off-nominal atmospheric conditions and navigational errors. To account for this then, the control needs to be tested over a range of likely atmospheric conditions and navigational errors (Chapter V).

To represent off-nominal atmospheric conditions we use a biased sine wave variation of the standard exponential atmosphere model similar to that used by Braun & Powell[50] and Thorp & Pierson[17].

$$\rho = \rho_{\exp}\left(1 + \delta + a\sin\frac{2\pi h}{h_{ref}}\right) \qquad \text{II.C.2.3.5-1}$$

where

$$\rho_{\exp} = \rho_o \exp\left(\frac{-h}{H}\right) \qquad \text{II.C.2.3.5-2}$$

as per eqn. II.C.2.3.1-1, though any atmospheric density model could be used (e.g. US-62 standard atmosphere)

The parameter δ is the bias and introduces a percentage offset from nominal density, a is the amplitude of the sinusoidal variations superimposed on the biased density profile, and h_{ref} the frequency of those variations.

Varied choice of these parameters will generate different atmosphere models, which, as the name implies, are sinusoidal oscillations about the nominal exponential atmosphere biased towards either high or low pressure conditions. Figure II.C.2.3.5.-1 shows the density values (within the likely perigee range for a lunar return aerobraking mission) for the nominal (exponential atmosphere) and four biased sine wave models. It can be seen that the models are biased towards either over- or under-dense compared to the nominal atmosphere but are not exclusively so. It is felt that this will result in greater fidelity with probable atmospheric variations.

II.C.2.3.6 Other Atmosphere Models

Other atmospheric models exist. Some, like the MSIS-83 model[51] are empirical in origin and provide accurate representations of variations in not only density but also temperature and composition. An analytic version of the Jacchia 1977 Static Density Model[52] exists which again gives detailed breakdown of the temperature and mass profiles within the various regions of the

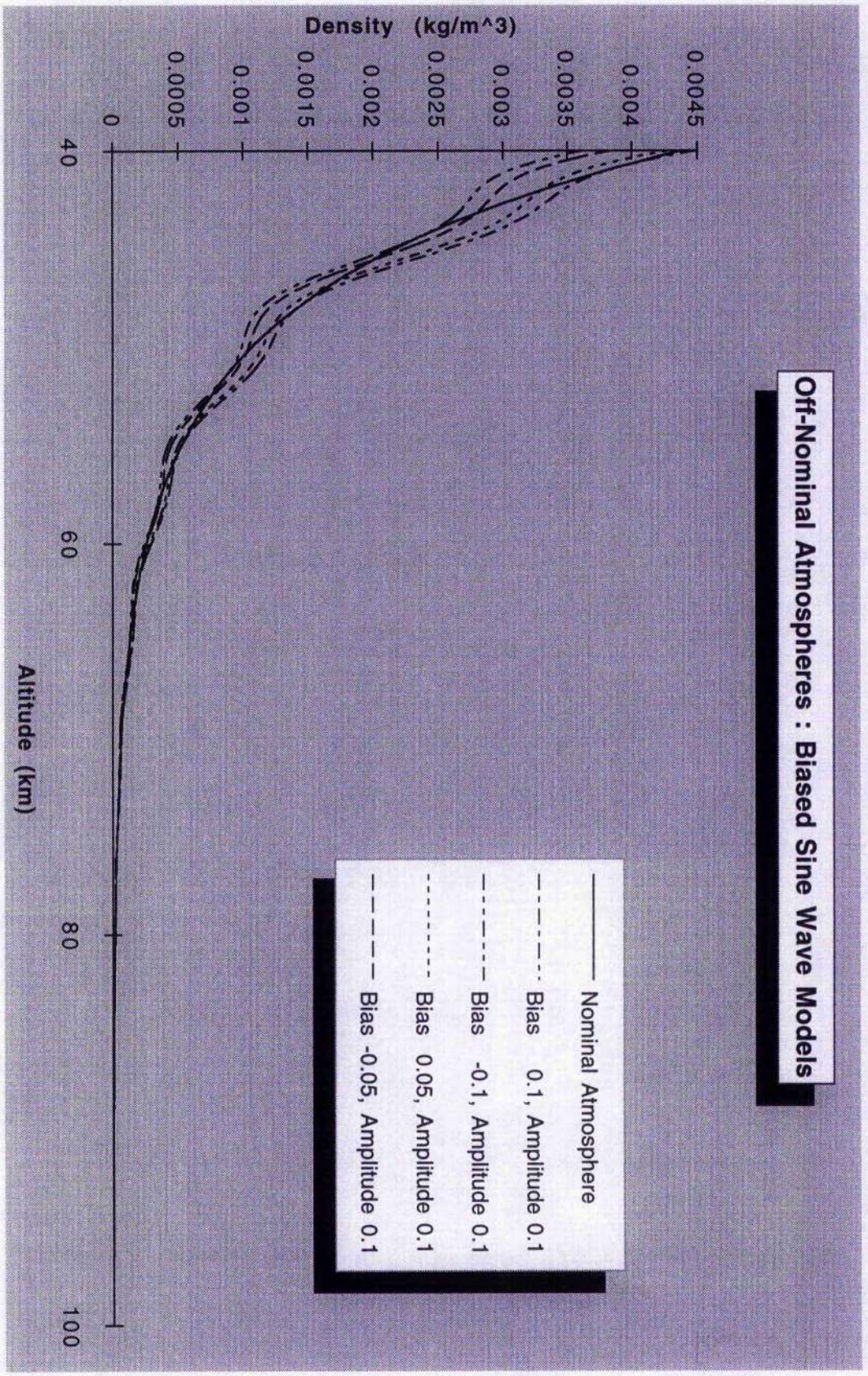

Fig. II.C.2.3.5-1 Off-Nominal Atmospheres : Biased Sine Wave Models

atmosphere. And again the GRAM (Global Reference Atmosphere Model)[53] used by NASA provides a highly accurate reference model, in this case including a spherical harmonic wind model.

All of these types of models can be considered overly-accurate for the analysis of transatmospheric vehicle motion for the reasons given previously. Some models, like the analytic Jacchia-77 Model and the GRAM model deserve consideration for inclusion in *genL*, to improve the modelling of satellite orbits and proximity manoeuvres. The existing models are, however, considered sufficient for the work to follow.

II.C.3. Solar System Orbit Model

The orbits of the planets in our solar system (with the notable exception of Pluto) all lie in orbit planes close to the ecliptic (the plane of orbit of the Earth about the Sun), following approximately circular orbits. For the purposes of examining the vanishingly small effects of the outer planets on an Earth re-entry vehicle it would be more than adequate to assume coplanar circular orbits for all these planets. However, when considering trans-lunar trajectories we cannot assume the same holds true for the orbits of the Earth and the moon.

In order to keep *genL* as generic as possible, elliptical orbit models were included for all nine planets and the six major moons: the Galillean moons of Jupiter, Titan, and our own Moon. The inclusion of a facility allowing the user to ignore the effects of any of these bodies when deemed insignificant is included allowing faster run times where appropriate.

A precise propagation of the orbits of these bodies would require numerical integration. It might be desirable if this integration were carried out in a vector formulation similar to that employed for vehicle motion. In this way the propagation of

the motion of all the bodies in the simulation would be consistent.

However, to integrate (to $4th$ order) the motion of fifteen bodies in addition to that of the vehicle being examined would drastically increase the run-time of the simulation, requiring three positional and three velocity integrations for each body. This would introduce an additional $16\times(3+3)\times4=384$ integration calculations for each time point if all the celestial bodies modelled in the simulation were to be included. In addition, for long term analyses cumulative integration errors could result in not insignificant departures from accurate orbits. As a result a semi-analytic propagation method was chosen which can be shown to possess a rapid rate of convergence.

The method is termed semi-analytic in that it requires an iterative solution of Kepler's equation but is otherwise analytic.

Kepler's equation relates two of the quantities used in evaluating the orbital state of a body at time t, for a known orbit.

$$E - e\sin E = M \qquad \textbf{II.C.3-1}$$

where M and E are the mean and eccentric anomalies, respectively, and e is the eccentricity of the orbit. If M were the required quantity and E and e were known the solution would be simplicity itself. Unfortunately, we require E with the other variables known. Somewhat more fortunately, the form of the expression is sufficiently well posed that we may avoid use of Newton-Raphson or secant methods and simply use a solution of the form

$$\begin{aligned} E_1 &= M + e\sin E_0 \\ E_2 &= M + e\sin E_1 \\ E_3 &= M + e\sin E_2 \ldots \end{aligned} \qquad \textbf{II.C.3-2}$$

until the value converges to a good degree of accuracy.

This requires a good guess for E_0 and again the problem is so nicely formulated that the approximation $E_0 = M$ will be sufficient for orbits with small eccentricities, though the more accurate approximation $E_0 = M + e\sin M$ is used here.

It has been shown that solution of Kepler's equation using this method requires no more than six steps to converge to an accuracy better than $\pm 1 \times 10^{-15} rads$.

Upon obtaining this solution the remainder of the orbital data is derived analytically. A description of the full orbital solutions can be found in Appendix I.

The simulated anomalistic Earth year resulting from these solutions is thirty minutes longer than a true year, an error of less than $6 \times 10^{-3}\%$, and the distance between the bodies in the solar system means that the resultant error in the solar system gravitational field estimation is negligible over time periods of interest.

II.D. Aerodynamics

The mechanics of interaction between an atmospheric entry vehicle and the atmosphere itself would constitute an entire study unto themselves and consequently the treatment given here may seem rather cursory.

The flow encountered by an entry vehicle may be considered in five regimes[47], ranging from free molecule flow to continuum flow. The region of continuum flow extends to about $275km$ from the surface of the Earth. Beyond this the flow cannot truly be considered to behave in the same manner. However, the air density above $275km$ is of order 10^{-17} and decreasing exponentially.

The flow above this altitude will then have a relatively insignificant effect in terms of aerodynamic lift and drag and so it is considered sufficient to assume continued continuum flow rather than introduce a new model for this region.

The discrepancy between the aerodynamic effects of an assumed continuum flow and a more realistic flow model may well be of the same order as the aerodynamic effects themselves

but the tiny magnitude of those effects makes this a reasonable operating assumption.

The widespread use of this assumption in re-entry vehicle dynamics supports this approach.

For the work presented here, the values of the various aerodynamic force and moment coefficients are taken from empirical test or representative data used in other studies. Although various methods exist for predicting coefficients it was not the intention of this study to accurately design an atmospheric vehicle .

All aerodynamic force evaluations are made in the wind axes reference frame which is standard to aeronautics.

The magnitudes of the aerodynamic forces are obtained from the usual relations, viz.

$$L = \tfrac{1}{2}\rho V_a^2 S C_L \qquad \textbf{II.D-1a}$$

$$D = \tfrac{1}{2}\rho V_a^2 S C_D \qquad \textbf{II.D-1b}$$

$$Y = \tfrac{1}{2}\rho V_a^2 S C_Y \qquad \textbf{II.D-1c}$$

where V_a is the vehicle airspeed, and the first unknown encountered in obtaining the aerodynamic force vector.

The airspeed, V_a, may be found from the value of the velocity vector in the current working frame. This vector is first rotated into equatorial planet axes. If we assume that the atmosphere rotates with the planet at the same speed or about the same axis we then establish a frame rotating with this atmosphere with origin coincident with that of the equatorial set. The angular velocity, ω, of the rotating frame with respect to the equatorial frame is then simply the speed of rotation of the atmosphere about the polar axis.

Using the velocity transformation

$$\underline{V}_{rotating} = \underline{V}_{fixed} - \underline{\omega} \times \underline{r} \qquad \textbf{II.D-2}$$

the velocity with respect to the rotating frame is found. Local wind conditions can now be taken into account and the resulting vector is then rotated back into PAO axes, our working reference

frame. This then defines the 'airspeed' vector with respect to our inertial reference and hence the vehicle airspeed.

Now using the working frame Euler angle set, the vector is rotated from inertial to body axes allowing derivation of the angles of attack and sideslip, α and β, in the usual way. Once these have been obtained it is possible to define the lift unit direction vector as (0,0,-1) in wind axes and using α, β and the Euler angles to rotate this into body and then PAO axes. Scaling by the magnitude of the aerodynamic lift produces the lift vector in inertial axes.

The drag and side force vectors are obtained more easily, the unit direction vectors being the negative velocity unit vector and the unit vector perpendicular to lift and drag forming a right handed set with the positive directions obtained by the cross product of these direction vectors. It should be noted that because of the axes conventions in aircraft dynamics both lift and drag act in the negative direction along the appropriate axes in steady level flight.

Aerodynamic moments are evaluated directly in body axes using the standard relations

$$L = \tfrac{1}{2}\rho V_a^2 S C_L \bar{c} \qquad \textbf{II.D-3a}$$

$$M = \tfrac{1}{2}\rho V_a^2 S C_M \bar{c} \qquad \textbf{II.D-3b}$$

$$N = \tfrac{1}{2}\rho V_a^2 S C_N \bar{c} \qquad \textbf{II.D-3c}$$

where $L, M, N,$ and C_L, C_M, C_N are the x, y, z moments and moment coefficients respectively, and $\bar{c}$ is a reference length, usually the distance from the centre of pressure to the centre of gravity.

L and C_L are not to be confused with L and C_L used for aerodynamic lift. Because these moments are evaluated directly in the axis set in which angular motion is propagated no transformation of data is necessary.

II.E. Integration

The integration method chosen is based on an adaptive Runge-Kutta-Fehlberg scheme of order four.

Adaptive algorithms automatically rescale the integration step size to the required accuracy of the solution as dictated by some predefined error tolerance. The difficulty with some of these schemes lies in the requirement to "step back" if the assessed error does not lie within the required tolerances.

For example, when the Adams-Moulton predictor-corrector algorithm presented by Cheney and Kincaid[54] encounters an unacceptable error, the scheme will step back four time points (data sets) and either half or double the step size, depending on whether the error exceeds either the lower or upper tolerance. This requires a very careful selection of integration tolerances if the scheme is to avoid being caught in a loop as this modification of the step size may result in a calculated error which exceeds the other tolerance. Obviously this is undesirable, although the facility to modify the step size according to the dictates of the problem is a very useful one.

As stated the scheme used here is based on an adaptive fourth-order Runge-Kutta-Fehlberg scheme. This scheme requires six evaluations to provide a fourth order solution with an error estimate. This estimate is provided by developing a fifth order solution and using this to assess the truncation error in the fourth-order solution. It was intended that this error estimate be used in controlling an adaptive scheme as mentioned, but, although this facility exists within *genL*, it was decided through experience that a fixed step fifth order solution provided the better results for hypervelocity trans-atmospheric modelling both in terms of run-time and accuracy of solution.

However, bearing in mind the large discrepancy in the speed of the dynamics between Keplerian and atmospheric motion, the use of a different size of integration step in each region would seem appropriate. Similarly, it would seem appropriate to differentiate between controlled and uncontrolled motion in order to model the

effects of the control more accurately. To this end step sizes are split into four "zones" (shown below) with a simple check for the presence of the vehicle in each zone. The time steps used in each zone are problem specific.

	Controlled	Uncontrolled	Keplerian	Atmospheric
Zone 1	√	—	√	—
Zone 2	√	—	—	√
Zone 3	—	√	√	—
Zone 4	—	√	—	√

Table II.E-1 Definition of integration step zones for transatmospheric motion

This was found to work well in verification with *Orbital Workbench*[38] and known analytic solutions to trajectory and orbit problems. An algebraic description of the algorithm can be found in Appendix IV.

Chapter III.

MATCHED ASYMPTOTIC EXPANSIONS & NON-LINEAR CONTROL

In this chapter preliminary discussions are presented of both the analytic prediction technique and the control method employed in chapters IV & V. A brief examination of the theory behind each approach is given as well as a discussion of their applicability to the problems considered.

III.A. The Method of Matched Asymptotic Expansions

III.A.1. Introduction

The method of matched asymptotic expansions is a technique which was developed for the treatment of singular perturbation problems in fluid mechanics[55].

Early applications of this technique to transatmospheric vehicle dynamics examined its use in lifting body hypervelocity atmospheric entry problems[56] and found that the trajectory predictions obtained corresponded well to those obtained from numerical simulations. Solutions have since been presented for atmospheric skips in two[57] and three dimensions[42] with similarly good results.

In using the method of matched asymptotic expansions we consider systems of differential equations where a small parameter multiplies the highest derivative. This derivative can then be ignored except in thin regions of rapid change where the value of the derivative becomes large enough to cancel the effect of multiplying by the small parameter. These thin regions are often found at one of the boundaries to the problem and hence may be referred to as boundary layers.

Solutions may then be developed for the boundary layer (inner region) and the outer region and the resultant expressions matched at the interface to ensure continuity. Combining the two sets of expressions results in a close approximation to the real system which is uniformly valid over the full value range of the independent variable. In transatmospheric vehicle dynamics this independent variable is usually non-dimensionalised altitude.

The atmospheric entry problem is a clear candidate for the application of the method of matched asymptotic expansions. The singular perturbation is the effect of atmospheric entry on the motion of the vehicle and the problem is constructed so that a small parameter multiplies the aerodynamic terms in the equations of motion. Obviously outside the atmosphere there are no aerodynamic effects and the dynamics of the motion are relatively slow. During atmospheric passage the dynamics are notably faster and so, in comparison to the slow regions above the Earth, the atmosphere fits nicely to the concept of a thin region of rapid dynamical change or boundary layer.

The problem then becomes the development of expressions for the inner and outer regions and a common solution. These may then be combined to produce a uniformly valid composite solution for the entire motion.

III.A.2. Theory Behind the Solution Method

The method of matched asymptotic expansions is an analytic technique for obtaining a close approximate solution to a singular perturbation problem. In describing the theory behind the solution method it is helpful to use a problem which possesses an exact solution.

Consider the differential equation

$$\varepsilon\frac{d^2y}{dx^2}+\frac{dy}{dx}=x \quad \text{in the region } 0<x<1 \qquad \textbf{III.A.2-1}$$

where

$$y=y(x,\varepsilon) \text{ with } y(0,\varepsilon)=0 \text{ and } y(1,\varepsilon)=1 \qquad \textbf{III.A.2-2}$$

and ε is a small parameter.
For fixed ε this system can be directly integrated to give

$$y=\frac{(1+2\varepsilon)\left(e^{(1-x)/\varepsilon}-e^{1/\varepsilon}\right)}{2\left(1-e^{1/\varepsilon}\right)}-\varepsilon x+\frac{x^2}{2} \qquad \textbf{III.A.2-3}$$

Then, for $x\neq 0$ fixed, as $\varepsilon\to 0$ this solution can be seen to tend towards

$$y(x,\varepsilon)=\frac{1+x^2}{2} \qquad \textbf{III.A.2-4}$$

This approximation to the solution is, however, not uniformly valid over the entire domain of x values. In the region approaching $x=0$ the other terms in eqn. III.A.2-3 are no longer exponentially small and can no longer be ignored. Consequently eqn. III.A.2-4 is found to lose validity near $x=0$ and the lower boundary condition is lost from the solution.

An alternative expression may be developed which is uniformly valid in this region. For $\xi = x/\varepsilon$ fixed, as $\varepsilon \to 0$, rewriting eqn. III.A.2-3 in terms of ξ, the solution tends towards

$$y(\varepsilon\xi, \varepsilon) = \frac{\left(1 - e^{-\xi}\right)}{2} \qquad \textbf{III.A.2-5}$$

This solution again loses validity towards one boundary condition, this time as $\varepsilon\xi \to 1$.

In this way a single expression may be represented by two separate functions, one describing each region. There is, however, some commonality in the solutions obtained, as evidenced by the factor 1/2 found in each solution. This commonality exists as a result of the overlap region where both solutions are valid.

These solutions are approximations to the exact solution and the description of their development outlines the theory behind the matched asymptotic solution to the problem.

III.A.3. Solution by Matched Asymptotic Expansions

In contrast to the solutions obtained above, solution by matched asymptotic expansions requires the exact solution of approximate sub-problems. Consideration of the initial problem (eqn. III.A.2-1) suggests that for small ε we might be able to singularly reduce the order of the problem, effectively treating it as a regular perturbation problem. This is done by letting $\varepsilon \to 0$ before solving the differential equation.
The reduced problem is then

$$\frac{dy}{dx} = x \quad \text{in the region } 0 < x < 1 \qquad \textbf{III.A.3-1}$$

again with $y = y(x, \varepsilon)$ and $y(1, \varepsilon) = 1$ **III.A.3-2**

Assuming an expansion of the form

$$y(x, \varepsilon) = \sum_{i=0}^{n} \varepsilon^i y_i(x) + O\left(\varepsilon^{n+1}\right) \qquad \textbf{III.A.3-3}$$

eqn. III.A.3-1 is solved to lowest order in the expansion as

$$y_o(x,\varepsilon) = \frac{x^2}{2} + C_1 \qquad \textbf{III.A.3-4}$$

Knowledge of the exact solution to the problem allows us to apply the upper boundary condition to this solution, which will be known as the outer. Application of this condition determines the value of the integration constant C_1, so that now

$$y_o(x,\varepsilon) = \frac{x^2}{2} + \frac{1}{2} \qquad \textbf{III.A.3-5}$$

which is identical to eqn. III.A.2-4.

As has been discussed the reduction in order of the differential equation is not valid where d^2y/dx^2 is large, i.e., where there are rapid changes in the value of y. The examination of this region is made using a stretched independent variable, $\xi = x/\varepsilon$. Using this stretched variable effectively magnifies the area of interest, such that the range $0 < x < \varepsilon$ becomes $0 < \xi < 1$.

Eqn. III.A.2-1 now becomes

$$\frac{1}{\varepsilon}\frac{d^2\tilde{y}}{d\xi^2} + \frac{1}{\varepsilon}\frac{d\tilde{y}}{d\xi} = \varepsilon\xi \qquad \textbf{III.A.3-6}$$

where $\tilde{y} = \tilde{y}(\varepsilon\xi,\varepsilon)$ and $\tilde{y}(0,\varepsilon) = 0$ **III.A.3-7**

Again we assume an expansion of the form

$$\tilde{y}(\varepsilon\xi,\varepsilon) = \sum_{i=0}^{n} \varepsilon^i \tilde{y}_i(\varepsilon\xi) + O(\varepsilon^{n+1}) \qquad \textbf{III.A.3-8}$$

and eqn. III.A.3-6 is then solved to lowest order as

$$\tilde{y}_o(\varepsilon\xi,\varepsilon) = \frac{C_2}{e^{\xi}} + C_3 \qquad \textbf{III.A.3-9}$$

In this example the lower boundary condition is known and may be used to help obtain the integration constants C_2, C_3.

Application of this condition gives

$$C_2 + C_3 = 0 \qquad \textbf{III.A.3-10}$$

The upper boundary condition may not be applied as the inner solution loses validity in this limit.

The lower boundary condition will not always be known. In this event the inner integration constants are found solely through the matching process described below.

As mentioned above, there exists a region in which both solutions are valid, i.e. where ξ is large and x is small. By forcing the two solutions to match in this region we may solve for the remaining integration constants. The matching process is performed by taking the two solutions to their respective limits of validity and equating to find the constants.

Thus eqn. III.A.3-5 becomes

$$y_o \to \frac{1}{2} \quad \text{as } x \to 0 \qquad \textbf{III.A.3-11}$$

and eqn. III.A.3-9 becomes

$$\tilde{y}_o \to C_3 \quad \text{as } \xi \to \infty \qquad \textbf{III.A.3-12}$$

Equating eqn.s III.A.3-11 & -12 gives

$$C_3 = \frac{1}{2} \qquad \textbf{III.A.3-13}$$

and hence from eqn. III.A.3-10

$$C_2 = -\frac{1}{2} \qquad \textbf{III.A.3-14}$$

completing the set of integration constants.

To form a useful single uniformly valid solution we combine the two solutions (eqn.s III.A.3-5 & -9) to form a composite. We know that there is a solution which is common to both regions and this must be subtracted from their sum lest it be included twice.

The common solution is found by expressing one solution in the independent variable of the other and taking the limit as $\varepsilon \to 0$. Here we will take the outer which becomes

$$y_o = \frac{(\varepsilon\xi)^2}{2} + \frac{1}{2} \qquad \textbf{III.A.3-15}$$

and in the limit $\varepsilon \to 0$

$$y_o = \frac{1}{2} \qquad \textbf{III.A.3-16}$$

The composite solution is then the sum of the inner and outer solutions less their common solution, viz.,

$$y_o(x,\varepsilon) = \frac{1}{2}\left(x^2 - e^{-x/\varepsilon} + 1\right) \qquad \textbf{III.A.3-17}$$

It can be seen that the composite solution differs slightly from the exact solution. A comparison of the solutions (fig. III.A.3-1) shows that the missing terms have a relatively minor effect and so the zeroth order solution obtained is shown to be valid over the full range of x values.

The largest discrepancy between the solutions is found in the overlap region where ξ is large and x is small. Comparison of the solutions suggests that this is a higher order effect and consequently a higher order solution might provide greater accuracy. It would certainly, however, increase the complexity of solution.

Fig. III.A.3-2 shows the variation in the absolute errors (dY) obtained using the matched asymptotic solution for $\varepsilon = 0.01$ compared with the exact solution.

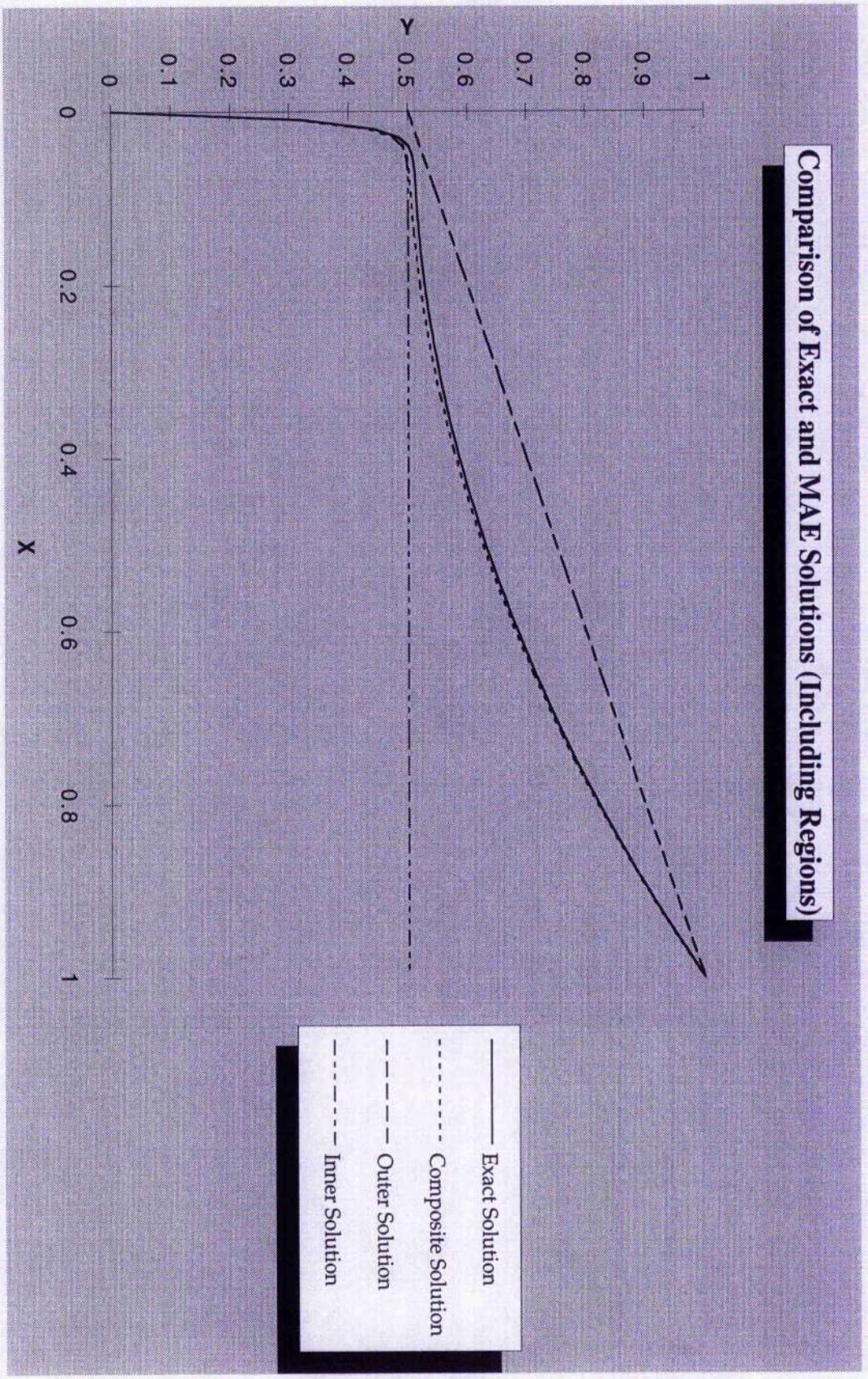

Fig. III.A.3-1 Comparison of Exact Solutions and MAE Solutions (Composite and Regional)

$\varepsilon = 0.01$

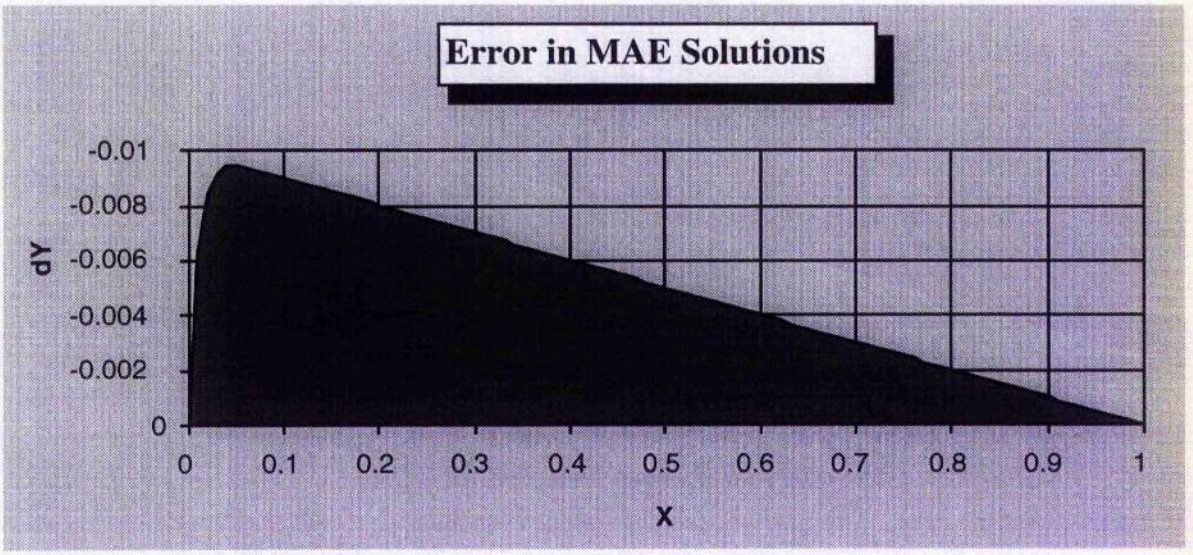

Fig. III.A.3-2 Absolute Errors in MAE Solutions, $\varepsilon = 0.01$

III.A.4. Inner Variables and Boundary Layers in the Atmospheric Entry Problem

In the discussion above we have used a second order problem with an exact solution to illustrate the solution method and theory. This allows us to determine from the size of the boundary layer and an appropriate scaling for this region. It is not always the case that one has an exact solution to help determine these factors and hence it might prove necessary to examine all the possibilities.

Similarly, a boundary layer might exist at the upper bound of the problem and this would have to be included in the modelling. Analysis of the problem assuming a boundary layer at the upper extreme results in an inner which is merely the outer expressed in a different variable, and it becomes clear that no such boundary layer exists at this extreme.

The atmospheric entry problem is well known and so may be treated like our example problem in that through numerical integration we may obtain an exact solution to the motion. This helps us to define the boundary layer(s) and to choose appropriate stretching parameters for those layer(s).

The boundary layer in this case is the atmosphere (thin relative to the surrounding space) in which we change from the slow dynamics of Keplerian motion to the rapid dynamics of hypervelocity aerodynamic motion.

The choice of inner variable is made using suitable parameters which will form part of the non-dimensionalising of the trajectory variables (section IV.B.2), such that the two regions considered are exoatmospheric/Keplerian (Outer) and atmospheric (Inner) motion.

Validation of the use of the atmosphere as a boundary layer and the choice of stretching parameter, ε (eqn. IV.B.2-12), is ultimately carried out through comparison of the resultant solutions to the 'exact' numerical solution.

III.B. Non-linear Transformation Guidance

III.B.1. Non-linear Systems

The stability or instability of a linear system is a characteristic of the system itself and is not affected by the magnitude of the input to the system or the initial conditions. The stability of a non-linear system, however, depends on the initial conditions and the magnitude of the input to the system. Whereas a linear system will always have the same "shape" of response to an input, the response of a non-linear system will vary in a complex way with respect to the input.

Much work has been done demonstrating and detailing the use of non-linear transformation, or feedback linearisation as a means of controlling non-linear dynamical systems.[30,33,35]

In employing feedback linearisation we use knowledge of the discrepancy between the current value of the state variables and some ideal value set to determine an appropriate control response which will act to return the system to this ideal state. Often we require to control only one or two system variables and these become the inputs to our control law. The magnitude of the applied control resulting from an off-nominal state is determined through a set of control gains.

In this way feedback linearisation is used to transform a non-linear system into a closed-loop, lincarised system to which we may then apply linear control theory. The development of an appropriate feedback control law, through construction and application, is outlined in section III.B.2 below.

The use of feedback linearisation has three main advantages:

- Reducing sensitivity of the system to variations in the system parameters.

  Exact knowledge of vehicle parameters, for example aerodynamic coefficients, etc., is not always possible particularly during transatmospheric motion where thermal expansion and ablation may alter the magnitude of such parameters. A suitable feedback control law would compensate for these and other variations, such as atmospheric uncertainties, in a robust manner.

- Control and time-response.

  By changing the gain applied to the control loop the time-response of the system is easily altered.

- Cancelling non-linearities in the state equations.

  The equations of motion for a transatmospheric vehicle are highly non-linear in themselves. Feedback lincarisation can make the vehicle behave as though its dynamics were linear.

There are, of course, disadvantages which accompany the use of feedback linearisation:

- Requires additional hardware and increases the complexity and cost of the system.

  The introduction of a feedback loop requires the addition of sensors and componentry which might not otherwise be present. Although a feedback law could be formulated to reduce the sensitivity of the system to variations in these parameters, it will still be desirable for these components to be made with a greater degree of precision than might be acceptable for other components so as to minimise the effect of uncertainties in the control hardware itself.

- Requires accurate knowledge of the system dynamics.

  Without an accurate representation of the system behaviour, the effectiveness and stability of the control cannot be assured.

- Possibility of the introduction of instability to the system.

  This is caused by the inherent time lags within the system, with the result that what was intended as negative feedback may turn out to be positive feedback.

- Partial linearisation.

  In some cases, state feedback will result in only partial linearisation of the system. The "linearised" system will also contain an unobservable non-linear subsystem which may cause problems. However, Mease and Kremer[33] demonstrate that such unobservable subsystems do not pose a problem for transatmospheric vehicle control.

In determining whether or not to use feedback control we must compare the improvements in control and stability to the

increased cost and complexity. Given the likely cost of any transatmospheric vehicle the additional cost of a feedback controller will probably not be significant and there is a recognised need for control of aeroassisted manoeuvres. In this case, the decision criterion would become the effectiveness of the controller in comparison to alternative methods.

III.B.2 State Feedback

Consider the general non-linear system

$$\dot{\mathbf{x}} = f(\mathbf{x}) + g(\mathbf{x})\mathbf{u} \qquad \textbf{III.B.2-1a}$$

$$\mathbf{y} = h(\mathbf{x}) \qquad \textbf{III.B.2-1b}$$

where $\mathbf{x}$ is the state vector, $\mathbf{u}$ the input (control) vector, and $\mathbf{y}$ is the output vector.

By differentiation of the system we may cause the input (control) to appear explicitly. The number of times the output must be differentiated to achieve this is termed the relative degree of the system. It has been shown[58,59], that when a non-linear system of this form has a clearly-defined relative degree, it is possible to feedback linearise the system with a state feedback law of the form

$$\mathbf{u} = \alpha(\mathbf{x}) + \beta(\mathbf{x})\upsilon \qquad \textbf{III.B.2-2}$$

where υ is an external reference input vector.
The choice of feedback law is such that the closed-loop system

$$\dot{\mathbf{x}} = f(\mathbf{x}) + g(\mathbf{x})\alpha(\mathbf{x}) + g(\mathbf{x})\beta(\mathbf{x})\upsilon \qquad \textbf{III.B.2-3}$$

will have a linear mapping from υ to $\mathbf{y}$.

To illustrate this we will outline the development of the constant altitude controller used later (Section V.B.5.1).

The purpose of this control is, as stated above, to track a constant altitude. The method of control is through roll-modulated aerodynamic lift and so our input vector **u** in this case is single-termed, viz.,

$$u = \cos\sigma \qquad \textbf{III.B.2-4}$$

where σ is the vehicle bank (roll) angle. This term appears explicitly in the second derivative of altitude $\frac{d^2h}{dt^2}$ and so the system considered is

$$\ddot{h} = \frac{d}{dt}V\sin\gamma = \frac{dV}{dt}\sin\gamma + V\cos\gamma\frac{d\gamma}{dt} \qquad \textbf{III.B.2-5}$$

Noting that $\frac{d\gamma}{dt}$ contains the control term explicitly and $\frac{dV}{dt}$ does not we save unnecessary expansion of terms here and write

$$\ddot{h} = f(V,\gamma,h) + g(V,\gamma,h)u \qquad \textbf{III.B.2-6}$$

Note that, in comparison with eqn. III.B.2-1a, on the right hand side we have terms for $f(\mathbf{x}) + g(\mathbf{x})\mathbf{u}$, but on the left we have $\ddot{h}$ which does not appear to fit the "rôle" of $\dot{\mathbf{x}}$.

In fact the expression shown above is only a part of the system.

Consider the state vector

$$\mathbf{x} = \left[\dot{V},\ \dot{\gamma},\ \dot{h},\ V,\ \gamma,\ h\right]^T \qquad \textbf{III.B.2-7a}$$

with derivative

$$\dot{\mathbf{x}} = \left[\ddot{V},\ \ddot{\gamma},\ \ddot{h},\ \dot{V},\ \dot{\gamma},\ \dot{h}\right]^T \qquad \textbf{III.B.2-7b}$$

Then we can see that the expression in $\ddot{h}$ is a part of the full system.

We do not consider the full system as the only system constraint is that it track a constant altitude. The other terms in the state vector derivative are not of concern provided this constraint is met. Also, as $\ddot{h}$ is a function of V, γ, h, and σ only, the other terms in the state vector are dropped from the notation in eqn. III.B.2-6.

It now remains to control the above system via a feedback law of the form given in eqn. III.B.2-2.

In this case the external reference input is given by the desired constant altitude, implicit in which is a null-valued reference climb/descent rate.

The desired transient response is that of a damped harmonic oscillator, which will guarantee stability of the system about the reference condition, viz.,

$$\ddot{p} = -\kappa\dot{p} - \lambda p \qquad \textbf{III.B.2-8}$$

where $\ddot{p}$ is defined as

$$\ddot{p} \equiv \ddot{h} \qquad \textbf{III.B.2-9}$$

and p and $\dot{p}$ are the altitude error and error rate respectively.

$$p = h - h_{ref} \qquad \textbf{III.B.2-10a}$$

$$\dot{p} = \dot{h} - \dot{h}_{ref} = \dot{h} \qquad \textbf{III.B.2-10b}$$

Now equating the left hand side of eqn. III.B.2-6 with that of eqn. III.B.2-8 and rewriting in terms of $\cos\sigma$ we obtain the feedback law

$$\cos\sigma = \frac{1}{g(V,\gamma,h)}\left(-f(V,\gamma,h) - \kappa\dot{p} - \lambda p\right) \qquad \textbf{III.B.2-11}$$

which can be shown to have the form required (eqn. III.B.2-2).

The parameters κ and λ are control gains which may be used to shape the system response to inputs.

In this manner control of the vehicle about a reference ideal may be effected. In the example above this reference ideal is a constant altitude trajectory. This controller is fully developed in Chapter V as well as an exit trajectory controller ("trajectory tracker") which utilises the method of matched asymptotic expansions to analytically produce the reference data as and when required.

Chapter IV

HYPERVELOCITY TRANSATMOSPHERIC VEHICLE MOTION

IV.A. Introduction

In this chapter we examine some aspects of hypervelocity transatmospheric vehicle motion, in particular we develop matched asymptotic expansions as both a modelling tool and as the basis for a simple, robust, controller. The aim is to produce in closed-form a set of analytic relations which describe the behaviour of state variables over the whole trajectory. These relations can then be used as a replacement for more costly sensors/instrumentation or as a low-cost monitor of the operation of such equipment, without the need to resort to onboard numerical integration.

The use of analytic modelling techniques such as the method of matched asymptotic expansions provides an insight into the basic mechanisms involved in the subject of study. An analytic approximation to the full equations of motion highlights the terms which most strongly influence the motion of the vehicle. In this case the solutions validate the approximation made by Allen and

Eggers[60], that aerodynamic forces predominate within the atmosphere to such an extent that gravitational forces may be neglected. As will be shown, a matched asymptotic analysis of transatmospheric motion shows that the effect of gravity tends towards zero during the atmospheric portion of the trajectory.

This might seem a rather backward way of proving a point as it is partly by use of this assumption that the system lends itself to solution by matched asymptotic expansions. Whilst recognising this fact, comparison with a high fidelity numerical solution to the motion can still be said to validate the operating assumption.

A close analytic approximation to real motion allows accurate determination of the trajectory variables without numerical propagation. In the work presented here the velocity and flight-path angle at any point along the trajectory may be obtained directly from input of the altitude. This allows the analyst to quickly predict related parameters such as dynamic pressure, axial acceleration and so on. Onboard a vehicle such a system could be used to replace complex sensors with analytically obtained values requiring knowledge of altitude alone, thus reducing the amount of instrumentation required and hence the cost. Initialisation of the analytic expressions would be done using data from exo-atmospheric state updates.

In addition, it will be shown that the validity of the constant drag coefficient approximation, also introduced by Allen and Eggers[60], may prove inadequate for certain applications. The applications referred to chiefly concern launch/entry vehicles with low bluntness ratios (ratio of nose radius to body radius) which are more susceptible to mach number related compressibility effects. For these vehicles the drag coefficient is mach number (and thus implicitly velocity) dependent. This dependence may be introduced into the matched asymptotic analysis introducing a new physical effect into the model and so broadening its applicability and improving its accuracy.

Typical examples of entry missions on which such a system could be used include planetary surface penetrators and Mars landers, as well as the obvious application to ballistic missiles

(section IV.B). Launch applications again include military uses as well as the direct launch concept which is discussed later (section IV.C).

IV.B. Ballistic Entry

Typical ballistic entry vehicles are low-drag configurations, the intention being to minimise trajectory curvature and thus reduce any possible targeting errors. One of the advantages of the low-drag configuration is that it minimises the dynamic and integrated heat loads experienced by the vehicle during atmospheric entry. One of the disadvantages is the increased stagnation-point heating rate incurred due to the sharpened nose-cone/leading edges. In addition, because the vehicle does not lose so much speed, surface impacts will occur at high velocities and may prove destructive to the vehicle. Not surprisingly the majority of uses for this type of vehicle are military although work on planetary surface penetrators[61,62] can also benefit from the techniques and technologies associated with ballistic missiles.

The lack of any lift force greatly reduces the controllability of the vehicle, as we shall see later (Chapter V) . The only means of affecting the vehicle trajectory once in-flight are by propulsive burns and variation in the vehicle drag parameters. Unfortunately because of the high speeds associated with re-entry it is likely that any deployable surfaces would be subject to enormous pressure loadings and would probably not remain attached to the vehicle for long. Changes in drag-coefficient are more usefully carried out by explosive release of, for example a heat shield, or, if/when sufficiently slowed by drag, by the deployment of a parachute.

In this section the trajectories of unguided hypervelocity atmospheric entry vehicles are investigated analytically using the method of matched asymptotic expansions. The use of the derived solutions is investigated both in the context of analytical modelling

and as the basis of a low-complexity guidance/control system. Both constant and velocity dependent drag coefficient models are employed in solving for the vehicle trajectory.

IV.B.1. Introduction

It has been suggested that the constant drag coefficient approximation introduced by Allen and Eggers[60] is insufficient when applied to some re-entry problems. To show this Barbera[63] presented a closed-form solution to the re-entry problem which incorporated an integrable, velocity dependent drag coefficient. The coefficient model used had been closely matched to inviscid drag data for typical re-entry vehicles. However, Barbera's closed form solution was actually separated into four zones, and was therefore not a uniform solution to the problem. These zones occurred as a result of a discontinuity in the drag coefficient /Mach number profile around $M = 10$, and Barbera's use of a two-zone patched atmosphere model. In order to produce a uniform solution for the complete trajectory a matched asymptotic analysis was used which employed Barbera's drag coefficient model.

Barbera's solution was found to be valid for trajectories resulting in velocities greater than $M = 1$ at impact. The work presented here is similarly aimed at high velocity entry vehicles. The operating assumption that we may neglect gravity within the atmosphere dictates that the aerodynamic forces experienced should be at least an order of magnitude greater than the gravitational forces. Hypervelocity atmospheric entry presents aerothermodynamic problems with regard to the high heating loads incurred, though ablative mass loss may be minimised by the use of suitable thermal-protection. In the case of the Huygens probe a beryllium nose cap and heat-shielding are used as low mass, non-contaminating protection[64].

The use of matched asymptotic expansions in the solution of launch and re-entry problems has been well documented[56,65,66]. The aim of this study was to provide an

analytical model for the entry trajectories of such vehicles in order to successfully predict some of the characteristics of a ballistic hypervelocity atmospheric entry vehicle. The introduction of a velocity dependent drag coefficient model should increase the scope of the current analytical model. The solutions obtained are investigated for potential use in onboard guidance and control systems, for example, in determining the altitude for release of the aforementioned heatshield or a decelerator system.

IV.B.2. System Dynamics

Fig.IV.B.2-1 shows a schematic of the geometry appropriate to a study of hypervelocity atmospheric entry vehicle motion.

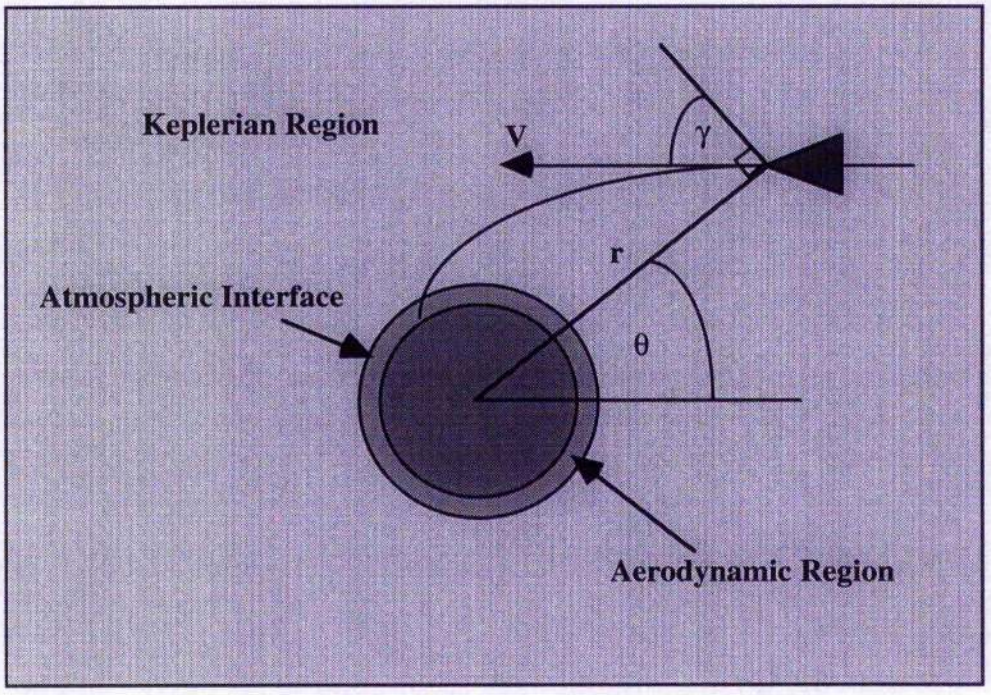

fig. IV.B.2-1 Schematic of Re-entry Trajectory

It is assumed that the atmosphere is non-rotating and that the vehicle experiences no transverse accelerations so that it remains in the plane containing the initial velocity vector and the planetary centre.

It is further assumed that the ablative mass loss from the heat shield is small and so the vehicle can be considered to have a constant mass. The equations of motion for this system[21] may then be written in a planetocentric frame as

$$\frac{dv}{dt} = -\frac{D}{m} + g\sin\gamma \qquad \textbf{IV.B.2-1}$$

$$v\frac{d\gamma}{dt} = -\left\{\frac{v^2}{r} - g\right\}\cos\gamma + \frac{L}{m} \qquad \textbf{IV.B.2-2}$$

$$\frac{dr}{dt} = v\sin\gamma \qquad \textbf{IV.B.2-3}$$

$$\frac{d\theta}{dt} = \frac{v}{r}\cos\gamma \qquad \textbf{IV.B.2-4}$$

where r is the orbital radius, t is time, v is velocity, and, $\gamma$the flight path angle measured positive up from the local horizon.

It is also assumed that gravity acts according to the spherically symmetric inverse square model for gravitational attraction

$$g(r) = -\frac{\mu}{r^2} \qquad \textbf{IV.B.2-5}$$

and the aerodynamic lift and drag accelerations are given by

$$\begin{Bmatrix} L \\ D \end{Bmatrix} = \frac{1}{2}\rho(r)v^2 \begin{Bmatrix} C_L(v) \\ C_D(v) \end{Bmatrix} S \qquad \textbf{IV.B.2-6}$$

where S is the aerodynamic reference area of the vehicle. It will later be assumed that the vehicle is non-lifting, i.e. $C_L = 0$ and models for C_D will be introduced in the form

$$C_D = bv^{2n} \qquad \textbf{IV.B.2-7a}$$

which models the velocity dependence of the drag coefficient.

A constant drag model of form

$$C_D = bv_E^{2n} = constant \qquad \textbf{IV.B.2-7b}$$

will also be used, where v_E is the atmospheric entry velocity and b and n are empirically derived constants.

The atmospheric model is a non-rotating, wind free, exponential model of the form

$$\rho(r) = \rho_o \exp(-(r-R)/H) \qquad \textbf{IV.B.2-8}$$

although any integrable expression may be used for the density-altitude profile.
The equations of motion are now transformed into a non-dimensionalised form via the following variable transformations,

$$\bar{v} = v\sqrt{\frac{R}{\mu}} \qquad \textbf{IV.B.2-9}$$

$$h = \frac{r-R}{R} \qquad \textbf{IV.B.2-10}$$

$$\bar{\rho} = \frac{\rho H}{m/S} \qquad \textbf{IV.B.2-11}$$

$$\varepsilon = \frac{H}{R} \qquad \textbf{IV.B.2-12}$$

Using h as the new independent variable the system is reduced to a set of three equations,

$$\frac{d\bar{v}^2}{dh} = -\frac{\bar{\rho}\bar{v}^2 C_D}{\varepsilon \sin\gamma} - \frac{2}{(1+h)^2} \qquad \textbf{IV.B.2-13}$$

$$\frac{d\cos\gamma}{dh} = -\frac{\bar{\rho} C_L}{2\varepsilon} - \cos\gamma\left\{\frac{1}{1+h} - \frac{1}{(1+h)^2\bar{v}^2}\right\} \qquad \textbf{IV.B.2-14}$$

$$\frac{d\theta}{dh} = \frac{\cot\gamma}{1+h} \qquad \textbf{IV.B.2-15}$$

Given this system of equations the method of matched asymptotic expansions is now employed to find a uniformly valid solution to the motion.

IV.B.3. Matched Asymptotic Solutions for a Ballistic Atmospheric Entry Vehicle

The method of matched asymptotic expansions (section III.A) considers differential equations involving a small parameter multiplying the highest derivative . This derivative can then be ignored except in thin regions of rapid change, or boundary layers, in this case the sensible atmosphere close to the surface of the planet. This boundary layer is known as the inner region, and the Keplerian exoatmospheric region as the outer. Expansions are made for $\bar{v}^2$ and $\cos\gamma$ in both these regions and solutions are found. Initial conditions are only known for one region, in this case the outer, so the two solutions are matched to find the constants of integration for the inner. A solution exists which is common to both regions and this must be subtracted from the sum of the two regional solutions to provide a composite solution to the original equations.

Following the approximation made by Allen and Eggers[60], aerodynamic drag predominates in the initial descent through the atmosphere and above the sensible atmosphere the motion is Keplerian. Employing a matched asymptotic analysis as described above, we develop solutions for the aerodynamic and Keplerian regions and then match them to produce a composite representation of the entire trajectory.

Using the atmospheric density model given in eqn.IV.B.2-8 we make the variable substitutions

$$u = \bar{v}^2 \qquad \textbf{IV.B.3-1a}$$

$$\omega = \cos\gamma \qquad \textbf{IV.B.3-1b}$$

The sine term in eqn.IV.B.2-13 is evaluated using the relation

$$\sin\gamma = \pm\sqrt{1-\omega^2} \qquad \textbf{IV.B.3-2}$$

taking the physical root.

In the case of the re-entry vehicle this is the negative root. Why this should be becomes clear when remembering that the flight path angle is defined as positive upward (away from the

local horizontal). In this case γ for a re-entry vehicle will be negative and consequently $\sin\gamma$ will also take a negative sign.

The equations of motion for this system are now,

$$\frac{du}{dh} = -\frac{\bar{\rho}_o u C_D \exp(-h/\varepsilon)}{\varepsilon\sqrt{1-w^2}} - \frac{2}{(1+h)^2} \qquad \textbf{IV.B.3-3}$$

$$\frac{d\omega}{dh} = -\frac{\bar{\rho}_o C_L}{2\varepsilon}\exp(-h/\varepsilon) - \omega\left\{\frac{1}{1+h} - \frac{1}{(1+h)^2 u}\right\} \qquad \textbf{IV.B.3-4}$$

These expressions are now evaluated for the (Keplerian) outer and (acrodynamic) inner regions of the motion.

IV.B.3.1 Outer Solution

The outer solution is obtained by applying the outer limit as $\varepsilon \to 0$ with h and all other non-dimensional variables held constant, viz.

$$\frac{du}{dh} = -\frac{2}{(1+h)^2} \qquad \textbf{IV.B.3.1-1}$$

$$\frac{d\omega}{dh} = -\omega\left\{\frac{1}{1+h} - \frac{1}{(1+h)^2 u}\right\} \qquad \textbf{IV.B.3.1-2}$$

The limit $\varepsilon \to 0$ has the effect of compressing the atmosphere to a vanishingly thin region on the surface of the planet. Remembering that $\varepsilon = H/R$ we can see that for fixed R this means that $H \to 0$, i.e. the atmosphere tends towards an infinitesimal size.

A series expansion of the form

$$u = \sum_{j=0}^{n} \varepsilon^j u_j(h) + O\left(\varepsilon^{n+1}\right) \qquad \textbf{IV.B.3.1-3}$$

$$\omega = \sum_{j=0}^{n} \varepsilon^j \omega_j(h) + O\left(\varepsilon^{n+1}\right) \qquad \textbf{IV.B.3.1-4}$$

is assumed for each of the variables under consideration. Substituting into equations IV.B.3.1-1 and IV.B.3.1-2, the relations become, to lowest order,

$$\frac{du_o}{dh} = -\frac{2}{(1+h)^2} \qquad \textbf{IV.B.3.1-5}$$

$$\frac{d\omega_o}{dh} = -\omega_o\left\{\frac{1}{(1+h)} - \frac{1}{(1+h)^2 u_o}\right\} \qquad \textbf{IV.B.3.1-6}$$

with higher order terms identically zero. The zero order terms give an exact representation of the Keplerian motion of the body outwith the atmosphere.

By integration we obtain the Keplerian expressions

$$u_o = u_{oo} + \frac{2}{1+h} \qquad \textbf{IV.B.3.1-7}$$

$$\omega_o = \frac{\omega_{oo}}{\sqrt{2(1+h)+u_{oo}(1+h)^2}} \qquad \textbf{IV.B.3.1-8}$$

where,

$$u_{oo} = u_i - \frac{2}{1+h_i} \qquad \textbf{IV.B.3.1-9}$$

and

$$\omega_{oo} = \omega_i\sqrt{2(1+h_i)+u_{oo}(1+h_i)^2} \qquad \textbf{IV.B.3.1-10}$$

The initial conditions, u_i, ω_i, h_i, will be obtained from transformation of the initial, exoatmospheric, vehicle state, V_i, γ_i, r_i, into non-dimensional form.

A solution will now be developed for the aerodynamic inner region.

IV.B.3.2 Inner Solution

The inner solution is similarly found by repeated application of the inner limit. In this boundary layer a new stretched inner variable is used to help obtain a solution. The variable used is $\tilde{h} = h/\varepsilon$ so that now as $\varepsilon \to 0$ we have $\tilde{h} \to \infty$,

effectively expanding the atmospheric region to an infinite distance. In this way the stretched variable may be considered a mathematical microscope, enlarging the area of interest.

In terms of this new independent variable eqn.s IV.B.3-3 and IV.B.3-4 now become,

$$\frac{1}{\varepsilon}\frac{d\tilde{u}}{d\tilde{h}} = -\frac{\overline{\rho}_o \tilde{u} C_D(\tilde{u}) \exp\left(-\tilde{h}\right)}{\varepsilon\sqrt{1-\tilde{\omega}^2}} - \frac{2}{\left(1+\varepsilon\tilde{h}\right)^2} \qquad \textbf{IV.B.3.2-1}$$

$$\frac{1}{\varepsilon}\frac{d\tilde{\omega}}{d\tilde{h}} = -\frac{\overline{\rho}_o C_L}{2\varepsilon}\exp\left(-\tilde{h}\right) - \tilde{\omega}\left\{\frac{1}{\left(1+\varepsilon\tilde{h}\right)} - \frac{1}{(1+\varepsilon\tilde{h})^2\tilde{u}}\right\} \qquad \textbf{IV.B.3.2-2}$$

Applying the inner limit and expanding $\tilde{u}$ and $\tilde{\omega}$ as below,

$$\tilde{u} = \sum_{j=0}^{n} \varepsilon^j \tilde{u}_j\left(\tilde{h}\right) + O\left(\varepsilon^{n+1}\right) \qquad \textbf{IV.B.3.2-3}$$

$$\tilde{\omega} = \sum_{j=0}^{n} \varepsilon^j \tilde{\omega}_j\left(\tilde{h}\right) + O\left(\varepsilon^{n+1}\right) \qquad \textbf{IV.B.3.2-4}$$

we obtain, to lowest order,

$$\frac{d\tilde{u}_o}{d\tilde{h}} = \frac{-\overline{\rho}_o \tilde{u}_o C_D\left(\tilde{u}_o\right)}{\sqrt{1-\tilde{\omega}_o^2}}\exp\left(-\tilde{h}\right) \qquad \textbf{IV.B.3.2-5}$$

$$\frac{d\tilde{\omega}_o}{d\tilde{h}} = \frac{-\overline{\rho}_o C_L\left(\tilde{u}_o\right)}{2\varepsilon}\exp\left(-\tilde{h}\right) \qquad \textbf{IV.B.3.2-6}$$

For the ballistic case under consideration $C_L = 0$ so eqn.IV.B.3.2-6 reduces to,

$$\frac{d\tilde{\omega}_o}{d\tilde{h}} = 0 \qquad \textbf{IV.B.3.2-7}$$

or

$$\tilde{\omega}_o = \tilde{\omega}_{oo} \qquad \textbf{IV.B.3.2-8}$$

Any integrable drag function may now be incorporated into the solution of eqn. IV.B.3.2-5. The function used is based on Barbera's velocity dependent drag model for hypersonic entry

projectiles[63], which assumes that the speed of sound is a constant over the range of interest. This relation takes the form

$$C_D = bv^{2n} = bu^n \qquad \textbf{IV.B.3.2-9}$$

which becomes

$$C_D = \tilde{b}\tilde{u}_o^{\,n} \qquad \textbf{IV.B.3.2-10}$$

When this is substituted into eqn. IV.B.3.2-5, with $\tilde{\omega}_o = \tilde{\omega}_{oo}$, we obtain

$$\frac{d\tilde{u}_o}{d\tilde{h}} = \frac{-\tilde{b}\tilde{u}_o^{\,n+1}\bar{\rho}_o}{\sqrt{1-\tilde{\omega}_{oo}^2}}\exp\left(-\tilde{h}\right) \qquad \textbf{IV.B.3.2-11}$$

This is integrated to give,

$$\tilde{u}_o = \left\{\frac{-\tilde{b}n\bar{\rho}_o}{\sqrt{1-\tilde{\omega}_{oo}^2}}\exp\left(-\tilde{h}\right) + \tilde{u}_{oo}\right\}^{1/n} \qquad \textbf{IV.B.3.2-12}$$

The two sets of solutions are now matched to find the unknown constants of integration, $\tilde{u}_{oo}$ and $\tilde{\omega}_{oo}$, for the inner solution. For the matching procedure the outer is first expanded for $h \to 0$, and the inner is then expanded for $\tilde{h} \to \infty$. The two solutions are then equated and the constants are found to be

$$\tilde{u}_{oo} = \left(u_{oo} + 2\right)^{-n} \qquad \textbf{IV.B.3.2-13}$$

$$\tilde{\omega}_{oo} = \frac{\omega_{oo}}{\sqrt{u_{oo}+2}} \qquad \textbf{IV.B.3.2-14}$$

The matched constants are now used in conjunction with the inner and outer solutions to produce a uniformly valid composite solution.

IV.B.3.3. Composite Solution

The composite solution is now obtained by combining the inner and outer solutions and subtracting the common solution. The common solution is obtained by expressing the outer solution in terms of the inner variable and finding the limit as $\varepsilon \to 0$ i.e.,

$$u_o = u_{oo} + \frac{2}{1+\varepsilon\tilde{h}} \qquad \textbf{IV.B.3.3-1}$$

and

$$\omega_o = \frac{\omega_{oo}}{\sqrt{u_{oo}\left(1+\varepsilon\tilde{h}\right)^2 + 2\left(1+\varepsilon\tilde{h}\right)}} \qquad \textbf{IV.B.3.3-2}$$

Therefore as $\varepsilon \to 0$ it is found that

$$u_o = u_{oo} + 2 \qquad \textbf{IV.B.3.3-3}$$

$$\omega_o = \frac{\omega_{oo}}{\sqrt{u_{oo}+2}} \qquad \textbf{IV.B.3.3-4}$$

The final expressions for the variation of non-dimensionalised velocity and flight path angle with altitude are now given as,

$$u = \frac{-2h}{1+h} + \left\{ \frac{-\tilde{b}n\bar{\rho}_o}{\sqrt{1-\tilde{\omega}_{oo}^2}} \exp\left(-\tilde{h}\right) + \left(u_{oo}+2\right)^{-n} \right\}^{-1/n} \qquad \textbf{IV.B.3.3-5}$$

$$\omega = \frac{\omega_{oo}}{\sqrt{u_{oo}(1+h)^2 + 2(1+h)}} \qquad \textbf{IV.B.3.3-6}$$

From input of the desired altitude we may now derive the velocity, flight-path angle, and any dependent variables, for the motion of an atmospheric entry vehicle.

In order to examine the need for a velocity dependent drag coefficient model we will now develop solutions using the constant drag coefficient assumption.

IV.B.4. Constant Drag Coefficient Solutions

It is clear that the Keplerian solution to the motion will remain the same regardless of whether we employ a constant or a velocity dependent drag coefficient. The two solutions differ only in the inner, aerodynamic region.
Substituting

$$C_D(\tilde{u}_o) = C_D \qquad \textbf{IV.B.4-1}$$

into eqn.IV.B.3.2-5 and integrating, we obtain the new solution

$$\tilde{u}_o = \tilde{u}_{oo} \exp\left(\frac{-\bar{\rho}_o C_D}{\sqrt{1-\tilde{\omega}_{oo}^{\,2}}} \exp(-\tilde{h}) \right) \qquad \textbf{IV.B.4-2}$$

As the body is non-lifting the solution for $\tilde{\omega}_o$ remains as before. The matching constants are found to be

$$\tilde{u}_{oo} = u_{oo} + 2 \qquad \textbf{IV.B.4-3}$$

$$\tilde{\omega}_{oo} = \frac{\omega_{oo}}{\sqrt{u_{oo}+2}} \qquad \textbf{IV.B.4-4}$$

and the common solution

$$u_o = u_{oo} + 2 \qquad \textbf{IV.B.4-5}$$

$$\omega_o = \frac{\omega_{oo}}{\sqrt{u_{oo}+2}} \qquad \textbf{IV.B.4-6}$$

The resulting composite solutions are

$$u = \frac{-2h}{1+h} + \tilde{u}_{oo} \exp\left(\frac{-\bar{\rho}_o C_D}{\sqrt{1-\tilde{\omega}_{oo}^{\,2}}} \exp\left(-\frac{h}{\varepsilon}\right) \right) \qquad \textbf{IV.B.4-7}$$

$$\omega = \frac{\omega_{oo}}{\sqrt{u_{oo}(1+h)^2 + 2(1+h)}} \qquad \textbf{IV.B.4-8}$$

We now possess two sets of analytic solutions which may be compared with solutions derived from *genL* (Chapter II) for both constant and velocity dependent drag coefficient models.

IV.B.5. Results

The trajectory predictions obtained from the two sets of analytical expressions are now compared with the results from *genL* (Chapter II) in order to assess their value in representing the motion. Both the velocity dependent and the constant drag coefficient models have been incorporated in the numerical simulations.

The atmospheric model employed is an exponential model of the terrestrial atmosphere (section II.C.2.3.1) with a scale height of $7.1km$ and base density $1.225kg/m^3$ whilst the entry vehicle data used is for the same sphere-cone configuration as will later be used for the launch case. Details of this vehicle can be found in Appendix V.

Relations for derived quantities such as convective heating rate[67] (radiative heating is assumed negligible), $\dot{Q}$, and dynamic pressure, q, may now be obtained using the expressions

$$\dot{Q} = C_Q \sqrt{\rho} V^3 \qquad \textbf{IV.B.5-1}$$

$$q = \frac{1}{2}\rho V^2 \qquad \textbf{IV.B.5-2}$$

Where C_Q is a function of the nose radius and the material properties of the heat shield.

Comparisons are also made for variations in axial acceleration and C_D.

Fig.s IV.B.5-1 to -6 show the errors in the velocity and flight-path angle-altitude histories over a range of entry velocities and angles. The errors are averaged over the entire trajectory.

Although no trends in the observed errors can be identified for a given entry angle, the majority of the errors themselves are so small as to suggest the possibility that they might be numerical in origin. Comparison with the constant drag coefficient numerical model disabuses us of this notion by producing similarly small errors, but with the velocity solution being consistently worse (fig. IV.B.5-7) and the flight-path angle solution consistently better (fig. IV.B.5-8) than the analytic relations. In addition, from cross-comparison of the entry cases, it can be seen that the errors decrease with an increasingly steep entry angle, as might be expected (see 'tip-over' below).

The improved accuracy in the flight-path angle solution obtained with the constant coefficient numerical model as opposed to the velocity dependent analytic model is not unexpected. The flight-path angle varies little enough for a slender re-entry vehicle and, as the inner solution (eqn. IV.B.3.2-8) suggests, it is insensitive to the velocity dependence of the drag coefficient. This being the case the constant coefficient numerical solution would be expected to closely follow that for the velocity dependent run.

The velocity solution is certainly not insensitive to the velocity dependence of the drag coefficient and hence the analytic relations improve over the constant coefficient numerical results.

The constant drag coefficient analytic solutions are shown in their best light for a steep high-velocity entry where the discrepancy between these solutions and those for the velocity dependent coefficient should be minimised. This is done in part to show the best case scenario, as stated, but also to show the peaks in the derived quantities such as heating-rate.

It can be seen that the analytic solutions match well to the velocity profile (fig. IV.B.5-9) but begin to over-predict the velocity as the vehicle decelerates, resulting in exaggerated predictions for peak heating rate (fig. IV.B.5-11) and dynamic pressure (fig. IV.B.5-12) and an error in the predicted altitude of those peaks. Accurate prediction of the altitude at which peak

heating rate occurs would be required by a vehicle such as the Huygens probe[64] in order to determine the appropriate altitude at which to jettison its heatshielding.

The derived relations for the flight path angle (eqn.IV.B.3.3-6 and eqn.IV.B.4-8) are identical. Upon closer inspection it can be seen that they represent the Keplerian contribution to the motion only. This is borne out by the trajectories obtained (fig. IV.B.5-10) which match exactly the numerical code up to the point of flight path tip-over (see-below).

The vehicle drag coefficient (fig. IV.B.5-13) and axial acceleration (fig. IV.B.5-14) expressed as functions of altitude show that the analytic expressions have been successful in modelling the Mach number dependence of the drag coefficient. It should be noted that the effect of the dependence on Mach number diminishes for large half-cone angles and bluntness ratios (ratio of vehicle nose radius to base radius).

Examination of the validity of the analytic solutions does highlight one problem in the derived trajectory model. That is that the expressions for the flight path angle are unable to model a change in the sign of the gradient on the flight-path angle curve as shown in fig IV.B.5-10. This condition, referred to here as 'tip-over', occurs for entries where the entry velocity is so high as to produce an initial increase in the flight-path angle (it should be remembered that γ is measured relative to the local horizon). Once the vehicle has been sufficiently slowed the variation in flight path angle is bent by gravity towards the downward trend noted for slower entries. It is this effect which is missing from the inner solution to the motion.

The range of velocities for which this is a problem is small in comparison to the full range which can be modelled using the analytic relations, particularly as for higher velocities the vehicle does not lose enough speed before impact for tip-over to occur (fig.s IV.B.5-16). These hypervelocity solutions (fig.s IV.B.5-15 to -18) also exaggerate the discrepancy between the two drag coefficient models whilst showing the accuracy of the analytic predictions in modelling the motion and hence in obtaining

predictions for parameters such as dynamic pressure (fig. IV.B.5-17) and peak heating-rate (fig. IV.B.5-18).

The expressions incorporating the variable drag coefficient were found to provide an excellent match to the numerical code, down to entry speeds of $1km/s$ (fig. IV.B.5-19 & -20) and below showing the wide range of validity of the solutions. Whilst atmospheric entry is not likely to occur at these velocities, proposed release velocities for Martian penetrator-beacons[61] are as low as $138m/s$ and the geometric design of a penetrator vehicle is similar to that of the vehicle modelled.

Again, comparison of the derived solutions with *genL* running the US-62 atmosphere model (section II.C.2.3.4) shows how the analytic model stands up to a 'real-world' simulation. Fig. IV.B.5-21 & -22 show the errors obtained for the predicted flight-path angle and velocity respectively when compared with *genL* running either the US-62 or the standard exponential model.

Fig. IV.B.5-21 shows that the variation in flight-path angle errors to match very closely to that obtained in comparison with the exponential model. This is an excellent result, but perhaps, somewhat expected given the nature of the trajectory modelled.

Fig. IV.B.5-22 also shows the expected result whereby the form of the relative error curve remains the same but its magnitude has increased. The form of the curve is explained in the same way as before whilst the increase in the magnitude of the errors is due to the discrepancy between the density profiles for the US-62 and exponential atmospheres (fig. II.C.2.3.4-1).

Again the results are of a very high quality. In spite of the apparently large increase in magnitude the average error in the velocity predictions never exceeds 0.1% of the vehicle velocity.

In order to compare the computing power required for the two atmospheric entry models the analytic code was benchmarked for CPU time and required storage space against a minimal simulation formulated in spherical polar co-ordinates which is representative of an onboard numerical propagator.

(This is the only occasion results for this simulation are presented. All other simulation results were obtained with the

full *genL* simulation, including the graphs presented in this section).

The results for a $200km$ to ground trajectory with updates every $500m$ are given in table IV.B.5-1.

It should be borne in mind that these are total times and as such flatter the numerical simulation. Each data set within the analytic solution requires milliseconds to evaluate and this can be done as and when required. Using the numerical approach each point requires the evaluation of previous points until the final point which relies on all previous evaluations. With this in mind, it can be seen that the analytic approach is capable of providing real-time data to an onboard system.

	Total CPU Time (secs)	Storage (kbytes)
Analytic Model	1.12	1.5
Numerical Simulation	4.78	10.5
Improvement	66%	86%

table IV.B.5-1 Comparison of codes

This then is the potential such analytic representations possess. Important data is obtained quickly and accurately without excessive use of computing power, freeing space for other tasks. Indeed the simplicity of the analytic expressions means that predictions for the entire trajectory could be produced using a simple spreadsheet package for mission design. Logically the computing power made available by the simplification of guidance and control systems could be utilised in expanding the experimental and observational capabilities of missions, or performing other operational functions.

In the results that follow 'absolute' refers to the modulus of the error and 'average' to the absolute error time-averaged over an entire trajectory for the initial conditions indicated. Heating rate values are for the nosetip or stagnation point heating rate.

All runs are from an initial altitude of $200km$ for the vehicle described in Appendix V.

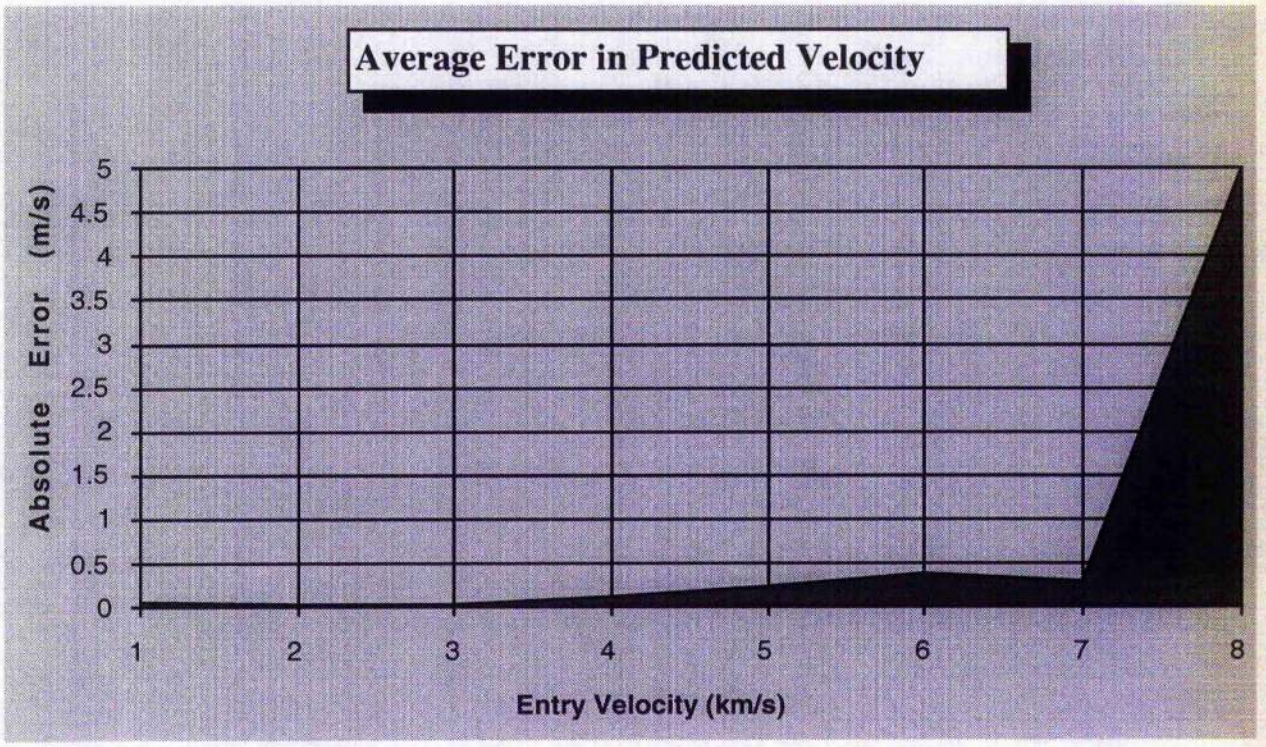

fig IV.B.5-1 Ballistic Entry : Entry Angle = -6°

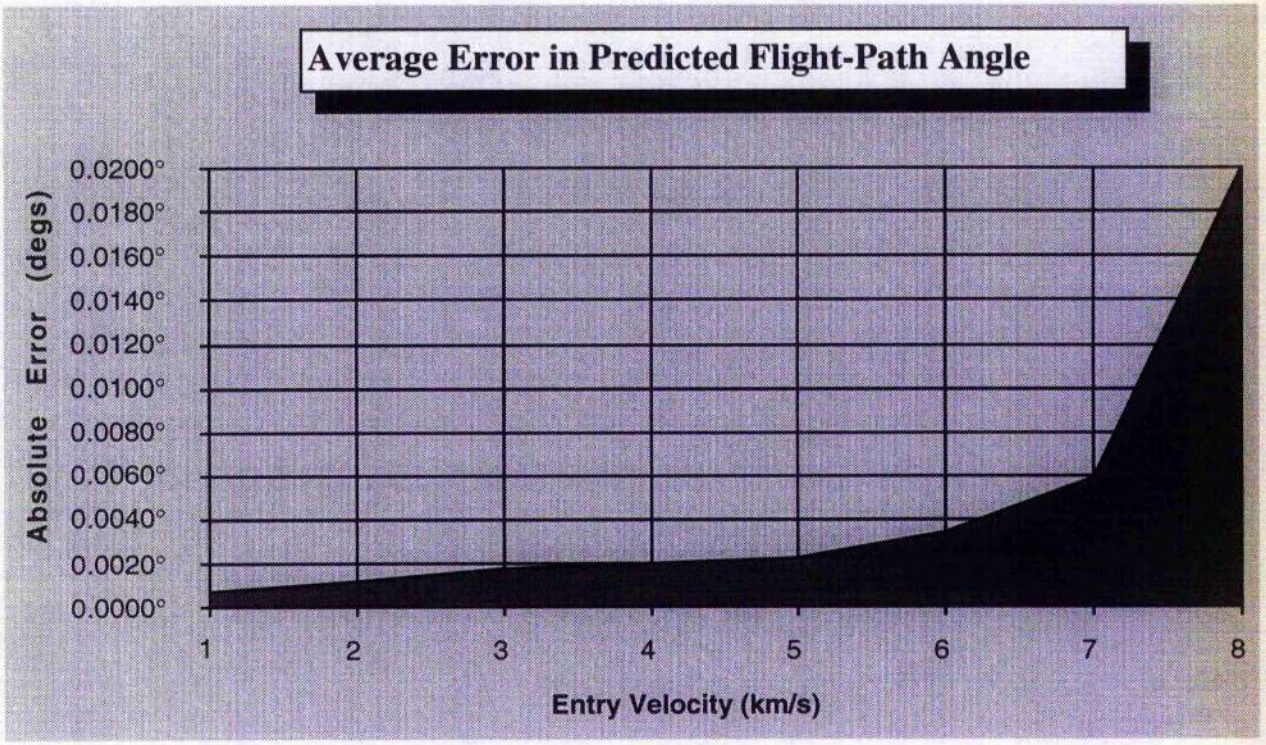

fig IV.B.5-2 Ballistic Entry : Entry Angle = -6°

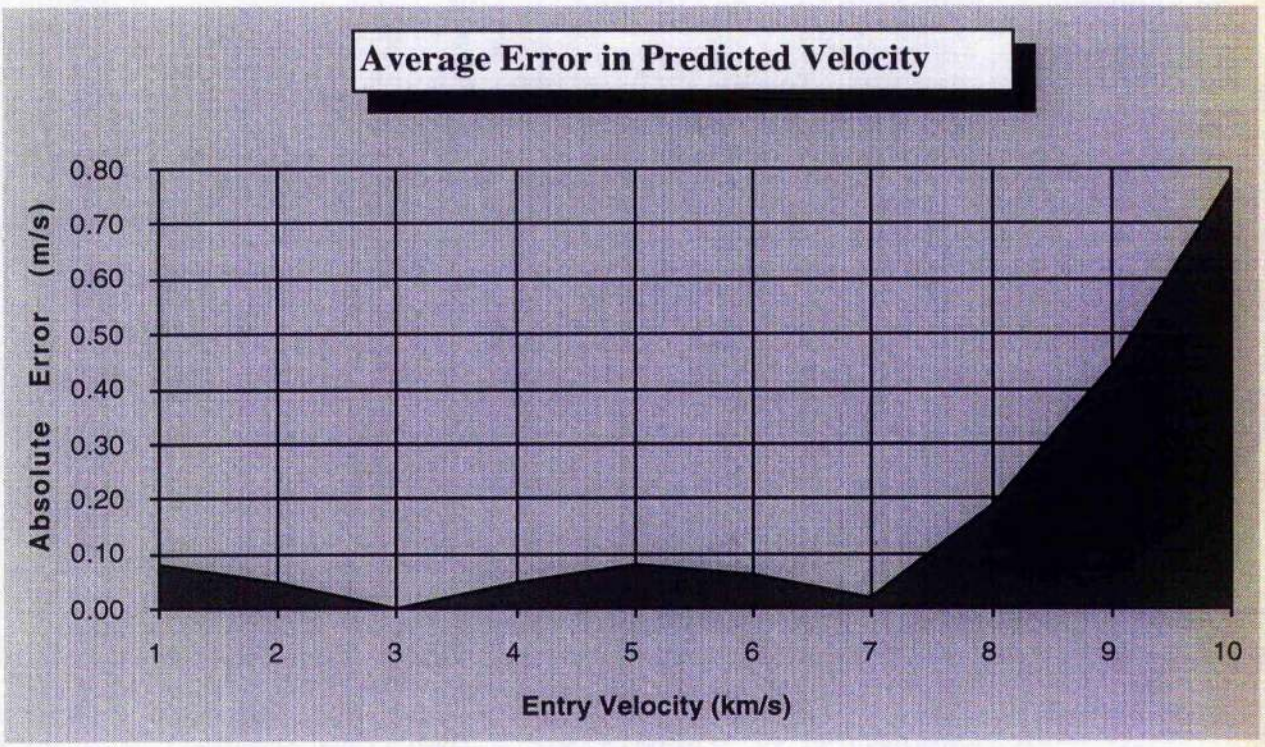

fig IV.B.5-3 Ballistic Entry : Entry Angle = -16°

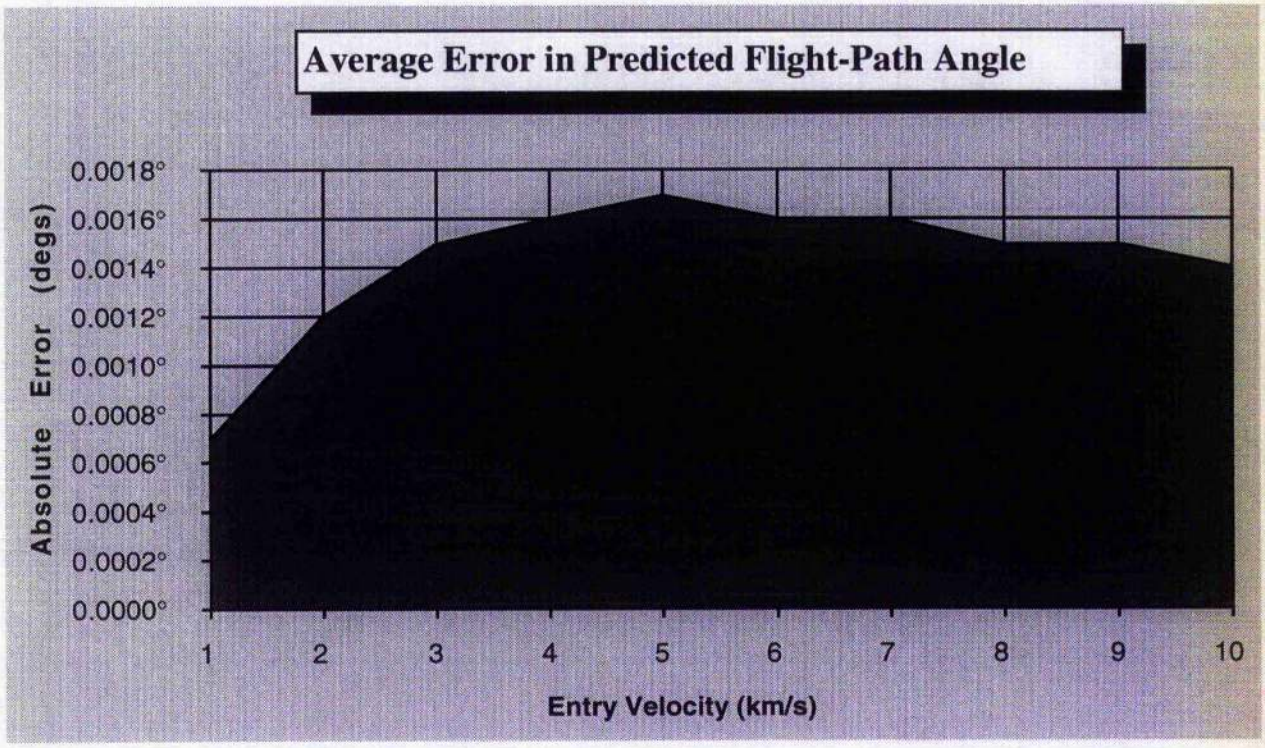

fig IV.B.5-4 Ballistic Entry : Entry Angle = -16°

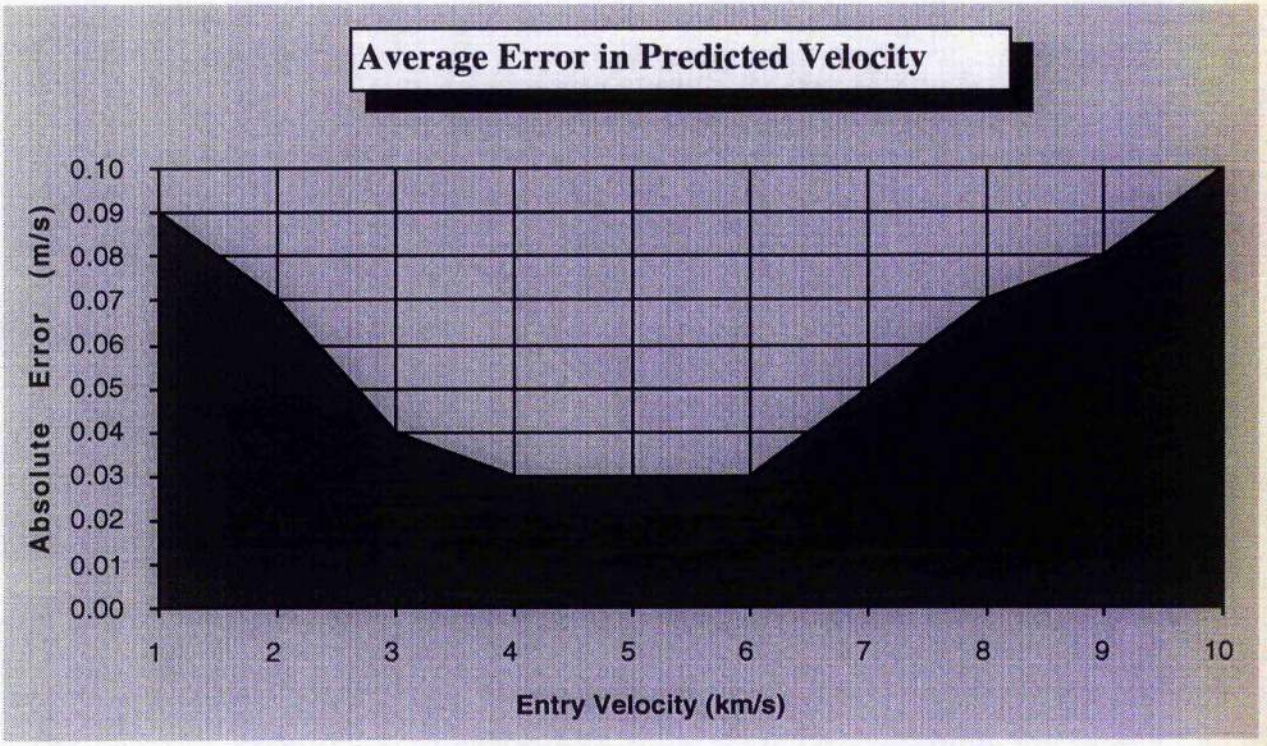

fig IV.B.5-5 Ballistic Entry : Entry Angle = -30°

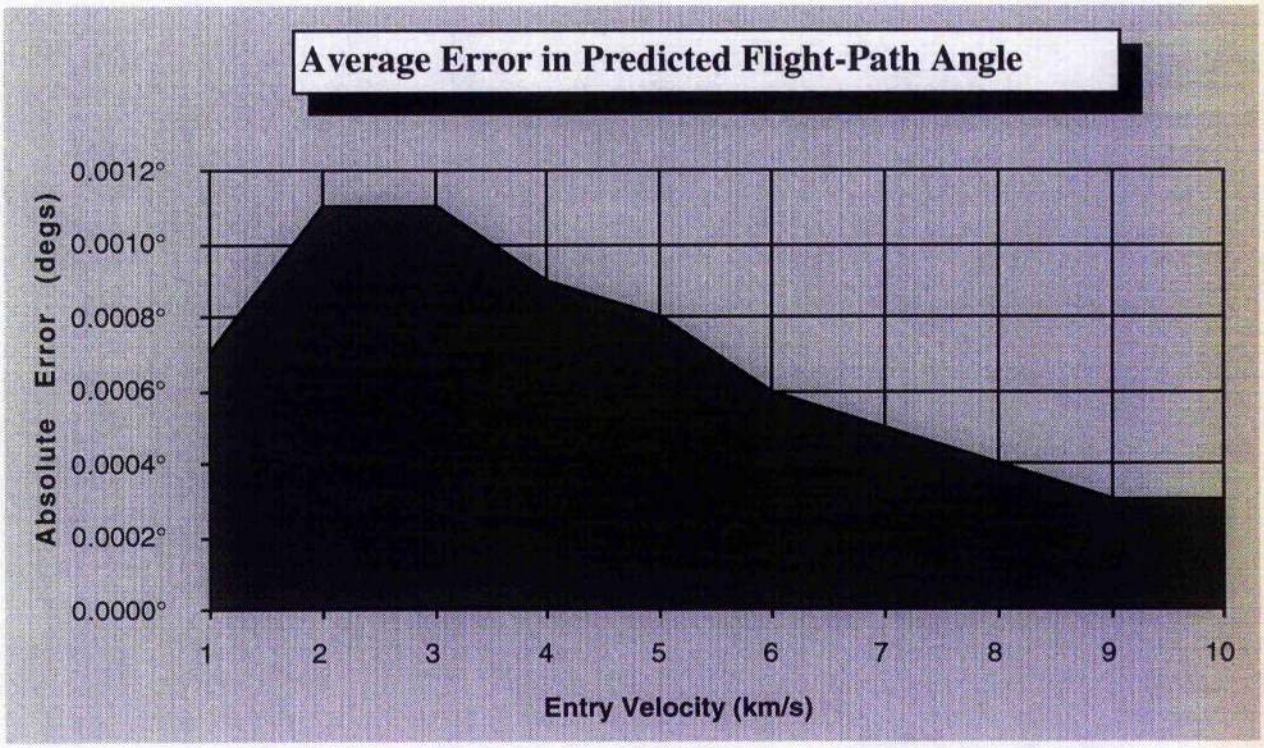

fig IV.B.5-6 Ballistic Entry : Entry Angle = -30°

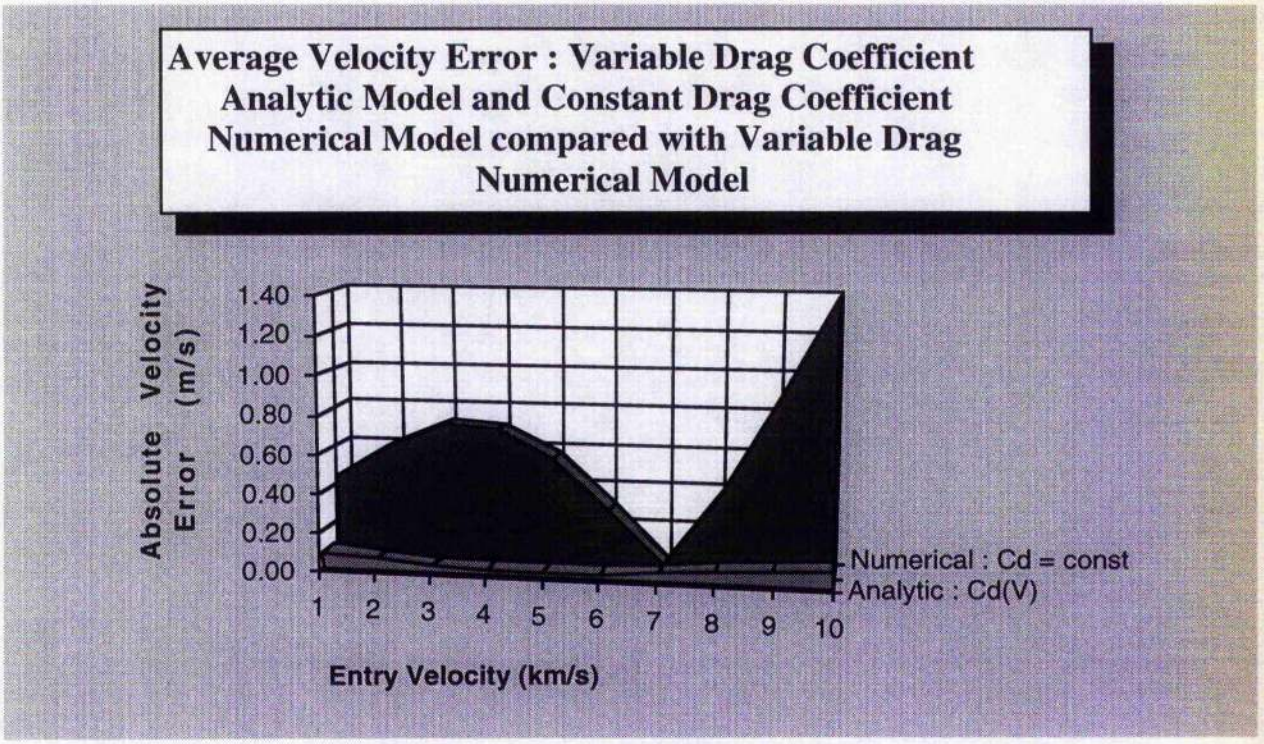

fig IV.B.5-7 Ballistic Entry : Entry Angle = -30°

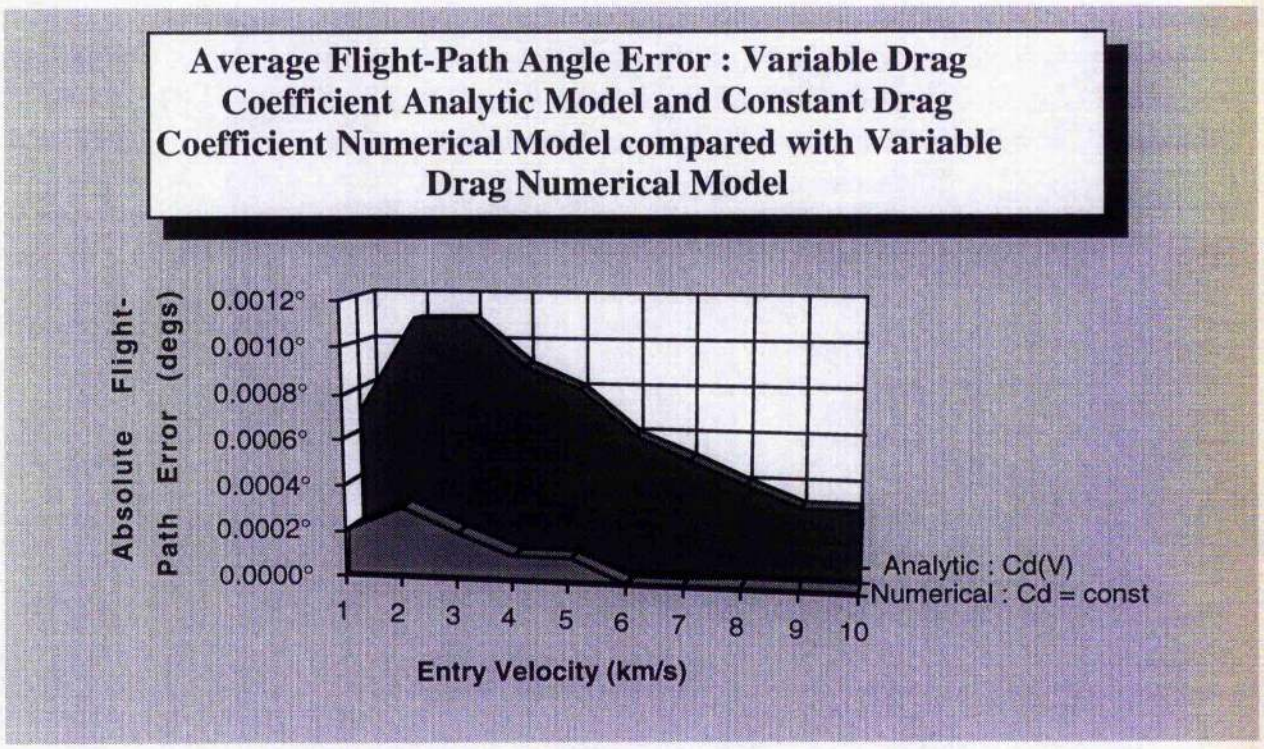

fig IV.B.5-8 Ballistic Entry : Entry Angle = -30°

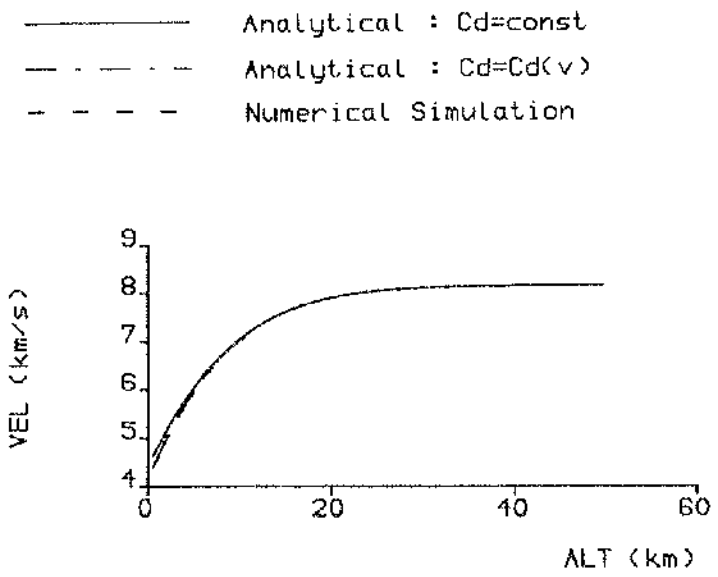

Fig. IV.B.5-9 : Velocity/Altitude Profile
Ballistic Entry : Entry Angle = -50°, Entry Velocity = 8km/s

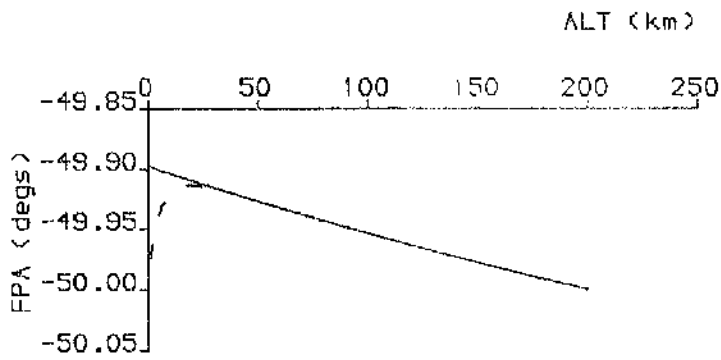

Fig. IV.B.5-10 : Flight-path Angle/Altitude Profile
Ballistic Entry : Entry Angle = -50°, Entry Velocity = 8km/s

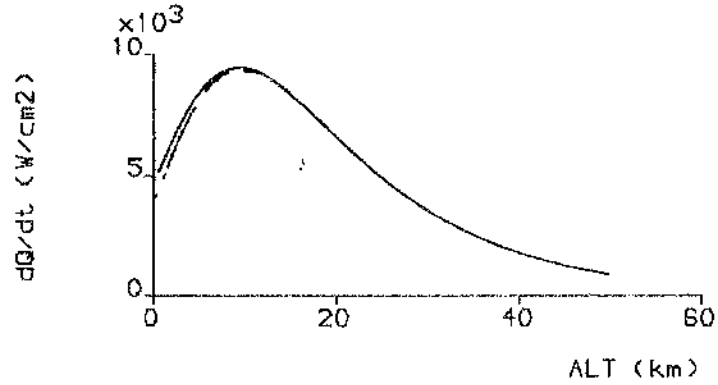

Fig. IV.B.5-11 : Nosetip Heating Rate/Altitude Profile
Ballistic Entry : Entry Angle = -50°, Entry Velocity = 8km/s

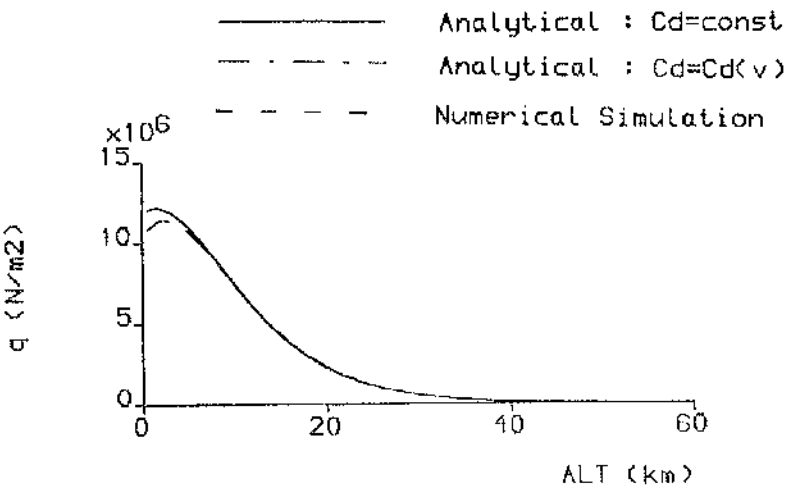

Fig. IV.B.5-12 : Dynamic Pressure/Altitude Profile
Ballistic Entry : Entry Angle = -50°, Entry Velocity = 8km/s

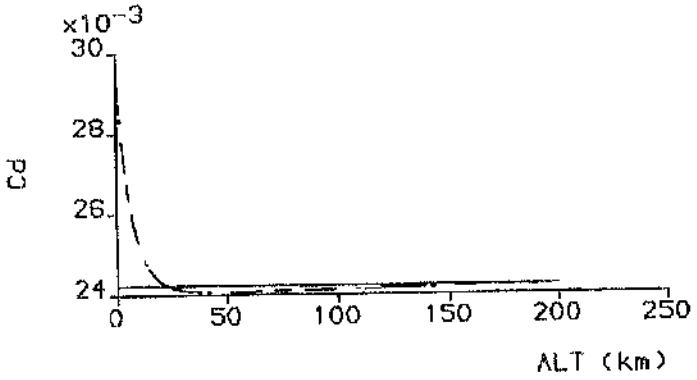

Fig. IV.B.5-13 : Drag Coefficient/Altitude Profile
Ballistic Entry : Entry Angle = -50°, Entry Velocity = 8km/s

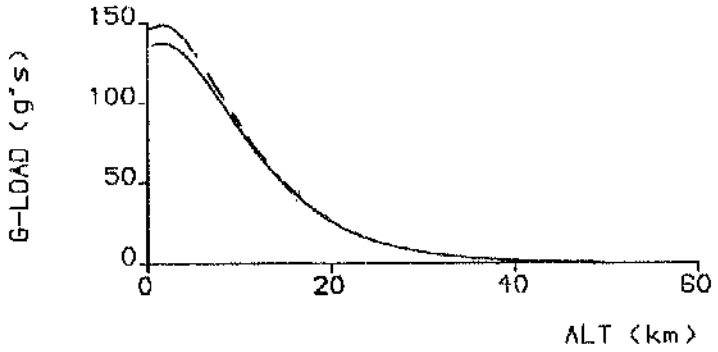

Fig. IV.B.5-14 : Axial Deceleration/Altitude Profile
Ballistic Entry : Entry Angle = -50°, Entry Velocity = 8km/s

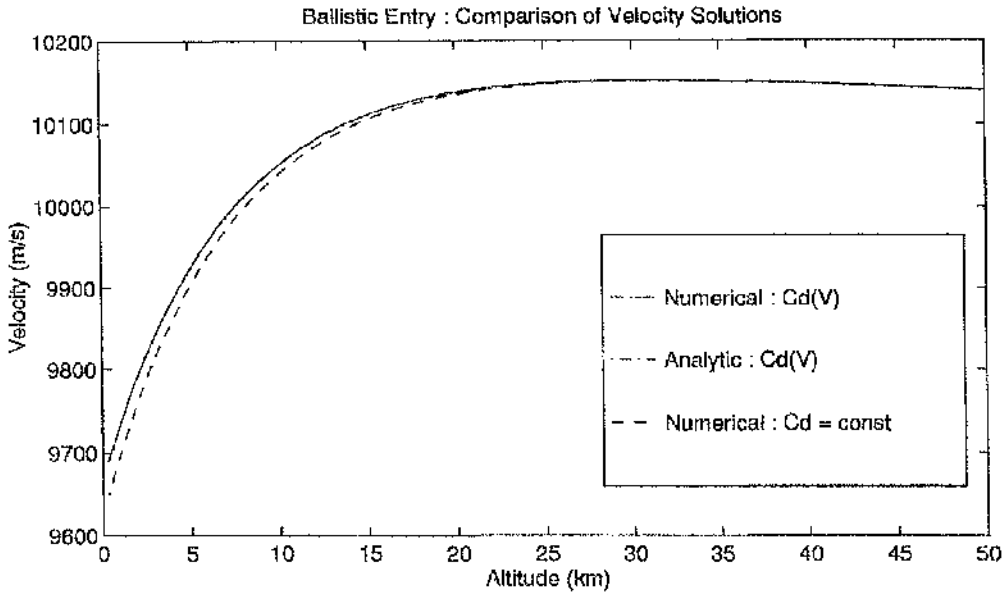

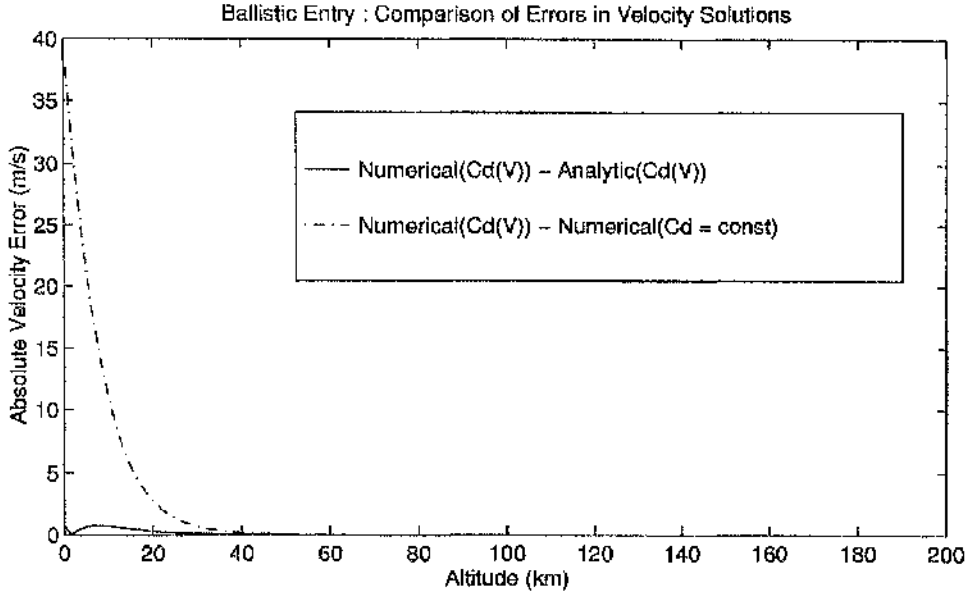

Fig. IV.B.5-13 Ballistic Entry : Entry Angle = -30°, Entry Velocity = 8km/s

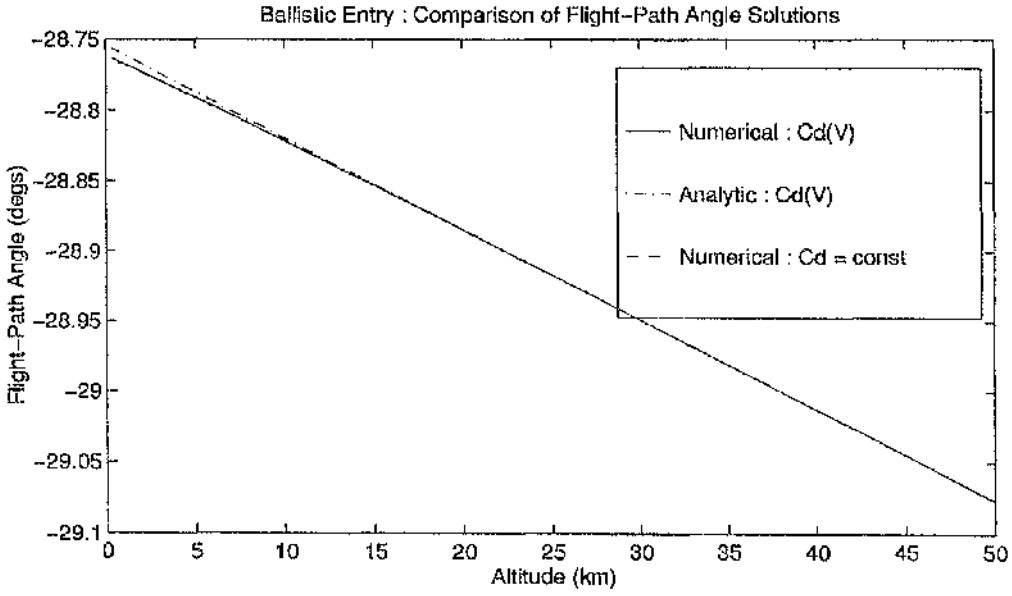

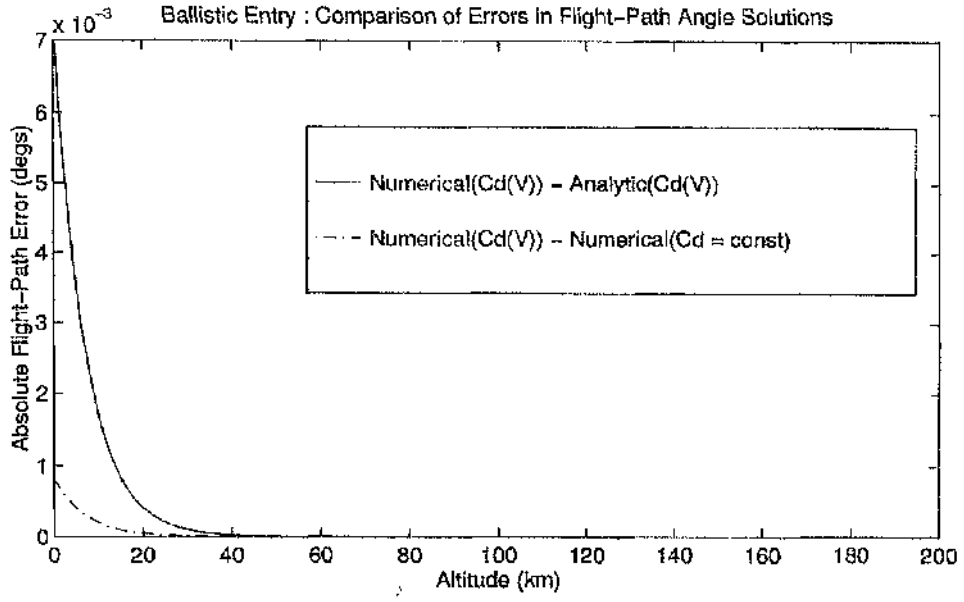

Fig. IV.B.5-16 Ballistic Entry : Entry Angle = -30°, Entry Velocity = 8km/s

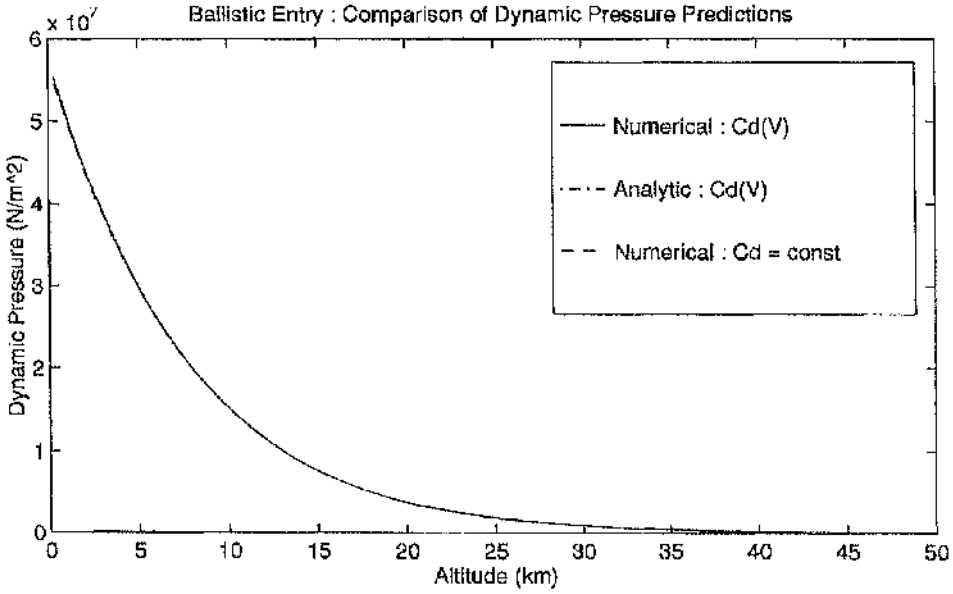

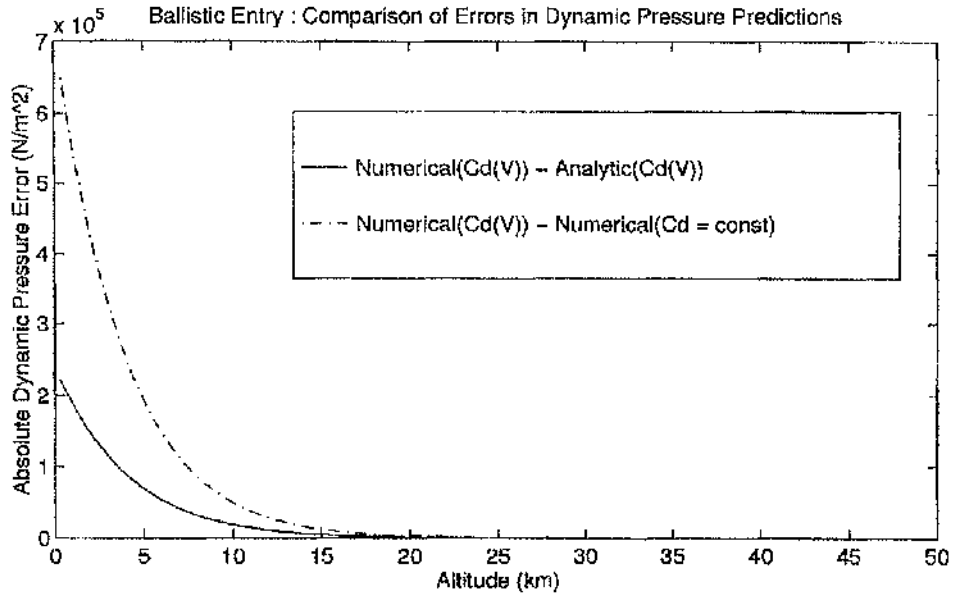

Fig. IV.B.5-17 Ballistic Entry : Entry Angle = -30°, Entry Velocity = 8km/s

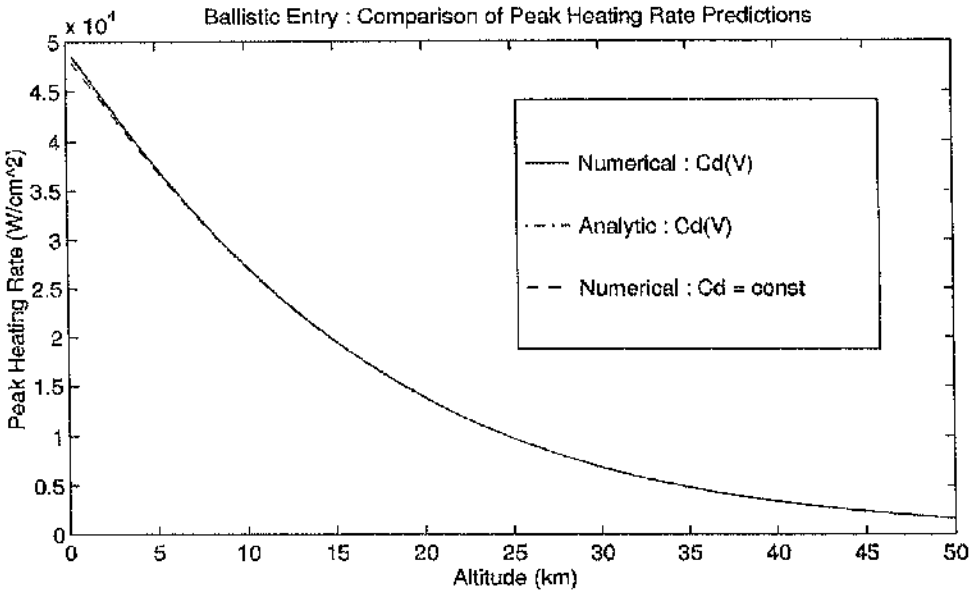

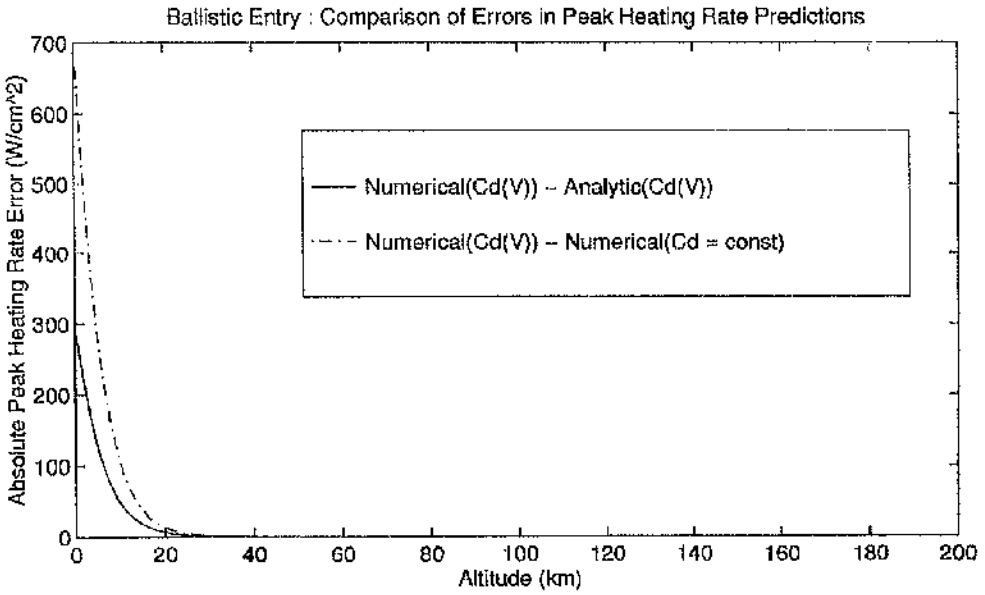

Fig. IV.B.5-18 Ballistic Entry : Entry Angle = -30°, Entry Velocity = 8km/s

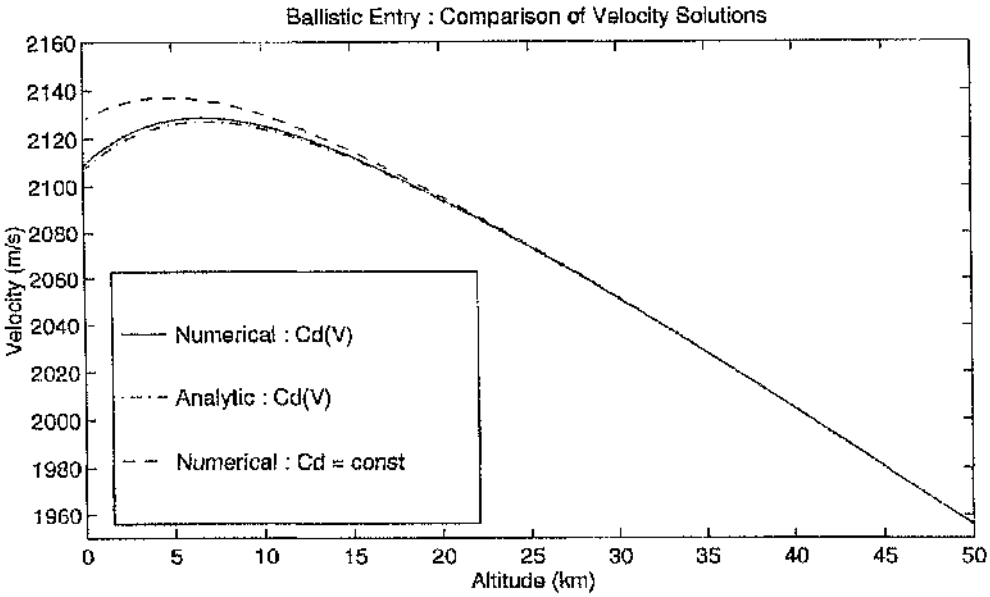

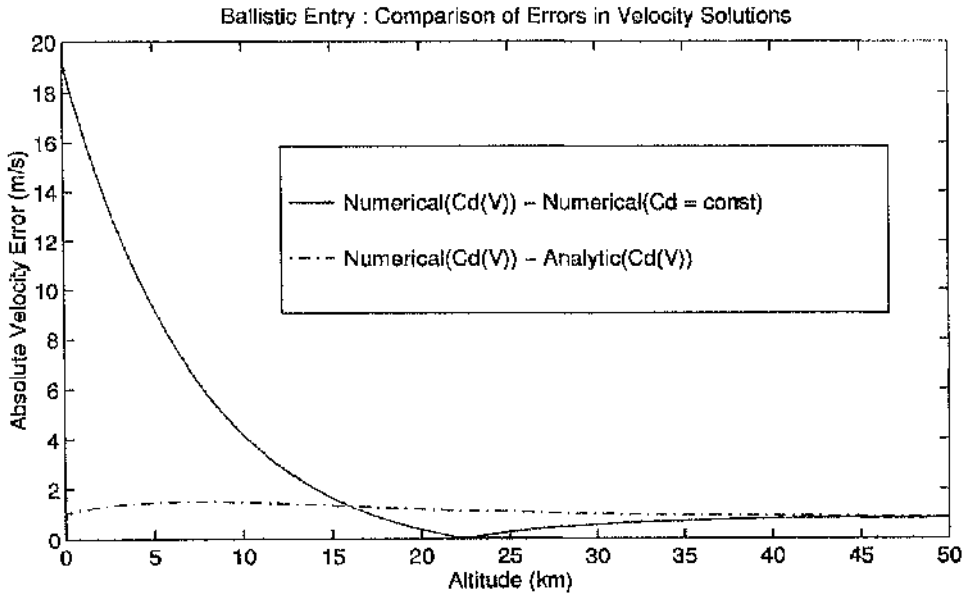

Fig. IV.B.5-19 Ballistic Entry : Entry Angle = -30°, Entry Velocity = 1km/s

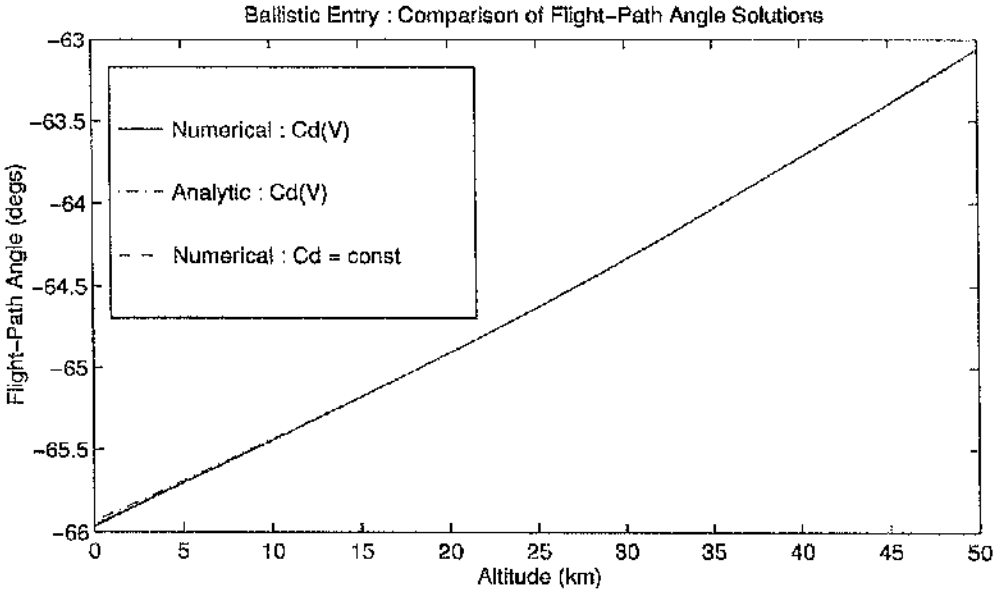

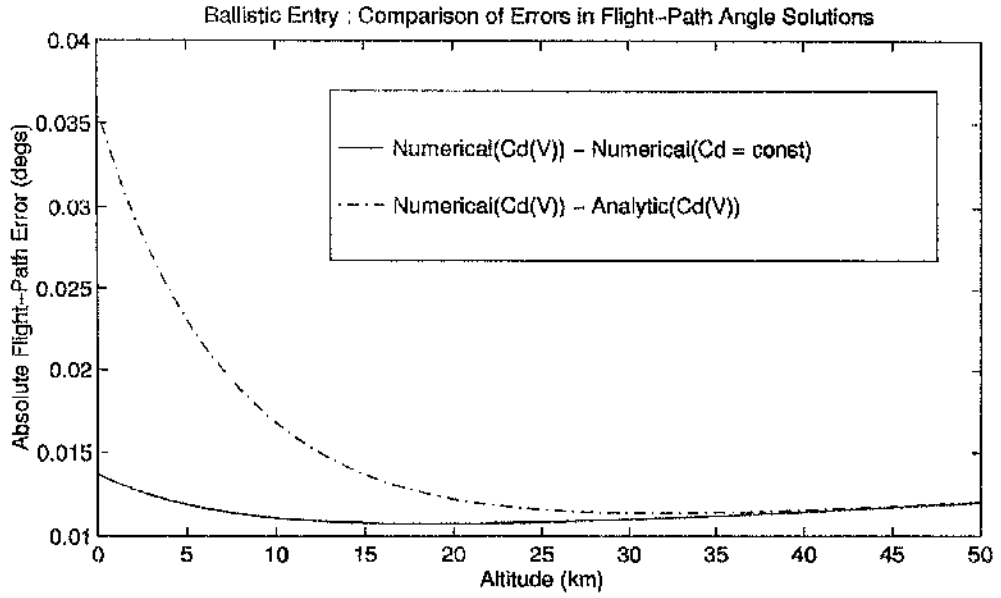

Fig. IV.B.5-20 Ballistic Entry : Entry Angle = -30°, Entry Velocity = 1km/s

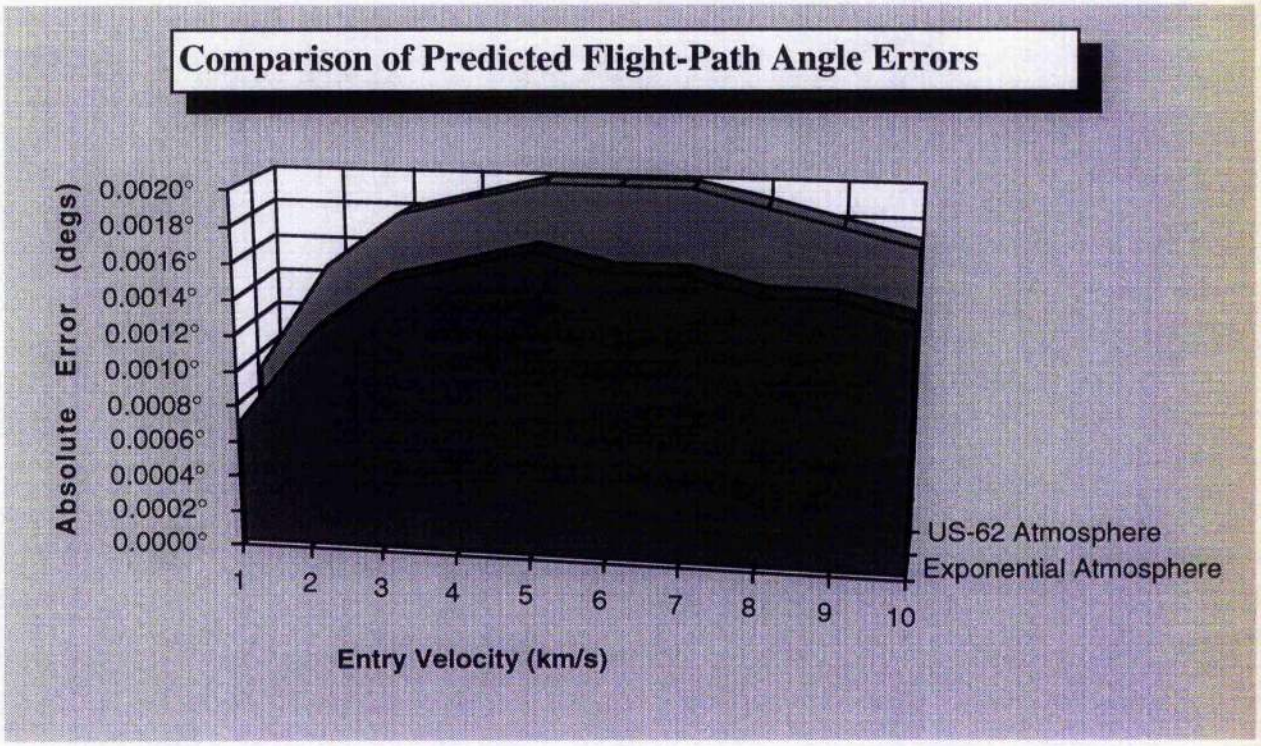

Fig. IV.B.5-21 Ballistic Entry : Entry Angle = -16°

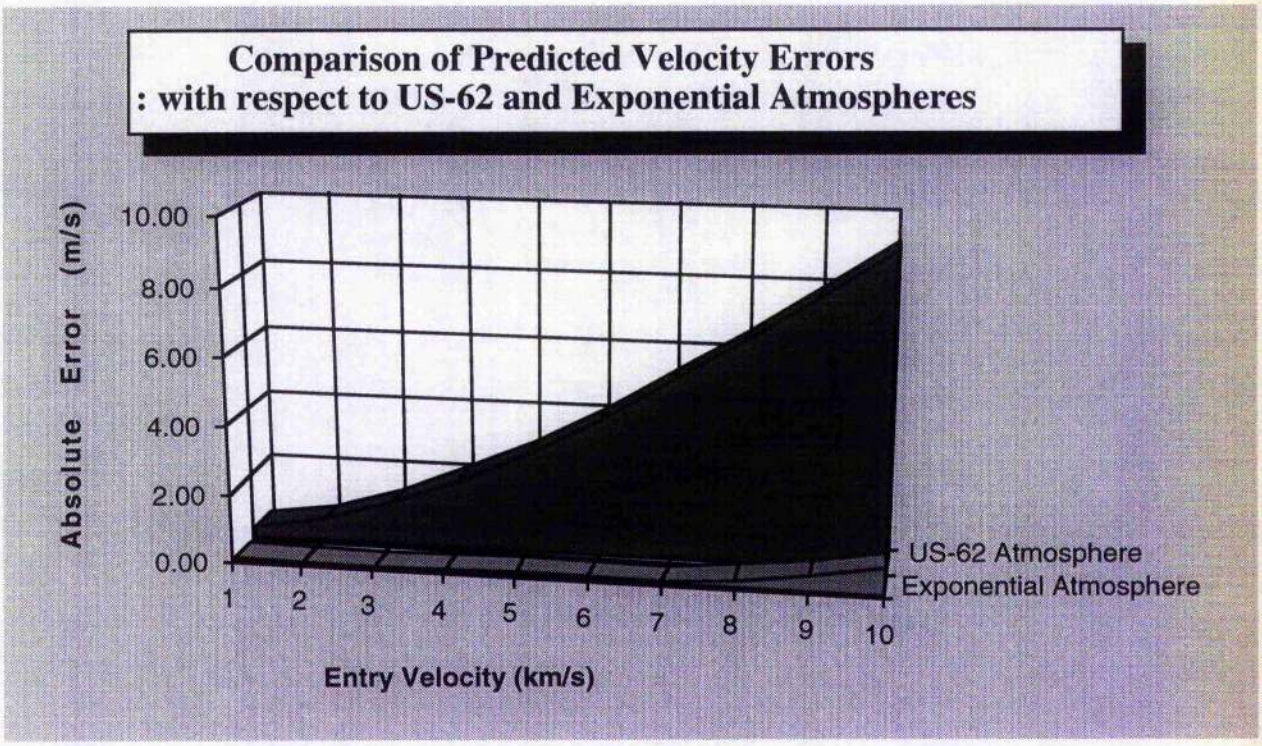

Fig. IV.B.5-22 Ballistic Entry : Entry Angle = -16°

IV.C. Ballistic Launch

The direct launch concept moves away from the traditional staged launch vehicle approach and towards the launch tube, within which a projectile containing the payload is accelerated up to orbital speeds. The projectile is targeted for a particular apogee and on achieving said apogee an impulsive burn places the payload into low Earth orbit (LEO).

Direct launch is seen as a means of reducing the costs involved in transferring payloads to orbit. Of particular concern is the transfer of acceleration insensitive payloads, such as raw materials and essentials like oxygen and water, which might be used in construction and maintenance either onboard the Space Station or by a future Lunar Base.

One of the major factors which have so far prevented the development of a large-scale infrastructure in space is the cost of transferring payloads to orbit, conventional launch requiring the transfer of a launch vehicle into space with payload release occurring after atmospheric exit.

With a direct launch the need for a launch vehicle is removed and consequently the total mass to be inserted into LEO is reduced. Payload mass fractions as high as 70% are predicted for successful launch systems and costs could be reduced to around $\$500/kg$ (payload to LEO) compared with $\$20{,}000/kg$ (payload to LEO) for the shuttle[68].

A number of different approaches have been presented as potential direct launch systems, varying from electromagnetic rail guns[69] to ram accelerators[70] to light gas guns[68].

The launch projectile itself can either be designed for low-drag or low-ablation. For equivalent vehicles the low-drag vehicle will lose more mass whilst requiring a lower launch energy.

The most promising of the current proposals for a direct launch system is the ram accelerator[70,48].

The ram accelerator concept (or 'ramjet-in-tube') considers a launch tube filled with a pressurised fuel-air mixture in which resides a projectile shaped like the centre-body of a ramjet

engine. Initial acceleration is provided by a conventional gas gun and then by external ignition of the fuel-air mix behind the projectile. At around $2.5km/s$ the projectile passes into a fuel-air mixture with a lower sonic velocity causing a sudden jump in the mach number. The vehicle then ignites fuel as it passes through an oblique compression wave which is formed by a sudden rise in the vehicle diameter aft of the its centre-point. The 'bump' is located such that the shock detonates the gas mixture behind the vehicle. The rapid expansion of the mixture provides the necessary forward thrust.

The estimated size of the launch tube required to accelerate a projectile up to orbital velocity is almost $4km$ and Kaloupis and Bruckner[48] propose Mount Kenya as a suitable launch site. Clearly the scale of the operation is large but the economies are there to be gained.

Ground tests for a light gas gun have been carried out at Lawrence Livermore National Laboratory in California where small projectiles have been launched to speeds in excess of $4km/s$[68], whilst scale ram accelerator tests have achieved velocities over $2.4km/s$[48].

IV.C.1. Solution by matched asymptotic expansions

Solutions for a direct launch vehicle are obtained in the same way as for the atmospheric entry case, the non-dimensional equations of motion differing only in the sign of the flight path angle term from eqn. IV.B.3-2. In this case, the physical root is now the positive root as the flight path angle is defined as positive upwards from the horizon.

Solutions are developed for the aerodynamic and Keplerian regions as before. In this case, however, the initial conditions for the motion are set by the launch, thus defining the inner integrations constants from which the outer constants are found through the matching process.

The expressions for the outer region are again the Keplerian relations given in eqn. IV.B.3.1-7 & IV.B.3.1-8. As before the flight path angle solution for the inner region is constant; viz.,

$$\tilde{\omega}_0 = \tilde{\omega}_{00} = \cos\gamma_i \qquad \textbf{IV.C.1-1}$$

The solution for the velocity term is now

$$\tilde{u}_o = \left\{ \frac{-\tilde{b}n\bar{\rho}_o}{\sqrt{1-\tilde{\omega}_{oo}^2}} \exp\left(-\tilde{h}\right) + \tilde{u}_{oo} \right\}^{-1/n} \qquad \textbf{IV.C.1-2}$$

and the constant of integration is found by application of the initial conditions to be

$$\tilde{u}_{oo} = \frac{-\tilde{b}n\bar{\rho}_o}{\sqrt{1-\tilde{\omega}_{oo}^2}} \exp\left(-\tilde{h}_i\right) + \tilde{u}_i^{-n} \qquad \textbf{IV.C.1-3}$$

Matching the inner and outer solutions the outer constants are found to be

$$u_{oo} = \tilde{u}_{oo}^{-1/n} - 2 \qquad \textbf{IV.C.1-4}$$

with

$$\tilde{\omega}_{oo} = \frac{\omega_{oo}}{\sqrt{u_{oo}+2}} \qquad \textbf{IV.C.1-5}$$

The common solutions take the same form as before (eqn. IV.B.3.3-3 & IV.B.3.3-4) and the resulting composite solutions are given below.

$$u = \frac{-2h}{1+h} + \left\{ \frac{-\tilde{b}n\bar{\rho}_o}{\sqrt{1-\tilde{\omega}_{oo}^2}} \exp\left(-\tilde{h}\right) + \left(u_{oo}+2\right)^{-n} \right\}^{-1/n} \qquad \textbf{IV.C.1-6}$$

$$\omega = \frac{\omega_{oo}}{\sqrt{u_{oo}(1+h)^2 + 2(1+h)}} \qquad \textbf{IV.C.1-7}$$

The constant drag coefficient solutions are found to be identical in form to eqn.s IV.B.4-7 & IV.B.4-8 with the

integration constants being obtained by application of the initial conditions to the inner solution and matching as before.

IV.C.2. Results

The derived trajectory predictions are now compared with results from the *genL* numerical simulation in order to assess their value in representing the motion. Fig.s IV.C.2-1 to -3 show the comparisons between the numerical and analytical solutions obtained for velocity, flight-path angle, and drag-coefficient, respectively, for an $8km/s$ launch at 30° to the horizontal. The launch vehicle used is of the ram accelerator type described in Appendix V and is derived from Kaloupis and Bruckner[48].

The simulation incorporates both constant and velocity dependent drag coefficient models in order to compare like with like and also to assess the validity of a constant drag coefficient assumption for a hypervelocity transatmospheric motion.

In contrast to the re-entry solutions, for the launch vehicle the flight path angle solutions (fig. IV.C.2-2) match well over the entire trajectory. This agrees with expectations as the variation in flight path angle is primarily a result of gravity bending the trajectory towards the Earth and this effect is modelled by the outer solution. For a re-entry vehicle atmospheric drag slows the vehicle to such an extent that gravity can no longer be ignored in the inner solution, invalidating our operating assumption, and so the flight path angle solution loses validity towards the end of the trajectory. For a ballistic launch, however, the vehicle travels out through the atmosphere away from the region of rapid change, such that, in the analysis of the projectile, the motion is actually in the direction of greater validity of solution; away from the approximation to the atmospheric motion and into the exact solution of a Keplerian orbit.

As anticipated the velocity solutions (fig. IV.C.2-1) provide an excellent match over the entire range of motion.

By examining how the accuracy of the solutions varies over a variety of launch velocities and flight-path angles we are able to determine a range of validity for the analytic solutions. Fig.s IV.C.2-4 to -13 show the average errors in the velocity and flight-path angle predictions and the average percentage error in the velocity predictions over a range of launch velocities from 1 to $9km/s$ for 16°, 22°, and 30° launches. Because of the relatively small magnitude of the flight-path angle percentage errors are not truly representative of the accuracy of the predictions. To justify this we consider the trajectory as it tends towards apogee. Towards this limit the flight path angle tends towards zero and consequently any error tends towards an infinite percentage error. This is illustrated in the absolute error shown in fig. IV.C.2-2.

In each case, the error in the velocity solution is found to have a local minimum at a launch velocity between 6 and $7km/s$. Broadly speaking, this occurs at the lowest value of the launch velocity which results in an apogee exceeding $300km$. The following explanation for this behaviour is offered:

For low-speed trajectories which do not achieve atmospheric exit the aerodynamic loads will be sufficiently low that gravitational forces cannot be completely ignored; thereby invalidating the assumption employed in obtaining the inner solution. This will lead to a decrease in accuracy with decreasing launch velocity.

For higher velocities, after exit is achieved the analytic and numerical solutions are effectively following separate orbits dictated by their exit conditions. Consequently one velocity solution will reach its minimum (at apogee) at a greater altitude than the other creating the discrepancy observed.

Launches with apogees in the range $300-500km$ are deemed to fall between these two extremes resulting in a higher degree of accuracy.

It is a fortunate coincidence that this range includes the proposed altitude for International Space Station Alpha, allowing highly accurate analytic modelling of direct launch trajectories for supply to the station.

Analysis of these trajectories using the analytic relations shows the potential benefits of direct launch. Consider a direct launch to Space Station orbit ($436.48km$):

Using the analytic relations developed, for a launch angle of 16° a launch velocity of $7.15km/s$ results in a predicted apogee of $434.20km$ and a required ΔV of $1.824km/s$ to achieve space station orbit from there. The fuel requirements for this manoeuvre are roughly half the vehicle mass ($923.87kg$). Using the masses of the other vehicle components given in Appendix V the resulting payload-mass fraction is 21.56%. Accurate numerical results obtained from *genL* put the final ΔV requirement at $1.825km/s$ for the same launch conditions. This demonstrates the success of the analytic predictions in providing highly accurate trajectory data whilst requiring a minimum of computing power. It can be seen that, using the derived analytic relations, direct launch trajectory analysis may be quickly carried out on a simple spreadsheet program without compromising the accuracy of the analysis, making them a powerful design tool.

Whilst acknowledging that an "optimum range of validity" exists, the relative error was still found not to exceed 0.10% for launches to apogees of over $5000km$.

The local maximum which occurs at lower launch velocities is somewhat misleading. The predictions at these lower velocities err both high and low of the numerical solutions crossing at around the midpoint of the altitude range, making these results more of a happenstance than an indication of increasing accuracy. This explanation is supported by an examination of the flight-path angle solutions, whose maximum error occurs without fail at the lowest examined launch velocity whilst also exhibiting the local minimum found in the velocity solutions.

Not surprisingly the accuracy of the solutions improves with increasing launch angle (fig. IV.C.2-13), a steeper launch resulting in a shorter atmospheric transit duration for the same launch velocity.

As for the entry case, comparison of the derived solutions with *genL* running the US-62 atmosphere model (section II.C.2.3.4) shows how the analytic model stands up to a 'real-world' simulation. Fig. IV.C.2-14 & -15 show the errors obtained for the predicted flight-path angle and velocity respectively when compared with *genL* running either the US-62 or the standard exponential model.

Fig. IV.C.2-14 shows that the variation in flight-path angle errors has lost its form and no real conclusions can be drawn about the form of this graph other than that it is simply the result obtained. Given that, the errors never exceed those found for comparison with the exponential model, and in some cases the error is reduced.

Fig. IV.C.2-15 shows the more expected result whereby the form of the relative error curve remains the same but its magnitude has increased. The form of the curve is explained in the same way as before whilst the increase in the magnitude of the errors is due to the discrepancy between the density profiles for the US-62 and exponential atmospheres (fig. II.C.2.3.4-1).

Again the errors are not large but do illustrate the difficulty in obtaining precise trajectory predictions when the exact atmospheric conditions to be encountered are unknown. This fact, combined with the inherent simplicity of the analytic relations, makes the use of the derived relations very attractive in the context of a preliminary design tool.

In assessing the validity of the constant drag coefficient assumption we consider the 30° launch case. For this steeper launch the atmospheric transit time is shorter and it follows that the difference between the constant and velocity dependent solutions should be minimised. Fig.s IV.C.2-16 to -18 show the comparison between the errors observed using the velocity dependent coefficient modelled by the analytic solution and a constant drag coefficient numerical solution. Both sets of errors are with respect to a numerical solution employing the velocity dependent drag coefficient model.

A quick look at the results obtained suggests that the inclusion of the improved drag model has a significant effect on

the accuracy of the results. This would seem to justify the use of the velocity dependent model.

The local minima observed in the constant coefficient solution at $7km/s$ occur as it crosses the actual solution, the errors being positive before and negative after. Again, this gives the illusion of increasing accuracy rather than any real improvement.

The observed improvement over the constant drag coefficient numerical simulation supports the case for utilising accurate analytic solutions in onboard guidance systems, be it as a replacement for sensors and other instrumentation, as a monitor for these systems, or for onboard updating of the vehicle state vector. After all, the improvement over the constant drag coefficient solutions has been obtained with a significant reduction in the amount of computer code and hence computing power.

The primary use for direct launch, however, would seem to be as a highly accurate, computationally efficient design tool.

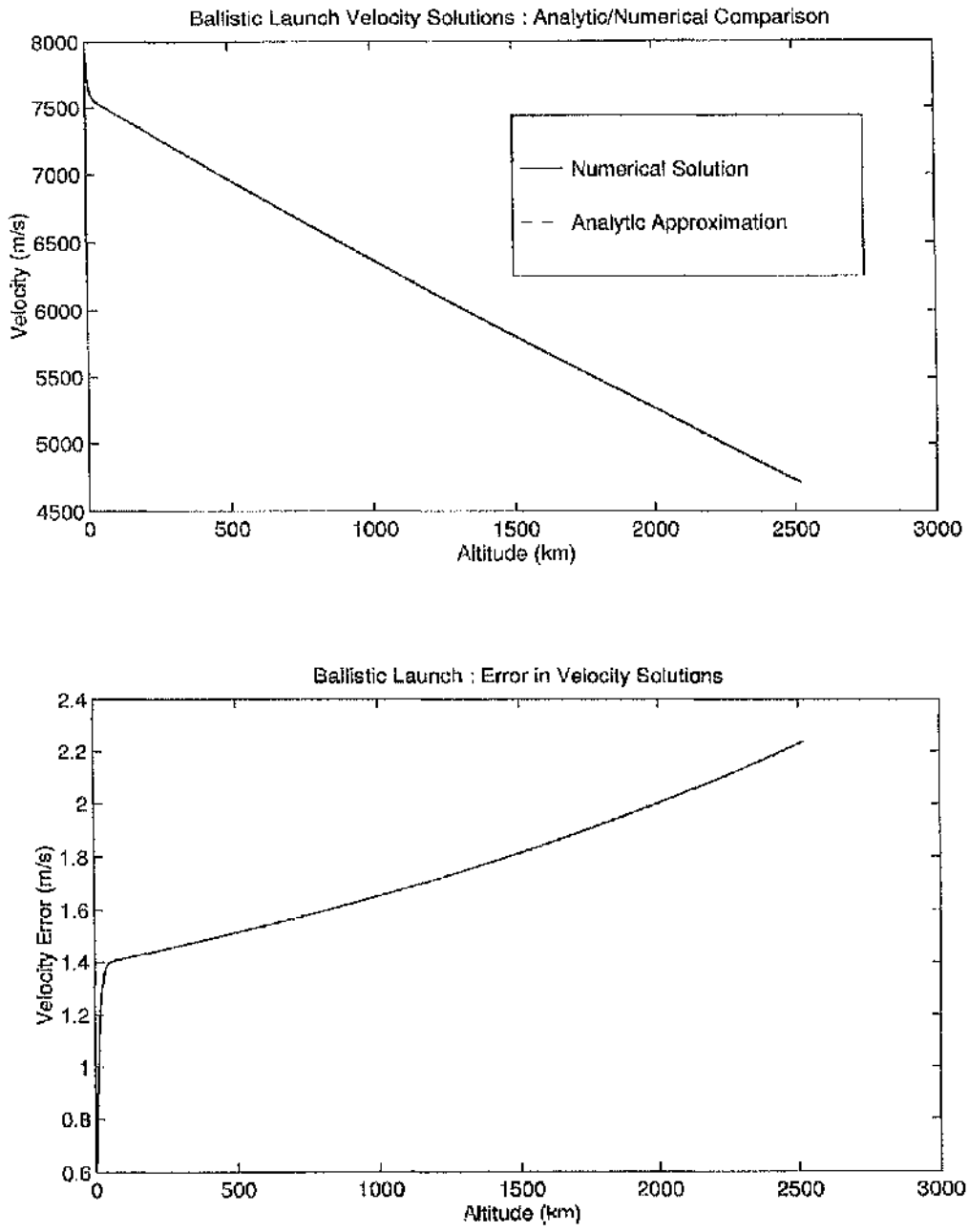

Fig. IV.C.2-1 Ballistic Launch : Launch Angle = 30°, Launch Velocity = 8km/s

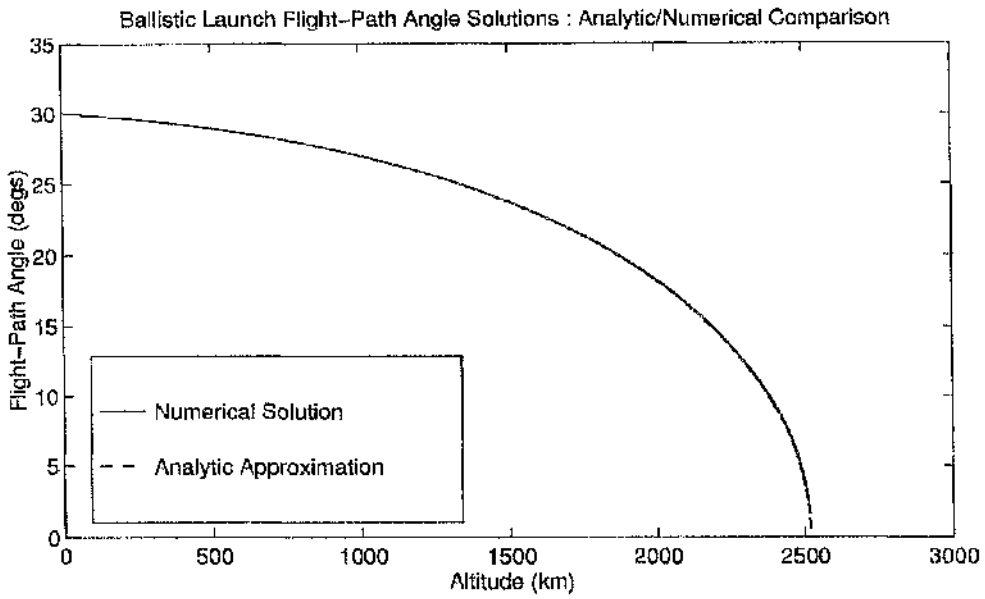

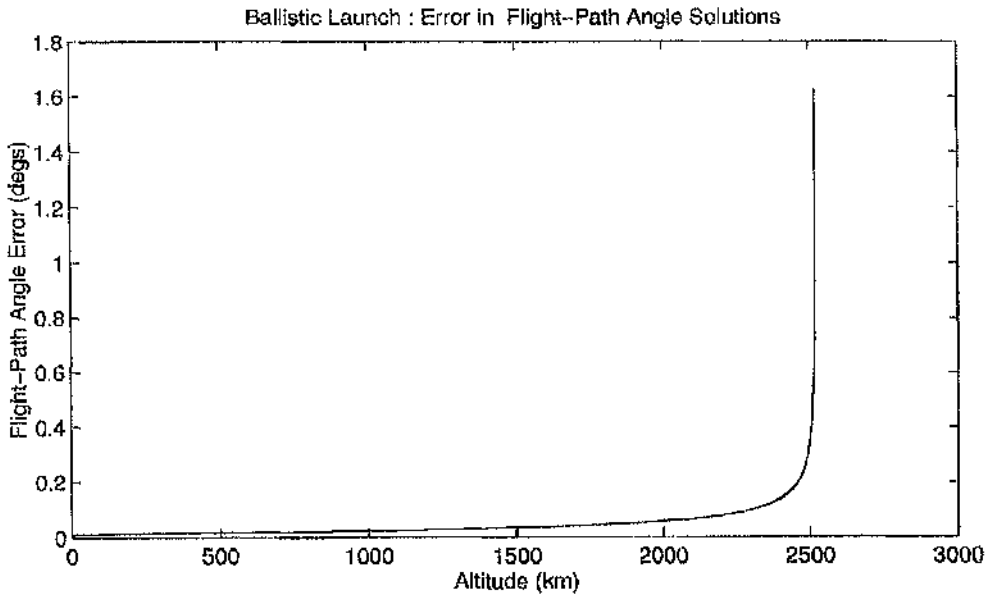

Fig. IV.C.2-2 Ballistic Launch : Launch Angle = 30°, Launch Velocity = 8km/s

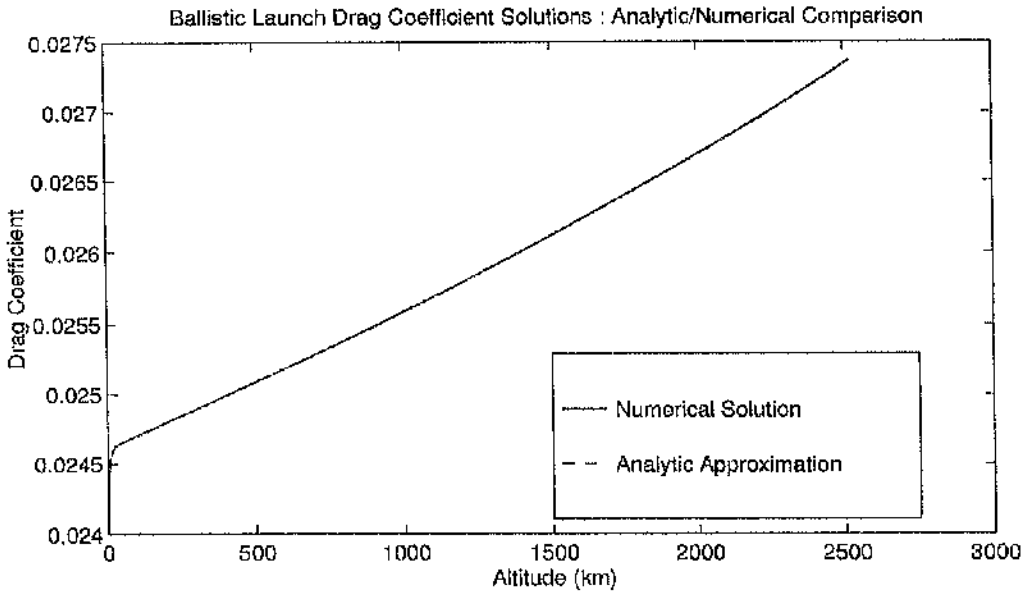

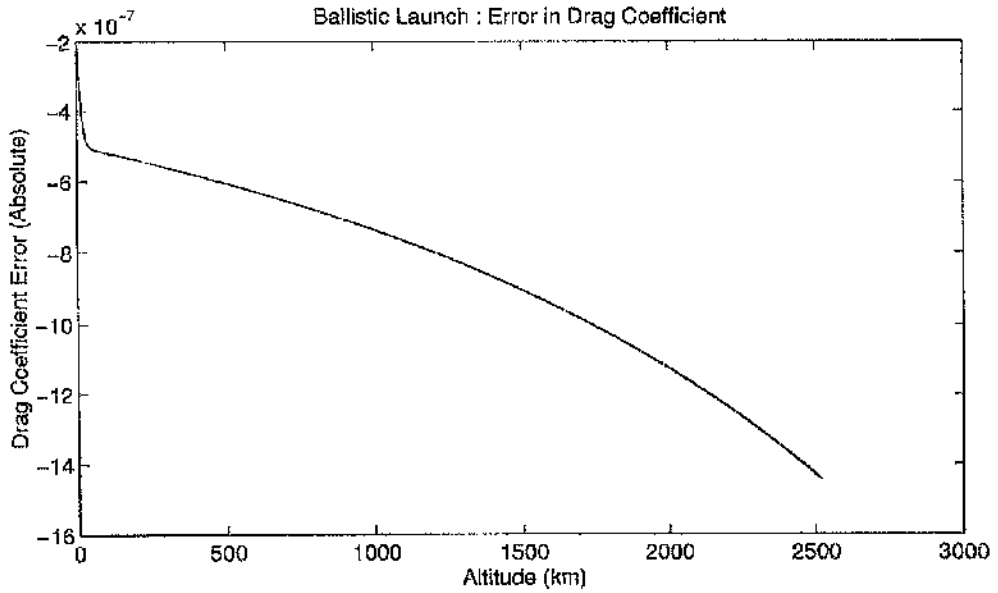

Fig. IV.C.2-3 Ballistic Launch : Launch Angle = 30°, Launch Velocity = 8km/s

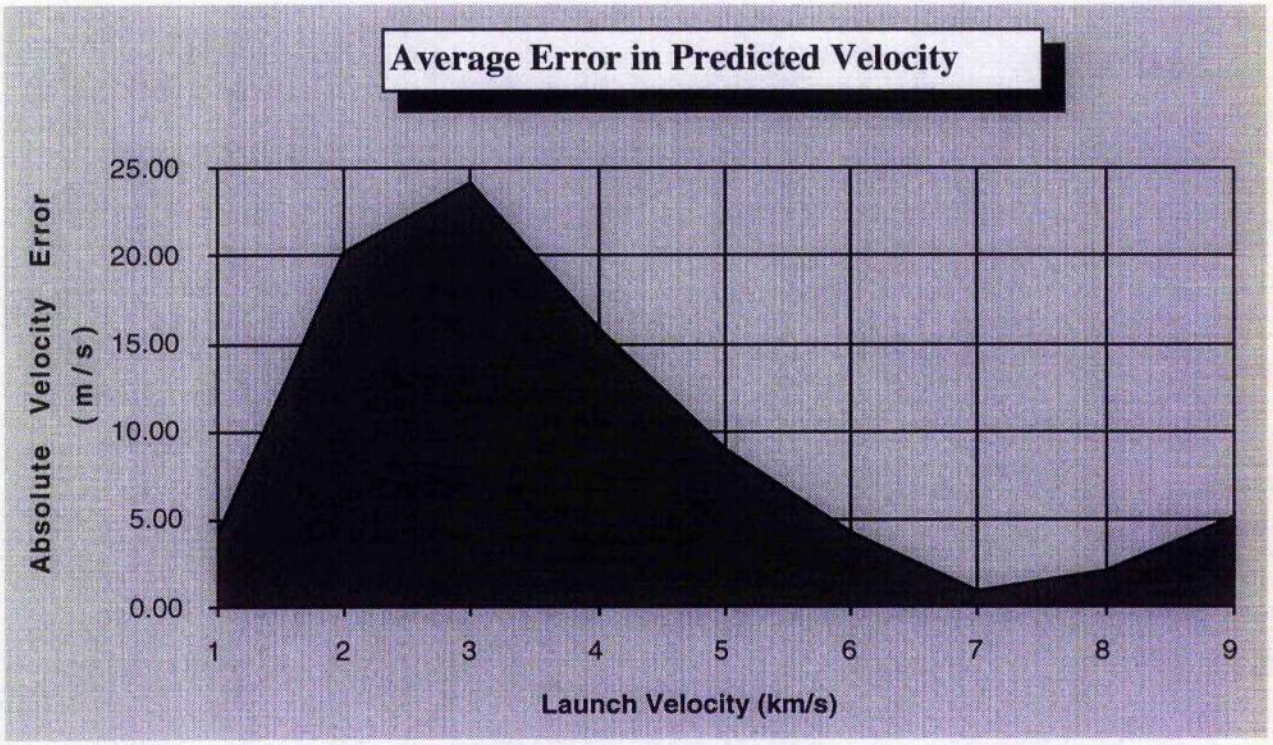

Fig. IV.C.2-4 Ballistic Launch : Launch Angle = 16°

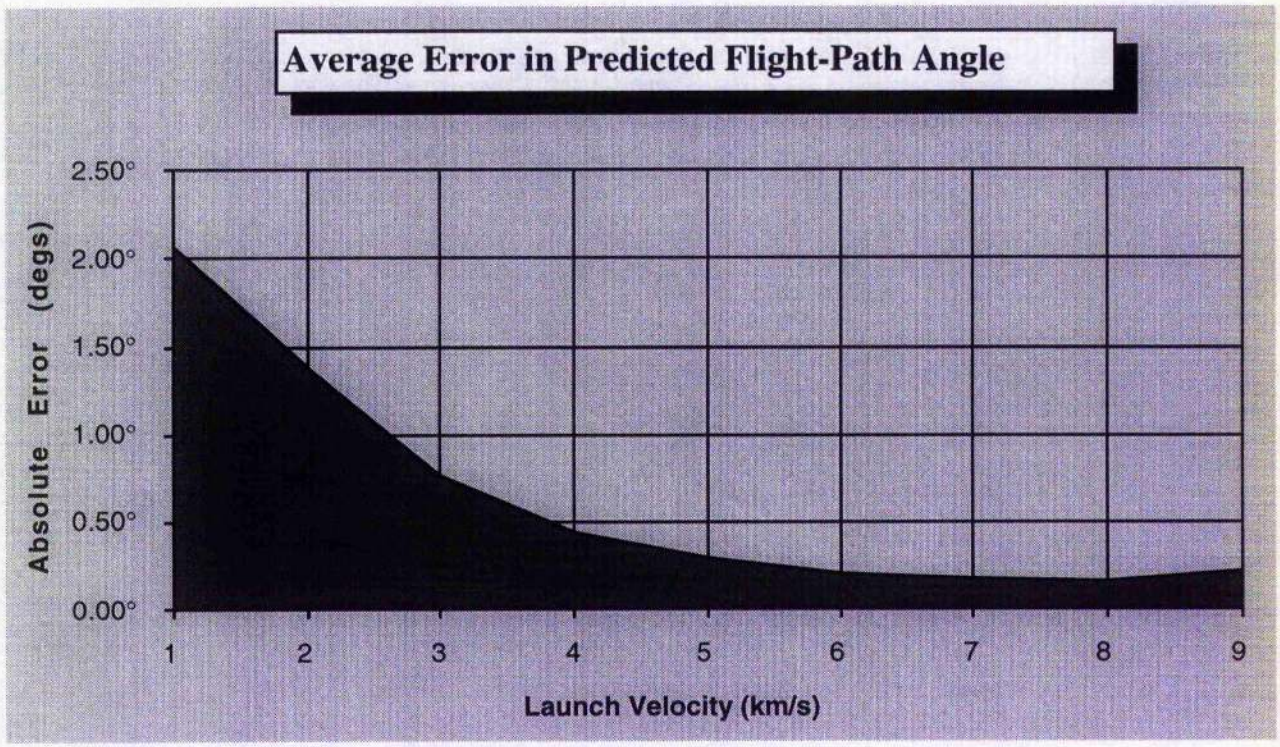

Fig. IV.C.2-5 Ballistic Launch : Launch Angle = 16°

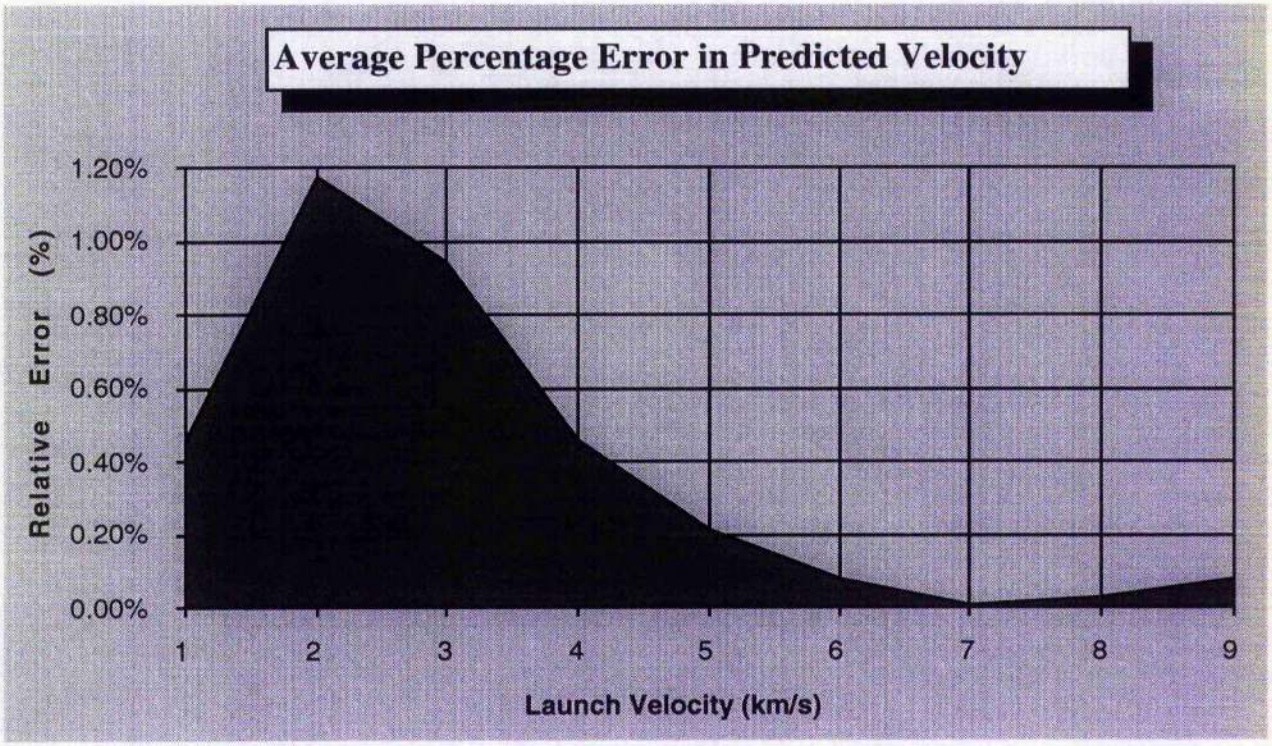

Fig. IV.C.2-6 Ballistic Launch : Launch Angle = 16°

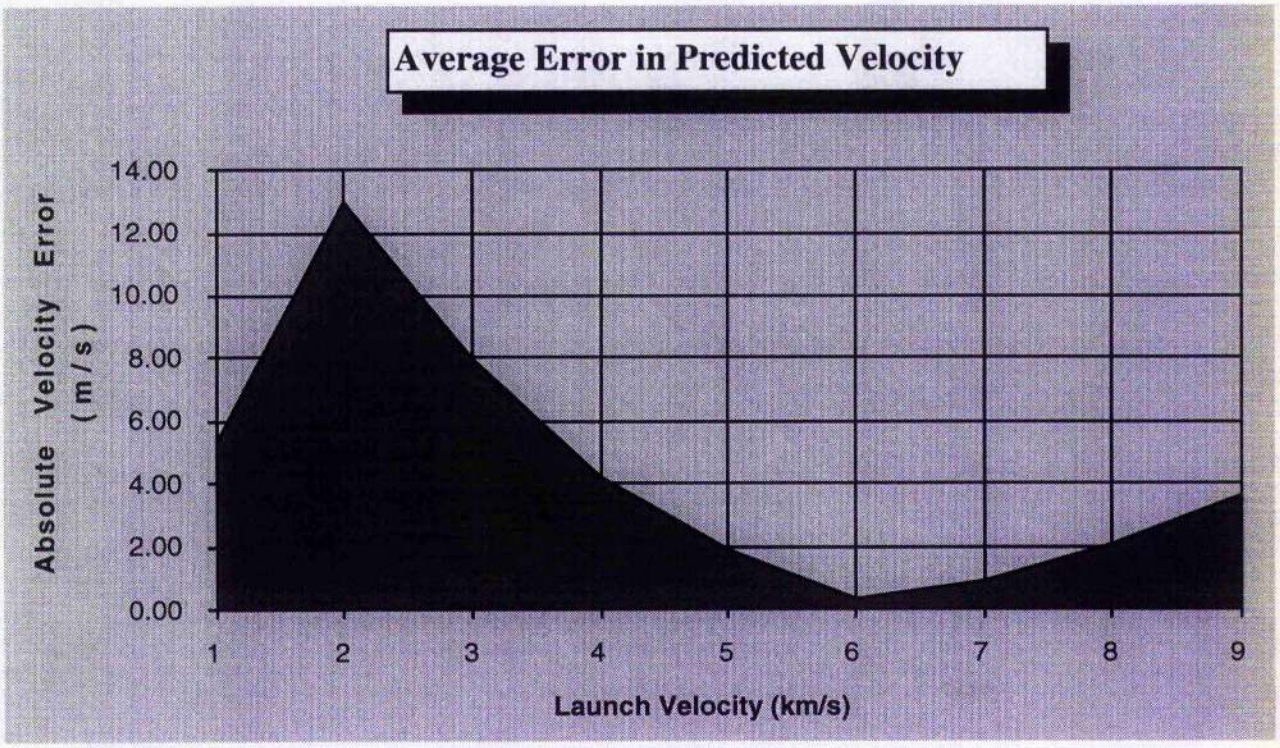

Fig. IV.C.2-7 Ballistic Launch : Launch Angle = 22°

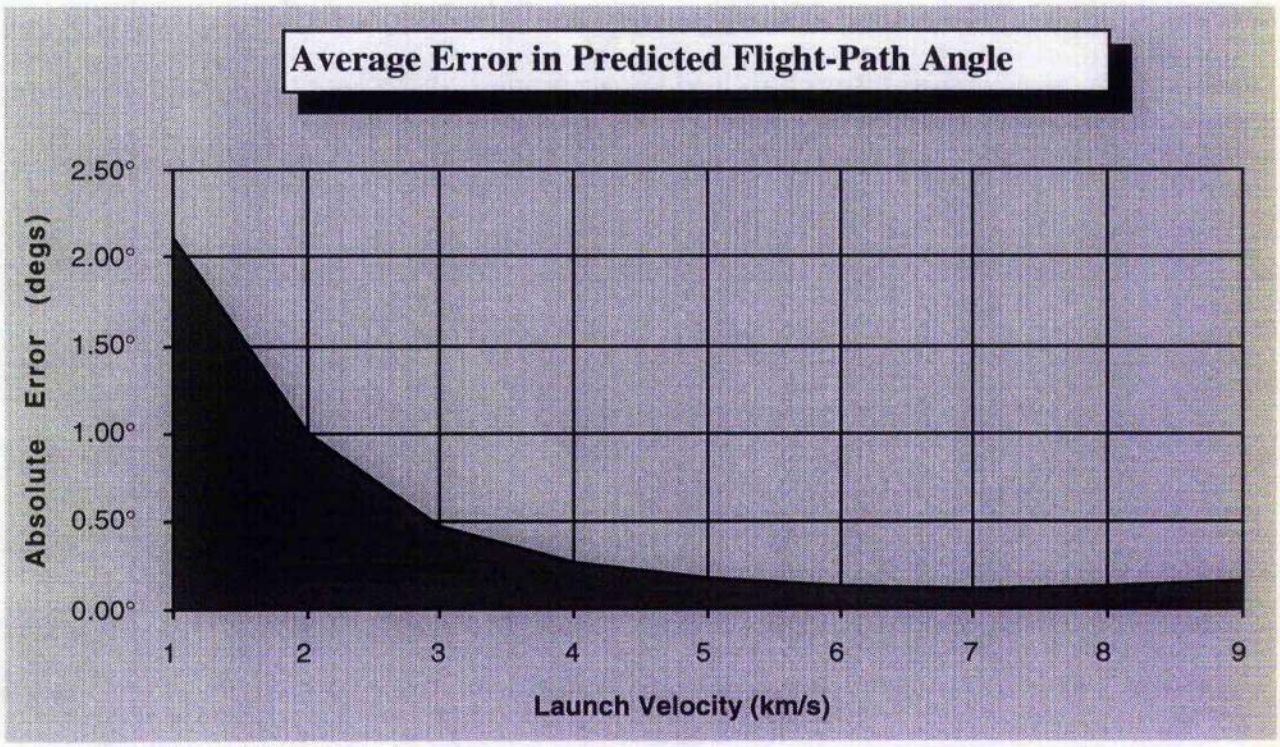

Fig. IV.C.2-8 Ballistic Launch : Launch Angle = 22°

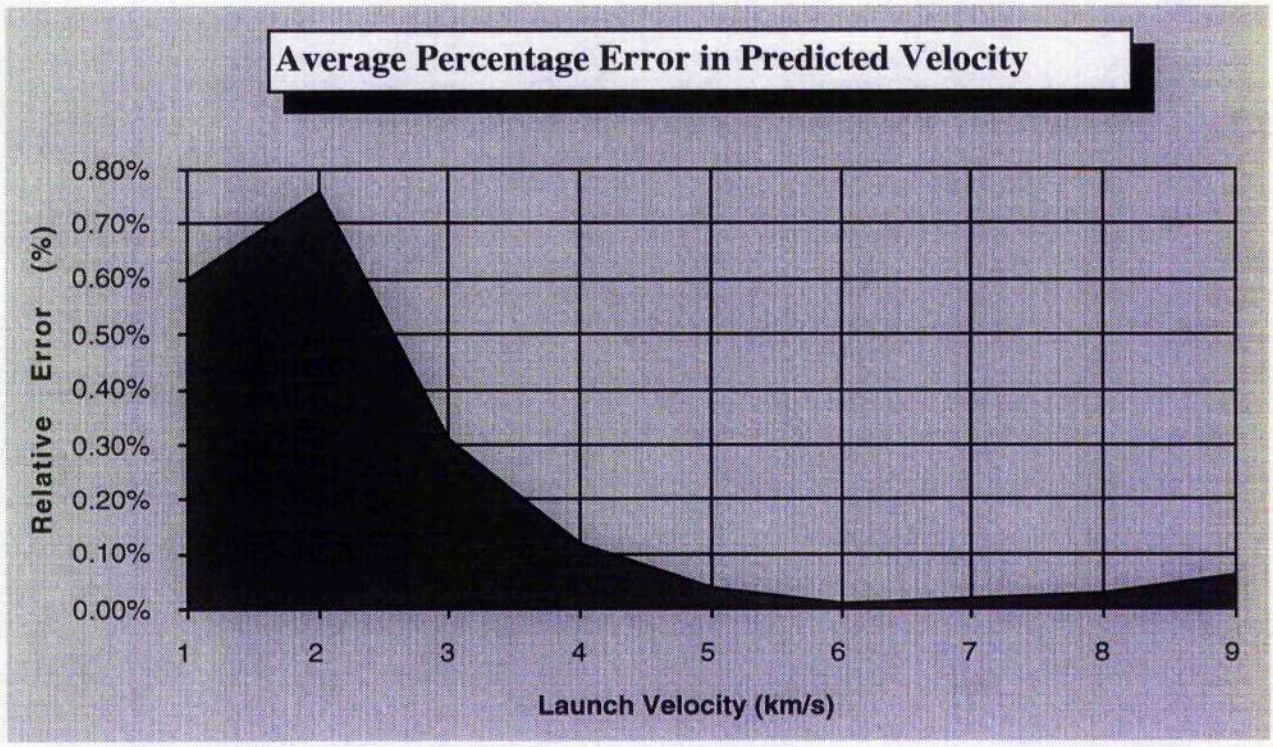

Fig. IV.C.2-9 Ballistic Launch : Launch Angle = 22°

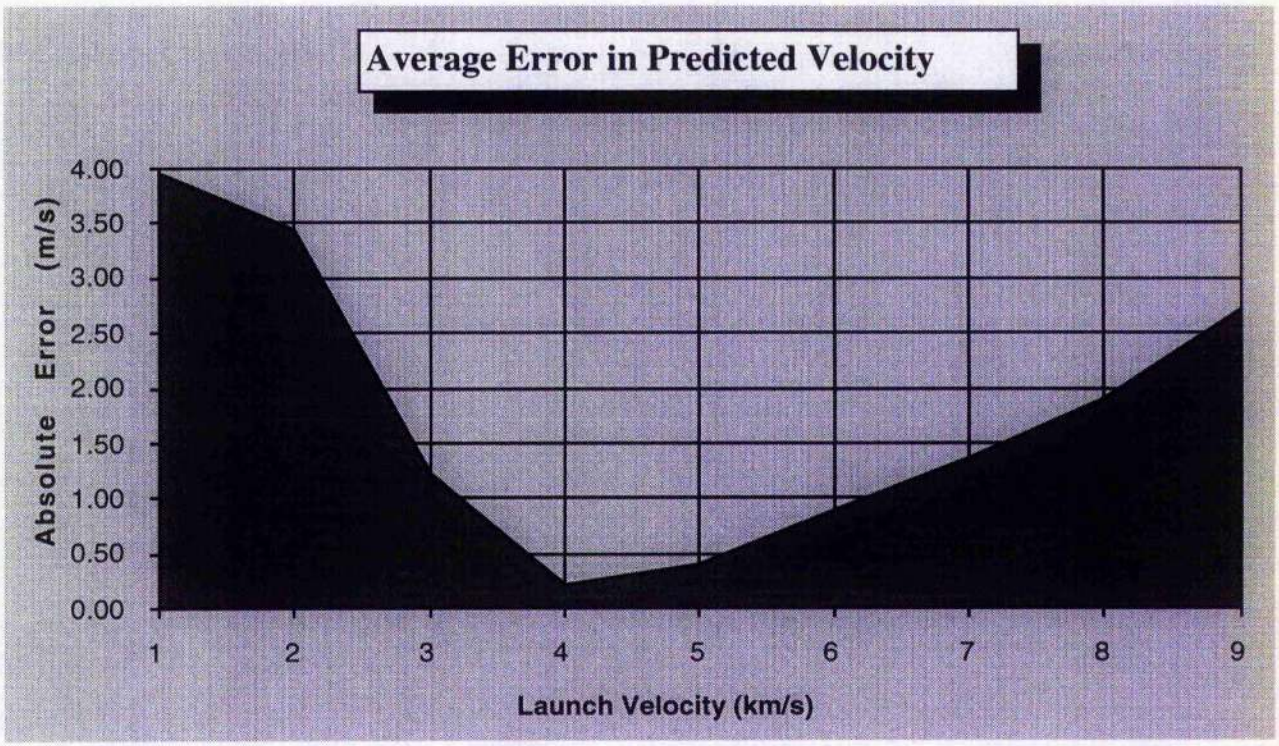

Fig. IV.C.2-10 Ballistic Launch : Launch Angle = 30°

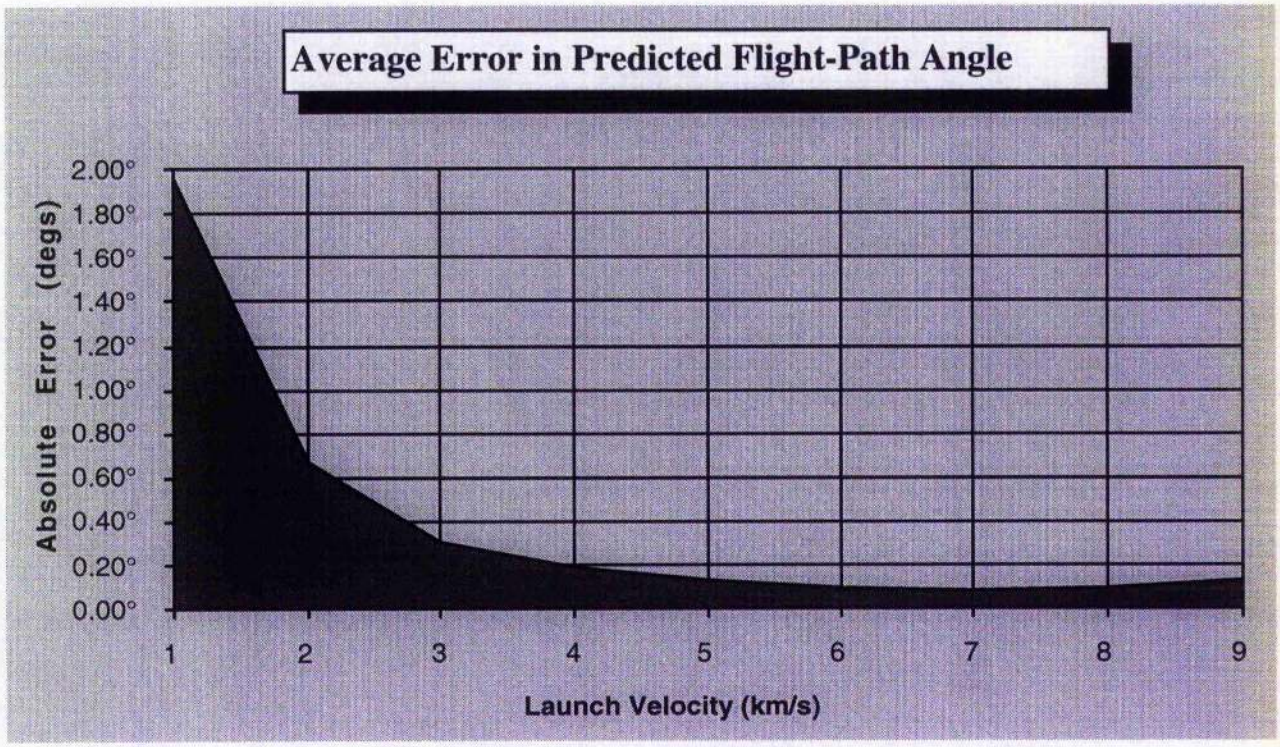

Fig. IV.C.2-11 Ballistic Launch : Launch Angle = 30°

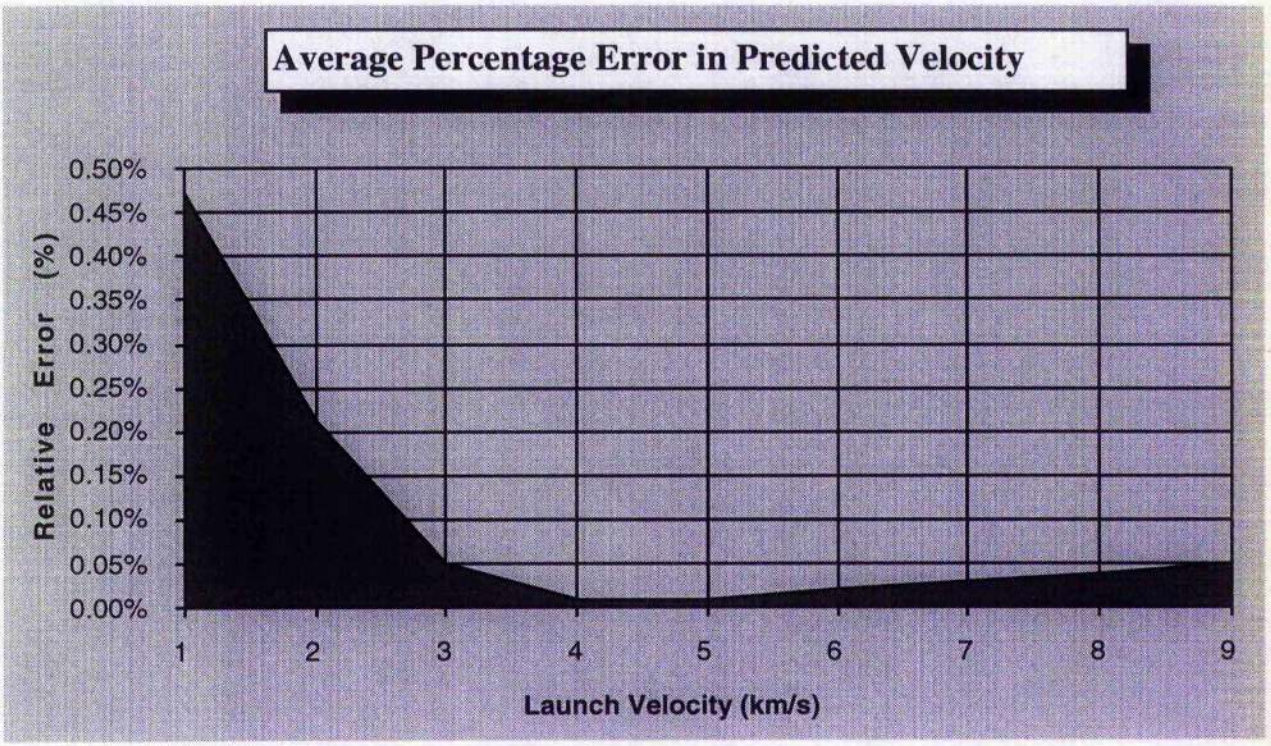

Fig. IV.C.2-12 Ballistic Launch : Launch Angle = 30°

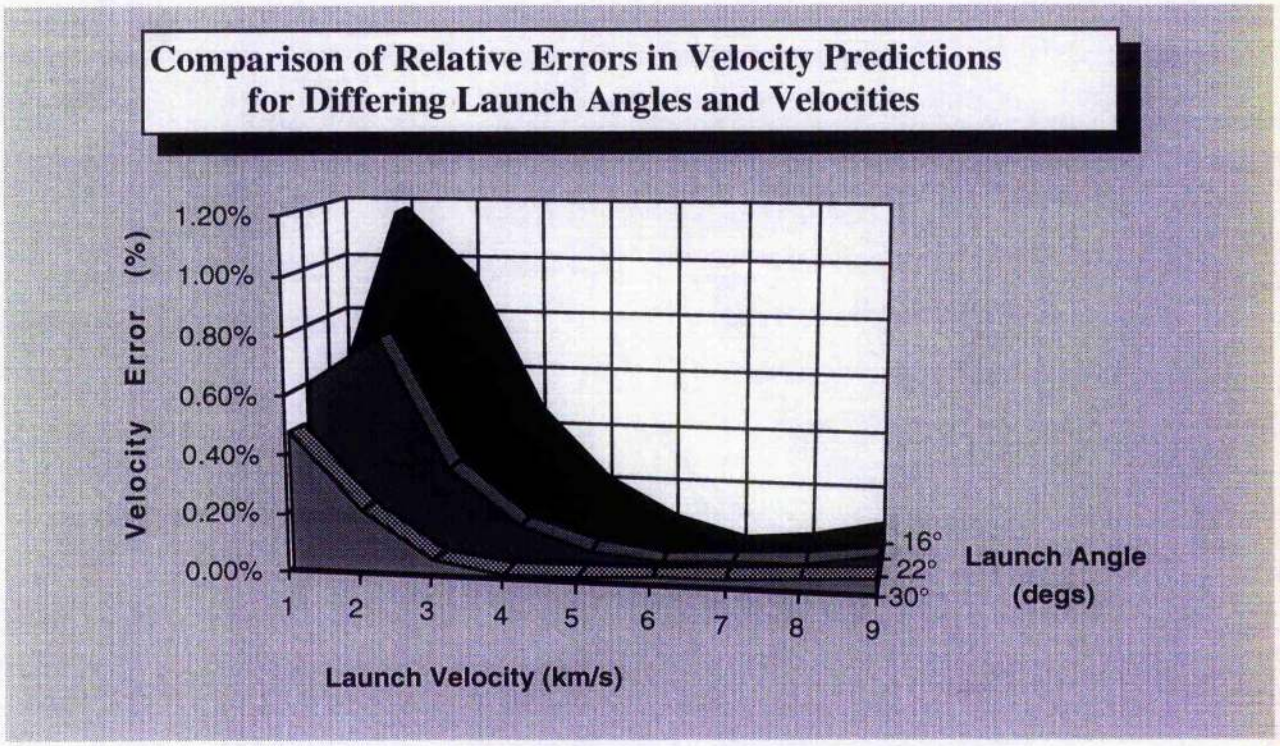

Fig. IV.C.2-13 Ballistic Launch : Comparison of Velocity Errors

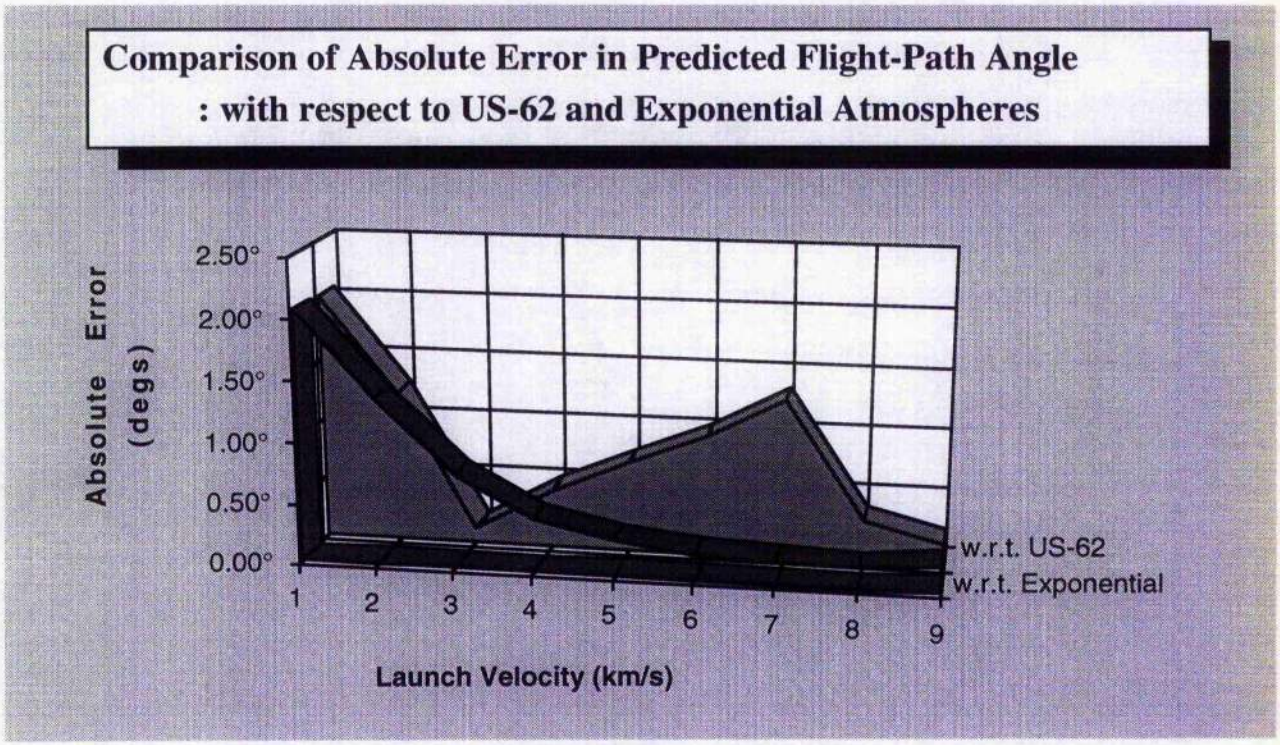

Fig. IV.C.2-14 Ballistic Launch : Launch Angle = 16°

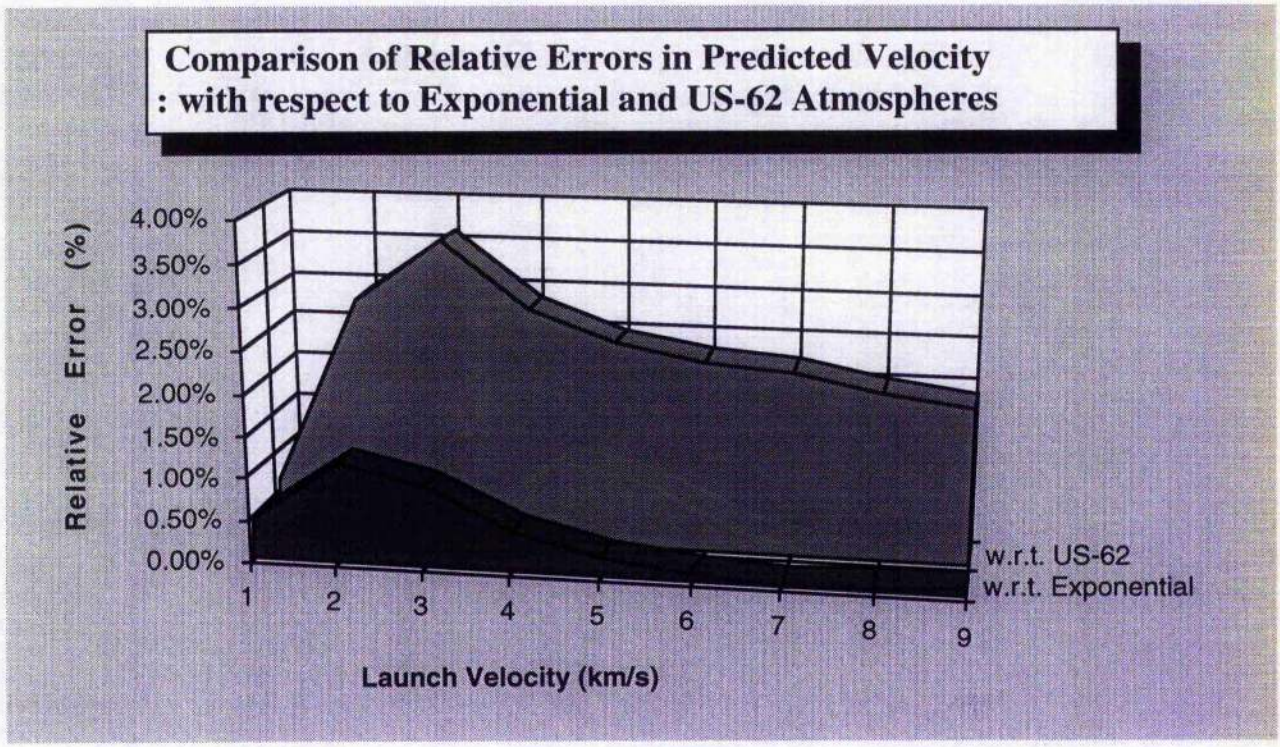

Fig. IV.C.2-15 Ballistic Launch : Launch Angle = 16°

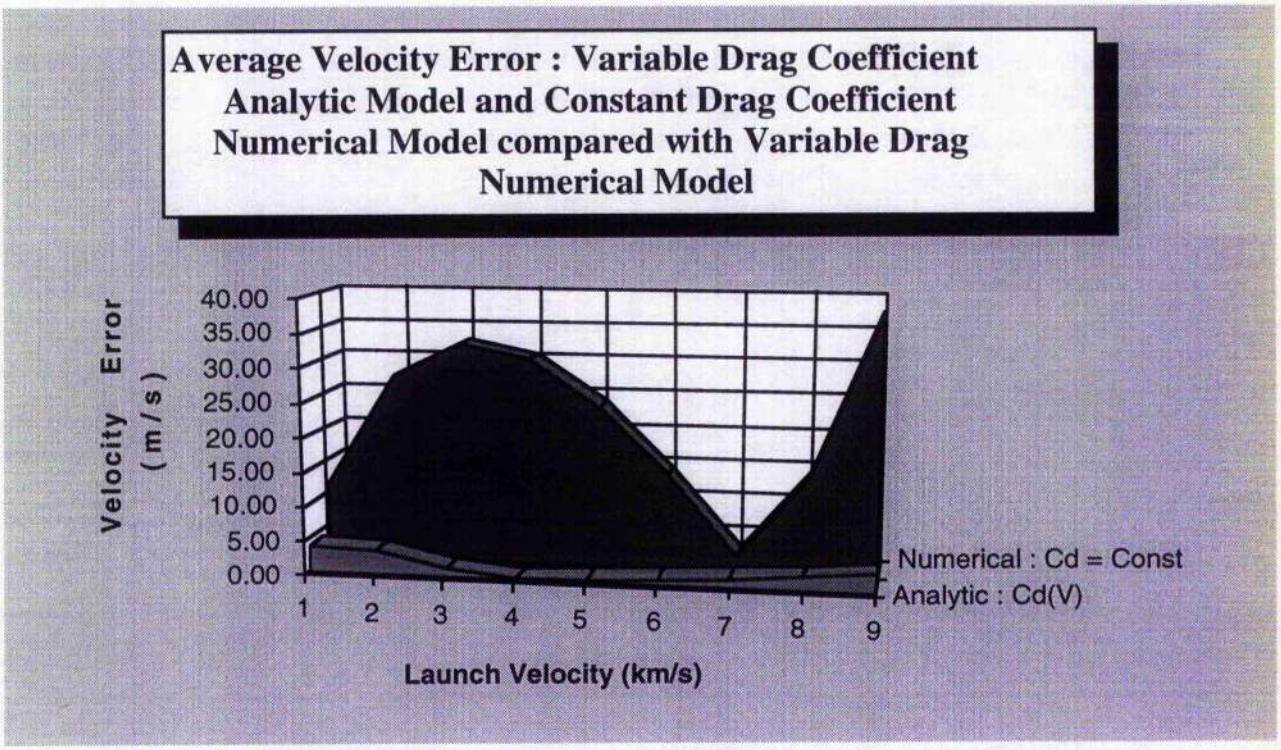

Fig. IV.C.2-16 Ballistic Launch : Launch Angle = 30°

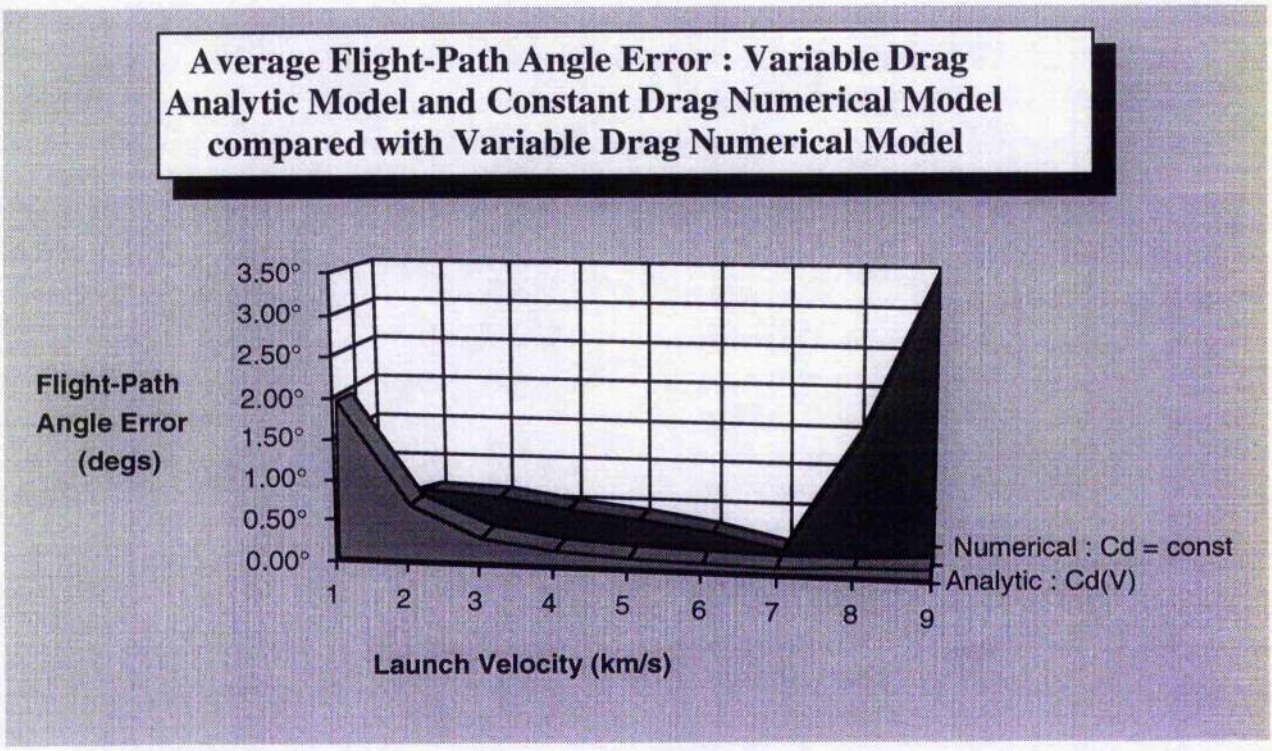

Fig. IV.C.2-17 Ballistic Launch : Launch Angle = 30°

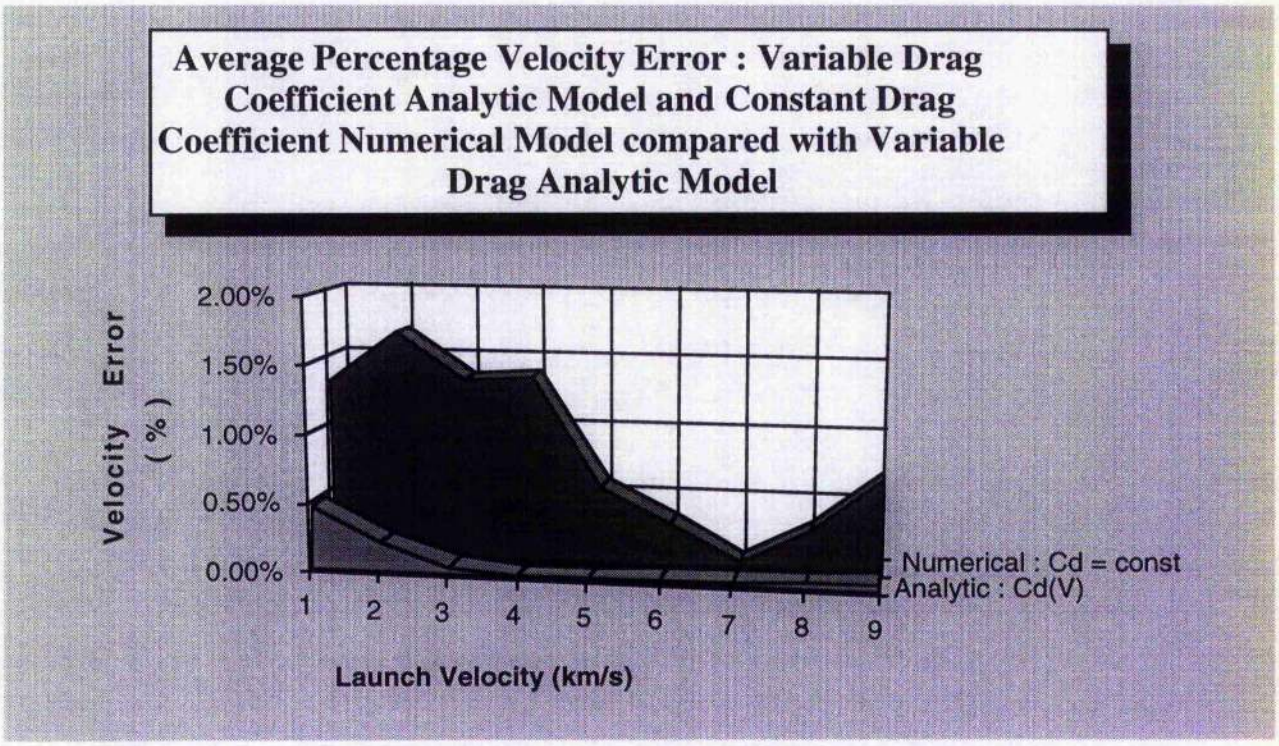

Fig. IV.C.2-18 Ballistic Launch : Launch Angle = 30°

IV.D. Conclusions

The method of matched asymptotic expansions has been used to analyse the trajectories of ballistic hypervelocity entry and launch vehicles and has shown excellent results for each. Comparison with a high-fidelity numerical model (*genL*) using the US-62 atmosphere model has shown similarly high quality results.

The incorporation of a velocity dependent drag coefficient has significantly improved the analytic model. Provided the function is integrable any suitable function could be used to model the drag coefficient (sections IV.B and IV.C) or the density profile.

The analytic expressions have been shown to accurately model the velocity dependence of the drag coefficient and comparison with a constant coefficient numerical simulation has vindicated its use for slender vehicles. The improvement in accuracy of the analytic solution over the constant coefficient numerical simulation highlights the potential of the analytic relations for use in onboard guidance and control systems in that it has been achieved in conjunction with a significant reduction in the amount of computing power required.

An optimum range of validity has been found to occur for the launch solutions for trajectories with apogees in the range $300-500km$. This is fortuitous as it encompasses the altitudes most likely to be used in supplying the Space Station, although excellent results are also found to either side of this range.

Atmospheric entry solutions produced relatively better results than those for launch except for the vehicle flight-path in the range where tip-over occurs. This was found to occur for entry velocities near orbital velocity. Sub-orbital velocity entries could be accurately modelled down to speed of less than $1km/s$. For entries above orbital velocity tip-over did not occur and the solutions were found to give excellent agreement with the numerical solutions.

In conclusion, in this chapter we have developed the capability of the analytic relations

- to accurately model the trajectories of ballistic launch and entry vehicles, even under off-nominal atmospheric conditions
- to accurately incorporate the effect of velocity dependence in the drag coefficient
- to produce quality trajectory predictions, simply and quickly.

The possible implementation of the derived relations and their ease of use is illustrated in figure IV.E-1. This figure shows a screen snapshot of a spreadsheet tool developed using the atmospheric entry relations derived in this chapter.

The user inputs the required parameters in the three input frames at the top of the sheet:

- Initial Values
- Vehicle Parameters
- Planetary Parameters

The frames below these are for the constants of integration and also three outputs:

- Point Solutions
  values at any altitude the user requests
- Impact Solutions
  values at impact
- Range of Solutions
  values over a range of altitudes

The derived tool is simple to construct and provides the same quality results described in sections IV.B and IV.C above.

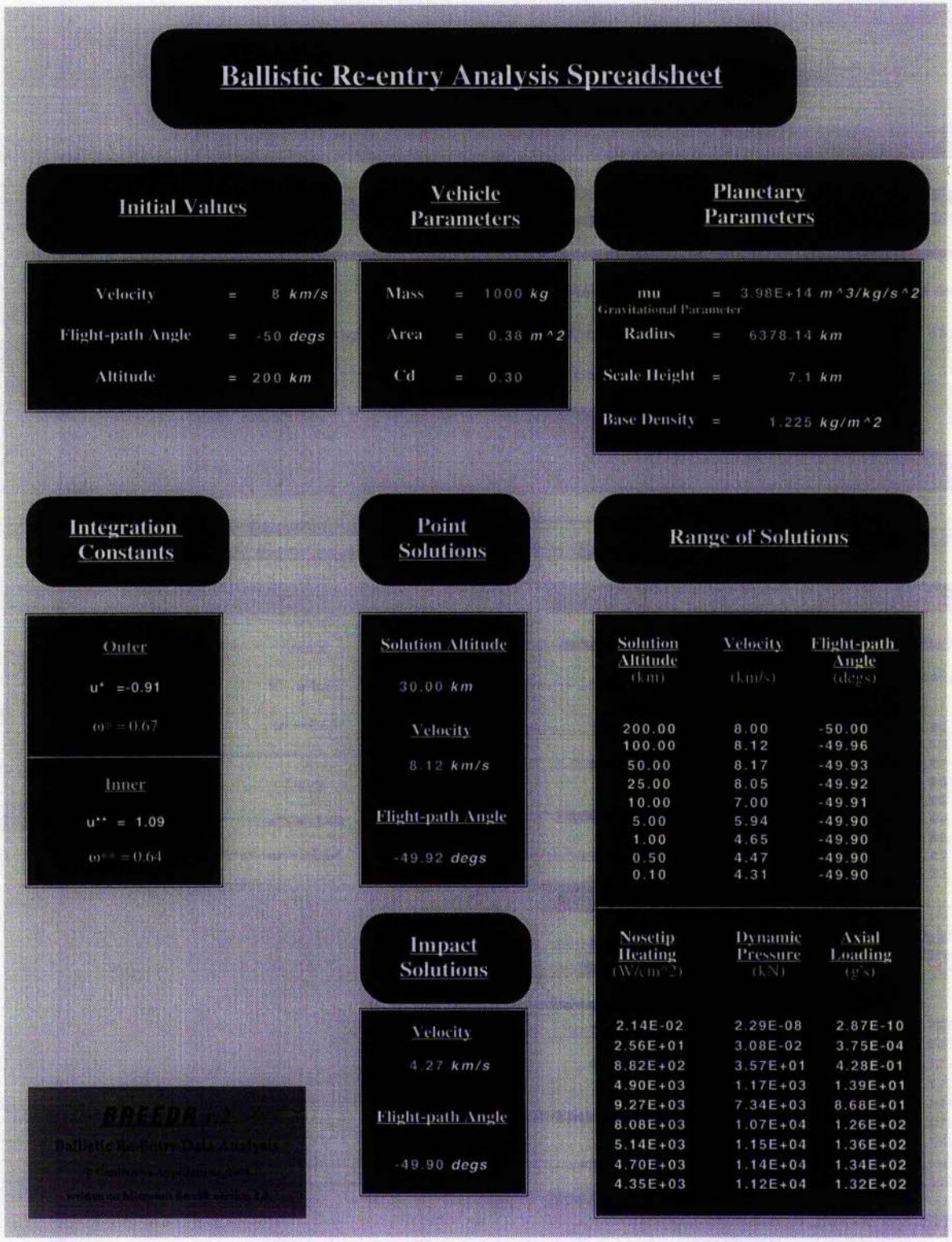

Figure IV.D-1 : Spreadsheet Prediction Tool Developed Using Re-entry Relations Derived in Section IV.B

The spreadsheet tool shown in fig. IV.D-1 uses the constant drag coefficient solutions derived in Section IV.B.4. Similar tools can be developed using the velocity dependent solutions and for direct launch with or without the velocity dependent drag coefficient model.

Chapter V.

LUNAR RETURN

V.A. Introduction

The human and scientific adventures of the early lunar missions are perhaps unparalleled in modern history. The achievements symbolised by the Apollo 11 landing are a clear example of what we can achieve when the will to do so is present.

"They proved that with skill and the desire to succeed ...[we] can indeed meet the most difficult tasks we set for ourselves."[71]†

As well as the human achievement, the Apollo missions had scientific goals: the collection of soil and rocks samples to help our understanding of the structure of the moon, and the deployment of instruments to measure solar-wind composition, seismic activity and lunar libration[72].

Apollo 11 achieved all its intended goals and returned some $20kg$[72] of lunar material to Earth. The preliminary science report alone contains just over 200 pages of observations and analyses made with this early data. Further analysis of this data and of that obtained during

† from preface to NASA SP-238, "Apollo 11 Mission Report", George M. Low, Acting Administrator, National Aeronautics and Space Administration, 1971

the remainder of the program (almost 400*kg* of lunar material were returned by the Apollo program[73]) have contributed greatly to our knowledge of our nearest neighbour, the Moon.

In the time since Apollo much of the data gathered on the moon has been from ground based observatories, the cost of launching a mission perhaps outweighing the perceived returns. In recent times, however, a return to the moon is again being considered as a cornerstone of future space exploration[6].

Some arguments for a return to the moon have been presented in Chapter I. In this chapter we address aspects of the practicalities associated with the lunar return mission.

V.A.1. Lunar Return

Early missions in the establishment of a Lunar base will include unmanned sample return missions, intended to bring samples of lunar rock and soil back to Earth for detailed analysis and later supply missions taking raw materials, water and oxygen as required. It is possible that the early supply vehicles could be constructed in such a way that they could be easily disassembled on the moon and the structural materials utilised in construction there, saving the cost of returning the vehicle to Earth. A sample return vehicle obviously cannot be used in this fashion, but the same vehicle could be used for supply purposes and then filled with lunar samples for its return leg.

Whether it be as a supply vehicle for a future lunar base or a sample return vehicle in the earlier stages of a continuation of the lunar exploration begun by Apollo, it is likely that there will be a requirement for the transport of a payload from the Moon back to Earth. The work presented here considers a small vehicle performing just such a return.

The representative vehicle used is too small to be manned, though this is not viewed as essential for the successful employment of the derived control. The physiological

constraints of the human body, however, will need to be considered if the type of return proposed here is to be considered for manned spaceflight.

V.A.1.1 The Transearth Trajectory

Transfer between Earth and Lunar orbits has been analysed intensively for the Apollo and Luna missions. The types of return available with today's technologies are no different than those used by the early lunar satellite launches although the guidance and control systems will have changed in sophistication.

Gapcynski and Woolston[74] showed the effects of Venus, Mars and Jupiter on the Earth-Moon trajectory to be negligible and this is used as the justification for ignoring their effects in the simulations performed for transearth trajectories. That having been said, their inclusion would result in only very minor changes to the initial conditions of the return and those could be arrived at empirically and to a great degree of confidence. Consequently the guidance and targeting required for transearth injection are not of issue here.

The transearth trajectory consists of three primary phases

- Transearth injection
- Transearth coast
- Earth entry/orbit insertion.

At transearth injection a high thrust rocket burn boosts the vehicle from lunar orbit to the velocity required for a transearth trajectory. The vehicle considered here is unmanned and consequently crew safety is not an issue in the choice of trajectory allowing greater flexibility for mission design. For example, the Apollo program utilised a free-return trajectory where the vehicle performs a figure of eight motion about the Earth-Moon system. In this way, should

there be a need to abort a landing attempt then the vehicle could progress around the moon and return to Earth with minimal course corrections and consequently minimal fuel usage.

Here, as stated above, we have no crew to concern us and the mission start point is the surface of the Moon itself. Consequently, free-return is not the only option and direct return (patched conic or cotangential transfer) is a possibility.

During the transearth coast phase the vehicle is, as implied, coasting and any control forces applied are so done as corrections suggested by telemetry. In the work following, a small course correction burn (of the order of $1 \rightarrow 2m/s$) is applied where necessary to fine tune the targeted entry conditions.

Finally, at the end of the coast phase the vehicle begins deceleration and is eventually brought to rest. Of concern here is with respect to what exactly is it brought to rest? The choices are simple: Firstly, the vehicle may be decelerated from its transearth velocity to rest at the surface of the Earth through some combination of propulsive, aerodynamic and surface impact forces; or secondly the vehicle may be caught into orbit about the Earth. This second option appears attractive at first as return-to-orbit will require a smaller velocity decrement than return-to-ground. However, the fuel requirements to achieve this decrement will be large unless we can utilise atmospheric forces as well.

This then is the first major choice in developing the return scenario for the vehicle.

Currently the choice is between Earth return and its more stringent requirements on heat shielding and consequently vehicle design, or return to orbit for retrieval by the shuttle. This second option is logistically inconvenient and possibly more expensive than the first although retrieval could be made a secondary shuttle mission to be performed after the primary, e.g. a satellite deployment. However, the imminent construction of International Space Station Alpha presents us

with the possibility of both an orbiting laboratory for analysis of lunar samples and an orbiting supply depot to which supplies for a lunar base could be delivered by shuttle before being transferred to the Moon by our transfer vehicle.

The vehicle considered in the work presented here is a small sample return vehicle representative of the size that might be used in demonstrating the techniques and technologies proposed herein.

The full-return problem considered later uses the free-return trajectory as this is likely to possess the greatest atmospheric entry velocity. Much of the earlier work considers entry speeds slightly lower resulting in a more benign heating environment which could be achieved through use of Hohmann-type returns. This allows us to consider a range of possible return types, and, within in each subgroup we could consider a range of actual return conditions and trajectories. This range of possible return trajectories is termed the entry corridor

V.A.1.2 Entry Corridors

As stated in Chapter I;

> *"The entry corridor is defined as the set of space trajectories for which aerodynamic capture within the atmosphere of the earth* [sic] *can be achieved and for which entry-trajectory control can be accomplished without exceeding either flight-crew or CM* [command module] *stress limits. Therefore, definition of the corridor limits includes four basic considerations: aerodynamic capture within the atmosphere, the aerodynamic load factor, aerodynamic heating, and landing-point control."* **12**†

Within this definition then the corridor becomes a set of trajectories which lie between two extremes. The difference between these two extremes is referred to as the corridor

† extract from Graves & Harpold, *Apollo Experience Report*, NASA TN D-6725

width, and this is usually given in terms of a range of atmospheric entry angles. It should be remembered that, for any given trajectory, the entry angle depends on the altitude at which atmospheric incidence is assumed to occur (fig.V.A.1.2-1).

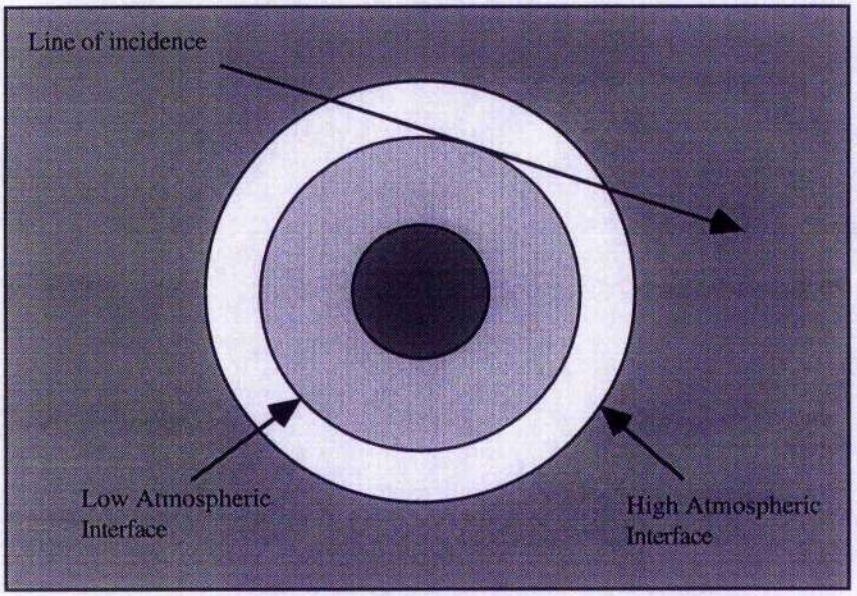

Fig V.A.1.2-1 - Effect of entry altitude on entry angle

If the constraints on the motion were purely aerodynamic then the two extreme trajectories are; the *overshoot*, where the vehicle does not get close enough to the desired state, and the *undershoot*, where it goes too far beyond the desired state.

Modifying the definitions from Chapter I for a lunar return aerocapture vehicle with a limited fuel load, these would be

- **overshoot** - the entry is too shallow and consequently the vehicle does not lose enough energy to achieve capture. The vehicle will then either continue out of the Earth's sphere of influence or will achieve an orbit with too great an apogee altitude to achieve space station rendezvous with the available fuel mass.

- **undershoot** - the entry angle is too steep and it is beyond the aerodynamic capabilities of the vehicle to achieve an acceptable exit state. The result in this case is either a surface impact or an orbit with too low an apogee to achieve space station rendezvous with the available fuel mass.

These then would be the corridor limits if capture were the only consideration and the vehicle's aerodynamic capabilities and fuel load the only constraints. This is not likely to be the case, however, as the definition above suggests.

Take for example the case of a manned return vehicle. Human physiological constraints require the imposition of a deceleration load limit on the trajectories. This is another constraint on the motion and may further reduce the entry corridor. Vehicle design constraints, such as the tolerable peak heating rate and (less likely) integrated heat load, may also reduce the corridor. These reductions in addition to constraints imposed by the abilities of the control algorithm(s) lead to what is called the flyable entry corridor.

Fig.V.A.1.2-2 below shows the entry corridor for Apollo 11.

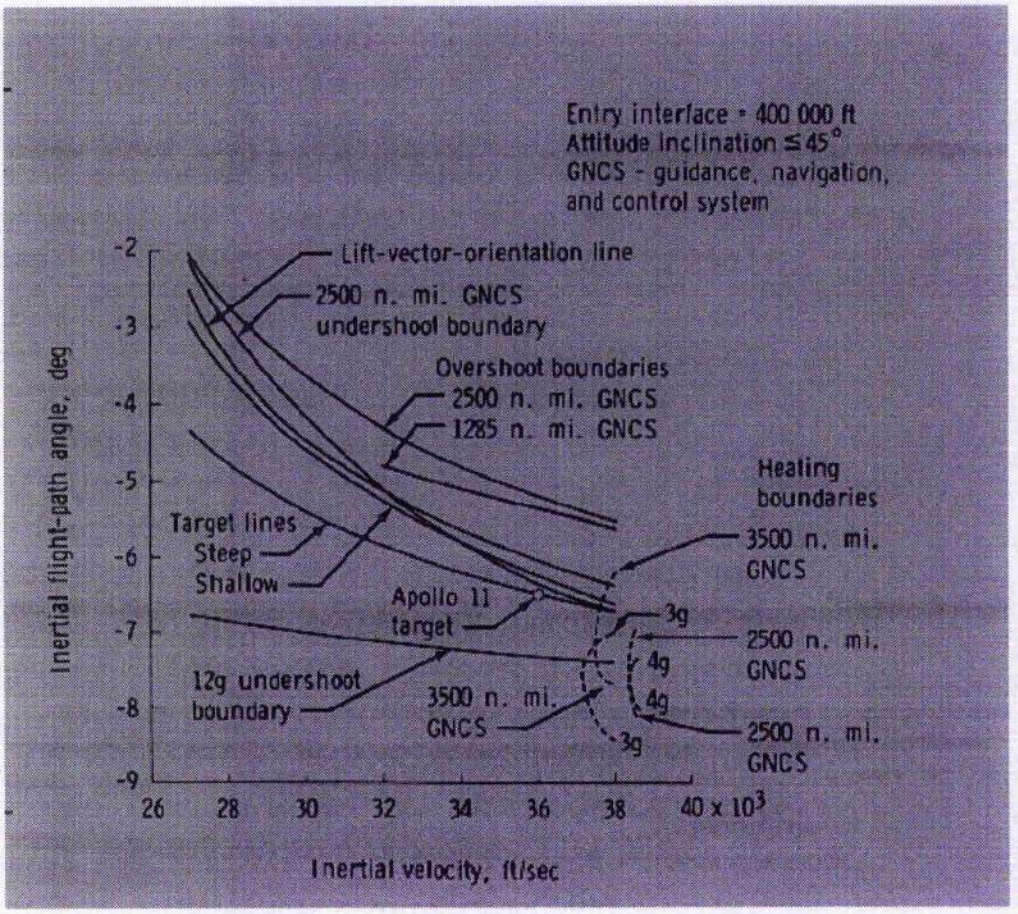

Fig. V.A.1.2-2 : Apollo 11 Entry Corridor[12]

The parameters used, flight path angle and velocity at the atmospheric interface are typical of those used to describe an entry corridor, whilst the additional constraints imposed by crew and vehicle considerations provide additional boundaries.

The types of limits imposed and the effects of such parameters as ballistic coefficient, and L/D ratio will be discussed in more detail when considering particular types of trajectory.

V.B. Return to a Space Station

V.B.1. Introduction

The planned construction of International Space Station Alpha (ISSA) may make feasible a larger scale return to the moon than the single mission programs such as Clementine which have been proposed or undertaken in recent years.

As the cost of mounting a multi-mission program from the Earth is likely to prove prohibitive, the construction of ISSA may provide a platform for the launch of lunar missions and an orbiting laboratory for sample study if the vehicles could return to the station rather than Earth[75].

One current ESA proposal is for a rover equipped lander mission to the south lunar pole, intended to assess the suitability of the moon as an off-world observatory. It is also proposed that the vehicle perform some soil sample analysis looking for oxygen and helium-3 for life-support/propellant and fusion fuel usage respectively[5]. More in-depth analysis of the lunar geology will be necessary if a manned base is to be established at some point in the future.

A single mission of the type proposed by ESA is limited in both the area it can cover and the experiments it may perform. A series of smaller sample return vehicles could achieve greater coverage in less time, and, with the possible use of ISSA as an orbiting laboratory, perform more detailed analysis for a lower financial outlay.

With autonomous on-board guidance the problem of communication loss with the return vehicle becomes less of a concern provided the guidance algorithms employed are sufficiently robust. The use of smaller vehicles would also minimise the loss, both financial and scientific of any single vehicle should a failure occur.

The use of small vehicles might also prove important in terms of safety. The aeroassist manoeuvre is highly unstable[30] and consequently there is the possibility, in a failure scenario, of a surface impact. However unlikely this scenario might appear, the use of small vehicles should make it easier to dispose of the vehicle, either by jettisoning the heatshield or self-detonation resulting in correspondingly small fragments and minimising the risk of any debris reaching the surface.

Returning to Earth would require an effective ΔV of the order of $11 km/s$ if the return is to ground. This compares with a ΔV of around $4 km/s$ to achieve space station altitude from the return trajectory, making return to the station the more attractive option in terms of the required ΔV and consequently the total heat load experienced by the vehicle.

In addition, although a ground return could be carried out using aerodynamic forces to provide a significant part of the required ΔV, the accuracy with which the landing site can be determined is limited. Historically this has led to ocean 'landings' and such an approach requires a large amount of hardware and personnel to be on hand to retrieve the vehicle.

If the vehicle were returned to ISSA then once its orbit had been circularised, rendezvous with the station could be achieved with a limited number of personnel, no more

hardware than would be on hand to track the vehicle anyway, and greater flexibility in time scale.

The $4km/s$ ΔV requirement for return to the station would still demand a significant fuel load for a purely propulsive return. Use of aeroassisted trajectories provides an alternative means of achieving the required ΔV for space station rendezvous, without incurring a large fuel penalty.

Previous work in the field of orbital transfer[21] has examined the use of analytic modelling techniques to predict the trajectories of aeroassisted orbital transfer vehicles and as the basis for non-linear guidance. The approach presented here uses the non-linear transformation technique discussed in Chapter III to ensure stability of a trajectory about a reference condition by compensating for the non-linear terms in the motion of the vehicle, and so artificially linearising the system dynamics.

Any suitable reference condition may be used in developing the control expressions. There are two reference conditions used here, a constant altitude and an analytically produced trajectory model. These are discussed further below.

The method of matched asymptotic expansions has proved a useful tool in the analysis of transatmospheric vehicle motion, and has been proposed as the basis for a number of guidance schemes[21,76,42]. As discussed in Chapter IV, solution by matched asymptotic expansions makes use of the approximation, first made by Allen and Eggers[60], that gravity may be ignored for high speed atmospheric motion in comparison with the aerodynamic forces experienced. Making this assumption, the motion of the vehicle can be considered in two parts, Keplerian and atmospheric. Individual solutions obtained for each of these regions are combined by asymptotic matching to produce a uniformly valid composite solution.

Such solutions have been shown to yield accurate predictions of transatmospheric trajectory data and these

predictions have enabled the development of some robust, low-complexity, inexpensive guidance schemes.

In this part of the study it is proposed to marry the use of feedback linearisation guidance with the analytic predictions obtained via the method of matched asymptotic expansions.

As the vehicle enters the atmosphere at a moderate bank angle ($\cos\sigma \approx 0.6$; σ measured from the vertical) analytic prediction of the resulting skip trajectory is used to estimate the minimum altitude that the vehicle will reach. Feedback linearisation is used to track this altitude while matched asymptotic expansions are used to predict the apogee which will result should the in-plane lift component be suddenly increased by rolling the vehicle to a predetermined pull-up bank angle ($\cos\sigma \approx 0.8$).

Once the predicted apogee altitude falls within acceptable tolerances of the desired apogee the vehicle "pulls-up". The pull-up bank angle is chosen such that the in-plane lift force is not saturated, leaving some degree of control authority over the exit phase.

The apogee that would be achieved by this manoeuvre would be close to the desired apogee and moderate correction needed as the analytic relations used to predict the apogee are an approximation to the motion. This correction could be achieved propulsively, however the scheme proposed here uses aerodynamic control during the exit phase. The predictions used to determine the pull-up point are used to provide an analytic reference trajectory. Non-linear transformations are then used to guide the vehicle along the reference trajectory, artificially improving the analytic predictions.

As the reference trajectory data is produced analytically it may be generated in flight removing the need for numerical integration or storage of trajectory data and so freeing valuable computer power for other functions. In addition, the trajectory data obtained is altitude dependent and consequently there will be zero altitude error for any given

point along the path towards apogee. Given this, convergence of the climb-rate to the reference condition will guarantee attainment of the desired apogee.

The concept of a reference trajectory is somewhat misleading in this application as the 'trajectory' used actually comprises the velocity and flight path angle prediction data, and the vehicle is guided along the altitude profiles obtained. The expression 'reference trajectory' will be used in this study for convenience.

Since the reference data is obtained from the same trajectory predictions used in determining the point of pull-up from level flight, the actual trajectory is guaranteed to be near the reference trajectory. How near that is obviously depends on the accuracy of the analytic model, but by guiding the vehicle along the predicted path it is found that the error in the predictions may be attenuated, matching the actual apogee as closely as possible to the targeted apogee.

The solution of the exit trajectory problem using asymptotic matching produces uniformly valid expressions for the velocity and flight path angle altitude profiles. Implementation of a feedback linearisation guidance scheme based on these then requires no more than the solution of simple algebraic expressions with no derivative terms involved.

In summary, vehicle control is implemented via bank angle modification of the in-plane lift component and it is assumed that the desired plane change is achieved using periodic roll-reversals. The control strategy falls into three sections:-

- **entry trajectory -**

The vehicle enters at a moderate bank angle ($\cos\sigma \approx 0.6$) and the minimum altitude is predicted analytically.

During this phase a prediction of the apogee resulting from a sudden increase in upward lift component ($\cos\sigma \approx 0.8$) is constantly made to allow for unfavourable atmospheric

conditions. This pull-up bank angle is only achieved if the predicted apogee lies within an acceptable tolerance of the desired apogee. At this stage the apogee prediction is really only a monitor, intended to check that the vehicle is not experiencing extreme atmospheric conditions.

- **constant altitude guidance -**

When the flight path angle approaches zero the vehicle tracks the predicted minimum altitude until the desired apogee is predicted. The vehicle is then rolled to the pull-up bank angle and commences atmospheric exit.

- **exit trajectory -**

The analytic trajectory solutions used to predict the apogee now provide a reference trajectory along which feedback linearisation is used to guide the vehicle to apogee.

The pull-up bank angle is chosen such that the vertical lift component is not saturated, thus leaving some control authority over the exit trajectory.

We will now explore the dynamics of the motion before developing the analytic model and thence deriving our control.

V.B.2 System Dynamics

In this part of the study a non-linear transformation guidance method is presented which is based on matched asymptotic predictions of the vehicle's trajectory. To assist solution of the problem in this manner it is assumed that only in-plane motion is considered about a spherical, wind-free, non-rotating Earth.

The equations of motion are solved in a similar manner to Chapter IV but with the addition of aerodynamic lift.

The equations of motion for this system are therefore

$$\frac{dV}{dt} = -\frac{\rho V^2 S C_D}{2m} - \frac{\mu}{r^2}\sin\gamma \qquad \textbf{V.B.2-1}$$

$$V\frac{d\gamma}{dt} = -\left\{\frac{-V^2}{r} + \frac{\mu}{r^2}\right\}\cos\gamma + \frac{\rho V^2 S C_L}{2m} \qquad \textbf{V.B.2-2}$$

$$\frac{dr}{dt} = V\sin\gamma \qquad \textbf{V.B.2-3}$$

where the variables are as defined in Section IV.B.2 and again the assumed density model has the standard exponential form

$$\rho = \rho_o \exp\left(\frac{-(r-R)}{H}\right) \qquad \textbf{V.B.2-4}$$

where R is the radius of the Earth and H the atmospheric scale height.

It is further assumed that both the lift and drag coefficients remain constant over the atmospheric passage. Finally, the range angle is not considered here as it does not influence the other state variables and has no effect on the guidance strategy.

In order to prepare these expressions for solution by matched asymptotic expansions the equations are non-dimensionalised and re-written in terms of non-dimensionalised altitude, h, as the independent variable.

As in Chapter IV, the following substitutions are used,

$$\overline{V} = V\sqrt{\frac{R}{\mu}} \qquad \textbf{V.B.2-5}$$

$$h = \frac{r-R}{R} \qquad \textbf{V.B.2-6}$$

$$\overline{\rho} = \frac{\rho H}{m/S} \qquad \textbf{V.B.2-7}$$

$$\varepsilon = \frac{H}{R} \qquad \textbf{V.B.2-8}$$

where μ is the Earth's gravitational parameter.

The reduced equation set in terms of non-dimensionalised altitude h, is now,

$$\frac{d\bar{v}^2}{dh} = -\frac{\bar{\rho}\bar{v}^2 SC_D}{\varepsilon \sin\gamma} - \frac{2}{(1+h)^2} \qquad \textbf{V.B.2-9}$$

$$\frac{d\cos\gamma}{dh} = -\frac{\bar{\rho}C_L}{2\varepsilon} - \cos\gamma\left\{\frac{1}{1+h} - \frac{1}{(1+h)^2\bar{V}^2}\right\} \qquad \textbf{V.B.2-10}$$

This system is now solved by the method of matched asymptotic expansions.

V.B.3 Solution by Matched Asymptotic Expansions

The skip-trajectory uses atmospheric drag to slow the vehicle, reducing the energy of the orbit such that the resultant apogee is as close as possible to the desired apogee.

Initially the motion of the vehicle is classical Keplerian, then, as the vehicle enters the atmosphere, aerodynamic forces take over and the contribution of gravity to the motion may be neglected. Finally, as the vehicle exits the atmosphere, aerodynamic effects disappear and the vehicle's motion is once again under the sole influence of gravity.

The clear dominance of gravitational force outwith the atmosphere and of aerodynamic force within allow the analysis of the motion to be split into two sections; the outer, or Keplerian region, and the inner, or aerodynamic region.

This approximation allows the closed-form solution of a simple skip trajectory by matched asymptotic expansions. In this approach expressions for the motion in each region are obtained separately and then combined by asymptotic matching to produce a uniformly valid composite solution.

The following variable substitutions are made for clarification,

$$u = V^2 \text{and } \omega = \cos\gamma \qquad \textbf{V.B.3-1}$$

The equations of motion for the system are now given by

$$\frac{du}{dh} = -\frac{\overline{\rho}_0 u C_D \exp(-h/\varepsilon)}{\varepsilon\sqrt{1-\omega^2}} - \frac{2}{(1+h)^2} \qquad \textbf{V.B.3-2}$$

$$\frac{d\omega}{dh} = -\frac{\overline{\rho}_0 C_L}{2\varepsilon}\exp(-h/\varepsilon) - \omega\left\{\frac{1}{1+h} - \frac{1}{(1+h)^2 u}\right\} \qquad \textbf{V.B.3-3}$$

Solutions are now obtained for the inner and outer regions.

V.B.3.1 Inner Region

As in Chapter IV, the boundary layer considered is the sensible atmosphere close to the surface of the planet. The variable $\tilde{h} = h/\varepsilon$ is again employed as our 'mathematical microscope', artificially expanding the region of interest.

With this substitution the system is now written as

$$\frac{d\tilde{u}}{d\tilde{h}} = -\frac{\overline{\rho}_0 \tilde{u} C_D}{\sqrt{1-\tilde{\omega}^2}}\exp\left(-\tilde{h}\right) - \frac{2\varepsilon}{\left(1+\varepsilon\tilde{h}\right)^2} \qquad \textbf{V.B.3.1-1}$$

$$\frac{d\tilde{\omega}}{d\tilde{h}} = -\frac{\overline{\rho}_0 C_L}{2}\exp\left(-\tilde{h}\right) - \varepsilon\tilde{\omega}\left\{\frac{1}{1+\varepsilon\tilde{h}} - \frac{1}{\left(1+\varepsilon\tilde{h}\right)^2 \tilde{u}}\right\} \qquad \textbf{V.B.3.1-2}$$

In the limit $\varepsilon \to 0$ the independent variable $\tilde{h} \to \infty$. In this limit the atmosphere is effectively expanded to an infinite distance. Applying this limit, with all non-dimensionalised variables held constant, and assuming the following expansions for the velocity and flight path angle terms,

$$\tilde{u} = \sum_{i=0}^{n} \varepsilon^i \tilde{u}_i\left(\tilde{h}\right) + O\left(\varepsilon^{n+1}\right) \qquad \textbf{V.B.3.1-3}$$

$$\tilde{\omega} = \sum_{i=0}^{n} \varepsilon^i \tilde{\omega}_i\left(\tilde{h}\right) + O\left(\varepsilon^{n+1}\right) \qquad \textbf{V.B.3.1-4}$$

the relations become, to lowest order,

$$\frac{d\tilde{u}_0}{d\tilde{h}} = -\frac{\overline{\rho}_0 \tilde{u}_0 C_D}{\sqrt{1-\tilde{\omega}_0^2}} \exp\left(-\tilde{h}\right) \qquad \textbf{V.B.3.1-5}$$

$$\frac{d\tilde{\omega}_0}{d\tilde{h}} = -\frac{\overline{\rho}_0 \tilde{\omega}_0 C_L}{2} \exp\left(-\tilde{h}\right) \qquad \textbf{V.B.3.1-6}$$

These expressions are then integrated to give

$$\tilde{u}_0 = \tilde{u}_* \exp\left(-2\tilde{\gamma}/\lambda\right) \qquad \textbf{V.B.3.1-7}$$

$$\tilde{\omega}_0 = \tilde{\omega}_* + \frac{\overline{\rho}_0 \lambda C_D}{2} \exp\left(-\tilde{h}\right) \qquad \textbf{V.B.3.1-8}$$

where $\lambda = C_L/C_D$ and $\tilde{u}_*$ and $\tilde{\omega}_*$ are constants of integration.

V.B.3.2 Outer Region

The solutions for the outer region are identical to those obtained in Chapter IV but are reproduced here for ease of reference.

Application of the limit $\varepsilon \to 0$ effectively shrinks the atmosphere to the Earth's surface, so that only exoatmospheric motion is considered.

The equations of motion for this region are then

$$\frac{du}{dh} = -\frac{2}{(1+h)^2} \qquad \textbf{V.B.3.2-1}$$

$$\frac{d\omega}{dh} = -\omega\left\{\frac{1}{1+h} - \frac{1}{(1+h)^2 u}\right\} \qquad \textbf{V.B.3.2-2}$$

Series expansions are again assumed for u and ω of the form

$$u = \sum_{i=0}^{n} \varepsilon^i u_i(h) + O\left(\varepsilon^{n+1}\right) \qquad \textbf{V.B.3.2-3}$$

$$\omega = \sum_{i=0}^{n} \varepsilon^i \omega_i(h) + O\left(\varepsilon^{n+1}\right) \qquad \textbf{V.B.3.2-4}$$

Integrating the resultant lowest order expressions the outer solutions are obtained as

$$u_0 = u_* + \frac{2}{1+h} \qquad \textbf{V.B.3.2-5}$$

$$\omega_0 = \frac{\omega_*}{\sqrt{u_*(1+h)^2 + 2(1+h)}} \qquad \textbf{V.B.3.2-6}$$

where u_* and ω_* are the outer constants of integration.

V.B.3.3 Composite Solution

The composite solution is again obtained by combining the outer and inner solutions and relating the integration constants by asymptotic matching.

Expanding the inner solution for $\tilde{h} \to \infty$ and the outer for $h \to 0$ and equating the equivalent expressions from each region the integration constants are found to follow the relations

$$u_* = \tilde{u}_* \exp\left(-2\tilde{\gamma}_*/\lambda\right) - 2 \qquad \textbf{V.B.3.3-1}$$

$$\omega_* = \tilde{\omega}_* \sqrt{u_* + 2} \qquad \textbf{V.B.3.3-2}$$

Finally, there exists a constant solution which is common to both the inner and the outer regions and this must be subtracted from the sum of the solutions for the two regions so that it is not included twice in the composite expressions.

The common solution is obtained by expressing the outer solution in the inner variable and taking the limit as $\varepsilon \to 0$, giving

$$u = u_* + 2 \qquad \textbf{V.B.3.3-3}$$

$$\omega = \frac{\omega_*}{\sqrt{u_* + 2}} \qquad \textbf{V.B.3.3-4}$$

The composite solutions for non-dimensionalised velocity and flight path angle in terms of altitude are now given as

$$u = (u_* + 2)\exp\left(-2(\tilde{\gamma} - \tilde{\gamma}_*)/\lambda\right) - \frac{2h}{1+h} \qquad \textbf{V.B.3.3-5}$$

$$\omega = \frac{\overline{\rho}_0 \lambda C_D}{2}\exp(-h/\varepsilon) + \frac{\omega_*}{\sqrt{u_*(1+h)^2 + 2(1+h)}} \qquad \textbf{V.B.3.3-6}$$

with

$$\cos\tilde{\gamma} = \cos\tilde{\gamma}_* + \frac{\overline{\rho}_0 \lambda C_D}{2}\exp(-h/\varepsilon) \qquad \textbf{V.B.3.3-7}$$

Having obtained the uniformly valid composite solution, it is noted that a problem occurs near $\gamma = 0$.

As the inner solution differs from the composite solution by terms of order ε, $\cos\tilde{\gamma}$ may reach unity before the composite solution. In this event the condition $\cos\tilde{\gamma} > 1$ arises near $\gamma = 0$ rendering the solution for u (eqn. V.B.3.3-5) indeterminate.

To avoid this the constant $\tilde{\gamma}_*$ is evaluated from the inner solution (eqn.V.B.3.1-8) by setting $\cos\tilde{\gamma} = 1$ at $h = h_{\min}$ i.e.

$$\cos\tilde{\gamma}_* = 1 - \frac{\overline{\rho}_0 \lambda C_D}{2}\exp(-h_{\min}/\varepsilon) \qquad \textbf{V.B.3.3-8}$$

where $h_{\min}$ is defined as the value of h at which the composite $\cos\gamma(\omega)$ becomes unity.

It should be noted at this point that the evaluation of $h_{\min}$ from eqn.V.B.3.3-6 requires prior evaluation of the constants u_* and ω_*. This concern is addressed more fully later (section V.B.5.2).

V.B.4 Exit Trajectory

The evaluation of the trajectory expressions does not assume either a negative or positive flight path angle and consequently the relations are equally applicable to both the atmospheric entry and exit portions of the skip, though obviously the initial conditions for each will be different. Recognising that the initial conditions for the exit are the final conditions from the entry it should therefore be possible to obtain the exit trajectory constants in terms of the entry constants.

Given that the flight path angle will take a positive value over the exit trajectory it is logical to assume that the constant $\tilde{\gamma}_*$ will also be positive. From eqn.V.B.3.1-8 it can be seen that the inner solution for the flight path angle is symmetrical about $h_{\min}$ and consequently

$$\tilde{\gamma}_{*_e} = -\tilde{\gamma}_* \qquad \textbf{V.B.4-1}$$

where the sub-subscript e denotes an exit trajectory constant. Equating the two sets of composite solutions at $h = h_{\min}$ the remaining exit constants are found as,

$$u_{*_e} = (u_* + 2)\exp(4\tilde{\gamma}_*/\lambda) - 2 \qquad \textbf{V.B.4-2}$$

$$\omega_{*_e} = \left(1 - \frac{\overline{\rho}_0 \lambda C_D}{2}\exp(-h_{\min}/\varepsilon)\right)\sqrt{u_{*_e}(1+h_{\min})^2 + 2(1+h_{\min})} \qquad \textbf{V.B.4-3}$$

The derived solutions are now complete and ready for implementation in an aerocapture guidance scheme.

V.B.5 Guidance

From the initial lunar return trajectory the vehicle is required to lose sufficient velocity that the resultant elliptical orbit has an apogee altitude as close as possible to some target altitude. It may not be possible for the vehicle to achieve the ΔV decrement necessary to attain the desired apogee on a simple skip and so a control is implemented at the bottom of

the skip to maintain that altitude until a release condition is satisfied where the vehicle then rolls to the pull-up bank angle.

Fig.V.B.5-1 below presents a schematic of the control methodology, where σ_c is the instantaneous command bank angle, determined by the onboard control.

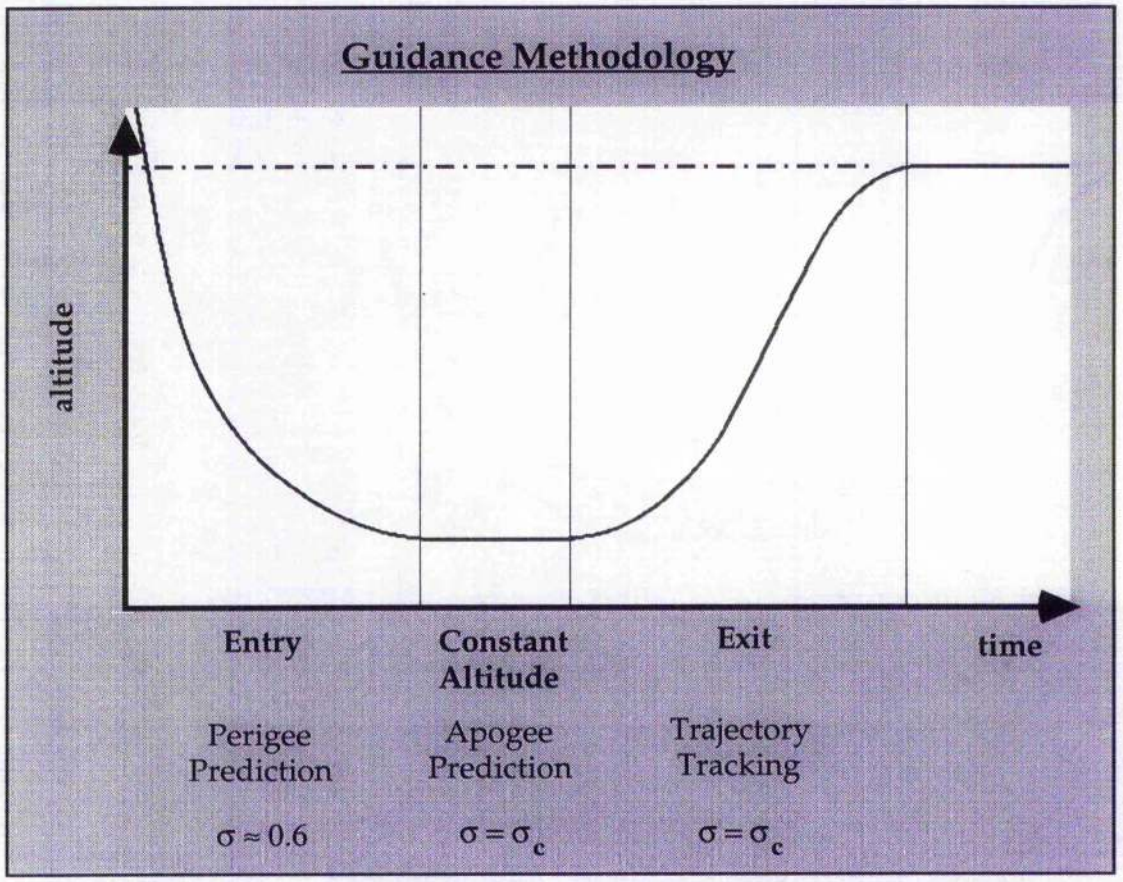

Fig V.B.5-1 - Schematic of Guidance Implementation

The control used to track this altitude is a non-linear transformation controller implemented via the vehicle bank angle.

The release condition referred to above is the prediction, using the analytic relations developed, that the desired apogee (within acceptable tolerances) would be achieved should the vehicle roll to a pre-determined "pull-up" bank

angle. This pull-up value is chosen so that the in-plane lift is not saturated, leaving some control authority for the exit leg.

Control over the exit trajectory is again implemented using non-linear transformations via the bank angle. The analytic predictions made in determining the pull-up point are used to provide a reference trajectory and the control is implemented to guide the vehicle along this path towards apogee.

Once at apogee, the vehicle's propulsion system would circularise the orbit and proceed from there to rendezvous with the station. Fig. V.B.5-2 presents a schematic of the onboard implementation of the control law.

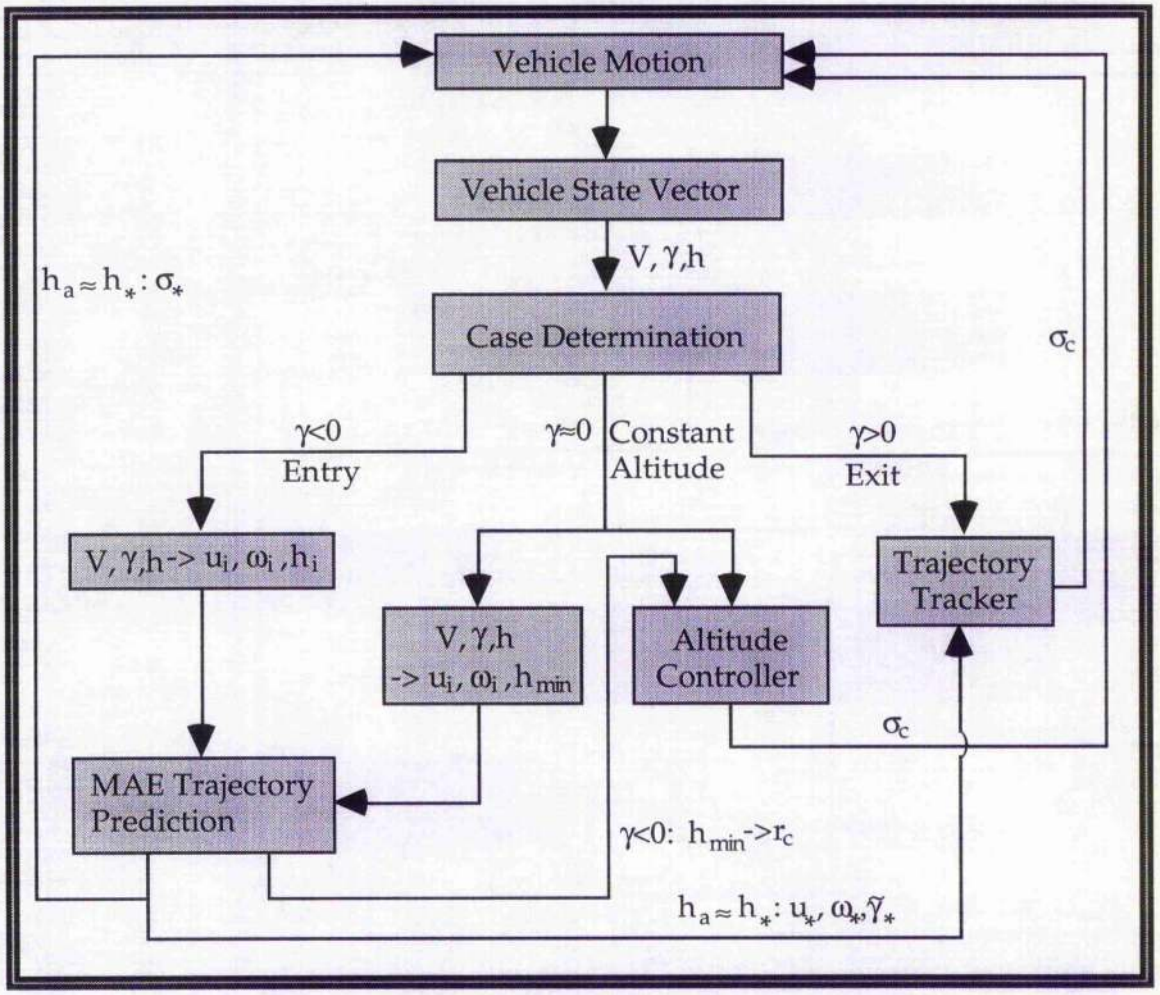

Fig.V.B.5-2 : Guidance Scheme Implementation

Although in this study the control laws are implemented by banking the vehicle, it should be noted that aerodynamic control can also be achieved by modulating the angle of attack. This approach would seem more suitable for manoeuvres requiring zero plane change as no out of plane forces are created by the control.

Implementation would appear to be more difficult, however, as the large pitching moments generated at hypersonic velocities would probably restrict the range of maintainable angles for a gliding vehicle lacking aerodynamic control surfaces. Gas jet control is possible but maintaining an off-trim pitch angle would require large amounts of fuel, far more than control of the bank angle which would also give access to the entire range of in-plane lift, from maximum outward to maximum inward[77]. There is also the added advantage of simplicity in the control law. Whereas a change in angle of attack will affect both C_L and C_D, a change in bank angle affects neither, rather it redirects the lift vector. It is also considered that the ability to control, to some degree, the plane of vehicle motion would be useful in correcting small changes in orbit plane.

V.B.5.1 Non-linear transformation controller for constant altitude.

The control used here is developed using non-linear transformations. As stated above the controller is implemented via the bank angle, which has the effect of redirecting the lift vector. It is assumed that the desired out-of-plane motion is achieved through periodic roll-reversals and so the variable λ is modified such that it becomes the in-plane lift-to-drag ratio, i.e.

$$\lambda = \frac{C_L \cos\sigma}{C_D} \qquad \textbf{V.B.5.1-1}$$

This definition will be used for the remainder of this section.

The control is required to track a given altitude, r_c, and so successive time derivatives of r are taken until the control σ appears explicitly in the relations. This occurs in the second derivative of r so a pseudocontrol P is defined as

$$P \equiv \frac{d^2r}{dt^2} = -\frac{\rho V^2 S C_D}{2m}\sin\gamma + \frac{\rho V^2 S C_L}{2m}\cos\sigma\cos\gamma + \frac{V^2}{r}\cos^2\gamma - \frac{\mu}{r^2}$$

...V.B.5.1-2

Stability is ensured by evaluating the pseudocontrol in terms of the altitude error and error rate, viz.,

$$P = -\phi_1(r - r_c) - \phi_2\left(\frac{dr}{dt} - \frac{dr_c}{dt}\right) \qquad \text{V.B.5.1-3}$$

where the reference climb rate, $\frac{dr_c}{dt}$, will be zero for a constant reference altitude.

The feedback gains ϕ_1 and ϕ_2 are chosen to produce the desired vehicle response in following the reference altitude. Rearranging eqn.V.B.5.1-2 the command bank angle is found to be

$$\cos\sigma = \frac{2m}{\rho V^2 S C_L \cos\gamma}\left[\frac{-V^2}{r}\cos^2\gamma + \frac{\mu}{r^2} + \frac{\rho V^2 S C_D}{2m}\sin\gamma + P\right]$$

...V.B.5.1-4

V.B.5.2 Apogee Targeting

Throughout the entry and constant altitude phases of the motion it is possible the apogee the vehicle will achieve for a particular value of $\cos\sigma$, using eqns.V.B.3.3-5 & V.B.3.3-6. In order to apply these equations, however, it is necessary to first evaluate the trajectory constants u_*, ω_* and $\tilde{\gamma}_*$.

During exoatmospheric flight the initial conditions are used to evaluate the two outer constants directly, and prediction of the minimum altitude yields $\tilde{\gamma}_*$. The procedure

becomes a little more complicated during the atmospheric phase of the motion.

A problem arises when considering the modified constant $\tilde{\gamma}_*$. Remembering that the modification of this constant is required to avoid ω taking a value greater than unity near the bottom of the skip, it is essential for accurate evaluation of the exit trajectory constants.

It has been noted that evaluation of $\tilde{\gamma}_*$ requires prior knowledge of u_* and ω_*, and, as the motion is now within the inner region these outer constants must be evaluated from their inner equivalents which are in turn evaluated from the current vehicle state.

The problem is that one of the inner constants, $\tilde{\omega}_*$, is the cosine of the very constant that is being modified. Obviously one cannot be changed without the other, though thankfully elimination of both from the minimum altitude evaluation is possible.

Eqn.V.B.3.3-5 is used to express both $\tilde{\gamma}_*$ and $\tilde{\omega}_*$ in terms of the minimum altitude. The inner velocity constant, $\tilde{u}_*$, may be evaluated with impunity, as it is depends only on the current velocity and flight path angle.

The outer constants are now obtained through the matching process. Substitution of the resultant expressions in terms of h_{min} into eqn.V.B.3.3-5 yields, with $h = h_{min}$,

$$1 = \frac{\bar{\rho}_0 \lambda C_D}{2} \exp\left(-h_{min}/\varepsilon\right) + \frac{\left(1 - \frac{\bar{\rho}_0 \lambda C_D}{2} \exp\left(-h_{min}/\varepsilon\right)\right) \sqrt{\tilde{u}_* \exp\left(-2\cos^{-1}\left(1 - \frac{\bar{\rho}_0 \lambda C_D}{2} \exp\left(-h_{min}/\varepsilon\right)\right)\Big/\lambda\right)}}{\sqrt{2\left(1+h_{min}\right) + \left(1+h_{min}\right)^2 \left(-2 + \tilde{u}_* \exp\left(-2\cos^{-1}\left(1 - \frac{\bar{\rho}_0 \lambda C_D}{2} \exp\left(-h_{min}/\varepsilon\right)\right)\Big/\lambda\right)\right)}} \quad \text{...V.B.5.2-1}$$

which is then solved for h_{min} using a Newton-Raphson iterative solver.

For computational simplicity, during the constant altitude portion of the motion the trajectory constants are evaluated using the assumption that for flight path angles very close to zero ($\pm 0.1^{o}$) ω may be taken as unity, implicitly defining the current altitude as the minimum altitude. Having so defined the minimum altitude the exit trajectory constants are readily evaluated from eqns.V.B.3.1-7, V.B.3.1-8, V.B.3.3-1, V.B.3.3-2 & V.B.3.3-8.

In predicting the apogee, rather than iterate to a solution as is done for the minimum altitude evaluation the predictions are used to evaluate the trajectory variables at a point outwith the atmosphere. The values of the trajectory variables at this exo-atmospheric point are then used as the initial conditions for the purely Keplerian motion to apogee.

Using the outer solution expressions alone then it can be shown that the resultant apogee, h_a, is given by

$$h_a = -\frac{\left(1+\sqrt{1+u_{*_{exo}}\,\omega_{*_{exo}}}\right)}{u_{*_{exo}}} - 1 \qquad \textbf{V.B.5.2-2}$$

where $u_{*_{exo}}$ and $\omega_{*_{exo}}$ are the outer constants obtained from eqns.V.B.3.2-5 & V.B.3.2-6 using the values of u and ω predicted at the exoatmospheric point.

In this manner the apogee predictions are constantly updated and the pull-up control value achieved when the predicted apogee lies within a specified tolerance of the target altitude.

V.B.5.3 Trajectory Tracking

The trajectory constants evaluated in predicting the point for the pull-up manoeuvre are now used to determine the ideal velocity and flight path angle at any point along the vehicle's trajectory. This data is then used as reference data for a feedback linearisation controller designed to guide the vehicle along the path defined by the analytic relations.

As the trajectory data is generated analytically in-flight the need for either storage of pre-planned trajectory data or repeated numerical integration of the trajectory is removed.

The control is devised as though it were following an altitude plan. As will be seen this allows account to be taken of errors in both velocity and flight path angle.
The altitude error y is defined as

$$y = r - r_{ref}(t) \qquad \textbf{V.B.5.3-1}$$

and consecutive time derivatives are taken until the control σ appears explicitly. This occurs in the second derivative which then defines a pseudo-control.

$$\dot{y} = V\sin\gamma - \dot{r}_{ref}(t) \qquad \textbf{V.B.5.3-2}$$

$$\ddot{y} = -\frac{\rho V^2 S C_D}{2m}\sin\gamma + \frac{\rho V^2 S C_L}{2m}\cos\sigma\cos\gamma + \frac{V^2}{r}\cos^2\gamma - \frac{\mu}{r^2} - \ddot{r}_{ref}(t)$$

...**V.B.5.3-3**

In order to assure stability the pseudo-control is evaluated from the altitude error and climb rate error as

$$\ddot{y} = -\alpha_1\dot{y} - \alpha_2 y \qquad \textbf{V.B.5.3-4}$$

It is noted at this time that, as the reference trajectory is altitude driven, that at any given point the altitude error is always zero and consequently the pseudo control is defined solely in terms of the climb rate error, i.e.

$$\ddot{y} = -\alpha\dot{y} \qquad \textbf{V.B.5.3-5}$$

where the feedback gain α is chosen to achieve the desired vehicle response.

Given that there are limits to the control which can be applied, judicious choice of α is required. This is discussed further in the implementation section of this chapter (section V.B.6 which follows).

The command bank angle may now be obtained from eqns. V.B.5.3-3 & V.B.5.3-4 as

$$\cos\sigma_c = \frac{2m}{\rho V^2 S C_L \cos\gamma}\left[\frac{-V^2}{r}\cos^2\gamma + \frac{\mu}{r^2} + \frac{\rho V^2 S C_D}{2m}\sin\gamma + \ddot{y} + \ddot{r}_{ref}(t)\right]$$

...V.B.5.3-6

As stated before, the reference trajectory is altitude driven and so the description of the reference variables as functions of time is somewhat misleading. The reference radial acceleration, $\ddot{r}_{ref}(t)$, for example, is found from the values of the trajectory variables for the altitude at which the vehicle finds itself at time t.

$$\ddot{r}_{ref}(t) = -\frac{\mu}{r^2} + \frac{\rho V_{ref}^2 S C_L}{2m}\cos\sigma_{ref}\cos\gamma_{ref} - \frac{\rho V_{ref}^2 S C_D}{2m}\sin\gamma_{ref} + \frac{V_{ref}^2}{r}\cos^2\gamma_{ref}$$

...V.B.5.3-7

The reference climb rate, $\dot{r}_{ref}(t)$, required for determination of the pseudocontrol, is also found in this manner as

$$\dot{r}_{ref}(t) = V_{ref}\sin\gamma_{ref} \qquad \text{V.B.5.3-8}$$

We will now examine the implementation of the control into *genL* and its performance in controlling the aerocapture manoeuvre.

V.B.6 Implementation and Results

The following section considers a small, unmanned, sample return vehicle, $1000kg$ in mass with an aerodynamic lift-to-drag ratio of 1.5 and a ballistic coefficient ($\beta = mg/C_D S$) of $19620Pa$, unless otherwise stated.

The vehicle is assumed to be sufficiently blunt (half-cone angle greater than about 7°) that a constant value for L/D can be used. For such a vehicle the small variations in hypersonic L/D will be dwarfed by the variations in air-density.

The vehicle is performing an aerobrake manoeuvre in the Earth's atmosphere. The manoeuvre is controlled such that the vehicle exits along a trajectory with an apogee as close as possible to the orbital altitude of the space station, $436.48km$.

In addition a fuel limit of $100kg$ is imposed on the vehicle, resulting in a ΔV capability of $310m/s$, for a specific impulse of $300s$.

Matched asymptotic expansions have been shown in the past to yield good results in comparison to numerical simulations[21,42,56,57,76,82]. Nothing new is added to the solutions in this chapter and so the justification for their use is taken as proven. It is the way in which they are implemented which is crucial here.

As has been said, the initial entry phase (see Fig V.B.5.1) is envisaged as monitored rather than guided. During this portion of the motion matched asymptotic expansions are used to predict the apogee which would result if the vehicle were rolled to the pull-up control value. In this way allowance is made for extreme variation in the atmospheric conditions experienced during entry.

Should the vehicle achieve the release condition during this phase pull-up would be effected at that point. In the worst case scenario the vehicle would be unable to achieve the desired altitude leaving the options of abort to lower orbit, abort to ground, or self-destruct. The most desirable of these would appear to be abort to lower orbit though this may not always be practical and indeed retrieval of the vehicle in a lower, faster decaying orbit may not prove feasible at all.

In implementing the control algorithm we take the vehicle state at $100km$ as the initial conditions for prediction of the minimum altitude using the derived analytic relations. Some iteration is needed to obtain the minimum altitude so the choice of $100km$ altitude is arbitrarily made to ensure the on-board computer has time to complete the calculations. In addition, $100km$ is deemed sufficiently high to be said to lie in the outer region for the analytic model.

For these reasons the results presented below are given in terms of the flight path angle at $100km$ altitude, referred to here as the "initial" flight path angle. There will be some disparity between this value and the entry angle. However, as there will inevitably be some error in the anticipated atmospheric conditions on entry, precise estimation of the flight path angle at the start of the first control phase would not be possible, though the disparity will likely be small. Given this, the choice of control gains is made such that a good degree of accuracy was maintained over a range of initial flight path angles rather than choosing a gain to precisely achieve the target altitude for one particular flight path angle. It was felt that this approach would be a more realistic test of the control algorithm.

Given the fast dynamics of the system, the data sample speed will be important for both state vector update and determination of the pull-up point.

Ideally, pull-up would be performed at the exact instant when the desired apogee is predicted. However, sample rates and computing speed make this impractical for now, and so pull-up is achieved when the predicted apogee lies within an acceptable range of the target.

A tolerance of $\pm 1.5km$ was chosen for this work, with an elapse time of one-tenth of a second between state vector updates and a first order filter applied to the control output to compensate for this and smooth out the control time history.

The filter takes the form

$$\Delta\sigma = (\sigma_c - \sigma_{ref})\exp(-\zeta t) \qquad \textbf{V.B.6-1}$$

where ζ is the filter gain, σ_{ref} the pull-up bank angle used as the reference bank angle in determining the command bank angle (eqn. V.B.5.3-7) so that the final control demand, σ_d, is

$$\sigma_d = \sigma_{ref} + \Delta\sigma \qquad \textbf{V.B.6-2}$$

This is the value of bank angle that will be demanded of the vehicle.

The performance of the routine was checked on *genL* running first with an exponential atmosphere and then a model of the 1962 U.S. standard atmosphere[78] (section II.C.2.3.4) representing the ideal atmosphere used by the on-board computer and the "real" atmosphere, respectively. Runs were carried out using the analytic apogee targeting system both with and without the trajectory tracking routine.

The comparison between the two runs (both using an exponential atmosphere model) with an initial flight-path angle of -6° (fig.V.B.6-1) shows a small overshoot for both cases with the trajectory tracking reducing the apogee error by over 25%. Fig.V.B.6-2 shows the absolute apogee error over a range of initial flight path angles from -5° to -8°, with a similar improvement in apogee error for each initial angle when the trajectory tracking is used.

The aforementioned fast dynamics of the system leave it susceptible to perturbations. It was intended that the relatively deep pass into the atmosphere and the use of a relatively high lift-to-drag ratio would exaggerate the differences between the ideal exponential atmosphere and the "real" atmosphere, again providing a more realistic test of the guidance.

Fig.V.B.6-3 shows the results for a pass through a model of the 1962 U.S. standard atmosphere. As expected the different density profile (Fig. II.C.2.3.4-1) introduces a new source of error to analytic predictions and without tracking of the predicted path the final apogee is in error by 36*km*. Using the trajectory tracking, however, this error is reduced by almost 86%.

From fig. V.B.6-4 it can be seen that the trajectory tracking again produces sizeable reductions in apogee error over the same range of initial flight path angles as before.

The absolute disparity between the apogees achieved for the two atmosphere models (fig. V.B.6-5) gives a guide to the robustness of the guidance algorithm. Once again, the trajectory tracking shows considerable improvement in

consistency over the apogee targeting alone. Fig.V.B.6-6 shows the altitude time histories of the four cases discussed so far. It can be seen that even the worse of the two results for the tracker improves on the better of the two for the free exit.

As has been stated, of primary importance in the testing of a control is the robustness of the control to state estimation and atmospheric errors. The results discussed above are the beginnings of such an analysis.

Errors in the predicted atmospheric conditions are the most likely errors to be encountered. Fig V.B.6-7 shows the apogee altitudes obtained in response to a range of off-nominal atmospheric conditions.

The off-nominal atmospheres are generated as per equations II.C.2.3.5-1 & -2. In each case the control assumes an exponential model for atmospheric density. Variations in bias were found to have a greater effect than the amplitude or frequency of the oscillations. Consequently the results shown here are for variations in bias, with $a = 0.1$ and $h_{ref} = 3.0km$ held constant.

Figure V.B.6-8 shows the control responses for these off-nominal atmospheric conditions. The vehicle enters the atmosphere at a constant bank angle, then saturates whilst pulling towards the predicted constant altitude. The control then gradually reduces this angle as required by the constant altitude controller. The spikes occur at the pull-up point and the consequent traces show the control acting to maintain alignment with the on-board generated reference data.

Figure V.B.6-9 shows the corresponding altitude histories. The spread appears wide but as Table V.B.6-1 shows the fuel savings over uncontrolled exit are significant and all within the $100kg$ fuel limit.

Clearly the trajectory tracking has reduced the apogee altitude error significantly. Figures V.B.6-10 & -11 show how this improvement translates to ΔV saving, firstly in absolute terms, and secondly by expressing the ΔV required to achieve

ISSA altitude from apogee as a function of that required for the uncontrolled exit. The savings are significant with ΔV requirements more than halved for most of the cases run.

Figure V.B.6-12 shows how the two sets of ΔV requirements compare to our ΔV budget of $310 m/s$. Without the trajectory tracking the system never achieves space station orbit within budget whilst using the tracking the budget is never exceeded. In software terms this has been achieved by a handful of lines of code.

What these ΔV savings mean in terms of the spacecraft design itself can be seen when we convert the ΔV data into fuel mass (assuming a specific impulse, I_{sp}, of $300s$):

Figure V.B.6-13 shows that the fuel saved with a controlled exit is actually greater (in all cases bar one) than the fuel actually required after such an exit.

Numerically (table V.B.6-1) we find that this equates to 80 or $90kg$ less fuel thanks to those few lines of code. Add to this the mass savings in the size of the fuel tanks (10% of the propellant mass[79]), and more importantly the ΔV savings by the reduced mass at transearth injection, and the significance of this mass reduction is even more readily appreciable.

bias β	fuel used (kg) (controlled)	fuel used (kg) (uncontrolled)	fuel savings (kg)
-0.05	89.20	177.41	88.21
-0.0375	80.85	170.05	89.20
-0.025	73.76	164.11	90.34
-0.0125	66.65	158.00	91.35
0 (nominal)	46.82	141.26	94.44
0.0125	52.46	145.31	92.86
0.025	46.80	140.13	93.33
0.0375	51.60	133.36	81.76
0.05	56.27	127.88	71.61

Table V.B.6-1 : Fuel Requirements and Savings

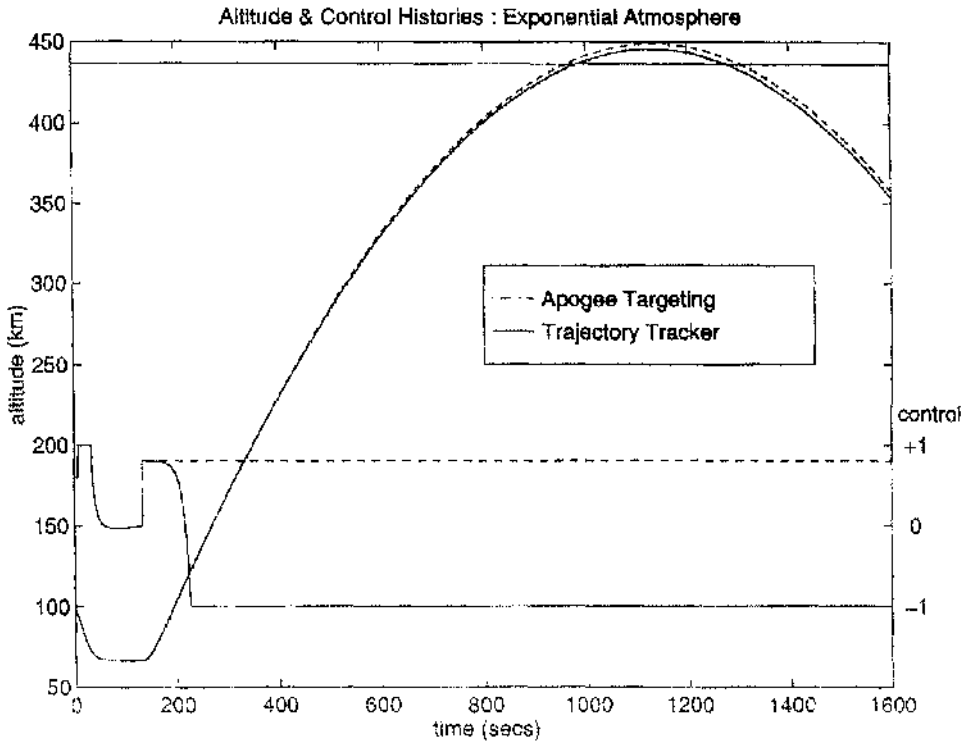

Fig. V.B.6-1 : Altitude & Control Histories : Exponential Atmosphere

$\alpha = 3,\ \zeta = 20$

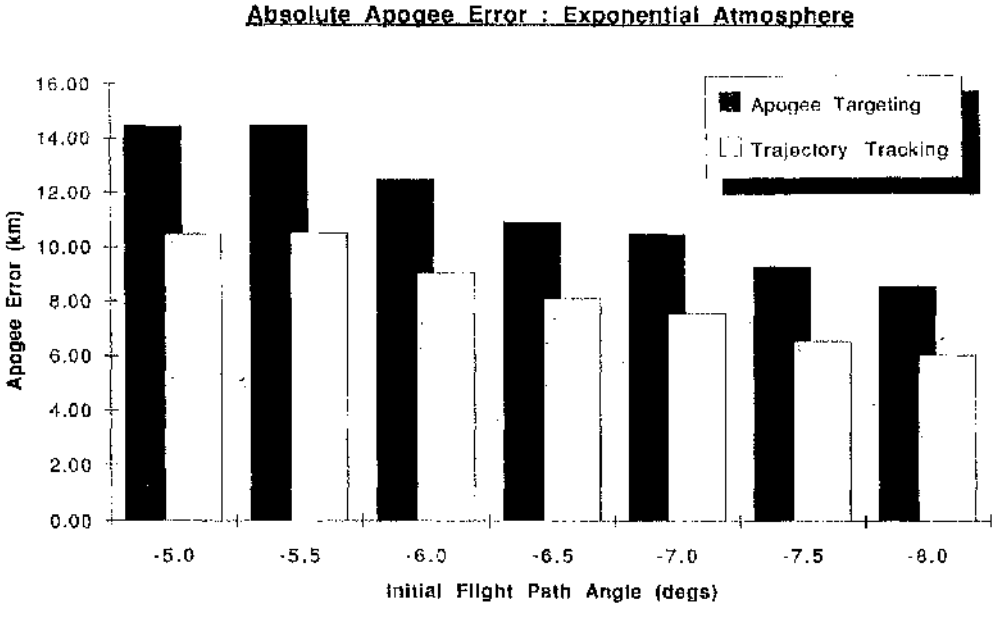

Fig. V.B.6-2 : Absolute Apogee Error : Exponential Atmosphere

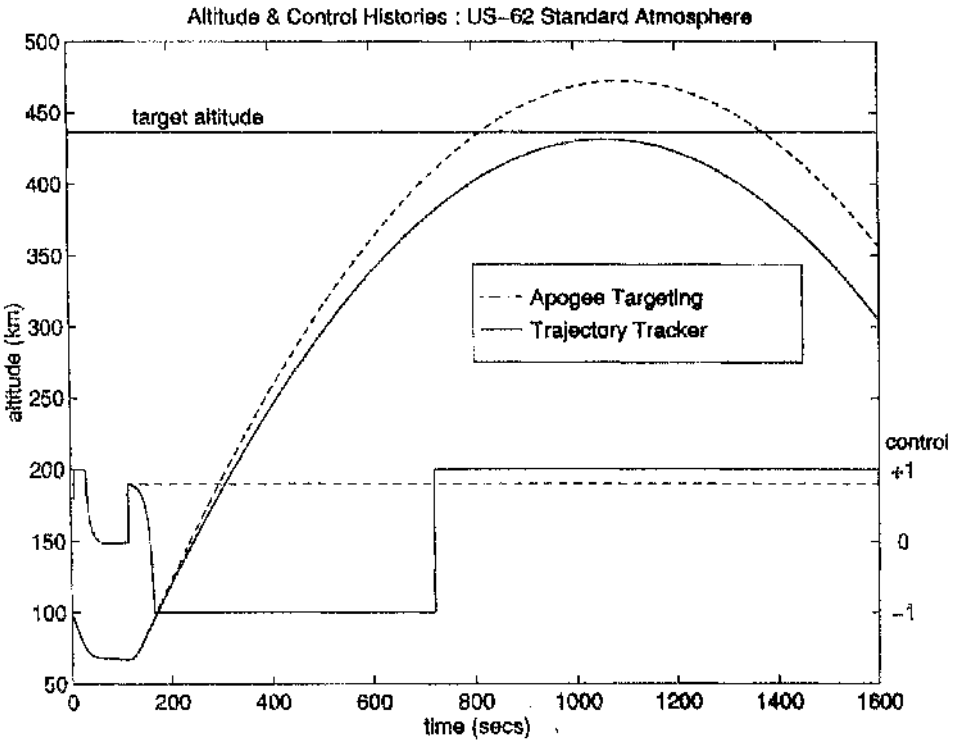

Fig. V.B.6-3 - Altitude & Control Histories : US-62 Standard Atmosphere

$\alpha = 3,\ \zeta = 20$

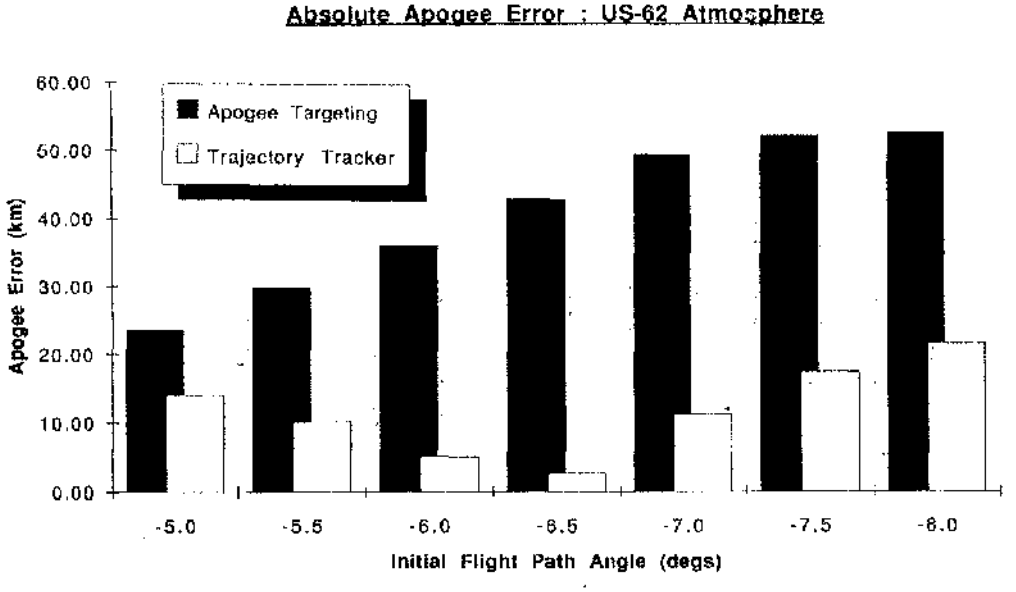

Fig. V.B.6-4 - Absolute Apogee Error : US-62 Standard Atmosphere

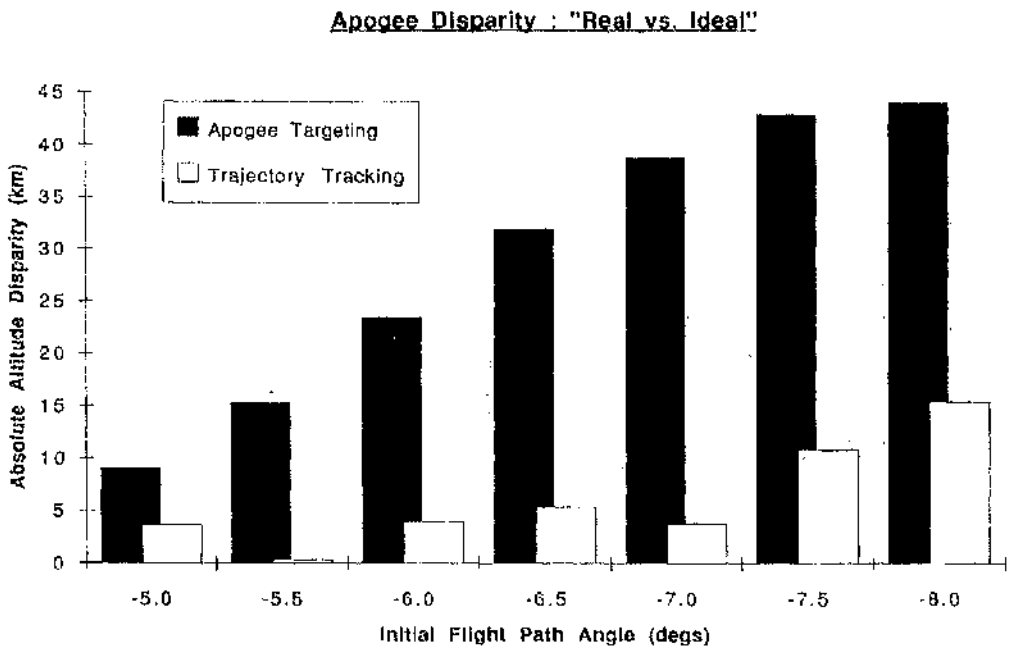

Fig. V.B.6-5 : Apogee Disparity : "Real" vs "Ideal" Atmospheres

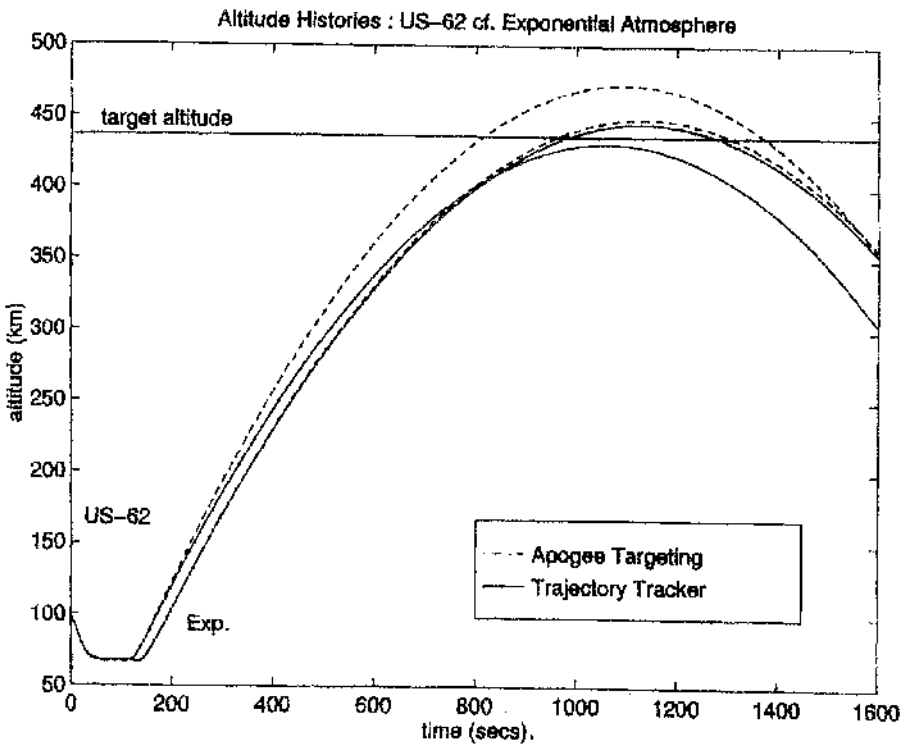

Fig. V.B.6-6 : Altitude Histories : US-62 cf. Exponential Atmosphere Controlled and Uncontrolled Exit

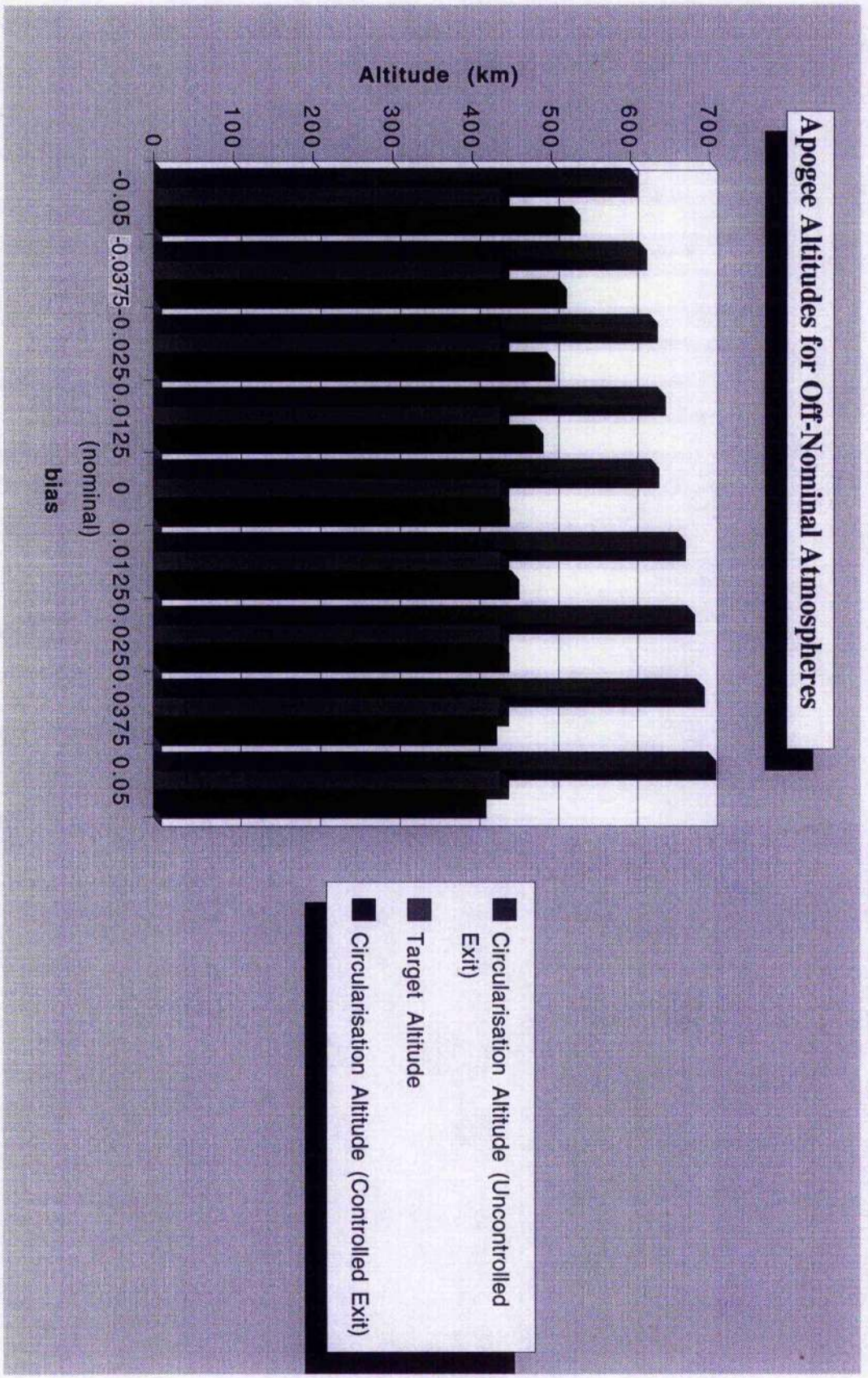

Fig. V.B.6-7 : Apogee Altitudes Achieved in Off-Nominal Atmospheric Conditions

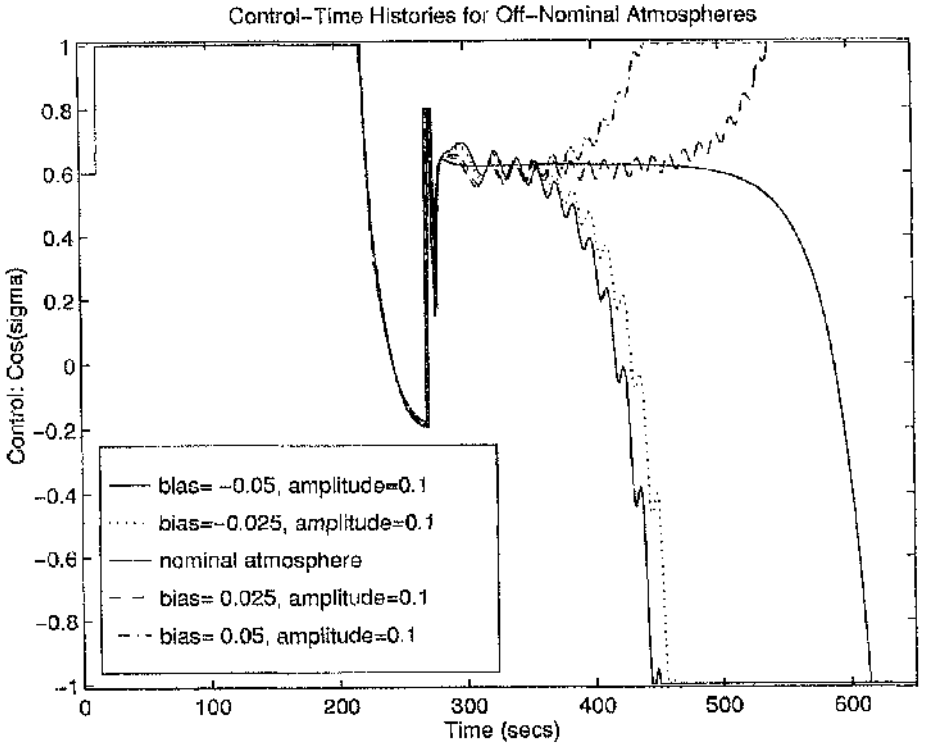

Fig. V.B.6-8 : Control Histories in Off-Nominal Atmospheric Conditions

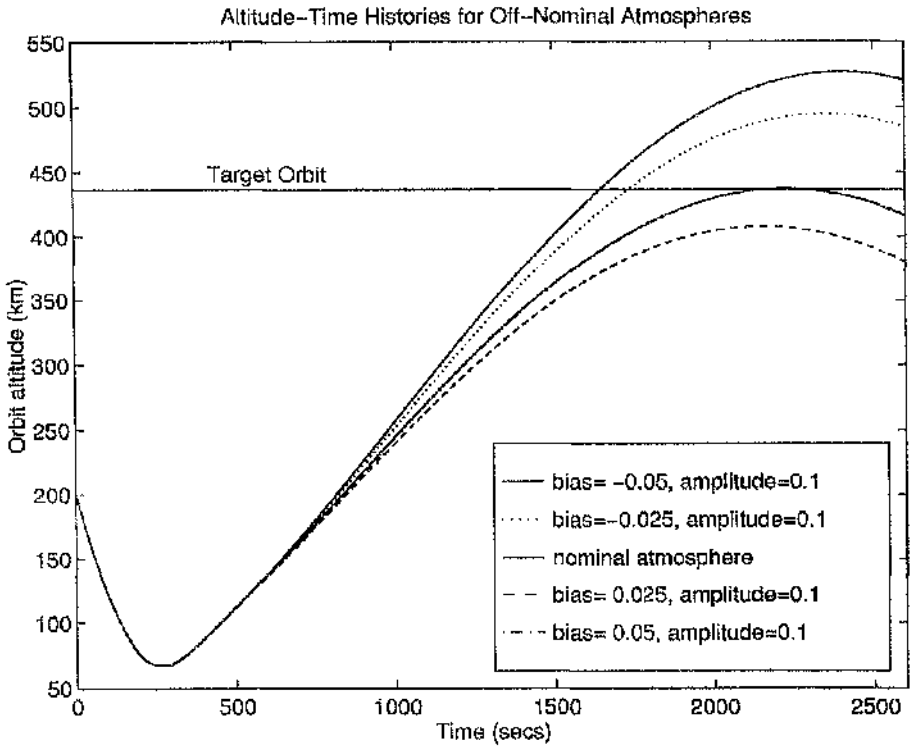

Fig. V.B.6-9 : Altitudes Histories in Off-Nominal Atmospheric Conditions

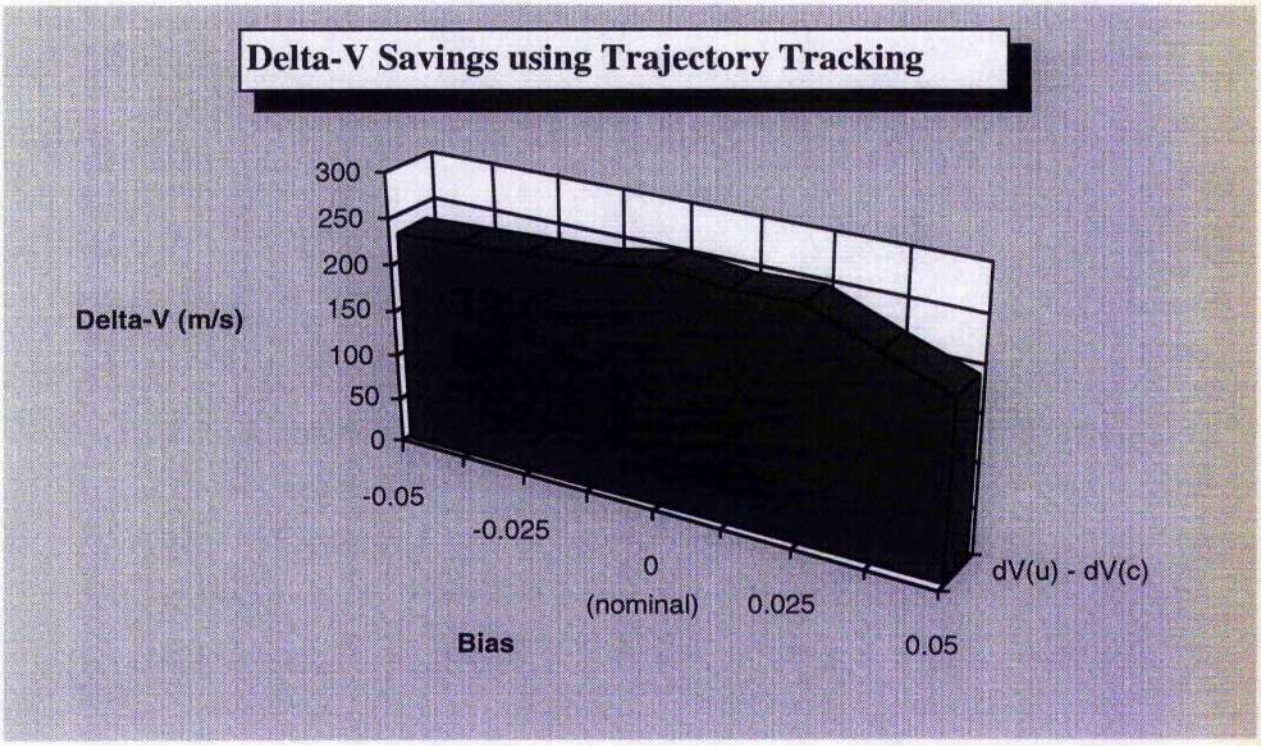

Fig. V.B.6-10 : ΔV savings using Trajectory Tracking†

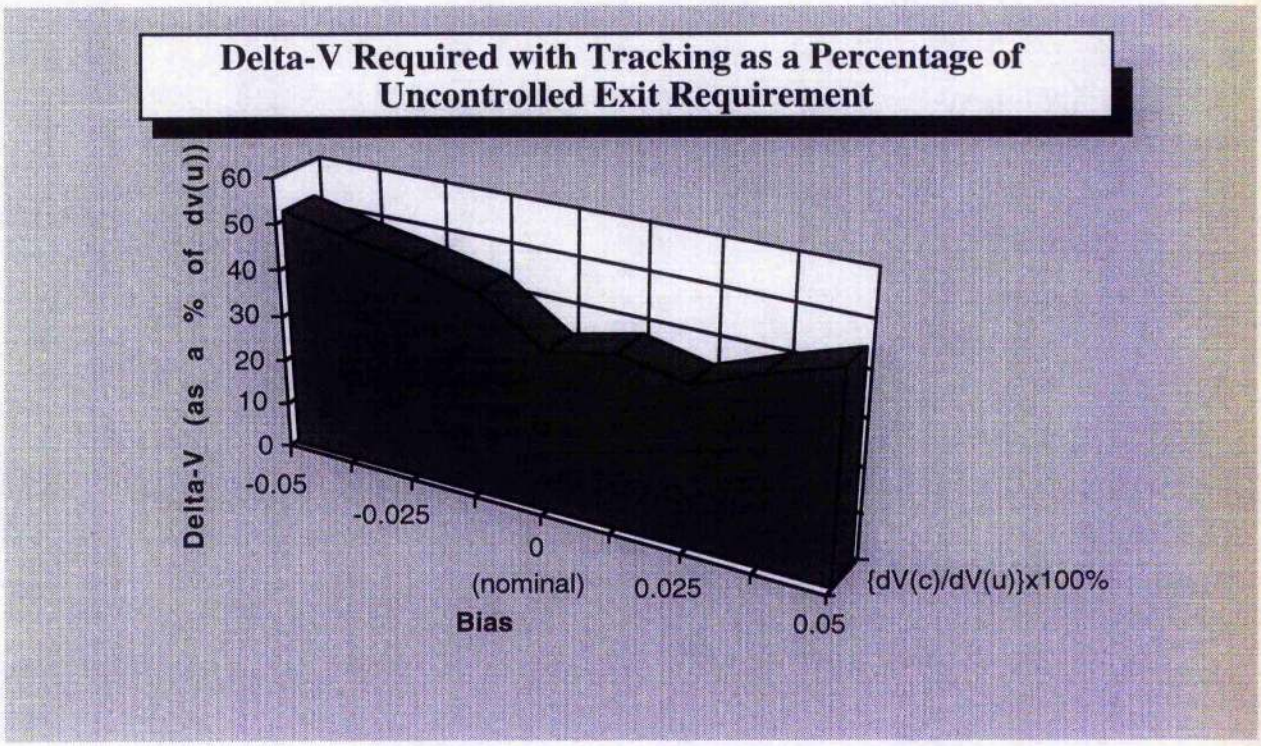

Fig. V.B.6-11 : Required ΔV as a percentage of uncontrolled trajectory requirement†

† dv(u) : ΔV for uncontrolled exit, dv(c) : ΔV for controlled exit

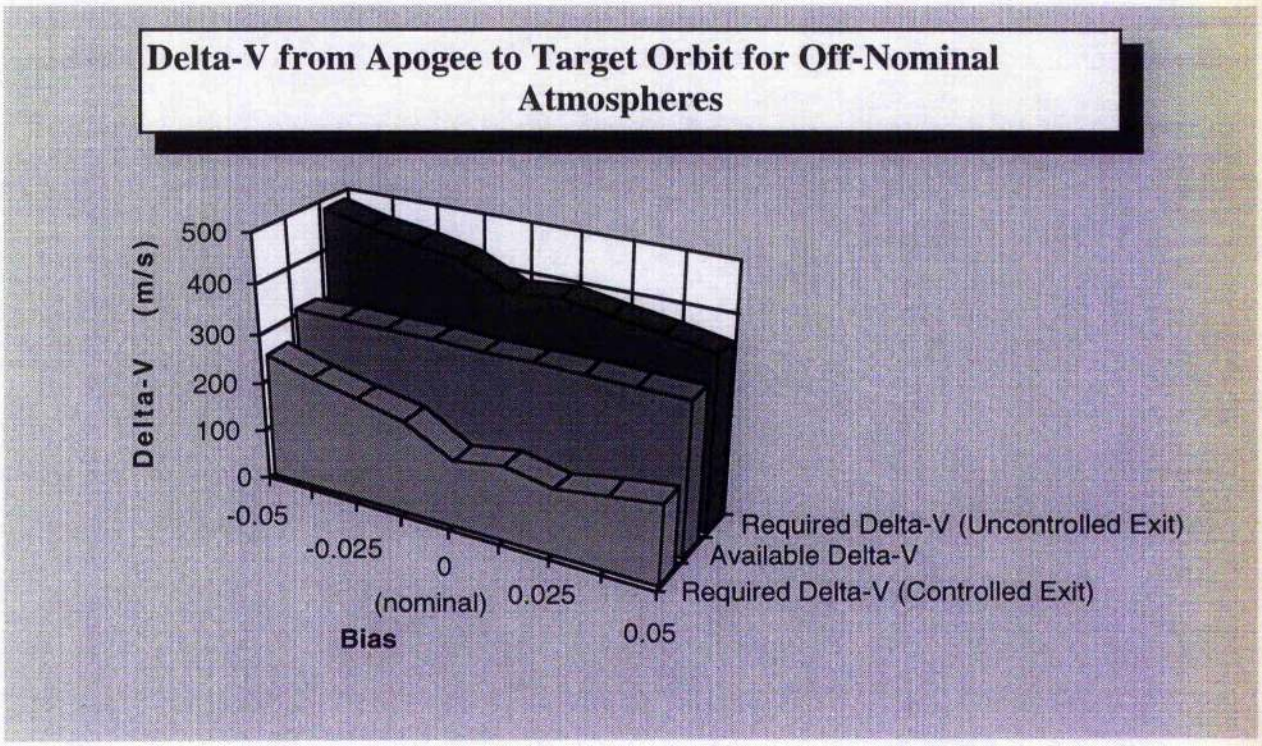

Fig. V.B.6-12 : ΔV requirements for controlled and uncontrolled exits

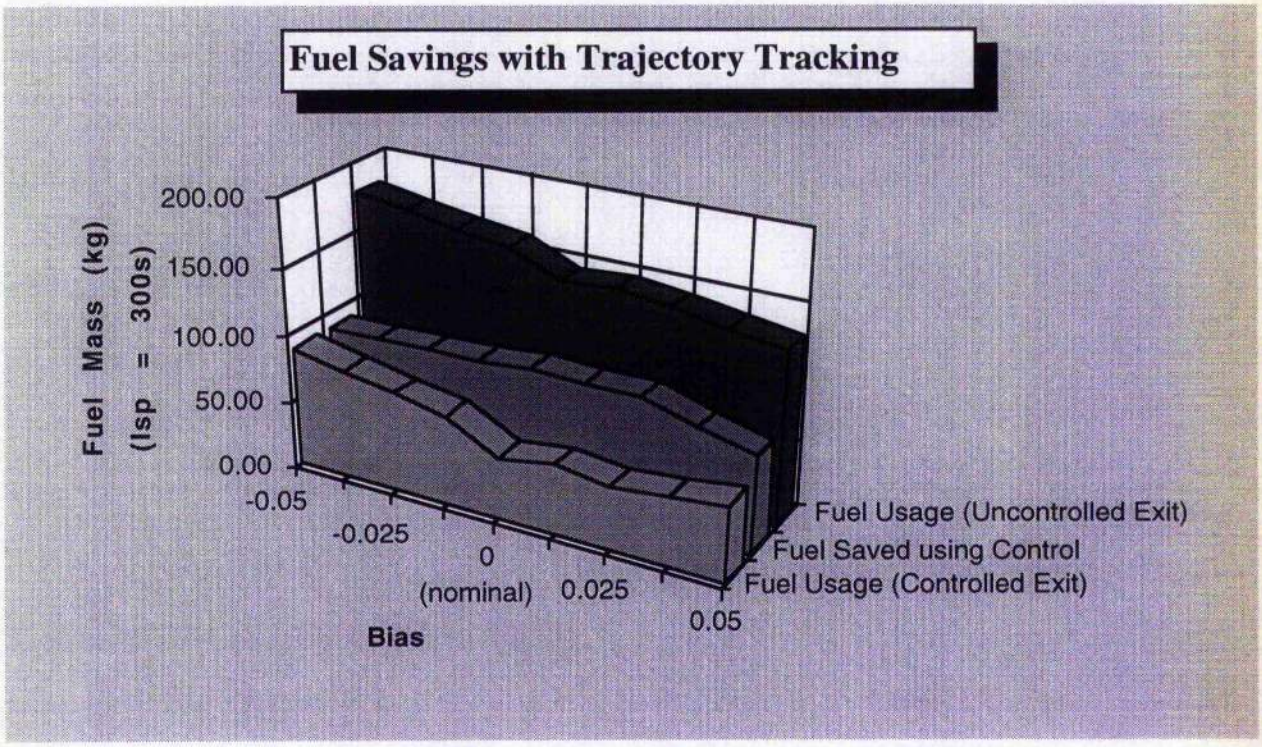

Fig. V.B.6-13 : Fuel requirements for controlled and uncontrolled exits.

Table V.B.6-2 below shows how one set of control gains copes with large variations in initial velocity, V_i. The control gains used were chosen to produce a minimum apogee error at $V_i = 9.20 km/s$.

Initial Velocity V_i (km/s)	Apogee Altitude h_a (km)	Apogee Error Δh (km)	Apogee Velocity V_a (km/s)	Required ΔV (m/s)
9.00	464.37	27.89	7.17	496.00
9.10	452.37	15.89	7.19	465.09
9.20	439.92	3.44	7.21	434.92
9.30	445.52	9.04	7.24	413.06
9.40	445.47	8.99	7.26	389.43
9.50	446.27	9.79	7.28	368.18
9.60	454.27	17.79	7.30	353.35
9.70	451.96	15.48	7.32	332.56
9.80	454.24	17.76	7.34	316.43
9.90	460.95	24.47	7.35	305.78
10.00	506.07	69.59	7.35	335.29
10.10	498.78	62.30	7.37	313.96
10.20	428.82	-7.66	7.41	245.20

Table V.B.6-2 : Variation in Apogee Altitude and Velocity for a range of Initial Velocities.

The first observation we make is that the apogee velocity is the predominate factor in determining the ΔV required to achieve space station orbit. Compare the results obtained for $V_i = 9.80 km/s$ with those for $V_i = 10.10 km/s$. The increase in attained apogee altitude is marked whilst the ΔV requirement actually drops.

The second observation we make concerns the stability of the control. From $V_i = 9.00 km/s$ to $V_i = 9.60 km/s$ there appears to be a local minimum in the apogee altitude results at $V_i = 9.20 km/s$. The trend continues up to $V_i = 9.90 km/s$, though with less consistency, and thereafter the changes become larger and less predictable until at $10.3 km/s$ the control fails completely and a surface impact occurs.

Mathematically the control guarantees stability, however the available limits to the control (±90° bank angle) and the inherent instability of the manoeuvre have rendered the particular gains used unstable in this instance. This theory is borne out as we examine the use of a further set of gains for entry velocities above $10.2 km/s$. Here the control produces very favourable results (table V.B.6-3) but loses applicability more rapidly, failing after $10.4 km/s$. Yet another set of gains can be employed for entry velocities above $10.4 km/s$ though this time the results are valid only for cases within $\pm 0.1 km/s$.

Initial Velocity V_i (km/s)	Apogee Altitude h_a (km)	Apogee Error Δh (km)	Apogee Velocity V_a (km/s)	Required ΔV (m/s)
10.30	435.41	1.07	7.42	222.53
10.40	432.16	4.32	7.44	212.67

Table V.B.6-3 : Variation in Apogee Altitude and Velocity for a range of Initial Velocities.

What explanations can we offer for this behaviour?
Firstly, the control operates in two phases : constant altitude and exit trajectory tracking.

The control over the constant altitude portion is implemented first and so we consider this first as a possible answer.

Increasing entry velocities will result in rapidly reducing perigee altitudes. Although the apogee altitude is still predicted internally to the system, this renders the control gains less applicable for off-design velocities and may result in over- or underdamping of the vehicle response. The higher the velocity the greater the disparity, this is likely to be a result of increasing duration and/or frequency of saturation of the control.

As a result, pull-up prediction does not actually occur along as smooth an altitude profile as intended in the control theory. Figure V.B.6-14 shows a schematic of the effect of an off-design entry velocity on the vehicle motion. This requires either the widening of the predicted apogee tolerances to avoid failure of

the control or a modification of the prediction technique to allow prediction from off-zero flight path angles.

Unfortunately this latter approach requires iteration to find the inner integration constants increasing the computational demands of the predictions. For a negative flight path angle this also introduces the additional complexity in that the apogee prediction is no longer for an exit trajectory with $\gamma_i = 0$ but rather for a skip with the initial conditions in the inner solution. It was found that knowledge of the additional integration constants required for a lifting skip trajectory was less reliable for initial conditions within the inner solution particularly so for small values of γ(see section V.B.5.2).

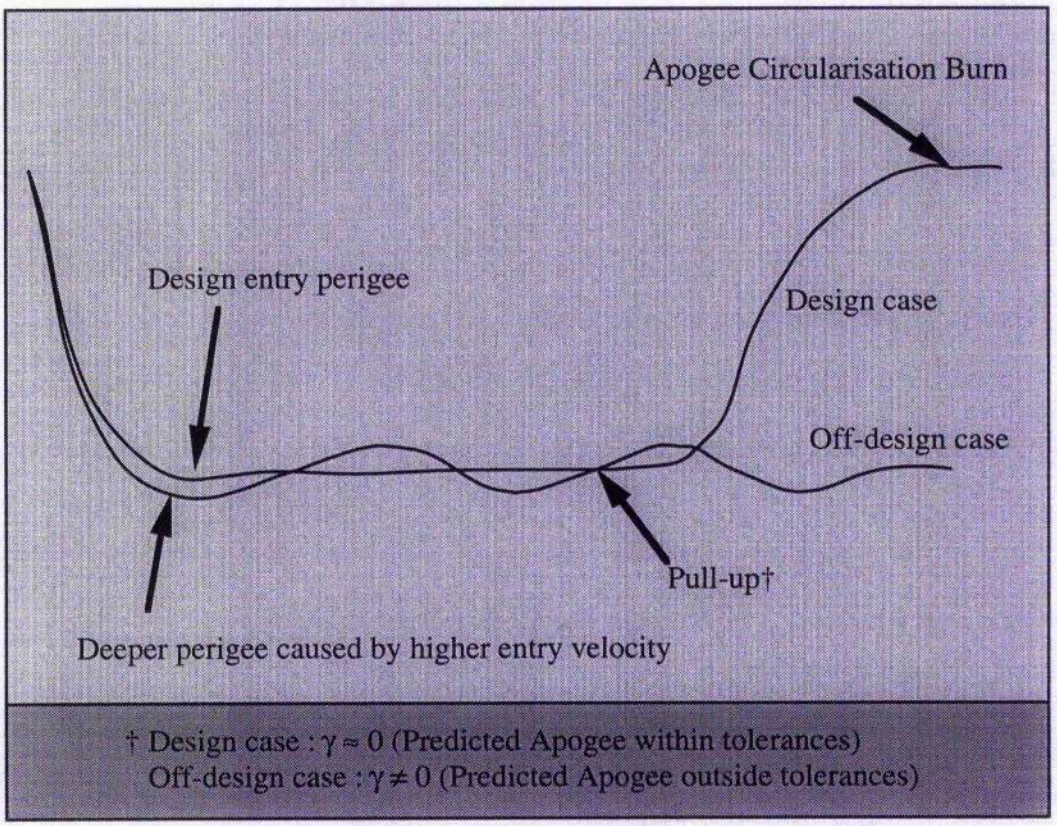

Fig. V.B.6-14 : Effect of off-design entry conditions

Increasing entry velocity seems to exaggerate the problem although the range of validity was found to remain around $\pm 50 m/s \rightarrow \pm 100 m/s$. The post-flight best-estimate trajectory for Apollo 11[12] calculated atmospheric entry velocity to within

$0.1m/s$ of the value supplied to the command module computer by ground support. This value was uploaded to the computer prior to entry at $124km$, and suggests that even these reduced ranges fall within attainable limits.

A similar analysis of the controls response to variations in initial flight path angle produces similar results. Here a spread of $0.7°$, well above targeting constraints, was found to be possible for lower entry velocities decreasing to around $0.2°$ for higher velocities. Again, the best estimate trajectory for Apollo 11[12] calculated a flight path angle at atmospheric entry of $-6.616°$ as compared to the uploaded entry condition of $-6.620°$.

Figure V.B.6-15 shows an entry corridor constructed from aerocapture analysis data obtained using *genL* and indicating primary regions of stability for single sets of applied control gains.

The construction of such a corridor proves to be complicated. The first and most significant problem is that described above, whereby particular control gains can be applicable for small regions requiring the choice of a new set of gains for entry conditions outside that region. This concern not only slows the process but causes a degree of uncertainty as to just how wide the corridor is. Although some trends were noted, no rule appeared to exist for determination of the control gains. For example, the overshoot boundary shown in fig. V.B.6-15 below is based on the majority of obtained results. However, a stable region was also found around $V_i = 11.0km/s$, $\gamma_i = -4°$. The conclusion drawn from this is that the entry corridor is indeed wide but that it remains for a globally applicable gain scheduling scheme to be derived.

For intermediate entry velocities, the choice of the constant altitude gains seemed to be least significant in determining the range of validity of any particular set of control gains. A large area of validity is found around $V_i = 10.0km/s$, $\gamma_i = -8°$, for example, with very little change in the constant altitude gains over this region, whilst the exit trajectory tracking gains require more regular alteration.

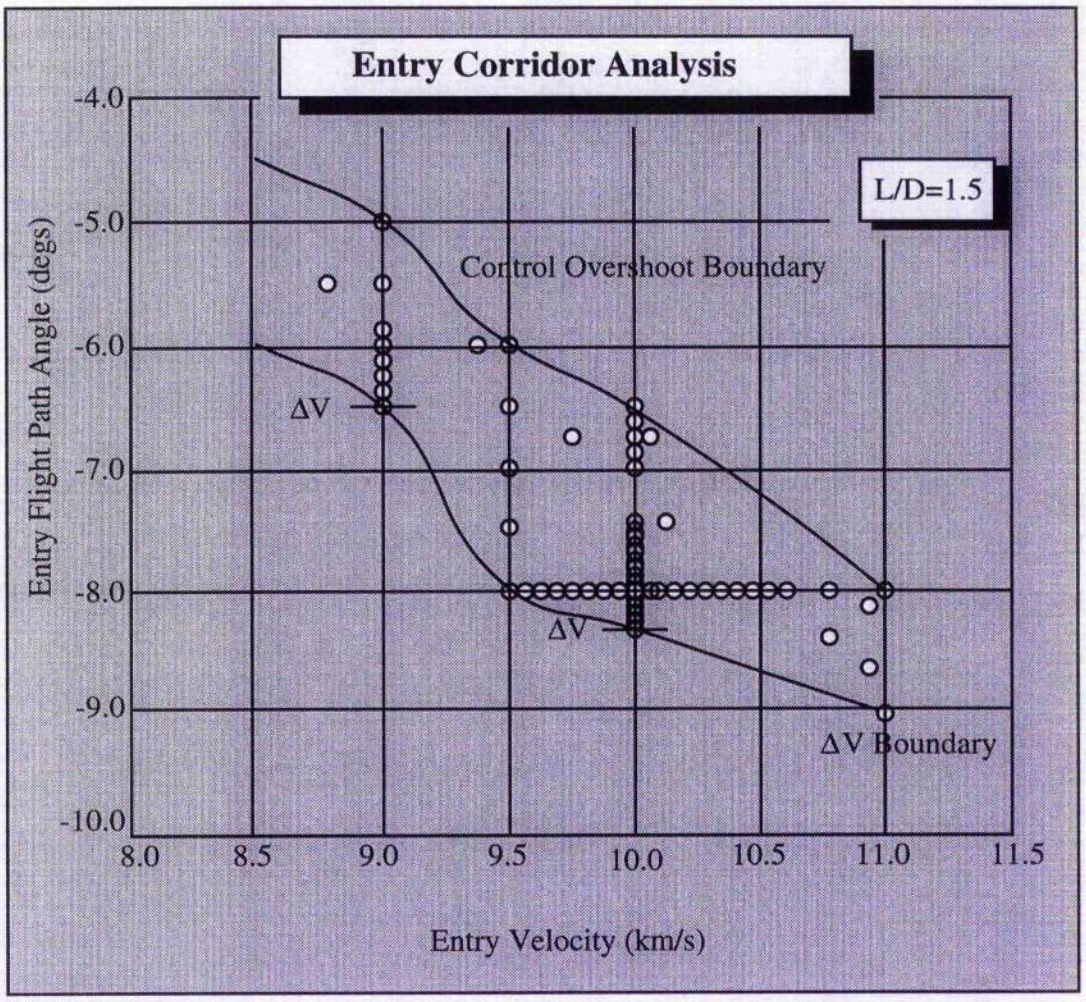

Fig. V.B.6-15 : Entry Corridor for Derived Control Indicating Primary Regions of Stability for Fixed Gain Groups.

Near the higher velocities however, the constant altitude gains require more significant modification reducing the range of applicability of any one control set. For this reason, and the increased pressure and heating limits encountered, entry velocities above free return entry velocity ($V_i \approx 11.0 km/s$) were not studied. Variation from the free-return trajectory only being deemed worthy if reductions in loadings could be achieved.

Again near the lower velocities it was found that the constant altitude gains required more frequent adjustment. Two explanations are offered for this observed effect. Firstly, that higher velocity entry requires a greater velocity decrement before

exit and consequently a longer duration constant altitude portion to the flight. The lengthening of this phase allows more time for the trajectory to be damped out towards constant altitude flight (where the pull-up predictions have greatest validity) thus giving greater flexibility in coping with off-design entry conditions.

The second, more pragmatic, explanation is the likelihood that more than one set of control gains can produce similar results and that those shown above may not possess the greatest range of applicability within that region of the corridor.

Figure V.B.6-16 illustrates one case where this effect was observed and figure V.B.6-17 shows the difference in the control histories used to obtain these results (figures are for $V_i = 10.0 km/s$, $\gamma_i = -10°$, and $L/D = 3.0$, a constant filter gain of $\zeta = 7$ was used). It can be seen from these results that gains of 3 and 5 result in similar trajectory profiles for quite different control histories.

Having accounted for the complexities in developing a true representation of the likely entry corridor it was pleasing to note that the lower limit of the corridor was predominately bound by the available ΔV or aerodynamic undershoot rather than by vehicle loading constraints (see table V.B.7-2 later). This result implies that the trajectories analysed would not require material or structural capabilities beyond those currently available. Indeed the $5g$ deceleration load limit was never breached and, although the specifications used are for a small sample return vehicle, the relatively benign environment encountered during the aerocapture manoeuvre suggests that the technique might also prove suitable for larger scale personnel transport vehicles.

The issue of a suitable lift-to-drag ratio was readily resolved. Four L/D values were considered, those being 0.5, 1.0, 1.5, and 3.0. For $L/D = 0.5$ the results were promising, however, the vehicle did not display the required control authority to deal consistently with off-design conditions, saturation of the control occurring rapidly. In addition, the entry velocities most suited to the lower value of L/D are significantly lower than typical entry

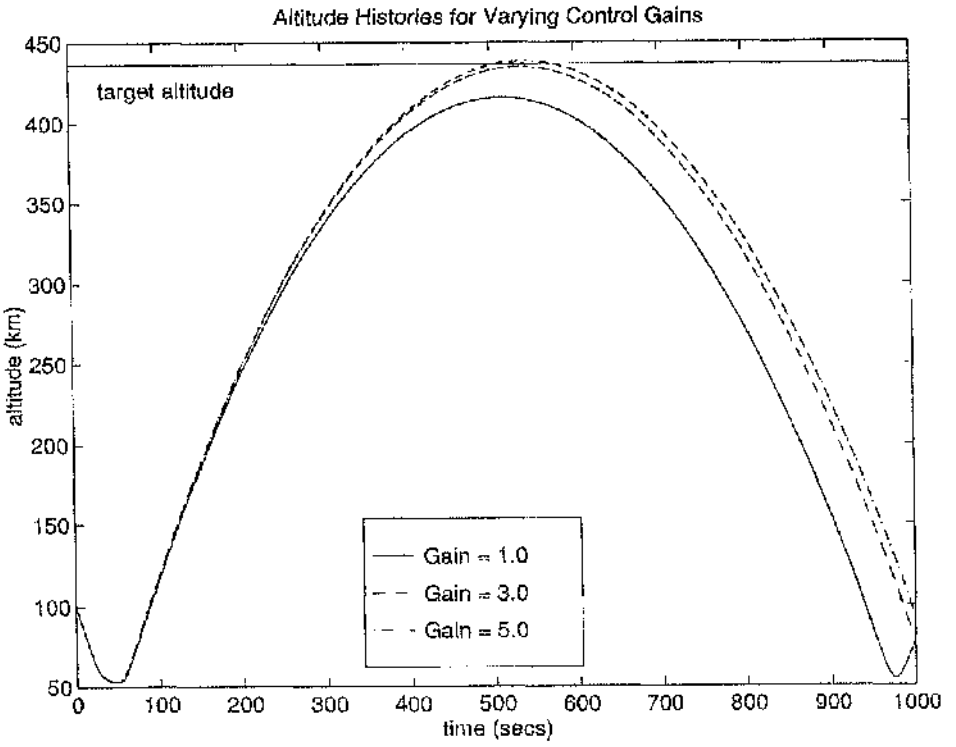

Fig. V.B.6-16 : Altitude Histories for Varying Control Gains

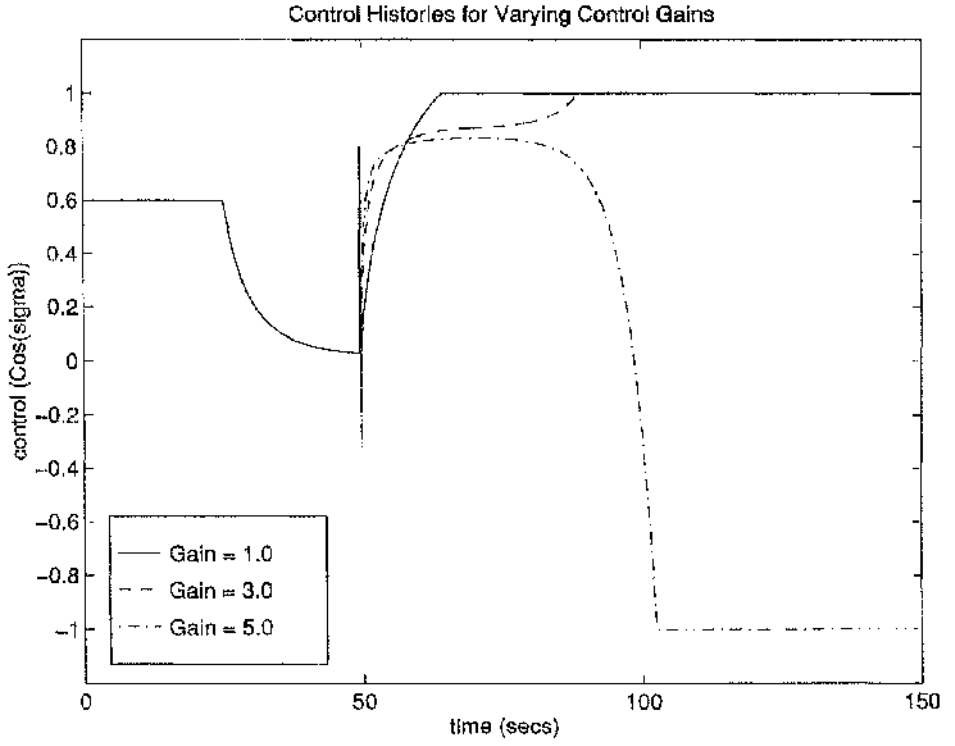

Fig. V.B.6-17 : Control Histories for figure V.B.6-16

velocities. Similar results were observed for $L/D = 1.0$ with the expected improvement in handling off-design conditions and increase in acceptable entry velocities.

The $L/D = 1.5$ vehicle performed as anticipated (see Chapter VI) with good accuracy and reliability in dealing with off-nominal conditions. The biconic shape corresponding to this value of L/D is still volumetrically efficient and it was later discovered that the design for the Japanese Hypersonic Flight Experiment (Hyflex) vehicle possesses similar dimensional and aerodynamic characteristics. Hyflex is intended to demonstrate surface to LEO operations for a reusable vehicle and will therefore have the capabilities required for the lunar return mission in terms of structural and thermal loading capacity. This option was deemed the most worthy of study and the majority of the derived results are presented for a vehicle with these specifications.

For $L/D = 3.0$ the accuracy is excellent and the consistency good. Off-nominal conditions are readily dealt with and the acceptable entry velocities are within the range expected. However, the reductions in volume efficiency and the increased material and technological requirements (see Chapter VI) in combination with the slight increase in ΔV requirements over the $L/D = 1.5$ vehicle were not adequately balanced by the cross-range ability of the vehicle to warrant further consideration.

One of the most likely causes of these errors would be an inaccuracy in the transearth injection burn which would be magnified as the vehicle approached Earth. Correction for these is possible during transit and this improves the prediction of the entry conditions. The second most likely cause is that of uncertainty in the atmospheric conditions at the time of entry. Models such as NASA's Global Reference Atmosphere Model (GRAM) contain wind models derived from past meteorological data which should help in choosing the control gains for actual flight vehicles.

As mentioned in Chapter II though, no atmosphere model can be totally reliable and, after taking the sensible precaution of allowing for expected seasonal variations etc., we still require a

control sufficiently robust as to allow for the possible variations. In this sense there is little point in optimising the aeropass manoeuvre as has been done in the past[19,42,78,82]. An optimal aerocapture solution might suggest a high entry velocity giving a correspondingly high exit velocity and hence a lower circularisation ΔV. However, as has been demonstrated above, the optimal gains might produce a highly unstable trajectory resulting in failure for only slight deviations from the design entry conditions.

V.B.7 Six-degree of Freedom, Transearth Trajectory

Having developed and tested the control technique and methodology it now remains for them to be implemented into the full return trajectory for six-degree of freedom analysis in the Sun-Earth-Moon system.

The motion is assumed to begin at the moment of transearth injection from a $105km$ lunar orbital altitude. At this point the vehicle state is measured relative to the moon (see table V.B.7-1), and so the velocity immediately after injection is $2.5243km/s$. The injection burn is made when the vehicle is in opposition to the Earth with respect to the moon.

The choice of these initial conditions is essentially arbitrary though they match broadly with those for Apollo 11. There is no reason to assume that transearth injection would not occur as an integral part of the lunar launch.

In the transearth cost phase which follows injection, a single course-correction of $1.4m/s$ (coincidentally a single course-correction of $1.46m/s$ was made by Apollo 11[71]) was applied one day into the coast phase.

Table V.B.7-1 outlines the schedule of operations over the duration of the mission. Additional tabulated points show the progress of the vehicle during transearth coast, these are plotted on fig V.B.7-1.

During the aeropass a simple time-based roll-reversal algorithm is employed which reverses the direction of bank every ten seconds. This results in an inclination change of $0.04°$ from the transearth trajectory to ISSA rendezvous. This is considered quite good performance for such a simple methodology. Though the robustness of this control has yet to be analysed and it is implicitly assumed that roll-reversal is instantaneous. It is also assumed that the transearth injection occurs with the vehicle's lunar orbit plane suitably aligned with ISSA's Earth orbit plane, so that no change of plane is required.

operation	time (secs)	altitude (km)	velocity (km/s)	flight path angle (degs)
transearth injection burn	0	105 ‡	2.524 ‡	0.0 ‡
1 day †	86400	2.749×10^5	1.133	–77.7
2 days †	172800	1.555×10^5	1.831	–76.2
2.31 days †	200000	1.006×10^5	2.424	–74.1
2.60 days †	225000	2.598×10^4	4.800	–62.8
2.64 days †	228000	1.191×10^4	6.480	–53.1
atmospheric entry	230400	200	10.940	–8.65
initiation of control	230540	59.7	10.900	–0.6
constant altitude achieved	230550	59.3	10.850	0.005
constant altitude end (pull-up)	230720	59.4	8.176	0.005
apogee burn	232510	435.43	7.646	0.007
$t = 25000$ †	250000	436.48	7.646	0.0

Table V.B.7-1 : Transearth Trajectory & Control History
† indicates point marked on Fig V.B.7-1
‡ indicates moon relative measurement

The propulsive ΔV requirement for a given inclination change, Δi, is found from

$$\Delta V = 2V \sin\frac{\Delta i}{2} \qquad \textbf{V.B.7-1}$$

which, for the case in question results in a propulsive inclination correction of $8.6 m/s$. This is not a significant ΔV and in combination with the circularisation ΔV requirement ($151.76 m/s$) falls well within the design onboard propellant load of $310 m/s$. (More detailed consideration of the return vehicle in Chapter VI puts the figure for fuel (+reserve) at $320 m/s$ ($+174 m/s$). In this case the total ΔV requirement is actually less than the designed reserve).

However successful this simple roll reversal scheme may have proved there is room for derivation of a suitable roll-reversal scheme to minimise this corrective ΔV.

Figure V.B.7-2a shows the velocity/altitude profile for the lunar return trajectory with figure V.B.7-2b showing the aeropass and the subsequent orbit circularisation in close-up. The velocity decrement of the aeropass is clearly shown.

These figures are all obtained using data derived from *genL* for the full six-degree of freedom transearth and aerocapture trajectory simulation.

The circularisation manoeuvre was implemented using a simple controller which calculated then applied the appropriate ΔV through knowledge of the current and the required states.

Table V.B.7-2 below gives the maximum vehicle pressure and heat loading data experienced during the aeropass in comparison to previous or existing design limits.

	Dynamic Pressure *kPa*	Axial Deceleration *g*	Nosetip Heating Rate W / cm^2
Experienced	16.9	0.867	726.1†
Limits	27.0‡	5.000∫	1600.0§

Table V.B.7-2 : Recorded Physical Maxima for Lunar Return Aerocapture Manoeuvre

† based on a nose radius of 0.40m ‡ shuttle limit[80] ∫ Apollo entry limit[12]

§ Experimental Data for Lightweight Ceramic Ablators[81]

As can be seen the experienced loadings do not exceed 65% of existing design limits. From this data we may conclude that current technology is easily capable of meeting the demands of lunar return aerocapture using the proposed control method.

Finally, figures V.B.7-3a & -3b show the aerocapture /circularisation manoeuvre as firstly an altitude-time history and secondly a plane view orbit trace around the Earth.

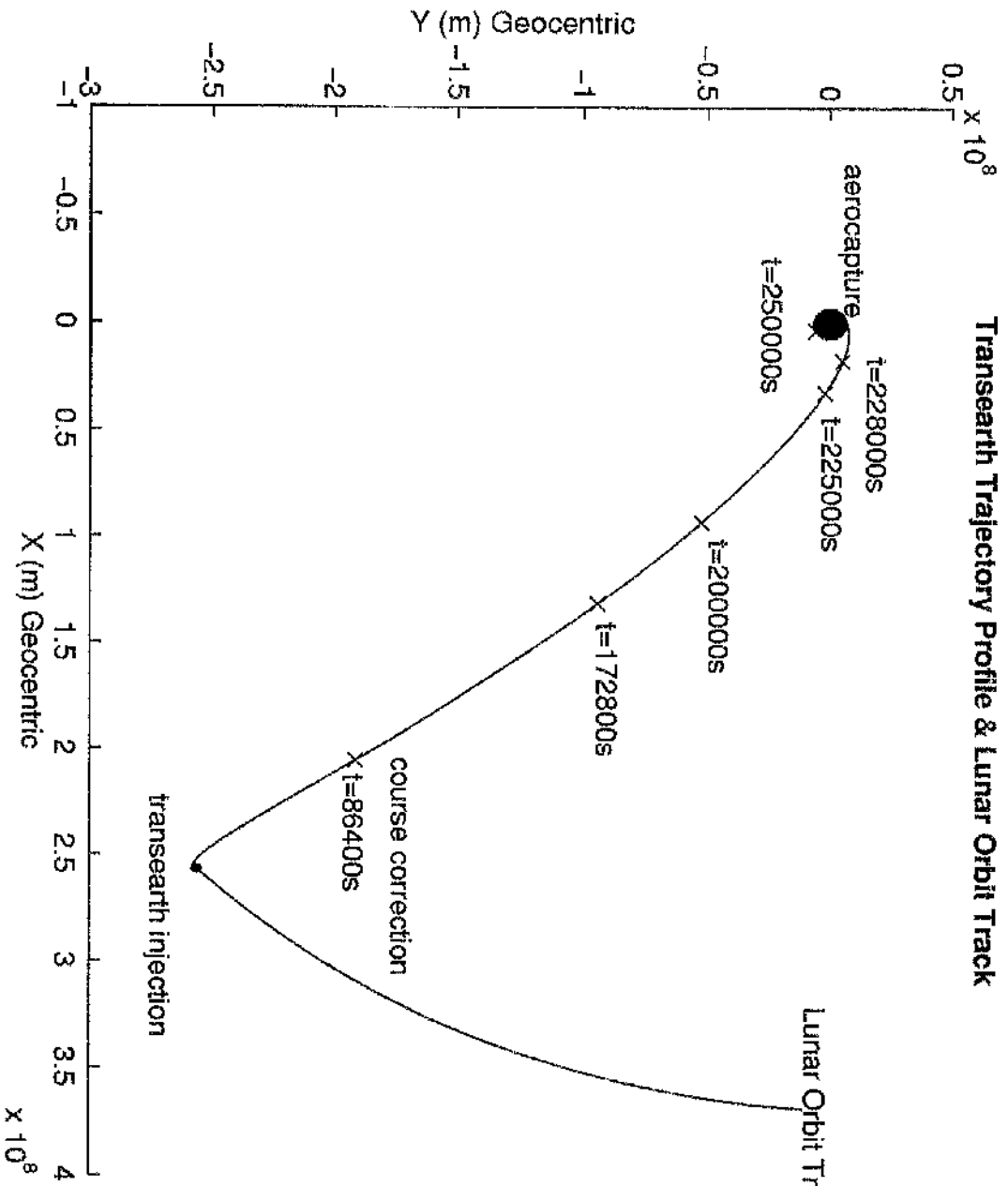

Fig. V.B.7-1 - Transearth Trajectory Profile

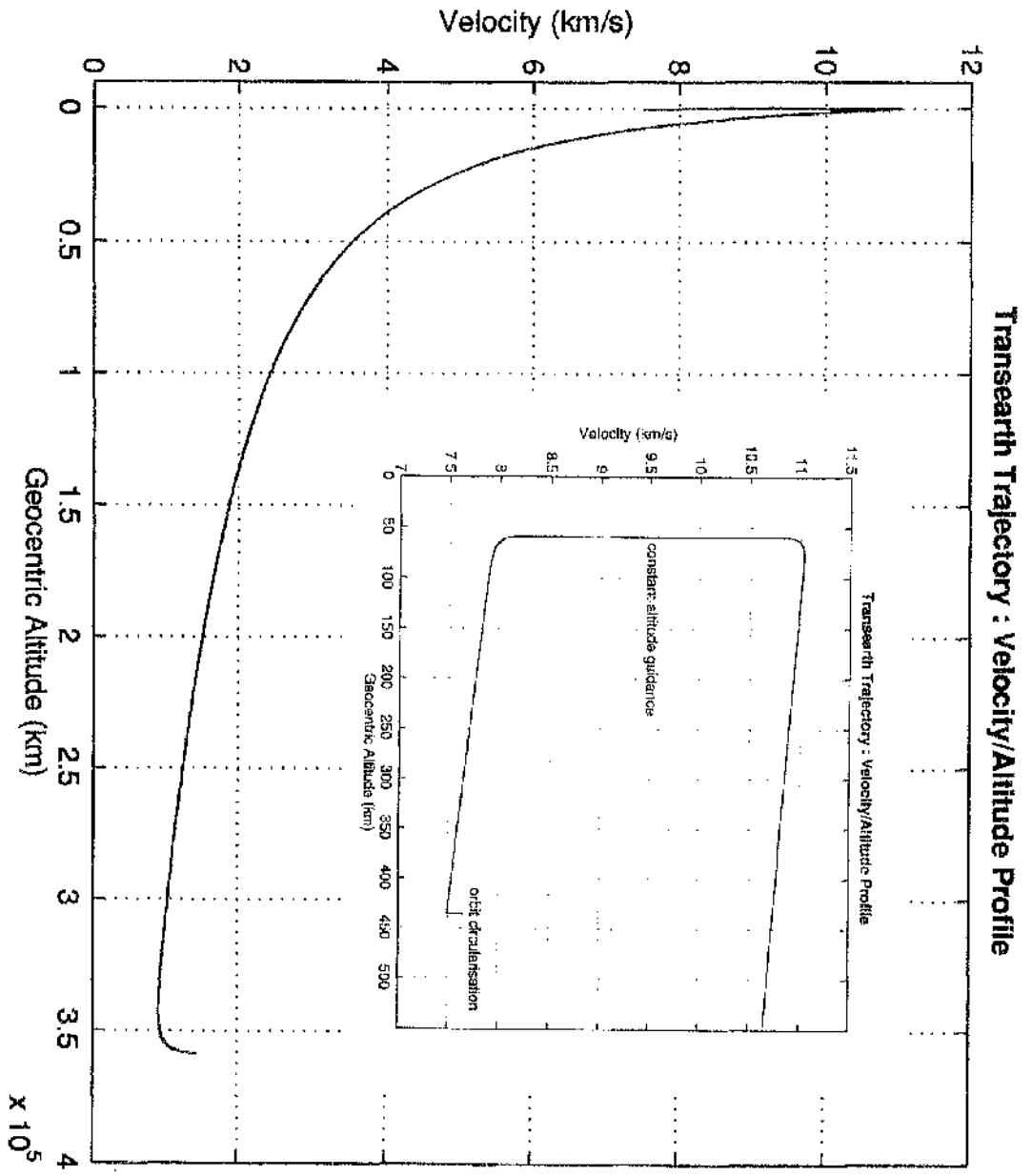

Fig. V.B.7-2a & Fig.V.B.7-2b - a) Transearth Trajectory Velocity/Altitude Profile & **b)** Insert: close-up of aeropass and orbit circularisation.

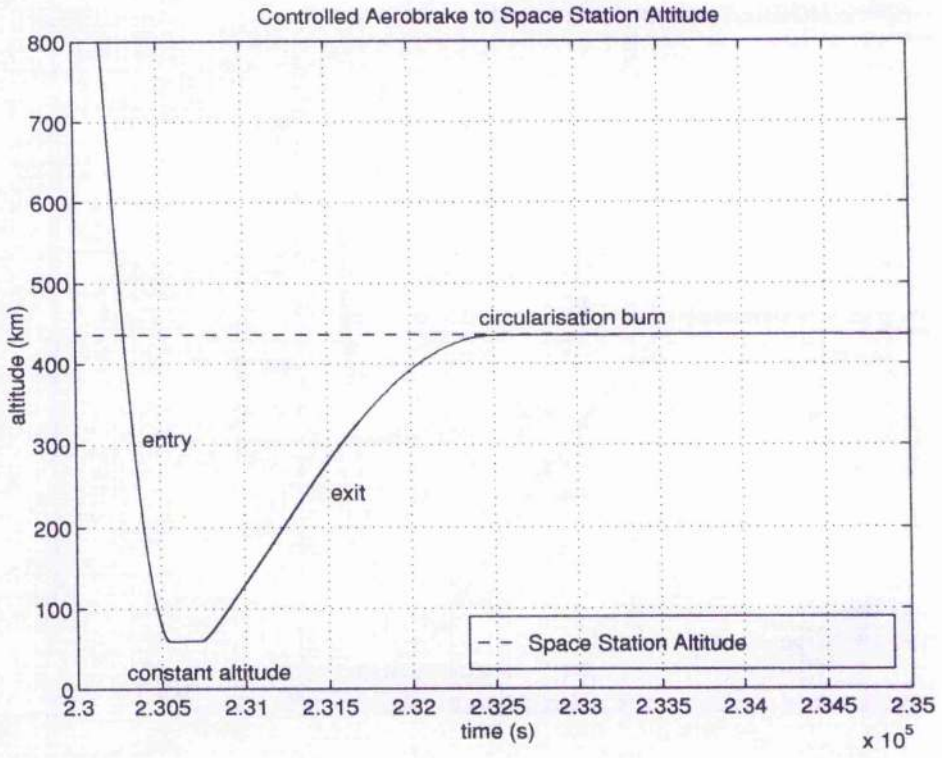

Fig. V.B.7-3a : Altitude-Time History for the Aerocapture/Circularisation Manoeuvre

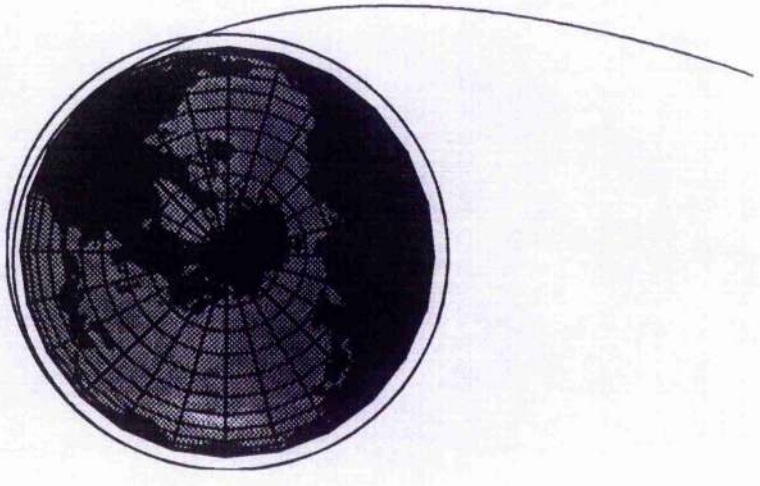

Fig. V.B.7-3b : Orbit Path for the Aerocapture/Circularisation Manoeuvre (Plan View)

V.B.8 Conclusions

It has been demonstrated using a robust, computationally efficient guidance method that lunar return to a space station can be achieved by successful use of an aerocapture manoeuvre. The motion of the vehicle has been analysed on the full six degree of freedom *genL* simulation.

Aerocapture to the space station is preferred to a return to ground for a number of reasons:

- logistic simplicity and flexibility

  The proposed return to ISSA leaves the return vehicle in a circularised orbit at the same altitude as ISSA. The vehicle may then rendezvous with ISSA 'at leisure', either autonomously or through ground or space station control. There is a clear advantage to this approach in comparison with the "four SH-3D helicopters from the U.S.S. Hornet, three E-1B aircraft, three Apollo range instrumentation aircraft, and two HC-130 rescue aircraft"[71] used for the Apollo 11 ocean landing, even allowing for the concern over the safety of the astronauts.

- lower load limits

  In comparison to the loads predicted for the proposed return scenario, a return to ground would incur higher heating and aerodynamic loads, requiring a more robust structural design, and thus reducing the payload mass fraction.

- improved payload margin

  In addition to the higher structural requirements mentioned above, there is the need for a parachute/propulsive deceleration system to avoid a high velocity surface impact. This will require a further reduction in the spacecraft payload mass fraction.

The use of aerocapture to achieve the required velocity decrement has reduced the fuel requirements for achieving ISSA orbit from transearth motion to those for orbit circularisation and rendezvous.

To achieve the required velocity decrement through propulsive means alone would require at least 65% of the

total vehicle mass to be purely propellant. A further 6.5% would be required for the mass of the fuel tanks, leaving less than 30% of the total mass for engines, systems, structure, and payload. The scenario proposed here requires only a 10% fuel mass fraction. As will be shown in the following chapter the mass fraction for aeroshell and propellant is only 30%, including a $50kg$ (5%) fuel reserve (section VI.B).

Clearly, this reduction in the fuel requirement greatly enhances the payload capabilities of the return vehicle.

The use of two periods of non-linear feedback guidance has achieved stability of the manoeuvre for satisfactory error ranges around any designed entry conditions.

Feedback linearisation has firstly been used to guide the vehicle along a constant altitude path until the appropriate ΔV has been decremented. Release from level flight is determined by the analytic prediction of the exit trajectory and the resultant apogee. These predictions are then used to analytically generate reference trajectory data in-flight negating the need for data storage or numerical integration.

Using this data, a second period of feedback linearisation guidance is initiated which guides the vehicle along the predicted path. This approach artificially improves the predictions obtained from the matched asymptotic solutions by using the feedback guidance to counter the effects not modelled in the predictions.

The use of non-linear feedback for tracking of the desired exit trajectory has proved highly successful and has further reduced the fuel requirements often by as much as 50% over the value for uncontrolled exit.

Further improvement of the analytic model will obviously improve the guidance algorithm by including some of these effects. The inherent simplicity of the scheme lends itself well to implementation on the limited computer resources available in terms of power, storage space and robustness.

Chapter VI.

Some Vehicle Design Considerations

VI.A. Introduction

As might be expected, the aeropass is one of the prime drivers in the design of a transatmospheric vehicle. The atmospheric entry trajectory is dominated largely by heating, dynamic pressure and axial load (g-load) considerations. All the vehicles considered herein are unmanned and this greatly reduces or removes axial loading concerns and allows greater design flexibility to cope with dynamic pressures. Ordinarily this would be of great help in simplifying the vehicle design process. Here, however, given the types of trajectory analysed, the heating constraint will almost always predominate anyway.

The Apollo 11 re-entry module had a $5g$ load limit applied to its entry corridor[12]. This was considered the maximum sustainable

load for astronauts, based on previous American experience and later verified by Soviet experience.

Modern sample return vehicles would not only be unmanned but would as far as possible employ solid state electronics and hence be largely acceleration insensitive. One concern might be the settling effect on any lunar samples of unnaturally high (for lunar material) acceleration loads. An examination of the results from Chapter V shows that typical g-loads are of the order of $1g$. This is not thought likely to cause significant change in any returned material.

The dynamic pressure environment is of concern largely in determining the required structural strength and integrity for the hull of the vehicle. In the case of the sample return vehicle proposed here this means the aeroshell, which is obviously also of concern in the design of the craft's heat-dissipating abilities. The aeroshell then becomes perhaps the most crucial component for the survival of the vehicle and its payload.

Comparing with existing designs again, this time the shuttle[80], we find a maximum dynamic pressure loading of over $27kN/m^2$, well above that required for our return vehicle (Section V.B.7).

It remains to establish the feasibility of the return with regards to the heat loadings both peak and integrated.

As has been stated before (section II.C.2.1) the kinetic energy associated with the typical re-entry trajectory is likely to be of the same order of magnitude as the heat of vaporisation of the vehicle. This assumes two things: Firstly, that all the energy is converted to heat during the passage; secondly, that all the heat is transferred to the vehicle. The survival of meteorites shows that this is not the case. Much of the energy is lost through aerodynamic friction to the surrounding air.

Knowledge has been gained, through experience and numerical modelling, of the mechanisms through which heat transfer occurs although this is not within the scope of this work. However, further analyses such as those intended for the Atmospheric Re-entry Demonstrator (ARD)[83] will be used to qualify thermal protection materials and evaluate the heat and pressure regime around the craft. More recently, examinations of effects such as surface catalycity

have revealed more complex interactions and new methods of reducing peak heating rates. The leading edges of the Shuttle are only partially catalytic and this has led to a 20% reduction in nosetip heating rate[84].

In this chapter we will discuss the issues associated with the design as we describe a mass breakdown for the lunar return system.

VI.B. Mass Breakdown

The vehicle considered in this work is a small ($1000kg$) vehicle of the type likely to be used in assessing the technologies associated with this type of return. Injection to transearth orbit is assumed to be provided by an expendable kick stage. Apollo 11 returned a lunar sample payload of $22kg$[72] and this is our start point for determining a mass breakdown, how much can we bring back?

The European Lunar Study Steering Group has been considering a sample return capsule carrying $50kg$ of soil samples or drill cores or $1 \rightarrow 2kg$ of refrigerated biological samples (from lunar experiments performed using Earth-originating specimens)[5]. The study assumes the use of a direct re-entry capsule for return of the material to Earth rather than to ISSA.

It is thought that the removal of the need for parachute and deployment mechanism and/or floatation devices might allow us to increase the payload mass to possibly as much as 10% of the gross weight of the vehicle. The parachute and propulsion systems required to decelerate a Viking vehicle ($731kg$) from $4.6km/s$ atmospheric entry velocity to rest on the surface of Mars would take approximately $18-22\%$ of the total vehicle mass[13].

The mass breakdown presented in table VI.B.1 below is based on standard designs[79,85] and empirical guide relations[79] except where otherwise referenced.

- **Aeroshell** (15% of Total Mass)

An aeroshell is a protective heatshield which completely encloses the vehicle. A shell will be used in preference to a partial shield in severe heating environments.

In section VI.A we have discussed the re-entry environment and the high heat loads experienced during atmospheric passage. There are three main ways of dealing with this heat load.

Component	% Total Mass	Mass
Aeroshell	15%	150*kg*
Fuel (Orbit Acquisition) (Rendezvous and Reserves)	15% (10%) (5%)	150*kg* (100*kg*) (50*kg*)
Engine Mass	10%	100*kg*
Systems	25%	250*kg*
Structure	25%	250*kg*
Payload	10%	100*kg*
Total	**100%**	**1000kg**

Table VI.B-1 : Guideline Mass Breakdown for Proposed Sample Return Mission

- Absorb

By using the body as a heat sink it is conceivable that it might be possible for some vehicles to absorb the total heat load into the structure. This will require a blunt-nose (with corresponding loss of L/D performance), a thick outer skin (with corresponding weight penalty) and ideally a steep entry trajectory to minimise the total amount of heat to be absorbed. Each of these considerations makes this method of thermal control unsuitable for aerobraking.

- Radiate

Radiation of the heat load is a viable option if the heat radiated from the vehicle can match that transferred to the vehicle. Ideally, this could be employed on a shallow entry lifting vehicle using a thin metal skin.

- Ablate

  Carbon or glass fibre composites can be bonded to a heat shield to provide ablative protection to the vehicle. Ablation essentially uses sublimation of the surface materials as a means of dissipating the heat, the high heat capacity of the materials absorbing large amounts of energy. Ablative heat shields or tiles have been used on re-entry vehicles and are the lightest known solution to the problem. In addition, the use of ablative shielding allows a greater degree of flexibility in determining the type of entry and hence entry corridor.

  The ablative loss of material from the surface of the vehicle will, however, result in uncertainty over the aerodynamic coefficients of the vehicle.

The choice of heatshielding becomes simpler when we recognise that aerobraking is only advantageous if the mass of the aerobrake/aeroshell is less than the equivalent required mass of propellant and propulsion system for an exo-atmospheric capture. General guidelines for a Lunar Transfer Vehicle (LTV) place this mass at 15% of the mass of the transfer vehicle[86]. A structural mass optimisation study[87] of a sandwich aerobrake for an LTV showed a graphite-epoxy honeycomb to be the lightest at 12.3% of the total vehicle mass, with a density around $1.6 g / cm^3$.

Less dense are the Lightweight Ceramic Ablators (LCAs) being developed at NASA Ames[81] with densities ranging from 0.224 to $1.282 g / cm^3$. The LCA consists of a ceramic matrix filled with an organic resin resulting in equivalent or improved performance when compared with conventional ablators. The study suggests that carbon-based LCAs would be the most mass-efficient at heating rates in the range up to around $1600 W / cm^2$.

- **Fuel** (15% of Total Mass)

The fuel margin assumed for the vehicle allows 10% or $100 kg$ of liquid bipropellant for the apogee circularisation burn and a 5% margin to allow for rendezvous and docking with the station

and/or to increase the ΔV available for the apogee circularisation manoeuvre.

Using these figures the available ΔV budget is then $320 m/s$ ($+174 m/s$ reserve) for both circularisation and rendezvous. This 5% margin was not assumed in the control work earlier and greatly expands the workable entry corridor.

- **Engine** (10% of Total Mass)

The figures used are broadly based on existing liquid bipropellant engines capable of achieving the required ΔV[79]. Advanced engine designs may help reduce this mass.

- **Systems** (25% of Total Mass)

Under the general heading of systems we consider the other components of the spacecraft which perform operations during flight, e.g.

- Thermal Control
- Avionics
- Electrical Power System
- Attitude Control System

Of these probably the most significant will be the thermal and attitude control systems:

The majority of the thermal control required to maintain onboard systems operating temperatures during the aeropass will be provided by the aeroshell, which, as a major structural component, has been addressed separately (see above). Even with the aeroshell, however, some heat will be conducted to the rest of the vehicle during atmospheric passage and this must be accounted for in the vehicle design. In addition some form of thermal control will be required during transearth coast. Typical electronic components will have an operational limit[79] of $0° \rightarrow 40°C$ and this may require active cooling (probably via a

pumped loop system) during the aeropass in order to prevent excessive heat being passed from the skin to these systems. It is conceivable that the craft's fuel supply might be used as the coolant since there is no overlap between the aeropass and the circularisation burn.

Attitude control will be one of the most crucial systems onboard the spacecraft.

Typical attitude control systems are concerned with maintaining pointing accuracy in perturbation free environments outwith the atmosphere.

The lunar return mission proposed will require a system which is effectively only concerned with roll control, if we assume pitch stability is provided by suitable aerodynamic design. However, the roll control required needs to be fast actuating in order to provide rapid roll-reversals and hence effective control of the orbital inclination. The baseline Aeroassisted Flight Experiment (AFE) assumes a maximum $15°/s$ roll rate[50] and Albert et al.[35] assume a limit of $20°/s$ for their control. In addition, a high degree of accuracy in achieving the commanded bank angle is necessary given the high aerodynamic forces encountered and the resultant possibility for error.

Chapter V provides some answers to these concerns. Firstly, it has been shown that a very simple roll reversal scheme produces a good degree of accuracy in maintaining the orbital plane (Section V.B.7). Secondly, the general robustness of the derived control to variations in air density (and hence lift force) strongly suggests that it will be able to accommodate some degree of uncertainty in the actual bank angle. A faster actuating control than those mentioned above remains desirable, though the design of such is outwith the scope of this study.

Reaction control jets would be the most obvious means of actuating roll control given that the flight environment is not well-suited for aerodynamic surfaces. That having been said, the proposed Japanese Hypersonic Flight Experiment (Hyflex[88]) will utilise an aft-mounted pair of control surfaces for attitude

control in conjunction with the aforementioned reaction control thrusters.

The 25% mass fraction is likely to be excessive for the systems mentioned above but also allows room for systems such as Inertial Measurement Units (IMU's, typically less than $25kg$[79]), for velocity and altitude data during atmospheric entry, and electrical power systems (Approximately $0.02kg\ per\ Watt$[79]).

- **Structure** (25% of Total Mass)

The figures used are arrived at by scaling down existing vehicle designs[85]. Advances in materials technology and future flight validation of existing materials may help to bring this figure down.

- **Payload** (10% of Total Mass)

The Apollo landings provide the only comparisons available for assessing a payload return mass sufficient to justify the likely cost of the mission. Apollo 11 returned 22kg of lunar material to Earth for analysis[72]. Having removed the human and surface return components (see above) of the mission the vehicle design is greatly simplified and it is likely that payloads of 10% or more of the total mass (after transearth injection) might be achieved.

VI.C. Vehicle Design Concepts

VI.C.1 Existing Glider Designs

A variety of design concepts exist for lifting entry vehicles ranging from simple sphere/cone shapes to winged gliders and waveriders. The most widely known is the Shuttle, a (manned) winged glider design which falls into the higher L/D bracket for existing entry designs. Other baseline designs include[9]:

- Sphere/Cones - $L/D = 0.0 \rightarrow 1.0$;

  Simple designs, such as the Apollo re-entry capsule have proven effective. The lack of any sharp edges leads to a lower peak heating rate, whilst the design is also aerodynamically quite stable. The low value of L/D is its major drawback, with controllability reduced.

- Biconics - $L/D \approx 1.5$;

  Most aerocapture studies have recommended the use of biconics for their missions[9], the accuracy of the aerocapture manoeuvre reaching a maximum around $L/D = 1.5$[89], this is again confirmed by the present study. These vehicles still retain the relatively low heating rates concurrent with the lack of any sharp edges.

- Winged Gliders and Lifting Bodies - $L/D \approx 2.0$

  More often than not these designs are relatively large manned vehicles where crew safety, operational flexibility, and return to a fixed landing sight(s) will be important concerns and hence we require greater manoeuvrability from the vehicle, in addition to the ability to fly at super-, trans-, and subsonic speeds.

  The Shuttle design uses rounded edges for both the nose and the leading edges of the wing to combat high heatings rates experienced during re-entry. The corresponding loss of slenderness of the vehicle reduces its lift-to-drag (L/D) performance whilst increasing its volumetric efficiency.

- Sharp-edged Winged Gliders - $L/D \approx 3.0$

  Sharp-edged winged gliders tend to be slender designs optimised for high L/D performance and are hence have a low volumetric efficiency and high leading edge heating rates. Most current mission analyses either do not require the L/D capabilities of these designs or have stepped over them directly to waverider concepts (VI.C.2).

From this information it would appear likely that our return vehicle will be a biconic design as confirmed by this study and the entry corridor analysis. Alternatives to such a design do exist, some of which are described below.

VI.C.2 Aeroassisted Flight Experiment (AFE)

The aeroassisted flight experiment[90] is a lifting aerobrake design intended to assess the aerodynamic environment of hypervelocity entry into the terrestrial atmosphere. The model design is that of an ellipsoidal nose blended with an elliptical cone and has been wind-tunnel tested at NASA Ames Hypervelocity Free-Flight Aerodynamic Facility to estimate lift, drag, and moment coefficients.

Also of significance has been the assessment of the longitudinal stability of the design. The importance of this is clear when we consider that the roll control used herein (and generally recognised as the best means of achieving hypervelocity aerodynamic control) requires a constant pitch angle to work effectively. Suitable aerodynamic design of the vehicle, specifically a large negative value of pitching moment coefficient, would seem to be the most appropriate means of achieving this goal.

VI.C.3 Waveriders

The waverider is a class of hypersonic high lift-to-drag vehicle based on a concept proposed by Nonweiler[28] whilst working at Glasgow University. Its name derives from the way it appears to ride the leading-edge shock wave generated during flight. The vehicle is shaped such that the shock wave is attached along the lower surface of the leading edge whilst the upper surface is subject to shock-free freestream flow. The resulting pressure differential is what gives the waverider its high lift characteristics.

The waverider vehicle has long been viewed as more of a scientific nicety than a practical design possibility. This has been due to the apparent need to optimise the design for a particular cruise speed and altitude and the sharp drop in performance for off-design conditions[91]. However, tests carried out by McDonnell Douglas on waverider models with blunted leading

edges have produced results which suggest that efficient performance is possible over a range of speeds and altitudes[91].

The tests showed that for a design speed of *Mach* 14 over a range of *Mach* and *Reynolds* numbers the variation in L/D was less than 10% with a maximum L/D value of 3.8.

Whilst the speed range tested is well below the typical entry speed for a Lunar Return Vehicle the corresponding value for L/D_{max} is approximately double that used in Chapter V and only 15% off the value for an optimised waverider design. In addition, designs for aero-gravity-assist manoeuvres aim at L/D_{max} values of around 10[27] and work towards this goal should produce vehicle designs with L/D values in the range useful for Lunar return aero-assist.

The low-drag characteristics of the vehicle would result in a longer trajectory arc to achieve the required velocity decrement. Whilst this is not necessarily desirable it is has to be considered whether or not the improvements in controllability available from using vehicles with such high L/D values as waveriders may outweigh any potential losses/problems[92].

VI.C.4 Single Stage?

In noting that the ΔV requirements for launch to LEO are of the same order as those from LEO to the Moon and back, it has been suggested that some current single stage to orbit (SSTO) concepts might be suitable for the supply of a lunar base[93]. The proposal is for a ground launch vehicle which would refuel at ISSA for the trip to the Moon.

One obvious drawback is the need to supply the station with the extra propellant required to refuel the SSTO before translunar injection. An estimated 87 SSTO launches would be required to supply the station with this fuel. The study need really go no further. What seems an interesting concept only really becomes feasible when we consider a vehicle capable of lifting the required amount of fuel in one or two steps. In this eventuality however, why stop at the station?

A further point of note is the requirement for a preentry braking ΔV of $800 m/s$ in addition to the $310 m/s$ required for circularisation and rendezvous. This is not a requirement for the return technique proposed here and suggests that a reusable vehicle capable of performing an unassisted aerocapture would make significant fuel savings.

VI.D Other Design Concerns and Conclusions

The means by which aerodynamic control is achieved is as much a design concern as heating and dynamic pressure loads. Control could be effected by angle of attack control and algorithms have been developed to this end. However, as has been discussed (section V.B.5), control by this means will require flight in off-design conditions and hence the application of large forces to stabilise the vehicle. The most likely means of actuating this control is through reaction control jets and consequently a significant amount of extra fuel may be required.

Control is therefore effected through bank-angle modulation. The aerodynamic rolling moments will not be as great as the pitching moments and hence control will be easier and more stable and hence require less fuel. In order to improve the response of the vehicle it should ideally have a small resistance to roll inputs. This reduces the stability of the vehicle and may require the use of full-time active control in an analogous manner to modern combat aircraft. Whichever choice is made the high aerodynamic loads which will be encountered will demand accurate determination of aerodynamic coefficients and trim angles for effective control[90].

Ordinarily an increase in the lift-to-drag ratio of an aerospace vehicle is desirable. In the context of aerocapture this may not necessarily be the case. Crouse and Lewis[92] assert that the accuracy of an aerocapture manoeuvre is a function of L/D for the vehicle. For a Martian aerocapture, accuracy is maximised near $L/D = 2.0$. During their study they discovered "only modest gains in entry

velocity" for the waverider design ($L/D = 5.0$) over a lower L/D vehicle ($L/D = 0.8$).

This expansion of the flyable entry corridor was offset by the increase in manoeuvre duration, increased heating rates and the corresponding technological advances required to withstand these rates.

Not surprisingly though, there was a marked improvement in achievable lateral range for the waverider vehicle, over 35° latitude as compared with less than 5° for the lower L/D vehicle.

That having been said the increased manoeuvrability provided by use of waveriders is not thought to provide enough benefit alone to justify their use in the short term. The mission frequency for the lunar return scenario will be very low initially and will not increase too rapidly. Given the low eccentricity of the lunar orbit and the relatively short orbit period of the ISSA it is not likely to prove too inconvenient to adjust the mission scheduling to align the transearth and ISSA orbits, thereby requiring minimal cross-range ability of the spacecraft.

Should waverider and material technologies develop sufficiently in the long run that manufacturing and operational costs become acceptable, then it is conceivable that the greater flexibility in scheduling provided by the increased manoeuvrability might lend waverider use to the increasingly frequent supply operations required by a growing lunar outpost.

Figure VI.D-1 presents a schematic of the design chosen for the sample return vehicle.

In the light of all the considerations covered in this chapter and the mission scenario analysed in Chapter V it is likely that the vehicle will have the following design characteristics:

- $L/D \approx 1.5$ produced by either a biconic or a lifting body design
- radiative heat shield and pumped loop cooling system (probably using the craft's liquid propellant as the coolant) for thermal control

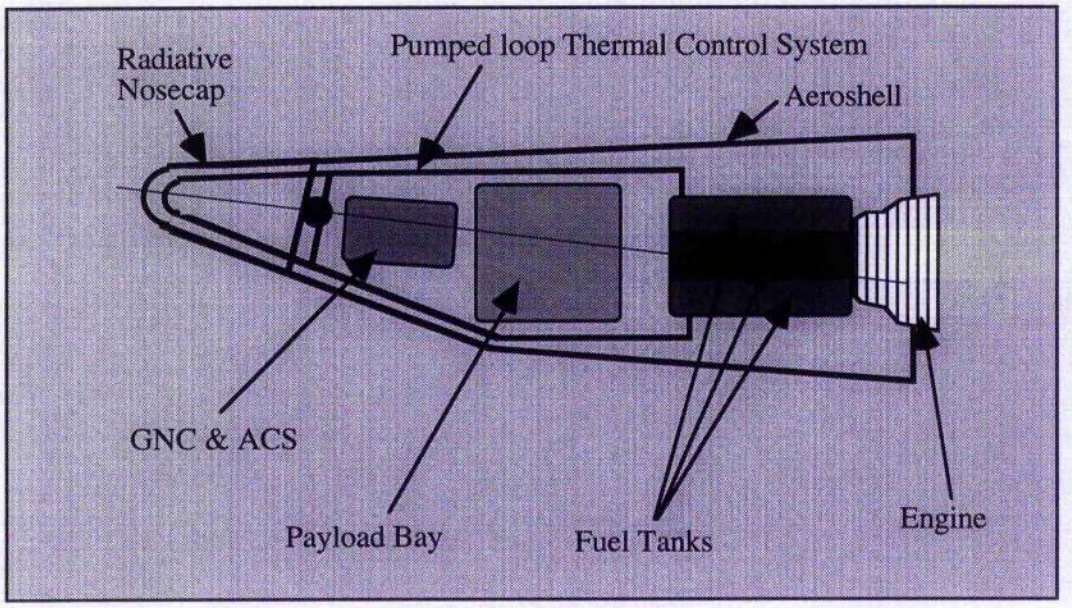

Fig. VI.D-1 : Schematic of the Sample Return Vehicle

- Mass breakdown as per Table VI.B-1
- Reaction jet attitude control systems utilising the same type of fuel as the main engine
- Liquid bipropellant fuel (probably N_2O_4 / MMH - mono-methyl hydrazine, $I_{sp} = 300 \rightarrow 340s$)

These design requirements for the sample return vehicle are well within contemporary capabilities and this makes the mission scenario a practical possibility for the early stages of a return to the Moon.

Chapter VII.

CONCLUSIONS

Overview

The prospect of a return to the moon must be treated seriously. The importance of such a venture in scientific terms alone cannot be understated. Now, with the rapid depletion of the world's fossil fuels and general concern over the safety of existing nuclear fission reactors the moon can also be looked on as a potential fuel source (section I.A). Whilst it is possible that in the future beamed energy concepts could be used to "transport" energy from Lunar reactors to Earth, it is likely that the first Deuterium/Helium-3 fusion reactors would be terrestrial, requiring the transport of Helium-3 from the Moon back to Earth. This commercialisation of space will prove to be of fundamental importance in the future as space exploration almost inevitably becomes a part of space exploitation.

Whether in the long run it would prove more cost effective to transport materials directly to the Earth or via an orbiting station will depend on the scale of the operations and the state of technology at the time.

To perform operations in stages would seem to be easiest as a single vehicle for the entire mission would either be required to

carry all the necessary fuel for LEO-to-ground for the entire trajectory or would need to be capable of controlled aerocapture to ground. This latter option will either require the transport of a complete parachute mechanism or a vehicle capable of aerobraking at a constant altitude (in a manner similar to that proposed here) before making a controlled gliding descent to ground. The cost of the Shuttle and the redefinition of "reusability" which accompanied it suggests that this latter option is not currently practical.

What is currently practical, as has been shown (Chapter V), is an aerobraking return to orbit. Either the Shuttle or a single-stage-to-orbit (SSTO) vehicle such as the proposed DC-X could then be used to transport material from LEO to the surface.

Aerocapture then has its purpose. In the more immediate future the concept could be demonstrated as part of an initial Lunar program performing sample return missions of the type described in this work. Here the advantages are clear as, with the presence of ISSA as an orbiting laboratory, there would be no need to transport the samples to the surface. This removes all the concerns associated with the extra $7km/s$ ΔV required by a surface return over return to the station.

To achieve the $4km/s$ ΔV required for the return to ISSA aerodynamically without the need to resort to single-use ablative heat-shielding is the icing on the aerocapture cake.

Once a proven technology, aerocapture could then form the basis of an Earth-Moon communications network, using ISSA (or its descendants) as an orbiting 'station' of a slightly different nature than is perhaps currently intended.

Ideally, as part of such a network, the aerobraking vehicle would be capable of the vertical landing required for lunar operations, so that it might also act as a supply vehicle to a lunar base. As mentioned in Chapter VI, a lift-to-drag ratio of 1.5 is more or less optimal in terms of the accuracy of the aerocapture manoeuvre, requiring either a lifting body or a biconic design. These designs may require more complicated controls to stabilise their descent to the lunar surface owing to their shapes. It may in the future prove possible to attach small winglets to the sides of a conic vehicle

making it capable of the desired L/D and also of controlling the manoeuvre. Such a capability would allow the design of more symmetrical vehicle, improving its performance for the lunar descent.

Transport of materials to LEO then becomes our next target. It is inevitable that much of this transport will be carried out by the vehicles which will retrieve materials (lunar or otherwise) from the Space Station. However, in the early stages of lunar exploration and in particular in the establishment of a lunar base, there will be a greater need for transport of material to the moon than from it.

Direct launch to orbit by a ram accelerator or gas gun (Chapter IV) is a more cost effective means of achieving transport to LEO. Conceivably the translunar transport vehicle could be housed within a protective sabot which could be discarded once in LEO before translunar injection. Such a launch approximately halves the ΔV capability required of the vehicle.

Direct launch to the translunar trajectory is likely to prove unfeasible for the foreseeable future, the heatshielding requirements (if achievable) probably negating any benefits obtained from such a launch.

In comparison with the efforts of the late fifties and the sixties recent progress in the space program appears slow. The space infrastructure has not yet been put in place to allow us to establish a manned lunar base and it is likely that the anticipated energy crisis will be the motivating factor behind the establishment of such an infrastructure, but it is this communications network which will form the backbone of future space efforts.

Controlled Aerocapture

The use of aerocapture is one of the keys to future space exploration. In the lunar return context an aerocapture return to the space station significantly alleviates the heating (approximately $25GJ$ less energy to be dissipated), dynamic pressure, and deceleration loadings on the vehicle, whilst also improving the operational flexibility of the mission over a surface return.

Of course, return to the station could be effected through purely propulsive means, but this would require a vehicle with an extra $4km/s$ ΔV capability requiring at least 65% of the vehicle mass to be propellant. The mass estimate for the aeroshell/circularisation propellant combination for the proposed aerocapture mission is 30% of the total vehicle mass. Clearly, for the same payload mass, a vehicle performing aerocapture will be significantly smaller than the equivalent all-propulsive vehicle.

Having justified the mission it is important to demonstrate it as an achievable practicality. This has been demonstrated in the following ways:

- **No Technological Advances Required**

  The manoeuvre may be performed by a vehicle using current materials and component technologies. A hypersonic L/D ratio of 1.5 is achievable using existing biconic and lifting body concepts. The Hyflex experimental vehicle is very similar in configuration to the proposed aerocapture vehicle.

- **Autonomously Controllable Manoeuvre**

  It has been shown that the aerocapture manoeuvre may be successfully performed by onboard guidance based on analytic trajectory predictions. Autonomy is important not only in maintaining the operational flexibility desired but, perhaps more significantly, because of the difficulty in transmitting control signals to a vehicle during a hypervelocity aeropass.

- **Robust Control**

  The use of non-linear feedback around reference trajectory data effectively damps out the non-linearities in the vehicle dynamics improving vehicle response in off-nominal conditions. A given set of control gains will not prove universally applicable owing to the presence of saturation limits on the control. This necessitates the careful choice of the control gains to achieve the desired trajectory, however, the observed robustness of individual sets of control gains is significantly greater than Apollo 11 re-entry state prediction errors and can more than satisfy entry corridor tolerances.

  The concept of optimisation is not truly applicable in the context of an aerocapture trajectory as robustness is the key. Precise optimisation of the trajectory is not possible as the atmospheric conditions to be encountered will be uncertain. It is possible to optimise the trajectory for the expected conditions but the control must be able to deal with the off-optimal conditions that may be encountered and in that sense it might be more practical to optimise for the maximum range of applicability of the control gains.

The analytic relations used in generating the reference data required for the feedback linearisation do so in a novel manner. Rather than storing the reference data onboard or downloading it before atmospheric entry the data is produced only as and when required. In addition, the onboard production of the reference data is specific to each phase of the motion and requires no prior estimation of the values of the state variables. The actual values of the required state variables at the initiation of each phase are used, making the data specific to the current motion.

In this way the actual vehicle state during the control phase is guaranteed to be close to the reference state. This is of importance in maintaining the applicability of the derived control.

The simplicity of the derived control is crucial to its success. There are no bugs or loopholes which the analyst cannot foresee. In

this case we have derived a control which, mathematically, guarantees stability of the manoeuvre.

Without the limits of the control saturation we could guarantee the desired end state from any initial conditions. The bounds on the applied control reduce this range and require careful choice of control gains to achieve the desired end state. What remains for the analyst then is to ensure that the control is sufficiently robust as to guarantee convergence within anticipated state variations. Once this has been asserted (through numerical simulation) the analyst can state with confidence that any failure will not occur as a result of a fault in the derived control.

With all this in mind it is clear that continued development of such analytic modelling techniques has merit. The accuracy to which they need be developed is debatable owing to the uncertain nature of the aeropass, but if the prediction data can incorporate new physical effects to improve its correlation with numerically obtained trajectory data then this should minimise the number and size of the control applications. Ideally the predicted exit trajectory should match the actual exit trajectory in the absence of off-nominal conditions.

To date it has proved difficult to incorporate velocity dependent effects into lifting body solutions through purely analytic means. A lifting solution may be obtained if we assume a constant lift coefficient. However, the value of a solution which incorporates a velocity dependence in one aerodynamic coefficient whilst assuming a lack of dependence in the other is questionable and hence it is not included in this work. In addition, the velocity dependence of the aerodynamic coefficients decreases rapidly with increasing nose-cone half-angle making its inclusion in the model superfluous. Other effects such as ablation are perhaps equally superfluous to this analysis, ablative shielding being unnecessary for the aerocapture vehicle.

The most likely cause of any discrepancy between the predicted and actual trajectory data is likely to be as a result of small angle concerns in the analytic solutions. As described in chapter V, angles approaching 0° create difficulties owing to the difference in order of the inner and outer solutions. If a technique can be found which removes or circumvents this concern it would be of great benefit in

analysing the optimal aerocapture solution whereby the vehicle skims the atmosphere at approximately 0° incidence thereby performing the aeropass as closely as possible to the desired end orbit.

Analytic Modelling

Away from aerocapture the use of analytic modelling techniques performs other functions. In particular they are of benefit in highlighting the important factors in the system dynamics and can be used to produce high quality predictions of important parameters quickly and easily.

In formulating the analytic solution to the re-entry problem we make use of the Allen-Eggers assumption that we may neglect the gravitational forces experienced during re-entry in comparison with the high aerodynamic loads. Indeed it is this assumption which first suggests that a matched asymptotic solution might prove appropriate for the analysis of this motion. By developing a mathematical solution using this assumption validation is possible through comparison with a numerical simulation which does not incorporate such an assumption. The very close correlation of the resulting trajectory data shows the operating assumption to be valid. In this way we have highlighted the important factors in the atmospheric pass.

Another operating assumption made by Allen and Eggers was that the vehicle drag coefficient could be considered constant over the range of interest. It had been suggested that this was not always the case and so we develop a solution incorporating a velocity dependent C_D model.

By comparing the constant C_D solutions and the velocity dependent C_D solutions with a numerical solution (also incorporating a velocity dependent C_D model) we have shown that, for craft with small nose-cone half-angles, this assumption is not valid. In this manner we have demonstrated that velocity dependence of the drag coefficient should be included in re-entry

trajectory analysis for relatively sharp-nosed vehicles whilst also developing a simple, quality analytic tool to facilitate such analyses.

A re-entry analysis tool of the type illustrated in Chapter IV allows the user to obtain any velocity or flight-path angle related data instantly, making it a very powerful tool in the analysis of re-entry scenarios. A similar tool could be developed for the direct launch mission, another for lifting launch/re-entry, another for a hypervelocity skip and hence for aerobraking missions, another for velocity dependent ballistic coefficients, and so on. Using these techniques a suite of tools could be generated allowing easy access to rapid, high quality trajectory predictions over a wide range of transatmospheric motion scenarios.

Numerical Simulation

The novel use of an arbitrary reference frame for propagation of vehicle motion has proved successful and the use of vectors has certainly facilitated both understanding of the problem and flexibility of the program. The choice of sphere of influence as the determining factor in the origin switching routine is intuitively obvious and appears to be a valid choice both philosophically and practically.

In spite of the continuing improvements in computing power the facilities available would not realistically permit a total vector formulation for *genL*. Although the vehicle state is expressed and propagated entirely in a vector formulation it would render *genL* computationally unwieldy to propagate planetary motion in the same format. Whilst this is desirable to the perfectionist mind, the engineering practicalities suggest that it is currently unfeasible and perhaps unnecessary. The influence of Jupiter, for example, on a transearth trajectory is not significant, its effect being noticeable only for studies of long duration orbital motion at best. If this is true of the largest planet in our solar system how much more so is it for Pluto?

The implication is that engineering judgement should be used in this context. When the effect is almost insignificant the accuracy with which it need be determined is reduced.

The *Holst* solar system model is a simple, quality model of planetary motion. The key to this model is the rapid convergence of the iterative solution to Kepler's Equation, $10^{-15} rads$ in no more than 6 steps. This makes the model what we have termed "semi-analytic", meaning that, apart from the small amount of iteration required to solve Kepler's Equation, the model is an analytic one.

Using this model, orbital motion is not propagated in the same sense as for vehicle motion but rather the state vector is evaluated as and when required in a similar manner to the reference data used in the aeropass controller. The model is surprisingly accurate, with the error in the Earth's anomalistic year (perigee to perigee) only 1 part in 17532.46 or 0.0057%.

As has been mentioned there is a tendency to develop simulations specifically for the subject of current study. *GenL* is an attempt to move away from this approach and develop a generic simulation package. As it stands *genL* can be used to analyse any type of motion. The adequacy of the atmospheric model for long term orbital motion is , however, questionable, though this can be rectified by incorporation of a new atmospheric data module without the need to rewrite the entire simulation.

The current choice of atmospheric model has been driven largely by the types of motion analysed, and this is perhaps the major shortcoming of the simulation as it currently exists.

The integration method has performed well. This is key to the simulation and hence careful thought must be given as to how to effect any improvements. Adaptive routines would seem to be desirable though there are some of the inherent difficulties with such routines (section II.E). It is suggested therefore that, in the absence of an acceptable alternative any upgrade of the integration routine should be a higher order scheme of the Runge-Kutta type.

It is hoped that at some point in the future a total vector representation of the Solar system could be included in the model. This will require significant amounts of computing power to run in

a reasonable period of time but if possible will model all the perturbations of the entire system implicitly within the simulation given a sufficiently accurate set of initial conditions. Such a formulation would be fully consistent within itself and should lend the simulation towards parallelisation.
